

HYDROLASES ON FUMED SILICA: CONFORMATIONAL STABILITY STUDIES TO
ENABLE BIOCATALYSIS IN ORGANIC SOLVENTS

by

JUAN CARLOS CRUZ JIMENEZ

B.S., National University of Colombia, Bogota, 2002

AN ABSTRACT OF A DISSERTATION

submitted in partial fulfillment of the requirements for the degree

DOCTOR OF PHILOSOPHY

Department of Chemical Engineering
College of Engineering

KANSAS STATE UNIVERSITY
Manhattan, Kansas

2010

Abstract

One area of considerable importance in modern biotechnology is the preparation of highly active and selective enzyme based biocatalysts for applications in organic solvents. A major challenge is posed by the tendency of enzymes to cluster when suspended in organic solvents. Because the clusters obstruct the transport of substrates to the active site of the enzyme, the observed activity is often severely reduced. Over the past two decades, many strategies have been proposed to mitigate this problem. We have tackled this major hurdle by devising an immobilization strategy that utilizes fumed silica as carrier for the enzyme molecules. Fumed silica is a non-porous nanoparticulated fractal aggregate with unique adsorptive properties. The enzyme/fumed silica preparation is formed in two steps. The buffered enzyme molecules are physically adsorbed on the fumed silica and then lyophilized. This protocol was shown to be successful with two enzymes of industrial relevance, *Candida antarctica* Lipase B (CALB) and *subtilisin Carlsberg*. The maximum observed catalytic activity in hexane reached or even exceeded commercial immobilizates and nonbuffer salt based preparations. The results demonstrated that catalytic activity has an intricate relationship with the nominal surface coverage (%SC) of the support by the enzyme molecules. *s. Carlsberg* exhibited an ever increasing activity as more surface area was provided per enzyme molecule. The activity leveled off when a sparse surface population was reached. CALB showed a maximum in catalytic activity at an intermediate surface coverage with steep decreases at both lower and higher surface coverage. It was shown that this maximum results from the presence of three distinct surface loading regimes after lyophilization: 1. a low surface coverage where opportunities for multi-attachment to the surface likely lead to detrimental conformational changes, 2. an intermediate surface coverage where interactions with neighboring proteins and the surface help to maintain a higher population of catalytically competent enzyme molecules, and 3. a multi-layer coverage where mass transfer limitations lead to a decrease in the apparent catalytic activity. Conformational stability analyses with both fluorescence and CD spectroscopy showed evidence that these regimes are most likely formed during the adsorption step of our protocol. A low conformational stability region was detected at low surface coverage while adsorbates with highly stable enzyme ensembles were observed at high surface coverage. Secondary structural analysis of the lyophilized nanobiocatalysts with FTIR confirmed a substantial decrease in the α -

helical components at low surface coverage. In summary, the work presented here traces the phenomenological observation of the catalytic behavior of a nanobiocatalyst to molecular-level: enzyme-enzyme and enzyme-support interactions, which are specific to the intricate properties of the enzyme molecules.

HYDROLASES ON FUMED SILICA: CONFORMATIONAL STABILITY STUDIES TO
ENABLE BIOCATALYSIS IN ORGANIC SOLVENTS

by

JUAN CARLOS CRUZ JIMENEZ

B.S., National University of Colombia, Bogota, 2002

A DISSERTATION

submitted in partial fulfillment of the requirements for the degree

DOCTOR OF PHILOSOPHY

Department of Chemical Engineering
College of Engineering

KANSAS STATE UNIVERSITY
Manhattan, Kansas

2010

Approved by:

Major Professor
Peter H. Pfromm

Copyright

JUAN CARLOS CRUZ JIMENEZ

2010

Abstract

One area of considerable importance in modern biotechnology is the preparation of highly active and selective enzyme based biocatalysts for applications in organic solvents. A major challenge is posed by the tendency of enzymes to cluster when suspended in organic solvents. Because the clusters obstruct the transport of substrates to the active site of the enzyme, the observed activity is often severely reduced. Over the past two decades, many strategies have been proposed to mitigate this problem. We have tackled this major hurdle by devising an immobilization strategy that utilizes fumed silica as carrier for the enzyme molecules. Fumed silica is a non-porous nanoparticulated fractal aggregate with unique adsorptive properties. The enzyme/fumed silica preparation is formed in two steps. The buffered enzyme molecules are physically adsorbed on the fumed silica and then lyophilized. This protocol was shown to be successful with two enzymes of industrial relevance, *Candida antarctica* Lipase B (CALB) and *subtilisin Carlsberg*. The maximum observed catalytic activity in hexane reached or even exceeded commercial immobilizates and nonbuffer salt based preparations. The results demonstrated that catalytic activity has an intricate relationship with the nominal surface coverage (%SC) of the support by the enzyme molecules. *s. Carlsberg* exhibited an ever increasing activity as more surface area was provided per enzyme molecule. The activity leveled off when a sparse surface population was reached. CALB showed a maximum in catalytic activity at an intermediate surface coverage with steep decreases at both lower and higher surface coverage. It was shown that this maximum results from the presence of three distinct surface loading regimes after lyophilization: 1. a low surface coverage where opportunities for multi-attachment to the surface likely lead to detrimental conformational changes, 2. an intermediate surface coverage where interactions with neighboring proteins and the surface help to maintain a higher population of catalytically competent enzyme molecules, and 3. a multi-layer coverage where mass transfer limitations lead to a decrease in the apparent catalytic activity. Conformational stability analyses with both fluorescence and CD spectroscopy showed evidence that these regimes are most likely formed during the adsorption step of our protocol. A low conformational stability region was detected at low surface coverage while adsorbates with highly stable enzyme ensembles were observed at high surface coverage. Secondary structural analysis of the lyophilized nanobiocatalysts with FTIR confirmed a substantial decrease in the α -

helical components at low surface coverage. In summary, the work presented here traces the phenomenological observation of the catalytic behavior of a nanobiocatalyst to molecular-level: enzyme-enzyme and enzyme-support interactions, which are specific to the intricate properties of the enzyme molecules.

Table of Contents

List of Figures	xiii
List of Tables	xxv
Acknowledgements.....	xxvii
Dedication	xxix
CHAPTER - 1 Introduction.....	1
1.1 Research Motivation	1
1.2 Research Objective	2
1.3 Dissertation Outline	3
1.4 References.....	4
CHAPTER - 2 Background.....	9
2.1 Enzymes in Organic Media.....	9
2.2 Activation of Enzymes in Organic Solvents.....	13
2.3 Interfacing Proteins with Nanomaterials	15
2.4 Enzymes and their Interactions at Aqueous/Solid Interfaces	19
2.5 Rearrangements in the Enzyme Structure upon Adsorption on Solid Surfaces.....	20
2.6 Physical Adsorption Enables Enzyme Immobilization on Fumed Silica	22
2.7 Protein Conformational Stability	23
2.7.1 Measuring Protein Conformational Stability	24
2.7.1.1 Spectroscopic Techniques to Monitor Structural Changes.....	25
2.7.1.1.1 Intrinsic Fluorescence Spectroscopy ^{126, 127}	25
2.7.1.1.2 Circular Dichroism.....	27
2.7.1.1.3 Infrared Spectroscopy	33
2.8 References.....	39
CHAPTER - 3 Immobilization of <i>Candida antarctica</i> Lipase B: Esterification of Geraniol in Hexane 51	
3.1 Abstract.....	51
3.2 Introduction.....	51
3.3 Materials and Methods.....	53

3.3.1	Materials	53
3.3.2	Enzyme Immobilization.....	54
3.3.3	Enzyme Adsorption Kinetics	54
3.3.4	Transmission Electron Microscopy (TEM) Analysis	56
3.3.5	Imaging of Enzyme Distribution on Fumed Silica Surfaces by Confocal Laser Scanning Microscopy.....	56
3.3.6	Analytical Methods for Assays in Hexane.....	56
3.3.7	Initial Reaction Rate Measurements and Kinetic Parameters.....	57
3.3.8	Thermal Stability Measurements	57
3.3.9	Storage Stability in Hexane	57
3.3.10	Long-Term Stability.....	57
3.4	Results and Discussion	58
3.5	Conclusions.....	69
3.6	References.....	70
 CHAPTER - 4 Immobilization of <i>Candida antarctica</i> Lipase B on Fumed Silica:		
	Enantioselective Transesterification of (RS)-1-Phenylethanol in Hexane	76
4.1	Abstract.....	76
4.2	Introduction.....	77
4.3	Materials and Methods.....	78
4.3.1	Enzymes.....	78
4.3.2	Chemicals and Materials.....	79
4.3.3	Enzyme Surface Coverage of the Support	80
4.3.4	Enzyme Immobilization.....	80
4.3.5	Mobile Phase.....	82
4.3.6	Analytical Methods for Reactions in Hexane	82
4.3.7	Initial Reaction Rates	82
4.3.8	Thermal Stability	83
4.3.9	Steady-State Conversion.....	83
4.3.10	Hexane Storage Stability.....	83
4.3.11	Long-term Stability for Storage at 4°C.....	83
4.3.12	Water Content Analysis	83

4.4	Results and Discussion	84
4.5	Conclusions.....	92
4.6	References.....	92
CHAPTER - 5 Conformational Changes and Catalytic Competency of Hydrolases Adsorbing on Fumed Silica: I. Tertiary Structure		
		97
5.1	Abstract.....	97
5.2	Introduction.....	97
5.3	Materials and Methods.....	100
5.3.1	Materials	100
5.3.2	Unfolding of Enzymes by GdmCl in Aqueous Buffer.....	100
5.3.3	Unfolded Fraction Inference for GdmCl Unfolding in Aqueous Buffer Solution..	103
5.3.4	Baseline for Kinetic Experiments	104
5.3.5	Kinetics of Tertiary Conformational Changes of Enzymes Adsorbing/Desorbing on Fumed Silica	104
5.3.6	Unfolded Fraction Inference for Kinetic Experiments with Fumed Silica in Aqueous Solution.....	105
5.3.7	Regions of Conformational Stability: 3D Filled Contour Plots.....	106
5.4	Results and Discussion	107
5.4.1	Deformation of Enzymes during Adsorption/Desorption on Fumed Silica in Aqueous Solution.....	107
5.4.2	Regions of Conformational Stability for Enzyme/Fumed Silica Adsorbates	111
5.4.3	Impact of Tertiary Structure Modifiers for Enzymes Adsorbing/Desorbing on Fumed Silica in Aqueous Solution.....	116
5.4.4	Regions of Conformational Stability for Enzyme/Fumed Silica Adsorbates in the Presence of Structure Modifiers.....	118
5.5	Conclusions.....	121
5.6	References.....	122
CHAPTER - 6 Conformational Changes and Catalytic Competency of Hydrolases Adsorbing on Fumed Silica: II. Secondary Structure		
		129
6.1	Abstract.....	129
6.2	Introduction.....	129

6.3	Materials and Methods.....	133
6.3.1	Materials	133
6.3.2	Circular Dichroism Conditions to Monitor Unfolding	133
6.3.3	Enzyme in Aqueous Buffer Solution: Unfolding by GdmCl/Urea and Unfolded Fraction Tracking by CD	133
6.3.4	Enzyme Adsorbed: Secondary Conformational Changes of Enzymes Interacting with Fumed Silica Nanoparticles in Aqueous Buffer Solution.....	136
6.3.5	Regions of Secondary Conformational Stability: 3D Filled Contour Plots	138
6.3.6	FTIR Analysis of Lyophilized Adsorbates	139
6.3.7	Second Derivative Spectral Analysis of Lyophilized Adsorbates	139
6.4	Results and Discussion	141
6.4.1	Unfolding of Enzymes Interacting with Fumed Silica in Aqueous Solution.....	141
6.4.2	Regions of Conformational Stability for Enzyme/Fumed Silica Adsorbates	146
6.4.3	Impact of Structure Modifiers for Enzymes Interacting with Fumed Silica in Aqueous Buffer Solution	149
6.4.4	Secondary Conformational Changes of Lyophilized Adsorbates.....	151
6.5	Conclusions.....	158
6.6	References.....	159
CHAPTER - 7	Conclusions and Recommendations	171
7.1	Conclusions.....	171
7.2	Recommendations.....	176
7.2.1	Strategies to Increase Conformational Stability	176
7.2.1.1	Computational Tools to Identify Regions of Low Conformational Stability in Proteins	177
7.2.1.2	Experimental Techniques to Identify Regions of Low Conformational Stability in Proteins	190
7.2.1.2.1	Calorimetric Techniques	190
7.2.1.2.2	Force Spectroscopy	190
7.2.2	Strategies to Control Interfacial Dynamics of Enzymes Adsorbing on Hydrophilic Surfaces.....	191
7.2.2.1	Adsorption Studies and Surface Chemistry Modification	191

7.2.2.2	Real-time Monitoring of Translational and Rotational Dynamics	196
7.2.2.3	Conformational Dynamics and Unfolding Events at Short-time Scales.....	200
7.2.3	Method Development.....	203
7.2.4	Additional Aspects of Enzyme Conformational Stability	204
7.2.5	Additional Applications	205
7.3	References.....	206

List of Figures

Figure 2.1. Solvent engineering strategies for enzymes in organic solvents ^{4, 46}	12
Figure 2.2. Active tumor targeting involves the use of proteins conjugated with nanostructured carriers. These proteins are able to specifically interact with cell receptors. Therapeutic compounds are delivered into the cell once the carrier is taken up by endocytosis. The efficacy of therapy mainly relies upon the ability to maintain an abundant population of structurally stable proteins on the surface of the nanocarrier ⁹⁸	17
Figure 2.3. Major factors controlling the adsorption of proteins on solid supports. Electrostatic interactions, hydrophobicity of the surface and conformational dynamics are all interdependent. The + sign represents a favorable pathway for adsorption while the – sign, unfavorable conditions for adsorption ¹⁰⁹	21
Figure 2.4. Individual fumed silica nanoparticle and the functional groups at its surface. This nanoparticle exhibits a diameter of approximately 10 nm	22
Figure 2.5. Guanidine hydrochloride (GuHCl) induced denaturation for the B-domain of protein A. Denaturation was tracked with circular dichroism at 222 nm ¹²⁵	25
Figure 2.6. Schematic of a typical spectrofluorimeter. Before impacting the sample, light from the source is filtered with an excitation monochromator. After impacting the sample the emitted light is collected through an emission monochromator and recorded with a photomultiplier sensitive between 200-1000 nm. The light at the source is usually generated with high-intensity xenon arc lamp or a laser in which case the monochromator is not required ¹²⁷	27
Figure 2.7. Schematic of a peptide bond and its corresponding transition dipoles (thick arrows) ¹²⁸	28
Figure 2.8. Basis for the CD effect: (I) resulting radiation when neither the L nor the R components are absorbed or they are equally absorbed, (II) preferential absorption of either the L or R components results in an elliptically polarized radiation ¹³⁰	28
Figure 2.9. Depending on the type of secondary structure, the CD spectrum shows a number of distinctive features. Solid line, α -helix; long dashed line, anti-parallel β -sheet; dotted line, type I β -turn; cross dashed line, extended α -helix or poly (Pro) II helix; short dashed line, irregular structure ¹³⁰	29

Figure 2.10. Schematic of a typical CD instrument. A very intense light source is required to extend into the far-UV. The circularly polarized light is generated by superposition of photons with different handedness. A piezoelectric crystal can be used to select either right or left circularly polarized light¹²⁷. 33

Figure 2.11. Mid-infrared spectrum of membrane protein Calcium ATPase. Vibrations that contribute the most to the observed absorption bands are: 3285 cm⁻¹- protein amide A; 2957 cm⁻¹- $\nu(\text{CH}_3)$; 2924 cm⁻¹- $\nu(\text{CH}_2)$; 2854 cm⁻¹- $\nu(\text{CH}_2)$; 1738 cm⁻¹- $\nu(\text{lipid C=O})$; 1653 cm⁻¹- protein amide I; 1542 cm⁻¹- protein amide II; 1455 cm⁻¹- $\delta(\text{CH}_3)$; 1389 cm⁻¹- $\nu(\text{COO}^-)$ of Asp and Glu; 1236 cm⁻¹- $\nu(\text{Lipid PO}_2^-)$; 1171 cm⁻¹- $\nu(\text{lipid C-O-O-C})$; 969 cm⁻¹- $\nu(\text{CN})$ of lipid; 820 cm⁻¹- $\nu(\text{lipid P-O})$ ¹³⁴. 34

Figure 2.12. Comparison of the most commonly used band-narrowing techniques of protein amide I. (a) IR absorbance spectrum of papain recorded at 2 cm⁻¹ resolution. (b) Second derivative of papain spectrum multiplied by -1. The emerging peaks can be assigned to different secondary structural components according to Table 2.6. (c) (—) Fine structure enhancement with a smoothing range of 12 cm⁻¹ and a weighting factor of 0.985; (---) Fourier self deconvolution using a Lorentzian line shape with a resolution enhancement factor of 2.6. All three methods generated very similar component bands¹³³. 36

Figure 2.13. Gaussian curve-fitting of bovine pancreatic trypsin amide I spectrum. Gaussian bands for the individual structural components are shown in colors. The original spectrum was band-narrowed with Fourier self deconvolution. The fractions of the secondary structural components were 26% α -helix and 41% β -sheet, which are in agreement with 26% α -helix and 45% β -sheet obtained with X-ray analysis¹³⁵. 37

Figure 2.14. Basic instrumental arrangement of a Fourier Transform Infrared spectrometer¹³⁴. .. 38

Figure 3.1. Transmission Electron Microscopy (TEM) image and schematic representation of a typical lyophilized fumed silica/enzyme preparation. 58

Figure 3.2. Adsorption kinetics of CALB on fumed silica in aqueous suspensions at pH7.8 (phosphate buffer, 0.1M; 25 °C). Surface coverage: (\diamond) 17%SC, (\square) 12%SC, (Δ) 4%SC, (\circ) 2%SC (y-error bars represent the standard error of multiple analyses of identical samples). 59

Figure 3.3. Surface loading of fumed silica with enzyme at different pH values as a function of the nominal surface coverage. (Δ) pH = 4.0, (\diamond) pH = 7.8, (\circ) pH = 9.5. Data obtained from

the final steady-state of the adsorption kinetics experiments. The solid line is calculated by dividing the mass of enzyme weighed in by the nominal surface area of the fumed silica that was used. The impact of pH relative to the isoelectric point is only important when surface area availability start to be reduced (Above 12%SC). 60

Figure 3.4. Schematic of surface charges for CALB and fumed silica nanoparticles in aqueous suspensions relative to the isoelectric point (pI). (Water molecules are not shown). Arrow widths illustrate the anticipated strength of the electrostatic interactions. 61

Figure 3.5. Confocal images of the distribution of CALB immobilized on fumed silica (FS). (A) 2%SC and (B) 4%SC. The corresponding surface fluorescence intensities are shown in panels A1 and B1. The doubling of the intensity corresponds roughly to a doubling of the enzyme loading per area of fumed silica (Figure 3.3, 4%SC and 2%SC, diamond symbols). The originally green fluorescence areas in panel B are emphasized by dashed contours. ... 62

Figure 3.6. Catalytic activity of CALB immobilized on fumed silica as a function of the nominal surface coverage in the final preparation. Geraniol: 0.1 M. (○) Experiments over the entire domain of %SC. Experiments to confirm the surprising decrease in reaction rate at high fumed silica content: (∇) first replica of 17%SC and 12%SC fumed silica, (□) second replica of 12%SC, 4%SC and 2%SC, (×) test to rule out mass transfer limitations, reaction volume 15 mL, 12%SC and 4%SC. Solid line represents Novozym 435®; dashed lines and y-error bars represent the cumulative standard error from the calculation of conversion and the linear assumption of the initial reaction rate. 63

Figure 3.7. Schematic model for enzyme/fumed silica interactions at different surface loadings. The enzyme arrangement changes from a crowded surface to approximately single molecule adsorption as the surface availability increases. The opportunity for maximum interaction of the enzyme with fumed silica is perhaps enhanced by surface topography (availability of “neck” positions) may lead to detrimental deformation of the enzyme molecule. (Based on concepts put forth by Gross et al.^{39, 40}. The schematic is roughly to scale, primary fumed silica nanoparticle diameter ~10 nm; CALB molecular diameter ~6 nm⁵¹). 65

Figure 3.8. Effect of temperature on the catalytic activity of CALB immobilized on fumed silica at various %SC. (◇) 17%SC, (□) 12%SC, (Δ) 4%SC, (○) 2%SC. Effect of temperature on the catalytic activity of Novozym 435 (*). y-error bars represent the cumulative standard

error from the calculation of conversion and the linear assumption of the initial reaction rate.....	67
Figure 3.9. Storage stability of CALB immobilized on fumed silica (FS) in n-hexane. (\diamond) 17%SC, (\square) 12%SC, (Δ) 4%SC, (\circ) 2%SC. (*) Novozym 435 shown for comparison. y-error bars represent the cumulative standard error from the calculation of conversion and the linear assumption of the initial reaction rate.....	68
Figure 3.10. Long-term stability of CALB immobilized on fumed silica as a function of the fumed silica content: (\square) fresh preparation, (\diamond) 6 months-aged preparation (4°C, closed glass vials). y-error bars represent the cumulative standard error from the calculation of conversion and the linear assumption of the initial reaction rate.....	69
Figure 4.1. Time evolution of the fractional conversion of R-1-phenylethanol during the transesterification with vinyl acetate for CALB/FS preparations with different nominal surface coverages %SC (30°C, 48 ml reaction volume, 35U of enzyme per preparation): 4 %SC (\bullet), 12 %SC (\square), 17 %SC (\blacksquare), 100 %SC (\triangle), 230 %SC (\diamond), 400 %SC (\blacklozenge).Novozym 435® during the initial 1.33 hours of reaction (X). Reverse reaction carried out with 230 %SC preparations (-); Solid lines added to guide the eye; y-error bars show the cumulative standard errors and are obtained from the kinetic parameter calculations.	84
Figure 4.2. Catalytic activity of CALB/FS preparations as a function of the nominal surface coverage %SC. (\diamond) Enantioselective transesterification of (RS) 1-phenylethanol in n-hexane. (\blacksquare) Esterification of geraniol with acetic acid in n-hexane. (---) Reaction rate for Novozyme435® in the enantioselective transesterification of (RS) 1 phenylethanol; (---) represents Novozyme435® in geraniol system. y-error-bars and short dashed lines represent the cumulative standard error from the calculation of the initial reaction rates. (30°C, 6 mL reaction volume, 35U of enzyme per preparation).	85
Figure 4.3. Schematic of the three regimes controlling the catalytic activity per enzyme molecule of FS/CALB preparations in hexane: 1. at low surfaces coverages, interactions with the surface are maximized leading to detrimental conformational changes. 2. at intermediate surface coverages, a transitional regime where enzyme structure is more generally maintained. 3. at high surface coverages multi-layer coverage leads to mass-transfer resistance and low apparent catalytic activity per enzyme molecule.....	86

Figure 4.4. Temperature stability of CALB/FS preparations with various surface coverages (%SC): 2 %SC (○), 12 %SC (□), 100 %SC (Δ), 230 %SC (◇). Temperature Novozym 435® preparations (X). (▲) *R. miehei* lipase immobilized in agar organogels based on lecithin, isooctane as solvent, shown for comparison (Zoumpantioti et al. 2008) Solid lines added to guide the eye; y-error bars show the cumulative standard errors from the kinetic parameter calculation. (Various temperature, 6 mL reaction volume, 35U of enzyme per preparation) 88

Figure 4.5. Solvent stability of CALB/FS preparations with various surface coverages %SC. After 4 days exposure to the solvent, the catalytic activity remains almost unaffected: 400 %SC (◆), 230 %SC (◇), 100 %SC (Δ), 2 %SC (○). Storage stability of Novozym 435® in n-hexane (X). y-error bars represent the cumulative standard error and are obtained from the initial reaction rate calculation. (30°C, 6 mL reaction volume, 35U of enzyme per preparation). 90

Figure 4.6. Long-term stability of CALB/FS preparations with various surface coverages %SC: (◇) fresh preparations, (□) one year-aged preparations (storage at 4°C, closed glass vials). Cumulative standard errors are obtained from the kinetic parameter calculation and are shown as y-error bars. (30°C, 6 mL reaction volume, 35U of enzyme per preparation). 91

Figure 5.1. Tryptophan fluorescence spectrum of the unfolding of CALB induced by GdmCl in aqueous buffer solution. (○) Native, (□) 1M GdmCl, (Δ) 2M GdmCl, (×) 4M GdmCl and (*) 8M GdmCl. Enzyme concentration of 0.5 mg/mL and pH 7.8. 101

Figure 5.2. Decrease in the maximum emission intensity of Tryptophan residues due to GdmCl induced unfolding. Enzyme concentration was maintained at 0.5 mg/mL and pH 7.8 in all cases. CALB unfolds to a larger extent when compared with *s. Carlsberg* and TLL which have tightly packed structures. y-error bars represent the standard error of multiple analyses of identical samples. 102

Figure 5.3. Normalized fluorescence intensity for the GdmCl induced unfolding of CALB in aqueous buffer. The tryptophan emission was monitored at 330 nm. Measurements were carried out at enzyme concentration of 0.5 mg/mL and pH 7.8. Similar calibration curves were obtained for *s. Carlsberg* and TLL (data not shown). 103

Figure 5.4. Unfolding data for CALB on fumed silica (z-axis) as a function of initial enzyme concentration (y-axis) and nominal surface coverage (x-axis). These data will be shown in

3D contour plots to identify regions of conformational stability and to subsequently correlate them with the surface loading regimes previously postulated for the lyophilized adsorbates..... 107

Figure 5.5. Unfolding kinetics of (●) CALB, (□) *s. Carlsberg* and (Δ) TLL adsorbing on fumed silica nanoparticles to form adsorbates with a nominal surface coverage of 2%SC. Data is normalized with the corresponding calibration curves and subsequently expressed as unfolded fraction. Enzyme concentration was maintained at 0.5 mg/mL and pH at 7.8.... 108

Figure 5.6. Unfolding kinetics of (●) CALB, (□) *s. Carlsberg* and (Δ) TLL adsorbing of fumed silica nanoparticles to form adsorbates with a nominal surface coverage of 100%SC. Data is normalized with the corresponding calibration curves and subsequently expressed as unfolded fraction using Equation 5.3. Enzyme concentration was maintained at 0.5 mg/mL and pH at 7.8. 109

Figure 5.7. Unfolding kinetics of (●) CALB, (□) *s. Carlsberg* and (Δ) TLL adsorbed of fumed silica nanoparticles to obtain a nominal surface coverage of 400%SC. Data is normalized with the corresponding calibration curves and subsequently expressed as unfolded fraction using Equation 5.3. Enzyme concentration was maintained at 0.5 mg/mL and pH at 7.8. 110

Figure 5.8. Regions of conformational stability for CALB/Fumed Silica adsorbates. The dotted vertical line at ~200%SC separates two different regions of conformational stability: Region I delimited by a long-dash-dot line where adsorbates exhibit low conformational stability, and Region III delimited by a short-dash-dot line where adsorbates have highly stable conformations. The presence of these two regions is likely to be responsible for the observed catalytic activity (r_0) of the lyophilized adsorbates in hexane (inset). The low catalytic activity observed at low %SC can be linked to Region I. Even though the structure is well preserved in Region III, multi-layer packing is likely responsible for diffusional limitations of catalysis. The maximum in activity between those two regions can be attributed to an optimal arrangement on the surface where the structure is relatively well maintained without excessive clustering (Region II, delimited by a dotted line)..... 112

Figure 5.9. Regions of conformational stability for *s. Carlsberg*/Fumed Silica adsorbates. The dotted vertical line at ~200%SC separates two different regions of conformational stability: Region I and III of low and high conformational stability, respectively. In this case, the catalytic activity (r_0) of the lyophilized adsorbates in hexane (inset) is constantly increasing.

As opposed to CALB, only partially unfolded enzyme molecules are present in the lower part of Region I at low initial enzyme concentrations. This resilience to denaturation could explain the higher activities observed for lyophilized adsorbates of *s. Carlsberg* at low surface coverages. The same type of lines as those in Figure 5.8 were used to delimit the regions of conformational stability. 114

Figure 5.10. Regions of conformational stability for TLL/Fumed Silica adsorbates. The dotted vertical line at ~250%SC separates two different regimes of conformational stability: Region I and III of low and high conformational stability, respectively. Across the whole Region I only partially unfolded conformations ($\phi_{FS} \sim 0.6$) were identified, which confirms the resilience of highly stable enzymes to denature at low surface coverages. The same type of lines as those in Figure 5.8 were used to delimit the regions of conformational stability. 115

Figure 5.11. Unfolding kinetics of hydrolases adsorbing on fumed silica nanoparticles in the presence of tertiary structure modifiers: (A) 30% (v/v) TFE and (B) 0.5 mg/mL DTT: (O) CALB, (■) *s. Carlsberg* and (▲) TLL. Data for unfolding in the absence of modifiers is superimposed for comparison: (●) CALB, (□) *s. Carlsberg* and (Δ) TLL. Components were mixed to form a nominal surface coverage of 100%SC. Data is normalized with the corresponding calibration curves and subsequently expressed as unfolded fraction. Enzyme concentration was maintained at 0.7 mg/mL and pH at 7.8..... 117

Figure 5.12. Impact of tertiary structure modifiers on conformational regions of CALB/FS adsorbates. This was tested by forming buffered suspensions with (A) 30%(v/v) TFE and (B) 0.5 mg/mL DTT. The previously identified Region III exhibits a higher unfolding in the presence of TFE. The extent of unfolding in Region I decreased in the presence of TFE. The addition of DTT resulted in a substantially large Region III for low %SC and low concentrations. The same type of lines as those in Figure 5.8 were used to delimit the regions of conformational stability. 119

Figure 5.13. Impact of tertiary structure modifiers on conformational regions of *s. Carlsberg*/FS adsorbates. This was tested by forming buffered suspensions with (A) 30%(v/v) TFE and (B) 0.5 mg/mL DTT. As in the case of CALB, TFE promoted a higher unfolding in the previously identified Region III. The maximum extent of unfolding in Region I decreased too. The addition of DTT showed no significant impact on the tertiary structure of *s.*

<i>Carlsberg</i> . The same type of lines as those in Figure 5.8 were used to delimit the regions of conformational stability.	120
Figure 6.1. CD spectra for native enzymes in aqueous buffer at an enzyme concentration of 0.7 mg/mL. CALB (●), <i>s. Carlsberg</i> (○), TLL (▼). The signal at 222 nm can be used as baseline to estimate the α -helical content in the presence of denaturants. Similar plots were obtained for enzyme solutions with other concentrations.....	134
Figure 6.2. Chemically-induced unfolding of enzymes. Equation 6.1 was employed to compute the unfolded fraction based on signal loss at 222 nm. The unfolding pathways in the presence of denaturants are similar to those reported previously based on intrinsic fluorescence spectroscopy. The relatively modest unfolding for <i>s. Carlsberg</i> and TLL after an initial unfolding can be attributed to their high conformational stabilities.....	135
Figure 6.3. Unfolding data for CALB on fumed silica (z -axis) as a function of initial enzyme concentration (y -axis) and nominal surface coverage (x -axis). These data will be shown in 3D contour plots to identify regions of conformational stability and to subsequently correlate them with surface loading regimes previously postulated for the lyophilized adsorbates. This approach was introduced in the previous chapter using tertiary unfolding data.....	138
Figure 6.4. CD spectra for CALB adsorbing on fumed silica nanoparticles at different %SC and at initial enzyme concentrations of: (A) 0.7 mg/mL and (B) 3.3 mg/mL. (Δ) Native, (●) 2%SC, (○) 100%SC, (▼) 400%SC. The signal loss at 222 nm is higher at low %SC for both low and high enzyme concentrations. This was attributed to reduced α -helical content. These results support the notion that increased surface interactions may lead to substantial conformational changes.	142
Figure 6.5. CD spectra for <i>s. Carlsberg</i> adsorbing on fumed silica nanoparticles at different %SC and at initial enzyme concentrations of: (A) 0.7 mg/mL and (B) 3.3 mg/mL. (Δ) Native, (●) 2%SC, (○) 100%SC, (▼) 400%SC. As for CALB, the signal loss at 222 nm is higher at low %SC for the two concentrations under consideration. This was attributed to a reduction in the α -helical content due to conformational changes upon contact with the surface.	143
Figure 6.6. CD spectra for TLL adsorbing on fumed silica nanoparticles at different %SC and at initial enzyme concentrations of: (A) 0.7 mg/mL and (B) 3.30 mg/mL. (Δ) Native, (●) 2%SC, (○) 100%SC, (▼) 400%SC. At low enzyme concentration, there is an observable	

loss of signal at 222 nm for 2%SC and 100%SC. When the enzyme concentration is increased, there is no significant loss of signal for 100%SC and 400%SC. This is most likely due to TLL's conformationally stable structure..... 145

Figure 6.7. Regions of secondary conformational stability for CALB/Fumed Silica adsorbates.

The dotted vertical line at ~250%SC separates two different regions of conformational stability: Region I delimited by a long-dash-dot line where adsorbates exhibit low conformational stability, and Region III delimited by a short-dash-dot line where highly stable enzyme ensembles are adsorbed on the surface. The presence of these two regions is likely to be responsible for the observed catalytic activity (r_0) of the lyophilized adsorbates in hexane (inset). The poor catalytic competency observed at low %SC can be linked to Region I while low activities at high %SC are linked to Region III where catalysis is severely reduced by mass transfer limitations. The maximum in activity between those two regions can be attributed to an optimal arrangement on the surface where the structure is relatively well maintained without excessive clustering (Region II, delimited by a dotted line). A very similar conformational diagram was previously found from intrinsic fluorescence spectroscopy experiments..... 146

Figure 6.8. Regions of secondary conformational stability for *s. Carlsberg*/Fumed Silica adsorbates.

The dotted vertical line at ~250%SC separates two different regions of conformational stability. Region I and III of low and high conformational stability, respectively. In this case, the catalytic activity (r_0) of the lyophilized adsorbates in hexane (inset) is constantly increasing. It appears that the extent of unfolding while operating in the lower part of Region I is less than that observed for CALB in the same region. This resilience to denaturation could be seen as a plausible explanation for the higher activities in this regime of surface loading compared with CALB. 148

Figure 6.9. Secondary unfolding of (A) CALB and (B) *s. Carlsberg* adsorbing on fumed silica nanoparticles in the presence of 30% (v/v) TFE and 0.5 mg/mL DTT.

Unfolding data for the untreated enzymes were added for comparison. The unfolded fraction (ϕ_{FS}) was calculated according to Equation 6.2. 150

Figure 6.10. FTIR spectra in the amide I and II regions of native lyophilized CALB (\square) and

lyophilized CALB/Fumed silica adsorbates: (\square) 2%SC, (*) 100%SC, (\circ) 150%SC, (Δ)

230%SC, (▪▪) 300%SC, and (◇) 1250%SC. A clear progression in the surface loading is evidenced by the higher signal intensities as the surface coverage increases.....	152
Figure 6.11. Second derivative of the amide I-FTIR spectra of CALB/Fumed silica lyophilized adsorbates. (A) 1250%SC and (B) 2%SC. The secondary structural components associated with the resolution-enhanced peaks obtained with this approach are subsequently identified according to Table 6.3.....	153
Figure 6.12. (A) FTIR spectra in the amide I and II regions of lyophilized CALB/Fumed silica adsorbates with 2%SC. Lyophilized nanobiocatalysts were prepared from enzyme solutions with different initial concentrations: (—) 0.15 mg/mL, (--) 0.25 mg/mL, (··) 0.5 mg/mL. Second derivative of the amide I-FTIR spectrum of nanobiocatalysts obtained from enzyme solutions with concentrations of (B) 0.15 mg/mL and (C) 0.5 mg/mL. The secondary structural components associated with the resolution-enhanced peaks obtained with this approach are subsequently identified according to Table 6.3.....	155
Figure 6.13. (A) FTIR spectra in the amide I and II regions of lyophilized CALB/Fumed silica adsorbates with 17%SC. Lyophilized nanobiocatalysts were prepared from enzyme solutions with different initial concentrations: (–) 0.3 mg/mL, (--) 0.5 mg/mL, (–··) 2.9 mg/mL, (··) 4.7 mg/mL. Second derivative of the amide I-FTIR spectrum of nanobiocatalysts obtained from enzyme solutions with concentrations of (B) 0.3 mg/mL and (C) 4.7 mg/mL. The secondary structural components associated with the resolution-enhanced peaks obtained with this approach are subsequently identified according to Table 6.3.....	157
Figure 7.1. Adding small molecules prior to adsorption could help to increase the stabilizing protein-protein interactions for “soft” enzymes at low surface coverages.	176
Figure 7.2. Stability constants for CALB residues as calculated from the statistical thermodynamic analysis of conformational ensembles implemented in the COREX algorithm. Residues 295 to 317 exhibit low stability and are good candidates for protein engineering.....	178
Figure 7.3. Single-molecule schematic of the different regions of stability in CALB’s structure. Residues in red exhibit the highest stability while those in yellow the lowest. In agreement with our experimental findings, CALB has regions of low stability that provide mobility and dynamism.....	183

Figure 7.4. Single-molecule schematic of the different regions of stability in <i>s. Carlsberg</i> 's structure. Residues in red exhibit the highest stability while those in yellow the lowest. In agreement with our experimental findings, <i>s. Carlsberg</i> as opposed to CALB exhibit a relatively stable structure.	183
Figure 7.5. Stability constants for <i>s. Carlsberg</i> residues as calculated from the statistical thermodynamic analysis of conformational ensembles implemented in the COREX algorithm.	184
Figure 7.6. Single-molecule schematic of the different regions of stability in TLL's structure. Residues in red exhibit the highest stability while those in yellow the lowest. In agreement with our experimental findings, TLL shows resilience to conformational fluctuations.	185
Figure 7.7. Stability constants for TLL residues as calculated from the statistical thermodynamic analysis of conformational ensembles with the COREX algorithm.	185
Figure 7.8. Location of CALB's cavities (blue, red, and blue regions) as calculated from Swiss PBD viewer. Internal cavities account for approximately 0.2% of the total volume.	187
Figure 7.9. Location of <i>s. Carlsberg</i> 's cavities (blue and green regions) as calculated from Swiss PBD viewer. Internal cavities account for approximately 0.1% of the total volume.	187
Figure 7.10. Location of TLL's cavities (blue, green, and red regions) as calculated from Swiss PBD viewer. Internal cavities account for approximately 0.8% of the total volume.	188
Figure 7.11. Adsorption isotherm for CALB on fumed silica at a surface coverage of 17%. C_{eq} is the equilibrium concentration of enzyme.	192
Figure 7.12. Adsorption isotherm for TLL on fumed silica at a surface coverage of 2%. C_{eq} is the equilibrium concentration of enzyme.	192
Figure 7.13. Silanization of fumed silica with aminopropyltriethoxysilane (APTES) ¹⁸ . The functionalized fumed silica can be subsequently coupled with one of the spacers in Table 7.7. This could help to control the number of reactive groups on the surface and ultimately the surface coverage, orientation, and conformation of the adsorbed enzymes.	193
Figure 7.14. Dendrimer-functionalization of fumed silica with poly-(propylene imine) dendrimers ¹⁸ . This approach is aimed at promoting an oriented assembly of enzymes on fumed silica. Orientational changes are thought to be present during the random adsorption events that normally occur on virgin fumed silica.	194

Figure 7.15. Confocal image of CALB adsorbed on a silica wafer with a SiO₂ layer of 100 nm. The nominal surface coverage was 150%..... 196

Figure 7.16. 3D intensity profile of image shown in Figure 7.15. Substantial enzyme aggregation was observed. This could support the idea that the structure is well maintained in this surface coverage regime due to the multi-layer packing. 196

Figure 7.17. Confocal image of CALB adsorbed on a silica wafer with a SiO₂ layer of 100 nm. The nominal surface coverage was 50%..... 197

Figure 7.18. 3D intensity profile of image shown in Figure 7.17. The enzyme molecules distributed more homogenously on the wafer. This could support the notion of increased surface-protein interactions that most likely lead to conformational changes..... 198

Figure 7.19. The dynamics of surface-protein interaction can be studied at the single-molecule level with the aid of state-of-the-art fluorescence imaging techniques. The complexity of this interaction is mainly due to the multidimensional landscape generated by the heterogeneity of the enzyme molecules. The ultimately goal of these studies is to engineer strategies to control the motion of the enzyme molecules as they assemble on the surface. A FRET strategy that involves energy transfer between donor and acceptor can be attempted to map small changes in the intermolecular distances between neighboring enzyme molecules and respect to the surface functional groups..... 199

Figure 7.20. Schematic representation of a theoretically predicted folding funnel for proteins in solution⁵³. This has been mainly predicted with the aid of computational tools. A similar landscape where enzyme ensembles contain a number of non-native intermediate species are likely to be generated upon interaction with solid surfaces. The inherent structural heterogeneity of these ensembles poses significant challenges for a complete experimental biophysical characterization⁵³. The arrival of ultra-high resolution methods will help to refine the structural ensembles produced..... 201

Figure 7.21. Overview of the major dynamical processes in proteins and their timescales. Some of the experimental and computational techniques that can be potentially used to access this information are added for reference⁵⁸. 203

List of Tables

Table 2.1. Advantages of incorporating enzymes in organic as opposed to aqueous media ²⁷	9
Table 2.2. Oxidation of <i>p</i> -anisidine catalyzed by Horseradish Peroxidase in different organic solvents ³²	10
Table 2.3. Representative examples of currently available excipients for activation of enzymes in organic media ²⁷	11
Table 2.4. Catalytic efficiency (k_{cat}/K_m) _{app} of free and immobilized α -chymotrypsin in different organic solvents for the transesterification of <i>N</i> -acetyl-L-phenylalanine ethyl ester. Upon immobilization the efficiency increased by 1 to 2 orders of magnitude respect to the free suspended native enzyme ⁷⁰	14
Table 2.5. Examples of Nanobiosensors based on Enzymatic Reactions ¹⁰³	18
Table 2.6. Assignment of amide I secondary structural components ¹³³	35
Table 3.1. Summary of the amount of fumed silica and buffer employed to prepare CALB supported nanobiocatalysts with different nominal surface coverages (%SC). In all cases, the amount of crude CALB was 5.83 mg.....	55
Table 3.2. Apparent kinetic constants and catalytic efficiency of CALB co-lyophilized with fumed silica (FS) compared to Novozym 435®	66
Table 4.1. Summary of the amount of fumed silica and aqueous buffer for the various enzyme preparations. In all cases, the amount of crude CALB was 5.83 mg.....	81
Table 4.2. Long-term stability (reaction conditions: 30°C, 6 mL reaction volume, 35U of enzyme per preparation) of various CALB/fumed silica preparations (storage at 4°C, closed glass vials).....	90
Table 5.1. Summary of the amounts of fumed silica and enzyme employed to form the suspensions with different nominal surface coverages. The enzyme concentration for each suspension was varied from 0.5 mg/mL to 4.70 mg/mL.	105
Table 6.1. Summary of the amounts of fumed silica and enzyme employed to form the suspensions with different nominal surface coverages. The enzyme concentration for each suspension was varied from 0.5 mg/mL to 4.70 mg/mL.	137
Table 6.2. Band assignments for proteins in the infrared amide I region of the spectrum ¹¹⁸	140
Table 6.3. Band assignments for CALB in the infrared amide I region of the spectrum ¹¹⁸	140

Table 7.1. List of the 15 most probable conformational states for CALB. The sequences indicate regions that have the tendency to either unfold or remain native-like.....	180
Table 7.2. List of residues with the lowest conformational stability constants for CALB ensembles.....	182
Table 7.3. Surface exposed and volume of internal cavities for CALB. The calculation was performed with Swiss PDB viewer.....	186
Table 7.4. Surface exposed and volume of internal cavities for <i>s. Carlsberg</i> . The calculation was performed with Swiss PDB viewer.....	186
Table 7.5. Surface exposed and volume of internal cavities for TLL. The calculation was performed with Swiss PDB viewer.....	186
Table 7.6. Packing density per residue for native CALB. Data calculated with Voronoia ¹⁴	189
Table 7.7. Commercially available spacer molecules ¹⁸ . Potentially any desired functional group can be incorporated for further interaction with the enzyme molecules.....	195

Acknowledgements

I would like to thank my advisors Dr. Peter Pfromm and Dr. Mary Rezac for their enormous support and excellent guidance during my doctoral studies at Kansas State. I feel really blessed to have had their continued dedication, passion, talent, and commitment as a model to pursue my lifetime dream of an academic career. My deepest and most sincere appreciation goes out to them. I would also like to acknowledge my advisory committee, Dr. John Tomich, Dr. Dan Boyle, and Dr. Vikas Berry for their valuable advice and thoughtful suggestions during the course of this project. I specially thank Dr. John Tomich for opening his lab to me and considering me part of his group. I will never forget Dr. Tomich's passion, creativity, and openness for discussion and new ideas. Thanks to Dr. Boyle for sharing with me all his knowledge and skills in microscopy. I am grateful to Dr. Berry for allowing us to use his lab facilities whenever we needed. I also want to thank Dr. Susan Sun for serving as Outside Chair representative from the Graduate School.

I wish to thank Dr. Robert Szoszkiewicz for spending precious time with me in front of the AFM. I would also like to thank Dr. David Moore and Heather Shinogle in the Microscopy and Analytical Imaging Lab at the University of Kansas. Their skills and resourcefulness while imaging in both the SEM and confocal microscopes are greatly appreciated. I also wish to acknowledge Dr. Bruce Law and Dr. Haeng Sub Wi for very profound discussions about ellipsometry and its applications in surface science.

I would like to thank all current and past members of the research group, especially Dr. Devinder Singh, Jacob Stern, Martin Kramer, Mohammed Hussain, Ronny Michalsky, Alex Brix, and Fan Zhang for sharing with me the wonderful experience of Grad School. It was very rewarding being part of such an amazing and supportive research group.

I am grateful to Dr. Tomich's lab members: Sushanth Gudlur, Nozomi Matsumiya, Yasuaki Hiromasa, Urska Bukovnik, Pinakin Sukthankar, and Xiao Yiao for their support and enjoyable time in the lab.

I would like to acknowledge all Faculty members and Staff in the Chemical Engineering Department. I specially thank Dave Threewit, Florence Sperman, and Lauren Muse for their continued support. Special thanks are to Dr. Larry Glasgow for the most amazing Transport Phenomena lectures I have ever attended. Dr. Glasgow's educational and didactic initiatives

were inspirational for my career. I also want to thank Drs. L.T. Fan and Andres Argoti for stimulating discussions about research and life.

Dedication

I would like to dedicate this dissertation to my lovely wife Sandra for supporting me during all these years. Without her support, this dissertation would have not been a reality.

CHAPTER - 1 Introduction

1.1 Research Motivation

Over the past two decades much effort has been invested towards the development of efficient enzyme based biocatalysts for synthetic applications in organic solvents¹⁻⁹. Enzymes are well suited for these applications due to their high specificity and selectivity⁹⁻¹². For instance, complicated multi-step synthesis schemes involving chemical catalysts can be effectively replaced with one-pot processes catalyzed by enzymes¹³⁻¹⁹. As a result, numerous research groups at both fundamental and applied levels have started programs to deepen understanding of some of the major issues raised by the use of enzymes in organic synthesis^{1, 5, 20-32}. These efforts have resulted in a plethora of methodologies, hypotheses, and general mechanistic descriptions that decipher and further exploit the aforementioned catalytic abilities of enzymes when operating in organic mixtures^{1, 5, 20-32}. In this regard, a major limitation for enzymes to be attractive candidates as catalytic agents is their tendency to deactivate in the presence of organic solvents, which are the preferred media in organic synthesis^{9, 27, 28}. Hitherto, however, this phenomenon remains poorly understood and despite the extensive experimental work to address it, no definitive chemical explanations have been elucidated. One important strategy to overcome this limitation is the immobilization of enzymes on solid porous and non-porous supports³³⁻³⁷. This approach has been quite successful, and indeed most of the commercially available enzyme preparations make use of it. For instance, the widely known enzyme *Candida antarctica* Lipase B (CALB) is commercially available through Novozymes Inc., as a supported biocatalyst. In this case, the enzyme is immobilized by adsorption on macroporous polymeric resins^{38, 39}. This preparation has been applied for the laboratory scale synthesis of a broad range of compounds of commercial interest including polymers and pharmaceuticals³⁸⁻⁴⁴. The large scale application, however, is still quite limited mainly because of the high price of the preparations^{38, 39, 41}. Additionally, unequal enzyme distributions and diffusional limitations due to the porous nature of the supports are somewhat worrisome^{38, 39, 41}. In general, the production of enzyme immobilizates with the desirable properties has been hampered by a lack of information on the complex protein-protein and surface-protein interactions taking place when enzymes are adsorbed on solid supports.

The advent of nanotechnology has brought to light a new set of nanostructured materials that can be examined as potential supports for addressing this major bottleneck. Due to the comparable size scale to that of enzymes, these materials also offer an opportunity for a molecular level understanding of the involved immobilization events. This is the case of the immobilization of enzymes on fumed silica nanoparticles. By immobilizing *subtilisin Carlsberg* and CALB on fumed silica, the apparent catalytic activity in hexane increased by nearly three orders of magnitude with respect to the lyophilized native enzyme suspended in the same solvent^{31, 45}. Nevertheless, much work remains to be done in order to decipher the relationships between activity/selectivity and conformation. Thus, next steps should be intended to develop strategies for the identification and assessment of the major parameters modulating the orientational and conformational arrangements responsible for the observed catalytic performance in organic media. The resulting correlations represent an unprecedented opportunity for a systematic nanoscale level tailoring of fumed silica supported enzyme biocatalysts. Hitherto, however, most developments in the field have resulted from purely empirical approaches, which have narrowed the applicability of the obtained enzyme preparations to processes for the production of costly specialty chemicals.

1.2 Research Objective

This PhD research project developed strategies for visualizing and quantifying the induced conformational changes that occur when enzymes are physically adsorbed on fumed silica nanoparticles. The new information can then be used to prepare highly active nanobiocatalysts in organic solvents. This will be accomplished by employing state-of-the-art spectroscopic techniques. These tools provide data at the molecular level which in turn advance our mechanistic understanding of the specific interactions and driving forces inherently present during the adsorption process. The detailed insight into the structure-catalytic function relationship gained from this project should allow for the tailoring and engineering of highly competitive and sustainable enzymatic technologies. This will ultimately expand the scope of non-aqueous enzymology to a broader range of commercially relevant nonaqueous applications.

1.3 Dissertation Outline

The chapters of this dissertation are reproductions of either already published/submitted papers or manuscripts ready to be submitted for publication. Detailed information of each chapter is shown below:

Chapter 2 describes the main attributes and challenges of incorporating enzymes as catalysts for synthesis in organic media. This is followed by a discussion of the different alternatives used to obtain highly efficient processes in organic media. The chapter also explains how emerging nanomaterials are interesting alternatives to produce biohybrid conjugates with unique functionalities of interest in different fields. Next, the discussion focuses on the myriad of interplaying factors present when nanomaterials are interfaced with proteins. Particular attention is given to interfacing processes based on physical adsorption. The chapter also shows how depending on the adsorption pathway, conformational changes in the protein structure may be important. Finally, the concept of protein conformational stability is introduced as well as some experimental methods to assess it.

Chapter 3 is a published paper⁴⁵ that discusses the development of CALB/fumed silica nanobiocatalysts for the esterification of geraniol with acetic acid. The paper describes the adsorption kinetics of CALB on fumed silica as a function of surface coverage. The enzyme distribution after lyophilization is experimentally assessed by confocal microscopy. The impact of the surface coverage on the catalytic activity is correlated with a possible model of surface loading. Finally, the solvent-, long-term-, and temperature- stabilities of the CALB/fumed silica preparations are discussed.

Chapter 4 is a manuscript submitted for publication to the Journal of Biotechnology. This chapter discusses the application of CALB/fumed silica nanobiocatalysts in the enantioselective transesterification of (R,S)-1-phenylethanol with vinyl acetate. A model of surface loading that involves three regimes of surface coverage is proposed to explain the observed catalytic activity. Finally, the solvent-, long-term-, and temperature- stabilities of the CALB/fumed silica preparations are also discussed.

Chapter 5 is a manuscript accepted for publication in Colloids and Surfaces B: Biointerfaces. This manuscript explores the applicability of intrinsic fluorescence spectroscopy in the detection of tertiary conformational changes of hydrolases adsorbing on fumed silica. The kinetics of unfolding is studied as a function of the surface coverage for hydrolases with low,

intermediate, and high conformational stabilities. The surface loading regimes of the lyophilized nanobiocatalysts are correlated with regions of enzyme conformational stability identified as a function of the surface coverage. The manuscript also explores the use of structural modifiers to elucidate the type of protein-surface interactions leading to the adsorption of the enzyme molecules.

Chapter 6 is a manuscript to be submitted for publication to *Colloids and Surfaces B: Biointerfaces*. This manuscript explores the applicability of CD spectroscopy in the detection of secondary conformational changes of hydrolases adsorbing on fumed silica. Unfolding is studied as a function of the surface coverage for hydrolases with low, intermediate, and high conformational stabilities. The manuscript further supports the correlation of enzyme conformational stability with the surface loading regimes proposed for the lyophilized preparations. Changes in the secondary structure for the lyophilized preparations are estimated from FTIR data.

Chapter 7 summarizes the major findings of the research project and foresees prospective avenues to continue to deeply understand and expand the scope of fumed silica based nanobioconjugates.

1.4 References

1. Carrea, G.; Riva, S., Properties and synthetic applications of enzymes in organic solvents. *Angewandte Chemie-International Edition* **2000**, 39, (13), 2226-2254.
2. Dordick, J. S., Enzymatic Catalysis in Monophasic Organic Solvents. *Enzyme and Microbial Technology* **1989**, 11, (4), 194-211.
3. Dordick, J. S., Nonaqueous Enzymology. *Current Opinion in Biotechnology* **1991**, 2, (3), 401-407.
4. Dordick, J. S., Designing Enzymes for Use in Organic-Solvents. *Biotechnology Progress* **1992**, 8, (4), 259-267.
5. Gupta, M. N., Enzyme Function in Organic-Solvents. *European Journal of Biochemistry* **1992**, 203, (1-2), 25-32.
6. Gupta, M. N.; Roy, I., Enzymes in organic media - Forms, functions and applications. *European Journal of Biochemistry* **2004**, 271, (13), 2575-2583.

7. Khmelnitsky, Y. L.; Rich, J. O., Biocatalysis in nonaqueous solvents. *Current Opinion in Chemical Biology* **1999**, 3, (1), 47-53.
8. Klibanov, A. M., Improving enzymes by using them in organic solvents. *Nature* **2001**, 409, (6817), 241-246.
9. Serdakowski, A. L.; Dordick, J. S., Enzyme activation for organic solvents made easy. *Trends in Biotechnology* **2008**, 26, (1), 48-54.
10. Gotor, V., Biocatalysis applied to the preparation of pharmaceuticals. *Organic Process Research & Development* **2002**, 6, (4), 420-426.
11. Gupta, A.; Khare, S. K., Enzymes from solvent-tolerant microbes: Useful biocatalysts for non-aqueous enzymology. *Critical Reviews in Biotechnology* **2009**, 29, (1), 44-54.
12. Schafer, T.; Borchert, T. W.; Nielsen, V. S.; Skagerlind, P.; Gibson, K.; Wenger, K.; Hatzack, F.; Nilsson, L. D.; Salmons, S.; Pedersen, S.; Heldt-Hansen, H. P.; Poulsen, P. B.; Lund, H.; Oxenboll, K. M.; Wu, G. F.; Pedersen, H. H.; Xu, H., Industrial enzymes. In *White Biotechnology*, Springer-Verlag Berlin: Berlin, 2007; Vol. 105, pp 59-131.
13. Capello, M.; Gonzalez, M.; Rodriguez, S. D.; Iglesias, L. E.; Iribarren, A. M., A mild and quantitative procedure for the removal of nucleoside alkoxy carbonyl groups using pig liver esterase or *Candida antarctica* B lipase. *Journal of Molecular Catalysis B-Enzymatic* **2005**, 36, (1-6), 36-39.
14. Capello, M.; Imanishi, L.; Iglesias, L. E.; Iribarren, A. M., Two new dialkoxy carbonylated nucleosides obtained through a regioselective enzymatic alcoholysis. *Biotechnology Letters* **2007**, 29, (8), 1217-1220.
15. Ferrero, M.; Gotor, V., Biocatalytic selective modifications of conventional nucleosides, carbocyclic nucleosides, and C-nucleosides. *Chemical Reviews* **2000**, 100, (12), 4319-+.
16. Garcia, J.; Fernandez, S.; Ferrero, M.; Sanghvi, Y. S.; Gotor, V., A mild, efficient and regioselective enzymatic procedure for 5'-O-benzoylation of 2'-deoxynucleosides. *Tetrahedron Letters* **2004**, 45, (8), 1709-1712.
17. Gotor, V., Biocatalysis applied to chemoselective transformations on Vitamin D and nucleoside derivatives. *Journal of Molecular Catalysis B-Enzymatic* **2002**, 19, 21-30.
18. Li, N.; Zong, M. H.; Liu, X. M.; Ma, D., Regioselective synthesis of 3'-O-caproyl-floxuridine catalyzed by *Pseudomonas cepacia* lipase. *Journal of Molecular Catalysis B-Enzymatic* **2007**, 47, (1-2), 6-12.

19. Wang, H.; Zong, M. H.; Wu, H.; Lou, W. Y., Novel and highly regioselective route for synthesis of 5-fluorouridine lipophilic ester derivatives by lipozyme TL IM. *Journal of Biotechnology* **2007**, 129, (4), 689-695.
20. Castillo, B.; Bansal, V.; Ganesan, A.; Halling, P.; Secundo, F.; Ferrer, A.; Griebenow, K.; Barletta, G., On the activity loss of hydrolases in organic solvents: II. a mechanistic study of subtilisin Carlsberg. *BMC Biotechnology* **2006**, 6.
21. Castillo, B.; Pacheco, Y.; Al-Azzam, W.; Griebenow, K.; Devi, M.; Ferrer, A.; Barletta, G., On the activity loss of hydrolases in organic solvents - I. Rapid loss of activity of a variety of enzymes and formulations in a range of organic solvents. *Journal of Molecular Catalysis B-Enzymatic* **2005**, 35, (4-6), 147-153.
22. Castro, G. R.; Knubovets, T., Homogeneous biocatalysis in organic solvents and water-organic mixtures. *Critical Reviews in Biotechnology* **2003**, 23, (3), 195-231.
23. Dabulis, K.; Klibanov, A. M., Dramatic Enhancement of Enzymatic Activity in Organic Solvents by Lyoprotectants. *Biotechnology and Bioengineering* **1993**, 41, (5), 566-571.
24. Dong, A. C.; Meyer, J. D.; Kendrick, B. S.; Manning, M. C.; Carpenter, J. F., Effect of secondary structure on the activity of enzymes suspended in organic solvents. *Archives of Biochemistry and Biophysics* **1996**, 334, (2), 406-414.
25. Eppler, R. K.; Komor, R. S.; Huynh, J.; Dordick, J. S.; Reimer, J. A.; Clark, D. S., Water dynamics and salt-activation of enzymes in organic media: Mechanistic implications revealed by NMR spectroscopy. *Proceedings of the National Academy of Sciences of the United States of America* **2006**, 103, (15), 5706-5710.
26. Ghanem, A., The utility of cyclodextrins in lipase-catalyzed transesterification in organic solvents: enhanced reaction rate and enantioselectivity. *Organic & Biomolecular Chemistry* **2003**, 1, (8), 1282-1291.
27. Gorman, L. A. S.; Dordick, J. S., Organic Solvents Strip Water Off Enzymes. *Biotechnology and Bioengineering* **1992**, 39, (4), 392-397.
28. Lee, M. Y.; Dordick, J. S., Enzyme activation for nonaqueous media. *Current Opinion in Biotechnology* **2002**, 13, (4), 376-384.
29. Lindsay, J. P.; Clark, D. S.; Dordick, J. S., Combinatorial formulation of biocatalyst preparations for increased activity in organic solvents: Salt activation of penicillin amidase. *Biotechnology and Bioengineering* **2004**, 85, (5), 553-560.

30. Ru, M. T.; Wu, K. C.; Lindsay, J. P.; Dordick, J. S.; Reimer, J. A.; Clark, D. S., Towards more active biocatalysts in organic media: Increasing the activity of salt-activated enzymes. *Biotechnology and Bioengineering* **2001**, 75, (2), 187-196.
31. Wurges, K.; Pfromm, P. H.; Rezac, M. E.; Czermak, P., Activation of subtilisin Carlsberg in hexane by lyophilization in the presence of fumed silica. *Journal of Molecular Catalysis B-Enzymatic* **2005**, 34, (1-6), 18-24.
32. Zaks, A.; Russell, A. J., Enzymes in Organic-Solvents - Properties and Applications. *Journal of Biotechnology* **1988**, 8, (4), 259-270.
33. Sheldon, R., Enzyme immobilization: The quest for optimum performance. *Advanced Synthesis & Catalysis* **2007**, 349, (8-9), 1289-1307.
34. Brady, D.; Jordaan, J., Advances in enzyme immobilisation. *Biotechnology Letters* **2009**, 31, (11), 1639-1650.
35. Secundo, F.; Carrea, G., Optimization of hydrolase efficiency in organic solvents. *Chemistry-a European Journal* **2003**, 9, (14), 3194-3199.
36. Wehtje, E.; Adlercreutz, P.; Mattiasson, B., Improved Activity Retention of Enzymes Deposited on Solid Supports. *Biotechnology and Bioengineering* **1993**, 41, (2), 171-178.
37. Kilbanov, A. M., Enzymes that Work in Organic-Solvents. *Chemtech* **1986**, 16, (6), 354-359.
38. Chen, B.; Miller, E. M.; Miller, L.; Maikner, J. J.; Gross, R. A., Effects of macroporous resin size on *Candida antarctica* lipase B adsorption, fraction of active molecules, and catalytic activity for polyester synthesis. *Langmuir* **2007**, 23, (3), 1381-1387.
39. Chen, B.; Miller, M. E.; Gross, R. A., Effects of porous polystyrene resin parameters on *Candida antarctica* Lipase B adsorption, distribution, and polyester synthesis activity. *Langmuir* **2007**, 23, (11), 6467-6474.
40. Ismail, H.; Lau, R. M.; van Rantwijk, F.; Sheldon, R. A., Fully enzymatic resolution of chiral amines: Acylation and deacylation in the presence of *Candida antarctica* lipase B. *Advanced Synthesis & Catalysis* **2008**, 350, (10), 1511-1516.
41. Chen, B.; Hu, J.; Miller, E. M.; Xie, W. C.; Cai, M. M.; Gross, R. A., *Candida antarctica* lipase B chemically immobilized on epoxy-activated micro- and nanobeads: Catalysts for polyester synthesis. *Biomacromolecules* **2008**, 9, (2), 463-471.

42. Mangas-Sanchez, J.; Rodriguez-Mata, M.; Busto, E.; Gotor-Fernandez, V.; Gotor, V., Chemoenzymatic Synthesis of Rivastigmine Based on Lipase-Catalyzed Processes. *Journal of Organic Chemistry* **2009**, 74, (15), 5304-5310.
43. Patel, R. N., Biocatalysis: Synthesis of chiral intermediates for drugs. *Current Opinion in Drug Discovery & Development* **2006**, 9, (6), 741-764.
44. Torres-Gavilan, A.; Escalante, J.; Regla, I.; Lopez-Munguia, A.; Castillo, E., 'Easy-on, easy-off' resolution of chiral 1-phenylethylamine catalyzed by *Candida antarctica* lipase B. *Tetrahedron-Asymmetry* **2007**, 18, (22), 2621-2624.
45. Cruz, J. C.; Pfromm, P. H.; Rezac, M. E., Immobilization of *Candida antarctica* Lipase B on fumed silica. *Process Biochemistry* **2009**, 44, (1), 62-69.

CHAPTER - 2 Background

2.1 Enzymes in Organic Media

The preparation of highly active and selective enzyme based biocatalysts for applications in organic media has proven to be an important field in modern biotechnology¹⁻¹⁴. A myriad of synthesis protocols involving enzymes in organic media have been developed for the production of various compounds of commercial interest. For instance, an increasing number of pharmaceuticals (e.g., anticancer and antiviral compounds) are produced by enzymatically catalyzed processes in organic solvents, which represents a multi-million dollar business¹⁵⁻²⁵. The exquisite ability of enzymes to catalyze selective chemistries is the driving force to incorporate them into these processes²⁶. Additionally, enzymes operate at ambient temperatures and pressures, which is quite advantageous from the processing standpoint²⁷. One major limitation, however, arises from the fact that enzymes are not fully active when immersed in typical organic processing media^{2-4, 6, 7, 13, 28-30}. These media are the choice for most applications due to the enhanced solubility and stability of the conventionally involved organic substrates^{2-4, 6, 7, 13, 19, 27-31}. Some other advantages of using organic over aqueous media are summarized in Table 2.1.

Table 2.1. Advantages of incorporating enzymes in organic as opposed to aqueous media²⁷

-
- The thermodynamic equilibrium can be shifted to favor synthesis over hydrolysis
 - Enzymes physically adsorbed on solid supports can be incorporated with minimal leaching.
 - Ease of product recovery due to low boiling and high vapor pressure of solvents.
 - Enhanced thermal stability of enzymes.
 - Possibilities for microbial contamination are highly reduced.
 - Ease for adaptation to currently established chemical processes.
 - High substrate specificity due to conformational rigidity.
-

Aqueous as opposed to organic media pose a tremendous challenge for the downstream processing because of its high boiling point and low vapor pressure²⁷. Additionally, the presence of water is likely to promote a number of unwanted side reactions (e.g., hydrolysis, racemization,

polymerization, and decomposition) that can ultimately suppress or compete with the main synthetic reaction. This will likely decrease the overall yield of the process²⁷.

A number of mechanisms have been proposed to explain the loss of activity exhibited by enzymes when operating in organic media^{2, 28, 30} including: (i) decrease in the polarity of the microenvironment surrounding the enzyme, (ii) decrease on the conformational dynamics and flexibility of the enzyme, (iii) loss of the critical water associated to the enzyme's surface and specific residues, (iv) disruption of the active site machinery by solvent penetration, and (v) changes on the delicate secondary structure of the enzyme when lyophilized for use in solvents.

Table 2.2. Oxidation of *p*-anisidine catalyzed by Horseradish Peroxidase in different organic solvents³².

Solvent	Reaction rate [$\mu\text{mol mg enzyme}^{-1} \text{min}^{-1}$][†]
Toluene	60.0
Benzene	54.0
Hexane	75.0
Methylene Chloride	9.6
Ethyl Acetate	45.0 [‡]
Diethyl Ether	105.0 [‡]
Methanol	0.0
Dioxane	0.0
Dioxane +5% aqueous buffer	7.5
Dioxane +15% aqueous buffer	33.0
Dioxane +30% aqueous buffer	129.0

[†] Conditions: 1mM *p*-anisidine, 0.2 mM H₂O₂, 1 μ g/mL peroxidase, 0.25% v/v acetate buffer, 10 mM, pH 5.

[‡] Solvents were saturated with acetate buffer prior to reaction.

Particular attention has been given to the role of the organic solvent in the loss of activity. The biological function of enzymes has been typically linked to the presence of water. Some studies suggest that nature has developed sophisticated mechanisms to strategically organize water molecules within the enzyme structure to maximize function^{33, 34}. It has been postulated that the presence of organic solvents could lead to the breakdown of the naturally occurring organizational dynamics of water molecules³⁵. Examples in nature, however, demonstrate that

bulk water where the thermodynamic activity is unity ($a_w=1$), is not necessarily required to sustain properly functioning enzymes. Halophilic enzymes, indeed, have adapted to function in very low water activity environments (i.e., $a_w \rightarrow 0$) where salt concentrations approach $4M$ ³⁶⁻³⁸. The ability to relocate water molecules is thought to be responsible for maintaining functionality even under the harsh conditions of these extreme environments. This ability is corroborated by the superior catalytic activities observed for some enzymes suspended in hydrophobic solvents (e.g., horseradish peroxidase) where low water activities are also commonly found. The case of hydrophilic solvents appears to be different; their presence promotes substantial denaturation and ultimately disruption of the catalytic machinery^{13, 28}. A number of hypotheses have been put forward to try to explain this phenomenon. One of them is the increased affinity of hydrophilic solvents towards polar and charged residues where water is tightly bound to the enzyme structure through electrostatic forces²⁸. This facilitates water desorption from the enzyme surface into the bulk of the solvent. The impact of solvent type is illustrated in Table 2.2 for the oxidation of *p*-anisidine catalyzed by horseradish peroxidase. When the aliphatic/aromatic solvents (i.e., hexane, toluene and benzene) are used as reaction media, relatively high values of activity were observed. As expected, the enzyme suspended in hydrophilic solvents showed no activity if no water is added to the reaction mixture. In summary, enzyme activity increases as solvent polarity decreases and hydrophobicity increases. Additional efforts have been devoted to further correlate some other solvent properties (e.g., dielectric constant, partition coefficient and solubility factor) to enzyme activity and selectivity³⁹. Hitherto, however, such relationships are not sufficiently reliable to make robust predictions.

Table 2.3. Representative examples of currently available excipients for activation of enzymes in organic media²⁷.

Excipient	Enzyme	Solvent	Degree of activation †
Trehalose	Subtilisin Carlsberg	Hexane	14
Methyl- β -cyclodextrin	Subtilisin Carlsberg	1,4-Dioxane	100
PEG	Soybean peroxidase	Acetone	35
KCl (98% w/w)	Subtilisin Carlsberg	Hexane	1920
CsAc (98% w/w)	Penicilin amidase	Hexane	35000

† This is calculated as the activity of treated enzyme in identical solvent conditions

Another example of retained functionality at low water activity is the lyophilization process. Lyophilization is a common practice in the biotechnology industry to prolong the lifetime of enzyme preparations⁷. In this process, water is removed by sublimation and reduced to a concentration of approximately 3-5% (w/w)⁴⁰. Even under this extreme condition of dehydration, numerous reports have described highly active preparations⁴¹. It has been hypothesized that the lyophilization process could promote substantial structural changes. FTIR, Raman and solid state NMR studies have shown, however, evidence that this hypothesis could be imprecise⁴²⁻⁴⁵. These studies came to the conclusion that the conformational changes induced by lyophilization are essentially reversible⁴⁵.

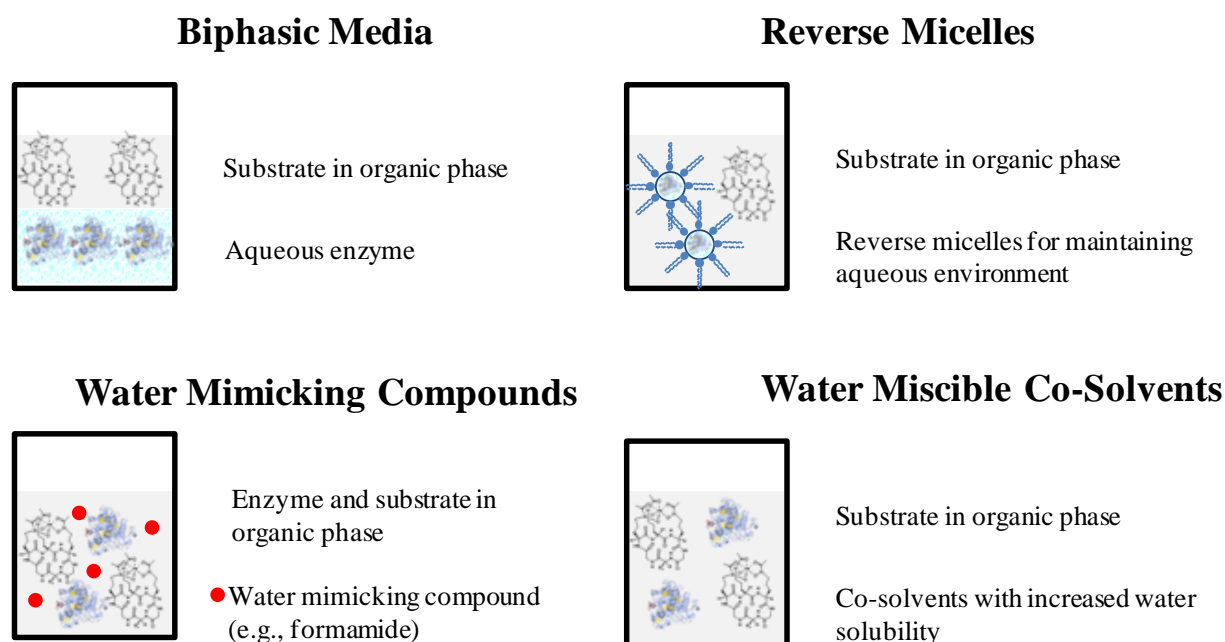


Figure 2.1. Solvent engineering strategies for enzymes in organic solvents^{4, 46}.

A number of research initiatives have been devoted to alleviate the unfavorable loss of activity in solvents by providing avenues to address some of the above discussed hurdles. The majority of available methodologies are based upon the lyophilization of the enzyme in presence of a variety of excipients. Table 2.3 shows representative examples of the currently available methods to activate enzymes in organic media via lyophilization.

Another important strategy is the engineering of the reaction media or “solvent engineering”^{4, 46}. In this approach, different reaction media are proposed to maintain the

structural integrity of enzyme molecules. Some of the engineered media include aqueous-organic biphasic mixtures⁴⁷, reverse micelles⁴⁸, and the addition of water mimicking compounds¹³. Figure 2.1 schematically shows some of the available solvent engineering strategies.

Along with the development of simple and successful experimental procedures, these initiatives have provided new insights into the mechanistic details that govern some of the aforementioned deactivation processes. Hitherto, however, there is not clear consensus among nonaqueous enzymologists about the hierarchy and relative magnitude of these processes.

2.2 Activation of Enzymes in Organic Solvents

Despite the significant number of factors detrimental to the activity of enzymes in organic solvents, several avenues have been explored to address this issue with strikingly positive results. A significant body of literature describes the activation of enzymes in non-aqueous media by their lyophilization in the presence of excipients. The compounds commonly used as excipients are carbohydrates^{49, 50}, polymers^{51, 52}, solid-state buffers⁵³, competitive inhibitors^{54, 55}, and nonbuffer salts^{31, 56-59}. It has been widely suggested that the increased catalytic activity is due mainly to the influence of the excipient as structure-preserving agent. For instance, the activation promoted by carbohydrates and polymers have been attributed to their lyo- and cryo- protectant properties, respectively^{7, 49, 60, 61}. It has been reported that in both situations, the excipient is capable of maintaining an increased fraction of the enzyme in its native conformation during lyophilization as compared with the excipient-free preparation^{44, 62}. This protected fraction of enzyme molecules will likely remain catalytically competent. Of particular interest, due to its simplicity and high activation levels, is lyophilization in the presence of nonbuffer salts. It has been hypothesized that the presence of salts is likely to maintain water mobility and lubricity in close proximity to the enzyme structure^{63, 64}, which in turn leads to an increased enzyme conformational dynamics and flexibility. In light of recent findings by Wurges et al.⁶⁵, however, this hypothesis may be imprecise. This study demonstrated that comparable activation levels are achievable by incorporating fumed silica as support prior to lyophilization. Unlike the nonbuffer salts, fumed silica is an inert nanoparticulated material of high surface area per unit volume and exceptional adsorptive abilities⁶⁶⁻⁶⁸. This suggests, therefore, that some other associated phenomena may be responsible for the observed levels of activity. Based on the physical properties of fumed silica, it has been proposed that a relaxation

of the diffusional limitations for the substrate is likely to be responsible^{65, 69}. Fumed silica is providing, therefore, means for the enzyme molecules to increase their interfacial contact with the solvent otherwise restricted by solubility reasons. In general, this immobilization protocol consists of two major sequential steps. First, the enzyme molecules are physically adsorbed on the nanoparticles from aqueous suspensions of fumed silica. Second, the resulting preparation is lyophilized to produce the supported nanobiocatalysts that can be further used in numerous solvents. The adsorption stage is thought to play a pivotal role in defining the resulting conformational/structural properties of involved enzyme molecules.

Table 2.4. Catalytic efficiency ($k_{\text{cat}}/K_{\text{m}})_{\text{app}}$ of free and immobilized α -chymotrypsin in different organic solvents for the transesterification of *N*-acetyl-L-phenylalanine ethyl ester. Upon immobilization the efficiency increased by 1 to 2 orders of magnitude respect to the free suspended native enzyme⁷⁰.

Solvent	$(k_{\text{cat}}/K_{\text{m}})_{\text{app}}$		Ratio [†]
	$[\text{M}^{-1}\text{min}^{-1}]*100$	$[\text{M}^{-1}\text{min}^{-1}]*100$	
	Free enzyme	Immobilized enzyme	
<i>n</i> -octane	221.0	19120.0	87
Carbon Tetrachloride	15.0	2150.0	141
Toluene	7.7	557.0	72
Diethyl Ether	33.0	1370.0	42
Tetrahydrofuran	7.2	91.0	13
Acetonitrile	0.0	56.0	-

[†]The ratio was defined as $(k_{\text{cat}}/K_{\text{m}})_{\text{app, immobilized}} / (k_{\text{cat}}/K_{\text{m}})_{\text{app, free}}$

The immobilization of enzymes on solid supports for biocatalysis in organic solvents has reached a stage of considerable maturity. Besides its applicability for decreasing potential diffusional limitations^{71, 72}, this approach has proven useful to enhance enzyme stability⁷³⁻⁷⁵. Both covalent and non-covalent chemistries have been used to attach enzymes to solid carriers. Examples of supports where covalent attachment is exploited for enzyme immobilization include glass, alumina, silica, stainless steel, charcoal, ceramics, gels, metallic oxides, resins, and chitosan^{76, 77}. The increased interfacial area obtained upon immobilization generally results in a significant increase of the reaction rates in solvents^{78, 79}. Additionally, some supports appear to

have the ability to bind water molecules that could be useful for catalysis⁸⁰. Table 2.4 clearly shows that the immobilization of α -chymotrypsin on glass beads increased the catalytic activity in solvents by nearly 1 to 2 orders of magnitude with respect to free enzyme⁷⁰. As in the case of immobilization on fumed silica, the resulting enhancement in catalytic activity does not appear to be related to significant changes in the final water activity of the preparation. This conclusion was supported experimentally with Karl Fisher titration and Electron Paramagnetic Resonance (EPR) spectroscopy⁷⁰. Substantial structural changes of the free enzyme were correlated with increased enzyme stability and a reduced tendency to form aggregates. Besides the relaxation of diffusional limitations and enhanced stability, immobilization is a convenient method of activation as it provides straightforward avenues for cyclic operation and reusability, enzyme and product recovery, and feasibility for continuous operation. More recently, the immobilization on nanostructured supports has been explored as an alternative for improving enzyme activity and stability⁸¹. The main attributes of these materials include their higher surface area, higher aspect ratio, higher thermal and chemical stability, lower diffusional resistance, and inertness. Successful examples include nanotubes^{82, 83}, nanofibers⁸⁴, and nanoparticles^{65, 85, 86}. During the past few years, considerable attention has been given to Single-Wall and Multi-Wall carbon nanotubes. Numerous chemistries have been considered to attach proteins including diimide-activation⁸⁷, physical adsorption⁸⁸, and functionalization with surfactants and polymers⁸⁹. Hitherto, however, the applicability of these supports in nonaqueous media remains poorly explored. It is expected, therefore, that the development of nanoscale-based immobilization strategies for applications in organic solvents will expand in the coming years.

2.3 Interfacing Proteins with Nanomaterials

Most attempts to interface proteins with nanomaterials have focused on the development of “smart” materials with specific biological functions. The impact of the nanomaterials’ physico-chemical properties on the structure and conformational stability of the proteins remains, however, poorly understood. Recent studies have suggested that the size of the nanostructured support may have a significant impact on the secondary structure of adsorbed proteins. Vertegel et al.⁸⁶ and Lundqvist et al.⁹⁰ studied the impact of nanoparticle size on the secondary structure of adsorbed lysozyme and carbonic anhydrase. They concluded that adsorption on small nanoparticles largely prevented secondary structural changes when compared with large

nanoparticles. They attributed the effect to changes in the surface curvature associated with particles of different size. High curvature was linked to the small particles while low curvature to the large ones. Roach et al.⁹¹ found, however, that fibrinogen denatured upon adsorption on small size nanoparticles. Similar results were found by Karajanagi et al.⁹² for chymotrypsin adsorbed on Single-Wall carbon nanotubes. Generalizations should be, therefore, done with extreme caution as proteins exhibit strikingly rich chemical and physical landscapes that may lead to multiple scenarios of conformational stability. The surface chemistry of the nanomaterials can be tuned to control the structural properties of adsorbed proteins. For instance, Rotello et al.⁹³ have recently shown that by functionalizing CdSe nanoparticles it is possible to control the surface loading and ultimately the population of active conformations. This conformational change was further exploited to control spacing in 3D architectures of self-assembled nanoparticles⁹⁴.

The ability to produce protein-nanomaterial conjugates with specific architectures and functionalities creates opportunities for new applications in various fields including nanobioelectronics, nanobiophotonics, biomedicine and biosensing. For instance, the preparation of highly efficient protein-based solar convertors could be enhanced. The commercial success of these devices mainly relies on the ability to produce highly ordered arrays of photosynthetic proteins on conductive materials^{95,96}. This can be accomplished by properly tuning the nanoscale environment for directional protein assembly⁹⁷.

The development of highly selective therapies could be also improved with biohybrid nanoengineered drug carriers⁹⁸. One strategy is based on the conjugation of nanomaterials (e.g., quantum dots, nanoshells, carbon nanotubes) with targeting proteins such as transferrin or antibodies for enhancing cellular uptake and tissue penetration^{99, 100}. This approach has proven useful for *in vivo* mitigation of breast carcinoma cells by increasing the temperature with externally applied NIR radiation¹⁰¹. It has been also an important alternative for the treatment of cardiovascular and immunological diseases. As pointed out by Farokhzad and Langer⁹⁸, the therapeutic efficacy largely depends on the proper distribution and stability of the targeting protein on the nanocarrier's surface. Figure 2.2 schematically describes drug delivery to cancer cells mediated by protein-functionalized nanocarriers. It is also important to discuss the application of nanobioconjugates in the development of sensors. The exquisite specificity of proteins can be exploited to detect minute changes in composition¹⁰². Hitherto, glucose detection remains as the most successful and perhaps the only protein-based sensing application of

commercial relevance^{102, 103}. Additional attempts remain circumscribed to the laboratory stage mainly due to proteins' inherent instability¹⁰². A marked decrease in sensitivity, stability, and selectivity is commonly detected as time passes¹⁰².

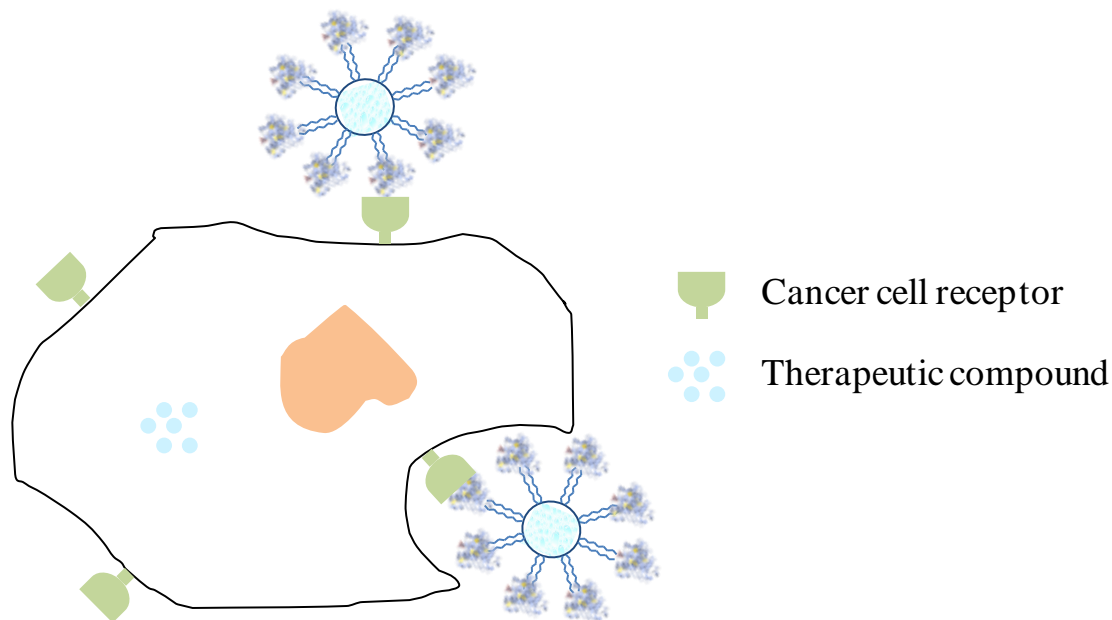


Figure 2.2. Active tumor targeting involves the use of proteins conjugated with nanostructured carriers. These proteins are able to specifically interact with cell receptors. Therapeutic compounds are delivered into the cell once the carrier is taken up by endocytosis. The efficacy of therapy mainly relies upon the ability to maintain an abundant population of structurally stable proteins on the surface of the nanocarrier⁹⁸.

The current myriad of available nanomaterials with unique electronic, optical, chemical, and mechanical properties has promoted a revival of this field by providing avenues to overcome the aforementioned hurdles¹⁰⁴. Some advantages of nanobiosensors include the reduction of mass transfer constrains due to their high surface area, detection in the attomolar range, and the possibility for multisubstrate detection^{103, 104}. The detection of biotinylated enzymes at picomolar concentrations was achieved with streptavidin-conjugated Single Wall carbon nanotubes¹⁰³. Antibody-conjugated carbon nanotubes have been also successfully applied for detecting antigens at nanomolar concentrations¹⁰⁵. Silica nanowire-based sensors have been incorporated in a label-free detection scheme where small molecules like ATP can be quantified at extremely low levels upon interaction with the immobilized proteins (e.g., tyrosine kinase)¹⁰⁶. The development of electrochemical nanobiosensors has also attracted considerable attention. This is due to the ease for directly linking enzymes to the surface of the nanomaterials, and to the

suitability for signal amplification upon biorecognition events^{107, 108}. These miniaturized devices also offer low cost and power requirements which make them very attractive for environmental and biomedical applications^{107, 108}. Among the electrochemical nanobiosensors, those based on enzymatic reactions have performed very well in detecting analytes of environmental and clinical importance. Redox enzymes like flavoenzyme, glucose oxidase (GOx), lactate oxidase, and peroxidase have been preferentially interfaced with nanoelectrodes due to the ease for monitoring changes in the electrochemical signal upon biorecognition events¹⁰³. The main challenge is to directly connect the redox center to the electrode to assure an efficient flow of electrons. This has been achieved with different approaches. For instance, GOx has been assembled on a nanoforest of carbon nanotubes that was linked to a gold electrode¹⁰³.

Table 2.5. Examples of Nanobiosensors based on Enzymatic Reactions¹⁰³

Nanostructure	Enzyme	Description
Gold Nanoparticles	GOx	Assembly of gold-nanoparticle-reconstituted GOx electrode with FAD on the dithiol-modified Au Electrode.
Zinc Oxide Nanoparticles	Peroxidase	Ultrasensitive Colorimetric Biosensor
SWCNT	Horseradish Peroxidase	Ultrasensitive Electrochemical Biosensor
CdTe QD + CNT	GOx	Relatively High Sensitivity
CNT	GOx	Assembly of carbon nanotube-reconstituted GOx electrode with FAD on the dithiol-modified Au Electrode.

GOx: Glucose Oxidase; SWCNT: Single Wall Carbon Nanotubes; QD: Quantum Dots; CNT: Carbon Nanotubes

The enzymatic reaction that allowed the electron flow was the conversion of glucose into gluconic acid. Another strategy for the alignment of enzymes on electrodes is the use of metallic nanoparticles as electron relays^{103, 104}. Conductive polymer-based nanobiosensors have been also considered as interesting avenues for *in vivo* detection due to their fast response and minimal

oxygen consumption¹⁰⁴. Table 2.5 shows examples of nanobiosensors that incorporate redox enzymes.

2.4 Enzymes and their Interactions at Aqueous/Solid Interfaces

When enzymes are in contact with solid surfaces, they are subjected to interactions that may ultimately lead to their adsorption^{109, 110}. This spontaneous accumulation of enzymes at the interface has been widely exploited as a mild method of immobilization¹¹¹⁻¹¹⁴. Most controlling events while immobilizing enzymes take place at the interface between the adsorbate (i.e., the enzyme molecules) and the adsorbent (i.e., the solid support)^{109, 115}. In general, the immobilization events are mainly driven by two types of interactions: electrostatic and hydrophobic¹⁰⁹. The former can be either attractive or repulsive depending on the net charges of the adsorbent and the adsorbate while the latter are mostly due to the presence of water molecules surrounding the enzyme molecules. These water molecules are likely to promote the association of the hydrophobic patches of the enzyme with similar groups at the surface of the adsorbent. A complete understanding of the enzyme adsorption mechanisms is challenging due to the immense variety of parameters involved in the process¹¹⁰. These can be classified into three major categories: (1) protein characteristics, including isoelectric point, net charge and distribution, three dimensional structure in solution, and conformational variability; (2) surface properties, including topography, electrical potential, water binding, and hydrophobicity; (3) medium conditions, including pH, temperature, ionic strength, and buffer type. Numerous studies have been attempted to elucidate the relationships and hierarchy of these factors. However, no comprehensive model has been reported with the capability of predicting such a complex intricacies and interdependencies. Of particular importance for this project are the conformational changes induced when enzymes are adsorbed on hydrophilic surfaces such as those present at the fumed silica surface. The extent of these structural modifications is crucial to determine the ultimate catalytic competency of adsorbed enzymes.

2.5 Rearrangements in the Enzyme Structure upon Adsorption on Solid Surfaces

As one of the modulating parameters for enzyme adsorption, the enzymes' native structural variability has attracted considerable attention from numerous biotechnological applications. For instance, in biocatalysis applications where it is important to consistently produce surfaces filled with catalytically competent and stable enzymes, this parameter plays a central role¹⁰⁹. It is well-known that when enzyme molecules undergo substantial conformational changes they are likely to become less active^{110, 111}. Despite the relative importance of the structural rearrangements, it is noteworthy to point out that their effects are not independent. These changes can also be involved in parallel processes such as charge redistribution and exposure of apolar residues^{109, 111}. In general, as soon as an enzyme molecule comes in contact with the adsorbent, the intramolecular hydrophobic interactions responsible for the stability of the enzyme are considerably altered. In fact, water at the interface of this ensemble is displaced and consequently, hydrophobic patches that tend to be buried in solution are exposed^{109, 111}. This exposure results in the destabilization of both the secondary and tertiary structures. Moreover, if the sorbent surface is able to form hydrogen bonds as is the case of oxides, a significant decrease in secondary structure is likely to be expected^{116, 117}. This general description suggests that the resulting surface-induced conformational changes of the adsorbed enzyme molecules can be minimized by properly balancing the energetically favorable interactions that facilitate the process. In this regard, experimental evidence indicates that the majority of enzymes, when interacting with hydrophilic surfaces, are likely to be less susceptible to conformational changes^{110, 118}. However, based on the extent of the structural rearrangements upon adsorption, proteins have been classified into two groups. Those proteins exhibiting minor changes on their conformation are referred as "hard" proteins¹⁰⁹. On the other hand, proteins with a tendency to spread when adsorbed are considered as "soft" proteins¹⁰⁹. These observations encouraged researchers to identify those conditions playing major roles as controlling agents for the adsorption pathways for each of the aforementioned protein groups. Thus, it was discovered that hard proteins only adsorb on hydrophilic surfaces if a net charge difference exists between the surface and the protein. In contrast, for the soft proteins adsorption is controlled by changes in the induced conformational entropy. In this case, even in the absence of charge differences, adsorption is possible at expense of a sufficiently large entropy change. Further research has

demonstrated that pH and ionic strength are factors exerting a significant impact on the electrostatic forces associated with these conformational changes^{119, 120}. In this regard, it has been demonstrated that the electrostatic effects on the structure can be reduced by adsorbing the enzyme at pH values near the enzyme's pI¹¹⁰. Additional reduction in denaturation events may be achieved by maximizing the surface concentration of enzymes¹¹⁰. These holistic remarks about protein adsorption have to be assumed with caution as great variability is expected among enzyme molecules due to their extremely rich surface chemistry and physics. Figure 2.3 shows a schematic description of the major factors involved on enzyme adsorption and their impact on the observed conformational changes.

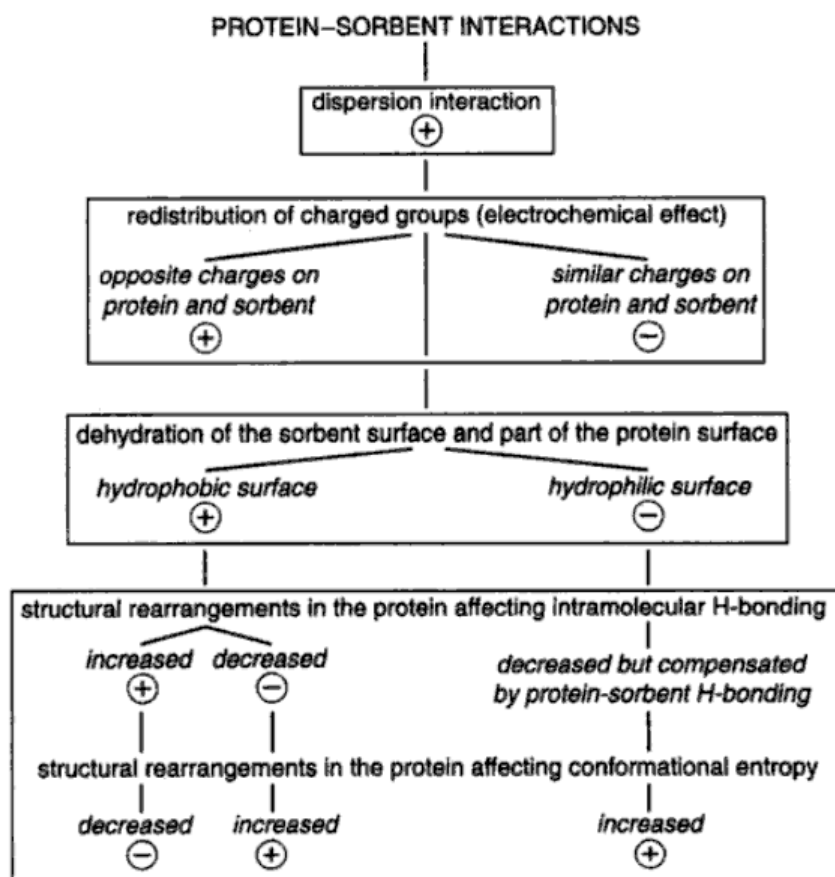


Figure 2.3. Major factors controlling the adsorption of proteins on solid supports. Electrostatic interactions, hydrophobicity of the surface and conformational dynamics are all interdependent. The + sign represents a favorable pathway for adsorption while the – sign, unfavorable conditions for adsorption¹⁰⁹

2.6 Physical Adsorption Enables Enzyme Immobilization on Fumed Silica

Fumed silica is described as an exceptional adsorbent due to facilitated adsorption pathways for a variety of compounds including polymers and proteins^{67, 68}. This is a direct consequence of the hydrophilic chemistry present at the surface of fumed silica. In fact, the majority of reactions at the fumed silica surfaces occur with the participation of highly reactive silanol groups ($=\text{Si}-\text{OH}$)¹²¹. Besides the favorable surface chemistry of fumed silica, many other factors govern the predominant adsorption pathways. In general, the mechanisms can be influenced by the chemical, spatial, and electronic structures of the adsorbates (i.e., the enzyme molecules); structural features of silica (e.g., surface area, surface topography, and particle size distribution) and availability of other components at the interfaces (e.g., adsorbed water)¹²². Some of these factors are markedly influenced by physicochemical properties resulting from the very synthesis of fumed silica. This material is synthesized by high temperature hydrolysis of SiCl_4 in an O_2/H_2 flame¹²³. Fumed silica is an amorphous material, nonporous, and exhibits a large specific surface area (up to $500 \text{ m}^2/\text{g}$). At the beginning of the synthesis process, protoparticles (1-2 nm) are produced followed by their agglomeration and coalescence. Subsequently, they are covered with additional silica layers to form primary particles (average diameter = 5-50 nm, density $\cong 2.2 \text{ g/cm}^3$). These particles tend to collide and fuse into aggregates of approximately 100 – 500 nm¹²².

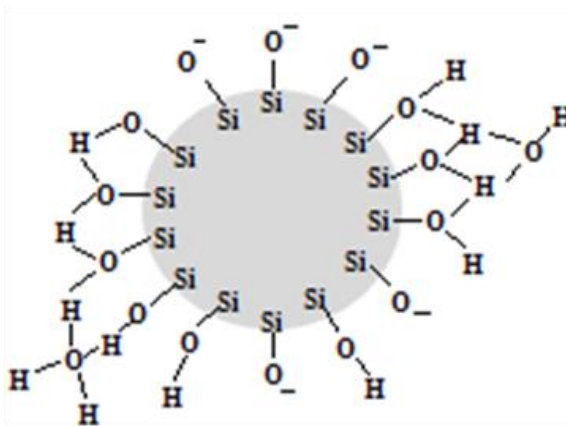


Figure 2.4. Individual fumed silica nanoparticle and the functional groups at its surface. This nanoparticle exhibits a diameter of approximately 10 nm

Figure 2.4 shows a schematic of a typical primary particle of fumed silica with their associated surface functional groups. The fractal dimension for these aggregates was calculated as 2.5, which represents a surface of relatively high roughness. The morphology of the

aggregates is in general determined by the temperature, coordination numbers, and type of bonding. Three major types of bonding have been described as pivotal for the stability of aggregates¹²¹: (1) chemical =Si-O-Si=; (2) intermolecular =SiOH ... O(H)Si=; and (3) with the participation of water molecules =SiOH ... (OH)₂ ... O(H)Si=. In order to mechanistically understand the adsorption process, the dynamical behavior of the complex enzyme/fumed silica aggregate should be examined in detail. Thus, from the support viewpoint, it is imperative to decipher the changes in morphology and surface chemistry induced by the presence of buffered enzymes. Previous attempts to address these issues have elucidated the main environmental factors susceptible of being modulated to effectively promote detectable changes. As a result, pH, ionic strength, and water concentration were determined as controlling parameters when selective changes in charge, electronic transfer, particle size distribution, and chemical bonding were desirable¹²¹. This may lead to engineer strategies for controlling the adsorption process for the production of target immobilizates for specific applications.

After examining the implications of adsorption on fumed silica from both the enzyme and the support viewpoints, the following general statements can be made. On one hand, the surface activity of an enzyme is a cumulative property influenced by a number of factors including size, charge distribution, hydrophobicity, and conformational stability. On the other hand, the adsorptive characteristics of fumed silica are mainly modulated by morphological/textural (e.g., particle size distribution and aggregation) and chemical properties (e.g., active silanol groups and their ability to form complexes). The environmental conditions that largely dominate both the enzyme and support physicochemical properties during adsorption are pH, and ionic strength. Due to the high diversity exhibited by enzymes in terms of structure and chemical functionality, one can expect that multiple adsorption pathways will lead to adsorption. The inherently associated changes in structure and consequently in catalytic activity are the main focus of this research project.

2.7 Protein Conformational Stability

The complex structure of proteins is essentially maintained by a number of intramolecular forces acting in a concerted manner^{124, 125}. These forces include hydrophobic interactions, hydrogen bonds, and dispersive and electrostatic forces. When the environmental conditions change, proteins continue to function properly by adopting different conformations¹²⁴,

¹²⁵. This is mainly achieved by altering the intramolecular forces which in turn promote folding into specific structures with minimized conformational energy. From this viewpoint the conformational stability is, therefore, a thermodynamic quantity^{124, 125}.

The formation of hydrogen bonds represents one of the major contributors to protein stability in solution, they are indeed involved in α -helix and β -sheet formation^{124, 125}. Each residue has the ability to form one hydrogen bond^{124, 125}. Protons are small in size and can become in contact with electronegative atoms easily. Proteins in the unfolded state tend to form intermolecular hydrogen bonds with water^{124, 125}. It appears that to maintain an energy balance, intramolecular hydrogen bonds need to form. The dispersion forces are important to maintain the packing density of the structure. Some proteins are as tightly packed as crystals in the folded state^{124, 125}. The presence of charged and ionizable groups creates attraction and repulsion between side chains. These forces define intramolecular distances in both native and denatured states^{124, 125}.

Among the intramolecular forces, hydrophobic are perhaps the most easily noticeable as they are involved in holding together the interior of proteins^{124, 125}. These forces are generally regarded as entropically driven due to their relation with the organizational dynamics of the surrounding water molecules. It has been suggested that the hydrophobic interactions may contribute to minimize the free energy of the protein by decreasing the exposure of nonpolar residues (buried in the structure) to the aqueous medium¹²⁵.

The environmental conditions largely define the protein stability. A large body of literature describes that extreme pH and temperatures may induce unfolding. Salts or ligands may selectively bind to the protein structure thereby increasing stability¹²⁵.

2.7.1 Measuring Protein Conformational Stability

The most common approach to determine the conformational stability of proteins is to perturb the unfolding equilibrium while monitoring structural changes¹²⁵. Biophysical methods to probe the structure include enzyme activity and spectroscopic methods such as UV-Vis absorbance, fluorescence, circular dichroism (CD), Fourier Transform Infrared (FTIR), Raman, Electron Spin Resonance (ESR) and Nuclear Magnetic Resonance (NMR). Unfolding is generally promoted by increasing the temperature (thermal denaturation) or by adding strong chemical denaturants (chemical denaturation)¹²⁵. The former generally leads to irreversible

denaturation while the latter is generally reversible. Figure 2.5 shows a typical guanidine hydrochloride denaturation curve. A similar approach was used in this research project to estimate unfolding levels of hydrolases in phosphate buffer solutions. An alternative method for measuring conformational stability that has gained considerable popularity is hydrogen/deuterium exchange. In this approach, regions that become exposed upon unfolding are accessible to exchange their hydrogen atoms with deuterons¹²⁵. The rate of exchanging can be further correlated with conformational stability and dynamics. For instance, this method has been particularly useful to determine the mobility of intramolecular regions in the protein structure¹²⁵.

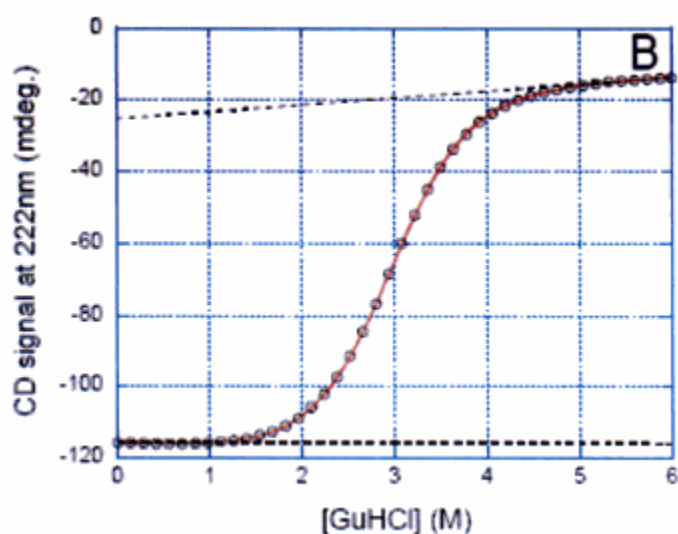


Figure 2.5. Guanidine hydrochloride (GuHCl) induced denaturation for the B-domain of protein A. Denaturation was tracked with circular dichroism at 222 nm¹²⁵.

2.7.1.1 Spectroscopic Techniques to Monitor Structural Changes

2.7.1.1.1 Intrinsic Fluorescence Spectroscopy^{126, 127}

Fluorescence spectroscopy is one of the most efficient techniques for the analysis of protein structure, high affinity interactions, and conformational dynamics. This is due to the remarkable sensitivity of some residues to chemical and environmental changes. For instance, the intrinsic fluorescence of tryptophan residues has been extensively used to understand the impact of solvent polarity on protein conformation. Three intrinsic residues in proteins may act as chromophores, namely tryptophan (Trp), tyrosine (Tyr), and phenylalanine (Phe). Trp has the highest quantum yield while Phe the lowest. Tyr fluorescence is very often quenched in close

proximity to Trp or by ionization mechanisms. This has made Trp residues the preferred choice for most studies. The intensity and position of the fluorescence signal strongly depend on environmental parameters such as polarity and hydrophobicity. This has allowed robust quantitative analyses in protein conformation studies. For instance, the emission maximum of Trp solvated in aqueous medium is approximately 350 nm and moves to shorter wavelengths (i.e., blue shift) as the residue is buried into the non-polar environment at the interior of the protein or upon insertion into membranes. Trp mutants have been generated to probe structural features of different regions in a protein. By replacing or eliminating Trp residues of multi-Trp proteins it is possible to simplify the analysis of fluorescence. This approach has to be followed with caution as the recombinant proteins may have altered spectroscopic properties or decreased structural stability.

An alternative approach considers Trp analogues such as 5-hydroxytryptophan (5H-W) or 7-azatryptophan (7A-W) to produce the recombinant proteins. These analogs showed no substantial modification of the physico-chemical properties of the obtained proteins and more convenient absorption and fluorescence spectra. The absorption spectrum of Tyr (Max. abs.: 275 nm) contains that of Phe (Max. abs.: 255 nm), the absorption spectrum of Trp (Max. abs.: 280 nm) contains those of Phe and Tyr. Trp dominates because it has the strongest $S_0 \rightarrow S_1$ transition. The emission maxima for Phe and Tyr are 275 nm and 303 nm, respectively. As described above, the emission maximum of Trp can be located in the region of 310-350 nm depending on the polarity of the medium. The overlapping of the absorption and emission spectra for the three aminoacids opens the opportunity for Foster resonance energy transfer (FRET) from Phe to Tyr or Trp, Tyr to Trp or Trp to Trp.

Trp residues are not typically present in various polypeptide hormones, in such a case, Tyr and Phe could be interesting alternatives. Shea et al.¹²⁶ investigated the binding of calcium to calmodulin with Phe and Tyr fluorescence. Calmodulin is a protein that regulates important cellular activities including glycogen metabolism and DNA replication. Fluorescence is detected with spectrofluorimeters, a typical instrumental arrangement for detection of fluorescence is shown in Figure 2.6.

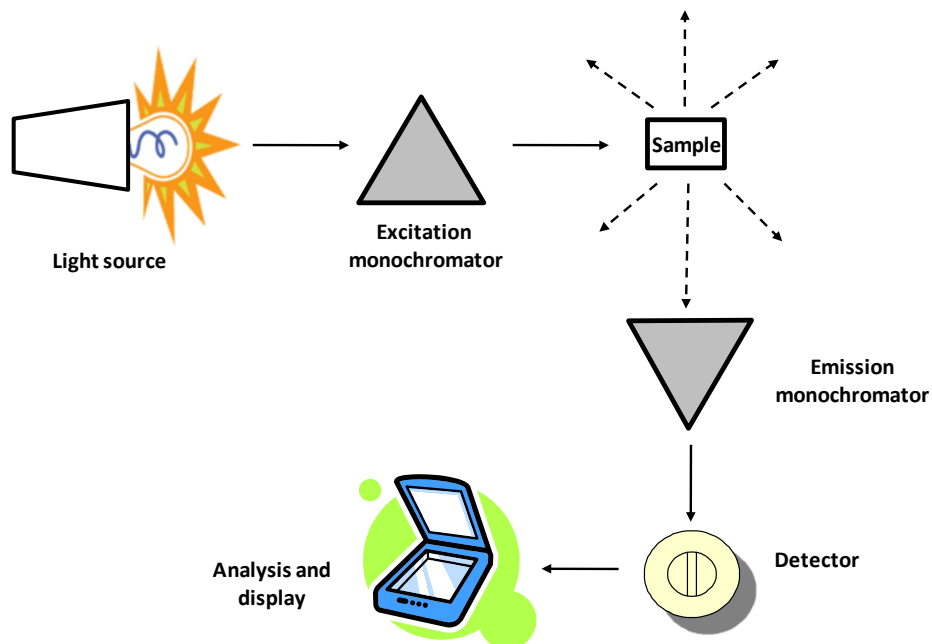


Figure 2.6. Schematic of a typical spectrofluorimeter. Before impacting the sample, light from the source is filtered with an excitation monochromator. After impacting the sample the emitted light is collected through an emission monochromator and recorded with a photomultiplier sensitive between 200-1000 nm. The light at the source is usually generated with high-intensity xenon arc lamp or a laser in which case the monochromator is not required¹²⁷.

2.7.1.1.2 Circular Dichroism

Circular dichroism (CD) spectroscopy is one of the most efficient techniques for determining the secondary structural content of proteins, polypeptides, and peptide structures. This method exploits the fact that these molecules (chiral in nature) may respond differently to left or right circularly polarized light¹²⁸. Particularly, the absorbance spectra in the far ultraviolet (UV) regions may exhibit slight differences. This is a direct consequence of the $n \rightarrow \pi^*$ and $\pi \rightarrow \pi^*$ of the amide groups (Figure 2.7). Moreover, the intensity and energy of these transitions are influenced by the geometry of the polypeptide bonds¹²⁸. As a result, the angles ψ and ϕ in Figure 2.7 will change according to the type of secondary structure present.

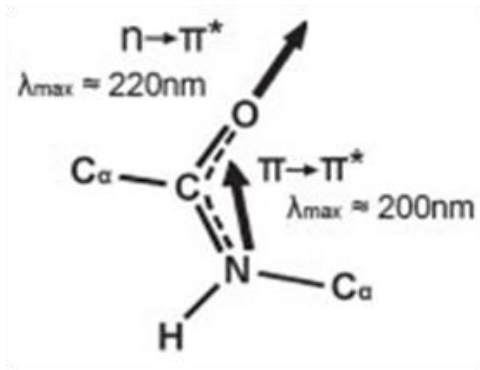


Figure 2.7. Schematic of a peptide bond and its corresponding transition dipoles (thick arrows)¹²⁸.

When light is circularly polarized the oscillating electric field vector rotates either to the left or to the right about the propagation axis of the electromagnetic wave. As a result, the tip of the vector follows a helical path along the beam^{129, 130}. CD is based on the differential absorption of these two components. If after passing through the sample the components of the light are not absorbed or equally absorbed, the emerging radiation will be in the original plane. If the components are differently absorbed; however, the emerging radiation will be elliptically polarized (Figure 2.8)^{129, 130}.

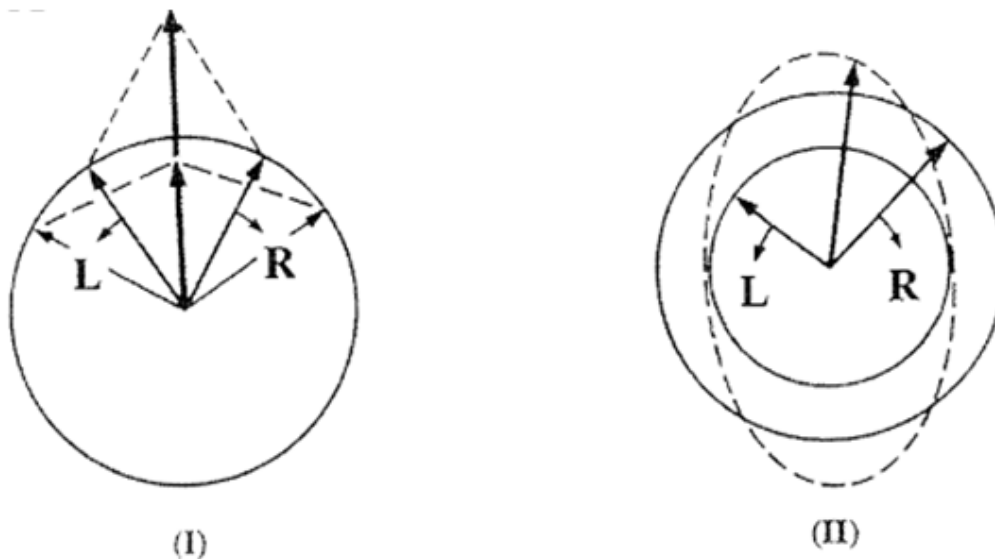


Figure 2.8. Basis for the CD effect: (I) resulting radiation when neither the L nor the R components are absorbed or they are equally absorbed, (II) preferential absorption of either the L or R components results in an elliptically polarized radiation¹³⁰.

CD instruments measure the difference in absorbance between the L and R components at a particular wavelength. Therefore, we have

$$\Delta A = (A_R - A_L) \quad \text{Equation 2.1}$$

Where

A_R is the absorbance of the R components of the polarized field.

A_L is the absorbance of the R components of the polarized field.

It is a common practice to describe CD data in terms of the ellipticity θ , in units of millidegrees.

The following expression allows for inter-conversion between θ and ΔA :

$$\theta = 32,980 * \Delta A \quad \text{Equation 2.2}$$

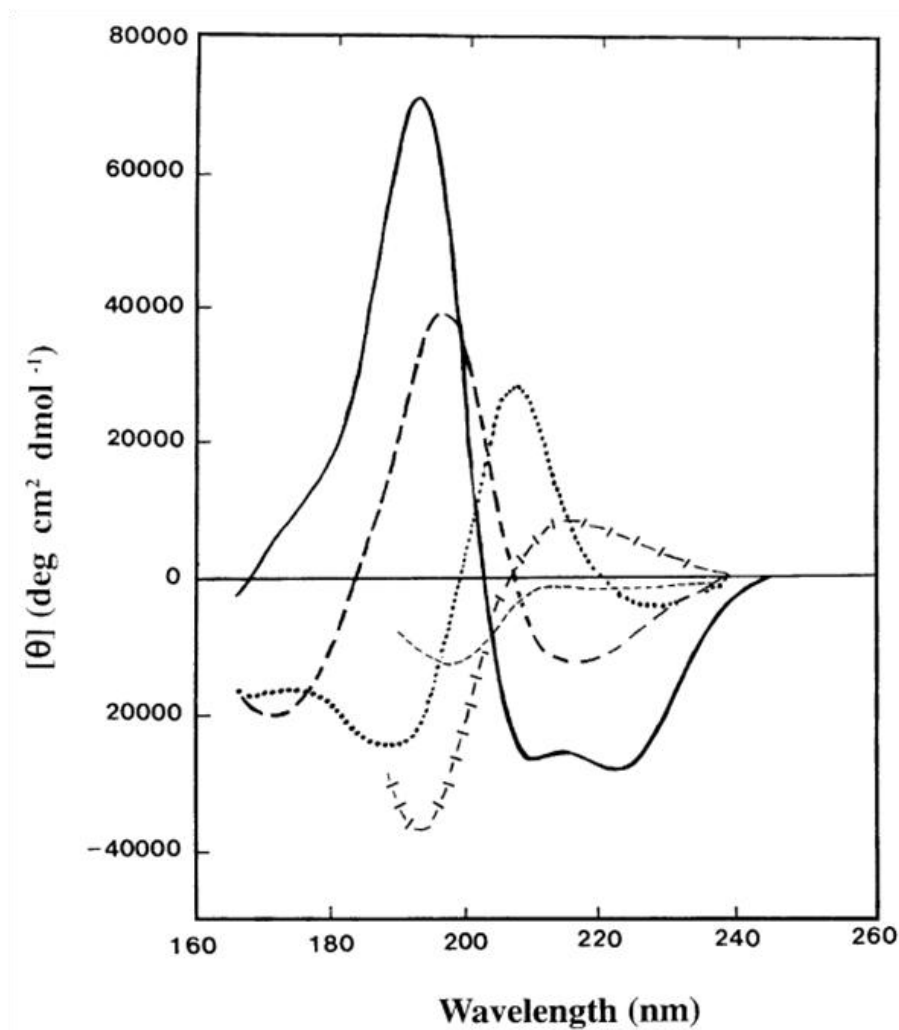


Figure 2.9. Depending on the type of secondary structure, the CD spectrum shows a number of distinctive features. Solid line, α -helix; long dashed line, anti-parallel β -sheet; dotted line, type I β -turn; cross dashed line, extended α -helix or poly (Pro) II helix; short dashed line, irregular structure¹³⁰.

A number of chromophores are present in proteins that can be successfully used to extract structural information including: (i) the peptide bond (absorption below 240 nm); (ii) aromatic amino acids such as phenylalanine, tyrosine, and tryptophan (absorption in the range 260 to 320 nm) and (iii) disulfide bonds (weak broad absorption bands centered around 260 nm)¹³⁰. Due to the presence of different types of regular secondary structure in proteins, characteristic CD spectra can be detected in the far UV (Figure 2.9). Particular attention has been dedicated to values of the CD signals at 208 nm and 222 nm since they are strongly influenced by the α -helical content¹³⁰. Besides estimation of the secondary structure, one may attempt to collect information on the tertiary structure of proteins with CD. In this case, spectra in the region from 260-320 nm must be collected. These data arise from the aromatic amino acids. Indeed, Trp shows a peak close to 290 nm with fine structure between 290 and 305 nm; Tyr a peak between 275 and 282 nm, with a shoulder at longer wavelengths often obscured by bands due to Trp; and Phe shows weaker but sharper bands with fine structure between 255 and 270 nm. Thus, the shape of spectra in this region can be linked with the mobility, nature of the environment, and spatial configuration of these residues in the protein¹³⁰.

CD spectroscopy can be also used to estimate the stability and folding state of proteins. It is possible to promote denaturation with chemical agents and track the changes in the CD signal. Similarly, it is possible to monitor the refolding process of denatured proteins and, therefore, to determine the time scales for rebuilding of secondary and tertiary structure¹³⁰.

CD data is generally presented either as ellipticity $[\theta]$ or differential absorbance (ΔA). However, software for data analysis may require normalization to molar concentrations. One approach is to normalize by the Mean Residue Weight (*MRW*) which is defined as follows:

$$MRW = \frac{M}{N - 1} \quad \text{Equation 2.3}$$

Where *M* is the molecular mass of the polypeptide chain (in Da), and *N* is the number of amino acids in the chain. For most proteins the *MRW* is 110 ± 5 Da.

The mean residue ellipticity at wavelength λ is, therefore, given by:

$$[\theta]_{mrw,\lambda} = \frac{MRW * \theta_{\lambda}}{10 * d * c} \quad \text{Equation 2.4}$$

Where

MRW is the Mean Residue Weight as defined above

θ_{λ} is the observed ellipticity in degrees.

d is the pathlength in cm.

c is the concentration in mg/mL.

A further conversion may be required into molar ellipticity which is given by:

$$[\theta]_{molar,\lambda} = \frac{100 * \theta_{\lambda}}{m * d} \quad \text{Equation 2.5}$$

Where θ_{λ} and d have the same meaning as above and m is the protein molar concentration. Both $[\theta]_{mrw,\lambda}$ and $[\theta]_{molar,\lambda}$ have the units

$$deg * cm^2 * dmol^{-1}$$

It is also possible to convert the collected absorbance into a differential molar CD extinction coefficient as follows:

$$\Delta\varepsilon = \frac{\Delta A}{m * d} \quad \text{Equation 2.6}$$

The units for $\Delta\varepsilon$ are $M^{-1} cm^{-1}$.

There is a simple numerical to inter-convert $[\theta]_{mrw,\lambda}$ or $[\theta]_{molar,\lambda}$ and $\Delta\varepsilon$:

$$[\theta]_{mrw,\lambda} = 3298 * \Delta\varepsilon \quad \text{Equation 2.7}$$

The accuracy of a CD experiment can be checked against the data for a hypothetical protein with 100% α -helical, which has a mean residue ellipticity at 222 nm of about $-34,000 \text{ deg cm}^2\text{dmol}^{-1}$ ($\Delta\varepsilon = -9M^{-1}cm^{-1}$).

After data collection, next step is to quantify the secondary structure of the sample. The simplest approach is to consider that the spectrum is a linear combination of each of the contributing secondary components weighted by their relative abundance in the protein¹³¹. This approach has proven, however, to be very inaccurate due to the absence of pure secondary standards. Two main alternative approaches have been developed to solve this issue. In the first one, polypeptide standards with known secondary structure (determined by IR and x-ray scattering) are used for reference¹³¹. The second approach compares spectra of unknown proteins to standards previously characterized by crystallography¹³¹. The algorithms for this comparison include least-square, ridge regression, singular value decomposition (SVD), SVD with variable selection, the self-consistent method, and neural network analysis. Some of the available packages to calculate secondary structural contents are described below¹³¹.

Linear regression. This method is primarily useful for globular proteins. It is based on direct comparison with polypeptide standards. The most basic fitting can be performed with the

program LINCMB. Recent refinements to the main algorithm include convex constrain (CCA) and nonconstrained multilinear regression (MLR). The major limitation is the absence of single standards for β -turns.

Ridge regression (CONTIN). Essentially fits the CD data by linearly combining spectra of known conformations. If mutations or denaturing agents are introduced new customized standards must be prepared.

Singular value decomposition (SVD). The program uses a set of spectra for known proteins to extract specific nodes. The data are subsequently incorporated in a weighting algorithm to determine the content of each secondary structural feature. The method is only useful for α -helical content.

Variable selection (VARSLC, CDSSTR). It uses a large database with known proteins. It operates with a reduction algorithm that provides the best candidates for fitting. It can be really slow due to the size of the database. It is not useful for polypeptides and protein fragments.

Self-consistent method (SELCON). It works with the same reduction algorithm as variable selection method. However, in this case the process is accelerated by the inclusion of the spectrum under analysis to the database. Hitherto, three versions of the program have been produced. It is not useful for polypeptides and protein fragments.

Neural networks (CDNN, K2D, SOMCD). These programs use a neural network to find the correlations in the CD data. The networks are trained with a reference set of proteins. This approach gives good results for both proteins and polypeptides.

The typical instrument arrangement of a Circular Dichroism spectropolarimeter is shown below (Figure 2.10).

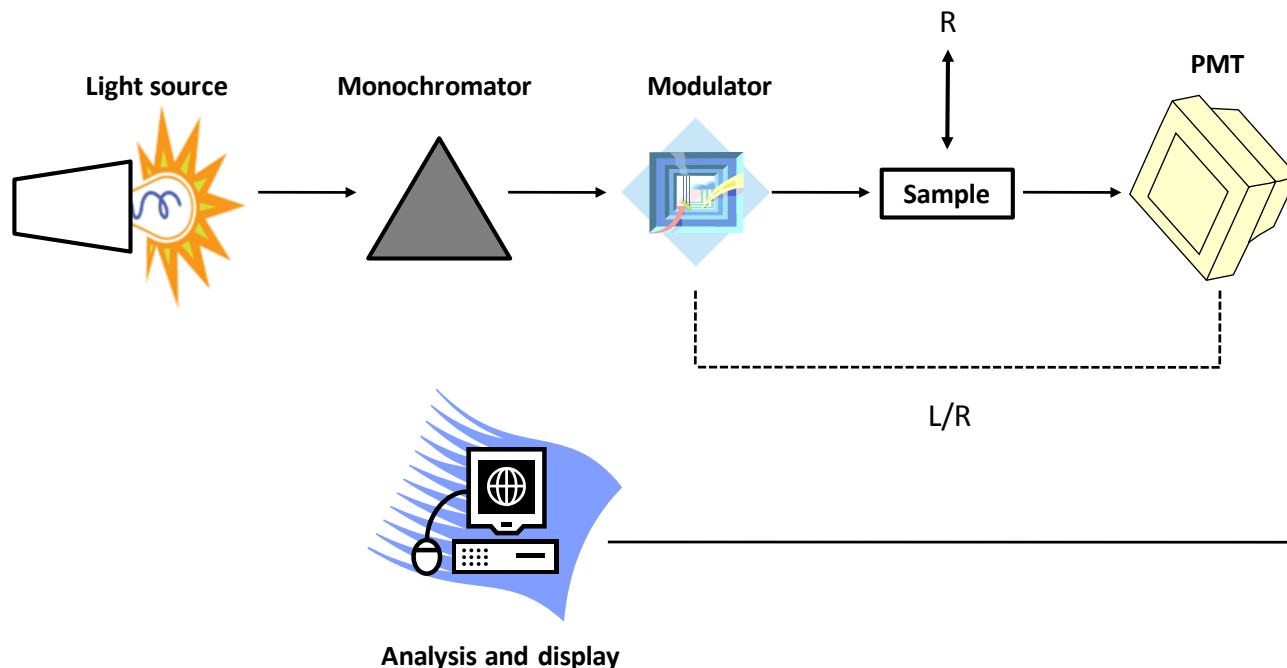


Figure 2.10. Schematic of a typical CD instrument. A very intense light source is required to extend into the far-UV. The circularly polarized light is generated by superposition of photons with different handedness. A piezoelectric crystal can be used to select either right or left circularly polarized light¹²⁷.

2.7.1.1.3 Infrared Spectroscopy

Infrared spectroscopy has been extensively used in protein structural analyses due to its exquisite sensitivity to chemical composition and architecture^{132, 133}. IR has been successfully applied to study molecular mechanisms of protein reactions, folding, misfolding, and unfolding^{132, 133}. IR analysis is also advantageous due to the ability to detect structural changes in small and large proteins, high resolution in very short times, moderate to low operational costs, and low sample amounts. Important structural information of proteins can be potentially extracted from the mid-infrared spectrum. A typical mid-infrared absorbance spectrum for a protein is shown in Figure 2.11. Even though the spectrum appears to be simple, meaningful structural information is highly convoluted. This is due to the superposition of various vibrational bands.

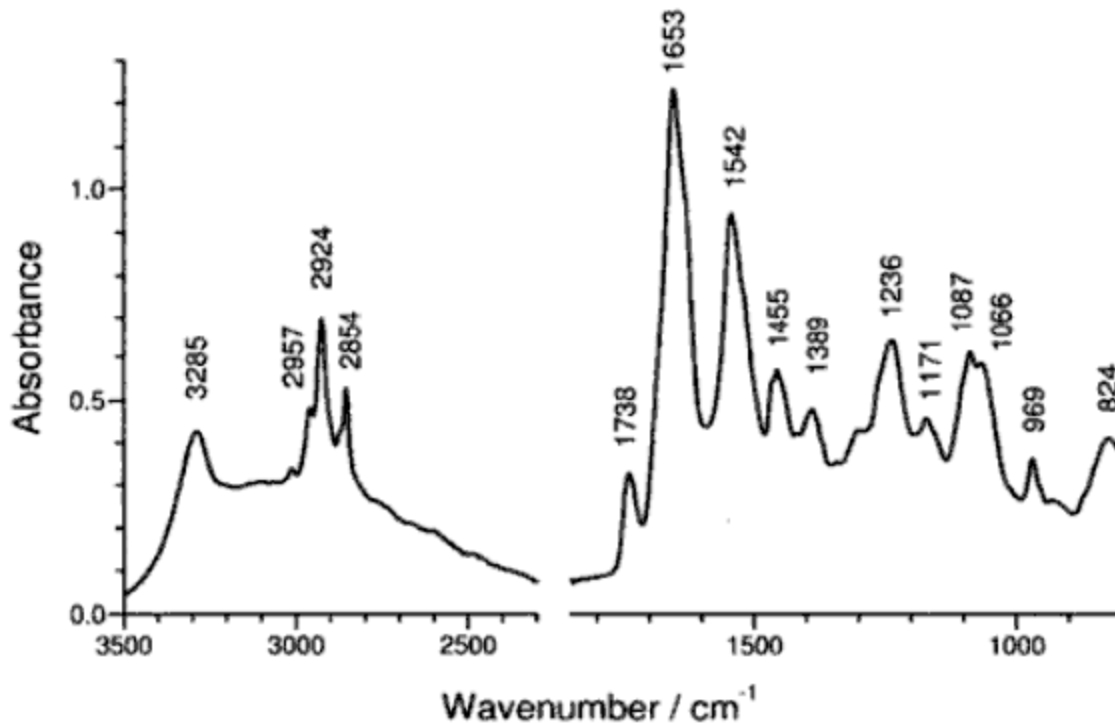


Figure 2.11. Mid-infrared spectrum of membrane protein Calcium ATPase. Vibrations that contribute the most to the observed absorption bands are: 3285 cm^{-1} - protein amide A; 2957 cm^{-1} - $\nu(\text{CH}_3)$; 2924 cm^{-1} - $\nu(\text{CH}_2)$; 2854 cm^{-1} - $\nu(\text{CH}_2)$; 1738 cm^{-1} - $\nu(\text{lipid C=O})$; 1653 cm^{-1} - protein amide I; 1542 cm^{-1} - protein amide II; 1455 cm^{-1} - $\delta(\text{CH}_3)$; 1389 cm^{-1} - $\nu(\text{COO}^-)$ of Asp and Glu; 1236 cm^{-1} - $\nu(\text{Lipid PO}_2^-)$; 1171 cm^{-1} - $\nu(\text{lipid C-O-O-C})$; 969 cm^{-1} - $\nu(\text{CN})$ of lipid; 820 cm^{-1} - $\nu(\text{lipid P-O})$ ¹³⁴.

A large body of literature has been devoted to develop strategies for deconstructing the IR information related to protein structure. In this respect, most studies suggest that special attention should be given to spectral regions where the same type of vibration is abundant in the protein structure. This is the case of the amide I region where C=O vibrations dominate. There are 8 more vibrational modes associated with the amide group, namely amide A and B, and amide II-VII. Due to its sensitivity to secondary structure, the amide I region has been preferred for correlating spectral information with structure¹³³.

The sensitivity of the amide I is attributed to the so-called transition dipole coupling (TDC). Depending on their relative location and orientation on the protein backbone structure, neighboring amide groups have the ability to resonate¹³³. This coupling interaction gives rise to the splitting of the amide I for β -sheet structures. Conformational changes will alter the transition dipole moments, which ultimately leads to a shift of the amide I frequencies. Thus, each

particular secondary structure component has a specific range of absorption as shown in Table 2.6.

Table 2.6. Assignment of amide I secondary structural components¹³³.

Secondary Structural Component	Frequency (cm ⁻¹)
α -helix	1642-1660
β -sheet	1615-1641, 1672-1695
Turns	1653-1691
Disordered	1639-1657

To recover quantitative information from the amide I band, two approaches have been mainly applied: (i) band-narrowing followed by curve-fitting of the component bands, and (ii) deconvolution into basis spectra with the aid of a calibration set of known proteins¹³³.

In the curve-fitting approach, the idea is to deconstruct the amide I into the contributing sub-bands to subsequently proceed with their assignment to secondary structural components. The procedure starts by applying a mathematical band-narrowing algorithm to determine the position and type of the component bands. At each position Gaussian curves are then fitted and integrated to estimate the percentage of contribution of each component. A variety of band-narrowing algorithms have been developed to resolve the amide I components including second derivative, Fourier deconvolution, and fine-structure enhancement. The minima of the second derivative are directly linked to each of the overlapping components.

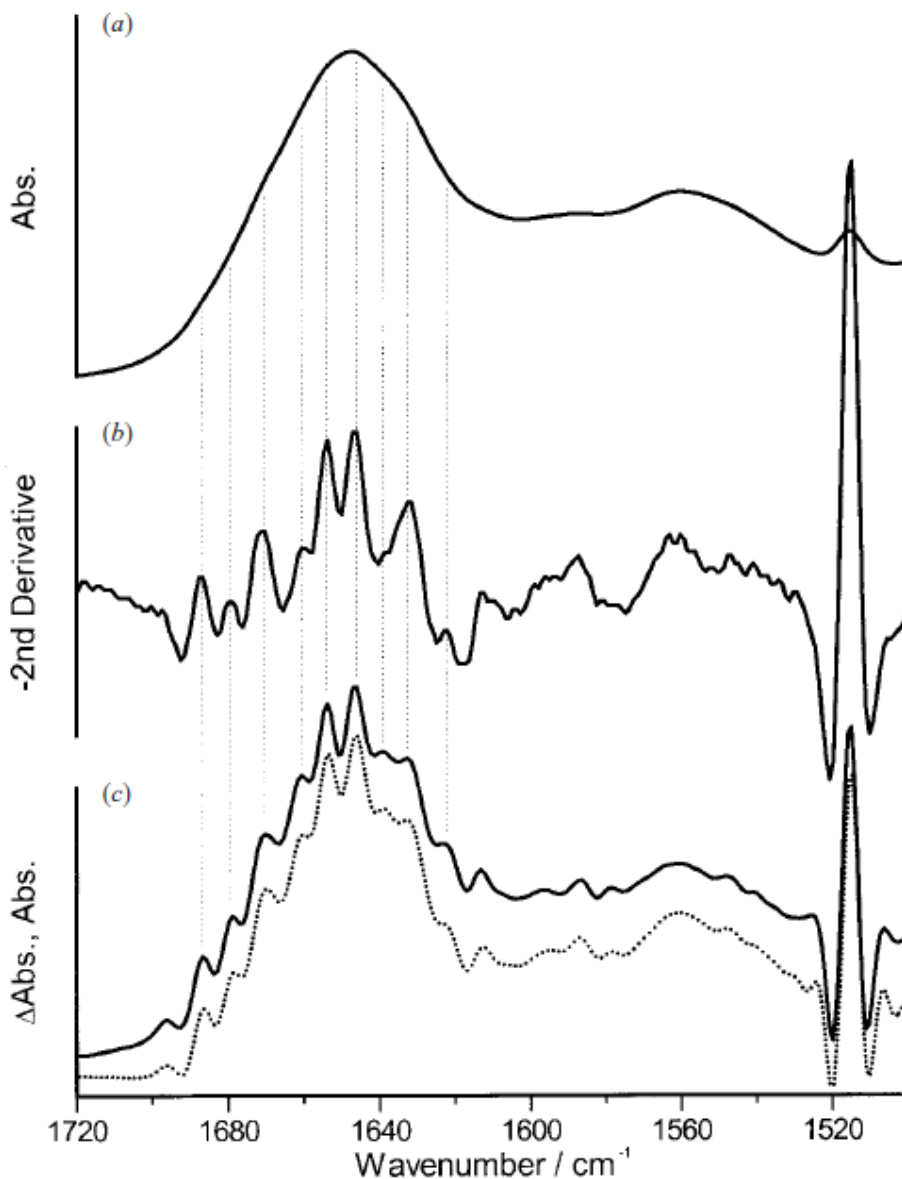


Figure 2.12. Comparison of the most commonly used band-narrowing techniques of protein amide I. (a) IR absorbance spectrum of papain recorded at 2 cm^{-1} resolution. (b) Second derivative of papain spectrum multiplied by -1 . The emerging peaks can be assigned to different secondary structural components according to Table 2.6. (c) (—) Fine structure enhancement with a smoothing range of 12 cm^{-1} and a weighting factor of 0.985 ; (---) Fourier self deconvolution using a Lorentzian line shape with a resolution enhancement factor of 2.6 . All three methods generated very similar component bands¹³³.

In the Fourier deconvolution method, the Fourier transform of the spectrum is multiplied by a line-shape-dependent function that produces sharper spectral characteristics where the component bands are located. In the fine-structure enhancement approach, the spectrum is smoothed out, multiplied by a factor, and subtracted from the original spectrum. This gives rise

to a much finer spectrum where structure details are exalted. The band-narrowing procedures are compared in Figure 2.12¹³³. After resolution enhancement with the band-narrowing algorithms, curve fitting procedures are applied to quantitatively estimate the contribution of each secondary structural component. One of the preferred methods is the Gaussian curve-fitting. In this approach, the spectrum is fitted by a sum of Gaussian bands. The area of each band can be estimated with conventional integration algorithms. The relative contribution of each structural component can be further calculated from their fractions of the total area of the amide I band. An example of the Gaussian curve-fitting procedure is shown in Figure 2.13.

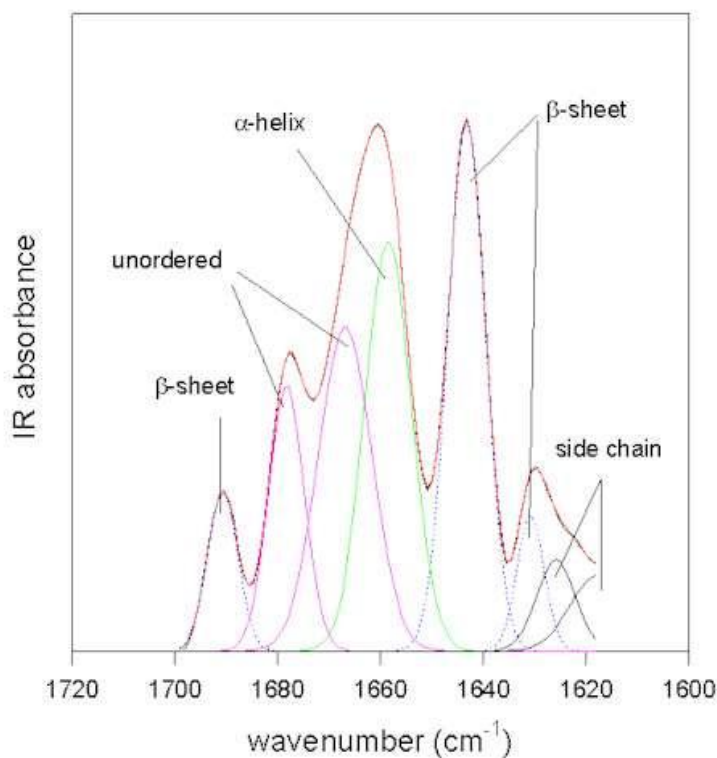


Figure 2.13. Gaussian curve-fitting of bovine pancreatic trypsin amide I spectrum. Gaussian bands for the individual structural components are shown in colors. The original spectrum was band-narrowed with Fourier self deconvolution. The fractions of the secondary structural components were 26% α -helix and 41% β -sheet, which are in agreement with 26% α -helix and 45% β -sheet obtained with X-ray analysis¹³⁵.

The second set of methods to quantify secondary structure mainly relies on the comparison with large databases of proteins with known structures. Partial least squares, factor analysis, and singular value decomposition algorithms are commonly implemented to reduce these large database sets to representative linearly independent spectra. These spectra are then

properly combined to reproduce the spectra of the unknown protein. This allows a complete quantification of the secondary structural content. IR spectra are collected with infrared spectrometers which are usually Fourier Transform Infrared Spectrometers (FTIR). In a conventional instrument layout, monochromatic light is generated by a source and subsequently divided in two with a beam splitter. The first beam, which is approximately 50% of the original beam, is reflected back to the splitter with a fixed mirror and passes through it to reach the detector.

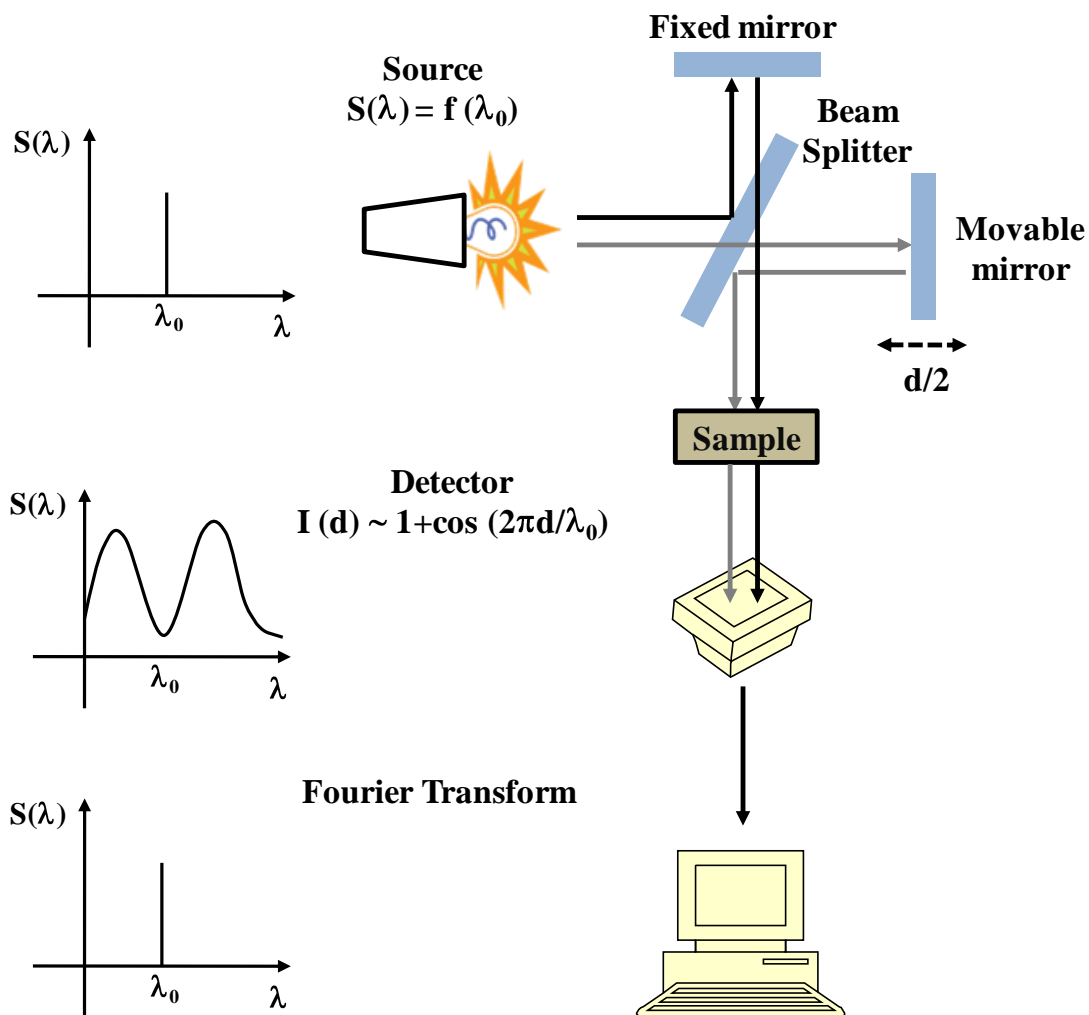


Figure 2.14. Basic instrumental arrangement of a Fourier Transform Infrared spectrometer¹³⁴.

The second beam is reflected in a movable mirror and returns to the splitter where only half passes and continues until is collected in the detector. These two beams have the chance to interfere with each other in the detector. Depending on the optical pathway (d) this interference

could be constructive or destructive. The instrument generates an interferogram of the light intensity relative to the position of the movable mirror. This interferogram is the Fourier transform of the spectrum ($S(\lambda)$). The measured data is then converted back into a spectrum ($S(\lambda)$) with a second Fourier transform. Figure 2.14 schematically describes a typical FTIR set up¹³⁴.

2.8 References

1. Carrea, G.; Riva, S., Properties and synthetic applications of enzymes in organic solvents. *Angewandte Chemie-International Edition* **2000**, 39, (13), 2226-2254.
2. Dordick, J. S., Enzymatic Catalysis in Monophasic Organic Solvents. *Enzyme and Microbial Technology* **1989**, 11, (4), 194-211.
3. Dordick, J. S., Nonaqueous Enzymology. *Current Opinion in Biotechnology* **1991**, 2, (3), 401-407.
4. Dordick, J. S., Designing Enzymes for Use in Organic-Solvents. *Biotechnology Progress* **1992**, 8, (4), 259-267.
5. Gupta, A.; Khare, S. K., Enzymes from solvent-tolerant microbes: Useful biocatalysts for non-aqueous enzymology. *Critical Reviews in Biotechnology* **2009**, 29, (1), 44-54.
6. Gupta, M. N., Enzyme Function in Organic-Solvents. *European Journal of Biochemistry* **1992**, 203, (1-2), 25-32.
7. Gupta, M. N.; Roy, I., Enzymes in organic media - Forms, functions and applications. *European Journal of Biochemistry* **2004**, 271, (13), 2575-2583.
8. Halling, P. J., Biocatalysis in low-water media: understanding effects of reaction conditions. *Current Opinion in Chemical Biology* **2000**, 4, (1), 74-80.
9. Hudson, E. P.; Eppler, R. K.; Clark, D. S., Biocatalysis in semi-aqueous and nearly anhydrous conditions. *Current Opinion in Biotechnology* **2005**, 16, (6), 637-643.
10. Khmelnitsky, Y. L.; Rich, J. O., Biocatalysis in nonaqueous solvents. *Current Opinion in Chemical Biology* **1999**, 3, (1), 47-53.
11. Kilbanov, A. M., Enzymes that Work in Organic-Solvents. *Chemtech* **1986**, 16, (6), 354-359.
12. Klibanov, A. M., Improving enzymes by using them in organic solvents. *Nature* **2001**, 409, (6817), 241-246.

13. Zaks, A.; Klibanov, A. M., Enzymatic Catalysis in Nonaqueous Solvents. *Journal of Biological Chemistry* **1988**, 263, (7), 3194-3201.
14. Zaks, A.; Russell, A. J., Enzymes in Organic-Solvents - Properties and Applications. *Journal of Biotechnology* **1988**, 8, (4), 259-270.
15. Ferrero, M.; Gotor, V., Biocatalytic selective modifications of conventional nucleosides, carbocyclic nucleosides, and C-nucleosides. *Chemical Reviews* **2000**, 100, (12), 4319-+.
16. Gotor, V., Biocatalysis applied to the preparation of pharmaceuticals. *Organic Process Research & Development* **2002**, 6, (4), 420-426.
17. Gotor, V., Biocatalysis applied to chemoselective transformations on Vitamin D and nucleoside derivatives. *Journal of Molecular Catalysis B-Enzymatic* **2002**, 19, 21-30.
18. Gotor-Fernandez, V.; Brieva, R.; Gotor, V., Lipases: Useful biocatalysts for the preparation of pharmaceuticals. *Journal of Molecular Catalysis B-Enzymatic* **2006**, 40, (3-4), 111-120.
19. Patel, R. N., Biocatalysis: Synthesis of chiral intermediates for drugs. *Current Opinion in Drug Discovery & Development* **2006**, 9, (6), 741-764.
20. Sharma, S. K.; Husain, M.; Kumar, R.; Samuelson, L. A.; Kumar, J.; Watterson, A. C.; Parmar, V. S., Biocatalytic routes toward pharmaceutically important precursors and novel polymeric systems. *Pure and Applied Chemistry* **2005**, 77, (1), 209-226.
21. Wang, H.; Zong, M. H.; Wu, H.; Lou, W. Y., Novel and highly regioselective route for synthesis of 5-fluorouridine lipophilic ester derivatives by lipozyme TL IM. *Journal of Biotechnology* **2007**, 129, (4), 689-695.
22. Wang, N.; Wu, Q.; Liu, B. K.; Cai, Y.; Lin, X. F., Enzyme-catalyzed regioselective synthesis of lipophilic guaifenesin ester derivatives. *Journal of Molecular Catalysis B-Enzymatic* **2004**, 27, (2-3), 97-102.
23. Wang, N.; Wu, Q.; Wu, W. B.; Quan, J.; Lin, M. F., Lipase-catalyzed regioselective synthesis of lipophilic inosine ester derivatives. *Journal of Molecular Catalysis B-Enzymatic* **2005**, 35, (1-3), 14-18.
24. Zinni, M. A.; Rodriguez, S. D.; Pontiggia, R. M.; Montserrat, J. M.; Iglesias, L. E.; Iribarren, A. M., Enzymatic alcoholysis of 3',5'-di-O-acetyl-2'-deoxynucleosides. *Journal of Molecular Catalysis B-Enzymatic* **2004**, 29, (1-6), 129-132.

25. Meyer, H. P.; Turner, N. J., Biotechnological Manufacturing Options for Organic Chemistry. *Mini-Reviews in Organic Chemistry* **2009**, 6, (4), 300-306.
26. Hudlicky, T.; Reed, J. W., Applications of biotransformations and biocatalysis to complexity generation in organic synthesis. *Chemical Society Reviews* **2009**, 38, (11), 3117-3132.
27. Serdakowski, A. L.; Dordick, J. S., Enzyme activation for organic solvents made easy. *Trends in Biotechnology* **2008**, 26, (1), 48-54.
28. Gorman, L. A. S.; Dordick, J. S., Organic Solvents Strip Water Off Enzymes. *Biotechnology and Bioengineering* **1992**, 39, (4), 392-397.
29. Klibanov, A. M., Why are enzymes less active in organic solvents than in water? *Trends in Biotechnology* **1997**, 15, (3), 97-101.
30. Lee, M. Y.; Dordick, J. S., Enzyme activation for nonaqueous media. *Current Opinion in Biotechnology* **2002**, 13, (4), 376-384.
31. Persson, M.; Mladenoska, I.; Wehtje, E.; Adlercreutz, P., Preparation of lipases for use in organic solvents. *Enzyme and Microbial Technology* **2002**, 31, (6), 833-841.
32. Kazandjian, R. Z.; Dordick, J. S.; Klibanov, A. M., Enzymatic Analyses in Organic-Solvents. *Biotechnology and Bioengineering* **1986**, 28, (3), 417-421.
33. Collins, K. D., Charge density-dependent strength of hydration and biological structure. *Biophysical Journal* **1997**, 72, (1), 65-76.
34. Cooke, R.; Kuntz, I. D., Properties of Water in Biological-Systems. *Annual Review of Biophysics and Bioengineering* **1974**, 3, 95-126.
35. Yang, L.; Dordick, J. S.; Garde, S., Hydration of enzyme in nonaqueous media is consistent with solvent dependence of its activity. *Biophysical Journal* **2004**, 87, (2), 812-821.
36. Soohoo, T. S.; Brown, A. D., A Basis of Specific Sodium Requirement for Morphological Integrity of *Halobacterium halobium*. *Biochimica et Biophysica Acta* **1967**, 135, (1), 164-&.
37. Lanyi, J. K., Salt-Dependent Properties of Proteins from Extremely Halophilic Bacteria. *Bacteriological Reviews* **1974**, 38, (3), 272-290.
38. Kim, J.; Dordick, J. S., Unusual salt and solvent dependence of a protease from an extreme halophile. *Biotechnology and Bioengineering* **1997**, 55, (3), 471-479.

39. Laane, C.; Boeren, S.; Vos, K.; Veeger, C., Rules for Optimization of Biocatalysis in Organic Solvents. *Biotechnology and Bioengineering* **2009**, 102, (1), 2-8.
40. Brulls, M.; Folestad, S.; Sparen, A.; Rasmuson, A., In-situ near-infrared spectroscopy monitoring of the lyophilization process. *Pharmaceutical Research* **2003**, 20, (3), 494-499.
41. Rupley, J. A.; Gratton, E.; Careri, G., Water and Globular-Proteins. *Trends in Biochemical Sciences* **1983**, 8, (1), 18-22.
42. Yu, N.; Jo, B. H., Comparison of Protein Structure in Crystals and in Solution by Laser Raman-Scattering .1. Lysozyme. *Archives of Biochemistry and Biophysics* **1973**, 156, (2), 469-474.
43. Gregory, R. B.; Gangoda, M.; Gilpin, R. K.; Su, W., The Influence of Hydration on the Conformation of Bovine Serum-Albumin Studied by Solid-State C-13-NMR Spectroscopy. *Biopolymers* **1993**, 33, (12), 1871-1876.
44. Prestrelski, S. J.; Arakawa, T.; Carpenter, J. F., Separation of Freezing-Induced and Drying-Induced Denaturation of Lyophilized Proteins Using Stress-Specific Stabilization .II. Structural Studies Using Infrared-Spectroscopy. *Archives of Biochemistry and Biophysics* **1993**, 303, (2), 465-473.
45. Griebenow, K.; Klibanov, A. M., Lyophilization-Induced Reversible Changes in the Secondary Structure of Proteins. *Proceedings of the National Academy of Sciences of the United States of America* **1995**, 92, (24), 10969-10976.
46. Schmid, A.; Dordick, J. S.; Hauer, B.; Kiener, A.; Wubbolts, M.; Witholt, B., Industrial biocatalysis today and tomorrow. *Nature* **2001**, 409, (6817), 258-268.
47. Fan, K. K.; Ouyang, P. K.; Wu, X. J.; Lu, Z. H., Prediction of aqueous phase pH for enzymatic synthesis of peptides in aqueous-organic biphasic systems. *Journal of Chemical Technology and Biotechnology* **2001**, 76, (8), 851-856.
48. Pavlidis, I. V.; Gournis, D.; Papadopoulos, G. K.; Stamatis, H., Lipases in water-in-ionic liquid microemulsions: Structural and activity studies. *Journal of Molecular Catalysis B-Enzymatic* **2009**, 60, (1-2), 50-56.
49. Dabulis, K.; Klibanov, A. M., Dramatic Enhancement of Enzymatic Activity in Organic Solvents by Lyoprotectants. *Biotechnology and Bioengineering* **1993**, 41, (5), 566-571.

50. Triantafyllou, A. O.; Wehtje, E.; Adlercreutz, P.; Mattiasson, B., How do additives affect enzyme activity and stability in nonaqueous media? *Biotechnology and Bioengineering* **1997**, *54*, (1), 67-76.
51. Murakami, Y.; Hoshi, R.; Hirata, A., Characterization of polymer-enzyme complex as a novel biocatalyst for nonaqueous enzymology. *Journal of Molecular Catalysis B-Enzymatic* **2003**, *22*, (1-2), 79-88.
52. Dai, L. Z.; Klibanov, A. M., Striking activation of oxidative enzymes suspended in nonaqueous media. *Proceedings of the National Academy of Sciences of the United States of America* **1999**, *96*, (17), 9475-9478.
53. Zacharis, E.; Moore, B. D.; Halling, P. J., Control of enzyme activity in organic media by solid-state acid-base buffers. *Journal of the American Chemical Society* **1997**, *119*, (50), 12396-12397.
54. Rich, J. O.; Dordick, J. S., Controlling subtilisin activity and selectivity in organic media by imprinting with nucleophilic substrates. *Journal of the American Chemical Society* **1997**, *119*, (14), 3245-3252.
55. Russell, A. J.; Klibanov, A. M., Inhibitor-Induced Enzyme Activation in Organic Solvents. *Journal of Biological Chemistry* **1988**, *263*, (24), 11624-11626.
56. Altreuter, D. H.; Dordick, J. S.; Clark, D. S., Nonaqueous biocatalytic synthesis of new cytotoxic doxorubicin derivatives: Exploiting unexpected differences in the regioselectivity of salt-activated and solubilized subtilisin. *Journal of the American Chemical Society* **2002**, *124*, (9), 1871-1876.
57. Lindsay, J. P.; Clark, D. S.; Dordick, J. S., Penicillin amidase is activated for use in nonaqueous media by lyophilizing in the presence of potassium chloride. *Enzyme and Microbial Technology* **2002**, *31*, (3), 193-197.
58. Ru, M. T.; Wu, K. C.; Lindsay, J. P.; Dordick, J. S.; Reimer, J. A.; Clark, D. S., Towards more active biocatalysts in organic media: Increasing the activity of salt-activated enzymes. *Biotechnology and Bioengineering* **2001**, *75*, (2), 187-196.
59. Khmelnitsky, Y. L.; Welch, S. H.; Clark, D. S.; Dordick, J. S., Salts Dramatically Enhance Activity of Enzymes Suspended in Organic Solvents. *Journal of the American Chemical Society* **1994**, *116*, (6), 2647-2648.

60. Triantafyllou, A. O.; Wehtje, E.; Adlercreutz, P.; Mattiasson, B., Effects of Sorbitol Addition on the Action of Free and Immobilized Hydrolytic Enzymes in Organic Media. *Biotechnology and Bioengineering* **1995**, 45, (5), 406-414.
61. Izutsu, K.; Yoshioka, S.; Terao, T., Effect of Mannitol Crystallinity on the Stabilization of Enzymes During Freeze-Drying. *Chemical & Pharmaceutical Bulletin* **1994**, 42, (1), 5-8.
62. Mi, Y. L.; Wood, G.; Thoma, L., Cryoprotection mechanisms of polyethylene glycols on lactate dehydrogenase during freeze-thawing. *Aaps Journal* **2004**, 6, (3), 10.
63. Lindsay, J. P.; Clark, D. S.; Dordick, J. S., Combinatorial formulation of biocatalyst preparations for increased activity in organic solvents: Salt activation of penicillin amidase. *Biotechnology and Bioengineering* **2004**, 85, (5), 553-560.
64. Eppler, R. K.; Komor, R. S.; Huynh, J.; Dordick, J. S.; Reimer, J. A.; Clark, D. S., Water dynamics and salt-activation of enzymes in organic media: Mechanistic implications revealed by NMR spectroscopy. *Proceedings of the National Academy of Sciences of the United States of America* **2006**, 103, (15), 5706-5710.
65. Wurges, K.; Pfromm, P. H.; Rezac, M. E.; Czermak, P., Activation of subtilisin Carlsberg in hexane by lyophilization in the presence of fumed silica. *Journal of Molecular Catalysis B-Enzymatic* **2005**, 34, (1-6), 18-24.
66. Gun'ko, V. M.; Zarko, V. I.; Voronin, E. F.; Turov, V. V.; Mironyuk, I. F.; Gerashchenko, II; Goncharuk, E. V.; Pakhlov, E. M.; Guzenko, N. V.; Leboda, R.; Skubiszewska-Zieba, J.; Janusz, W.; Chibowski, S.; Levchuk, Y. N.; Klyueva, A. V., Impact of some organics on structural and adsorptive characteristics of fumed silica in different media. *Langmuir* **2002**, 18, (3), 581-596.
67. Gun'ko, V. M.; Voronin, E. F.; Nosach, L. V.; Pakhlov, E. M.; Guzenko, N. V.; Leboda, R.; Skubiszewska-Zieba, J., Adsorption and migration of poly(vinyl pyrrolidone) at a fumed silica surface. *Adsorption Science & Technology* **2006**, 24, (2), 143-157.
68. Gun'ko, V. M.; Mikhailova, I. V.; Zarko, V. I.; Gerashchenko, II; Guzenko, N. V.; Janusz, W.; Leboda, R.; Chibowski, S., Study of interaction of proteins with fumed silica in aqueous suspensions by adsorption and photon correlation spectroscopy methods. *Journal of Colloid and Interface Science* **2003**, 260, (1), 56-69.
69. Pfromm, P. H.; Rezac, M. E.; Wurges, K.; Czermak, P., Fumed silica activated subtilisin Carlsberg in hexane in a packed-bed reactor. *AIChE Journal* **2007**, 53, (1), 237-242.

70. Suzawa, V. M.; Khmel'nitsky, Y. L.; Giarto, L.; Dordick, J. S.; Clark, D. S., Suspended and Immobilized Chymotrypsin in Organic Media - Structure-Function-Relationships Revealed by Electron-Spin-Resonance Spectroscopy. *Journal of the American Chemical Society* **1995**, 117, (32), 8435-8440.
71. Adlercreutz, P., On the Importance of the Support Material for Enzymatic-Synthesis in Organic Media - Support Effects at Controlled Water Activity. *European Journal of Biochemistry* **1991**, 199, (3), 609-614.
72. Sheldon, R., Enzyme immobilization: The quest for optimum performance. *Advanced Synthesis & Catalysis* **2007**, 349, (8-9), 1289-1307.
73. Polizzi, K. M.; Bommarius, A. S.; Broering, J. M.; Chaparro-Riggers, J. F., Stability of biocatalysts. *Current Opinion in Chemical Biology* **2007**, 11, (2), 220-225.
74. Asuri, P.; Bale, S. S.; Pangule, R. C.; Shah, D. A.; Kane, R. S.; Dordick, J. S., Structure, function, and stability of enzymes covalently attached to single-walled carbon nanotubes. *Langmuir* **2007**, 23, (24), 12318-12321.
75. Asuri, P.; Karajanagi, S. S.; Yang, H. C.; Yim, T. J.; Kane, R. S.; Dordick, J. S., Increasing protein stability through control of the nanoscale environment. *Langmuir* **2006**, 22, (13), 5833-5836.
76. Wehtje, E.; Adlercreutz, P.; Mattiasson, B., Improved Activity Retention of Enzymes Deposited on Solid Supports. *Biotechnology and Bioengineering* **1993**, 41, (2), 171-178.
77. Hyndman, D.; Lever, G.; Burrell, R.; Flynn, T. G., Protein Immobilization to Alumina Supports.1. Characterization of Alumina-Organophosphate Ligand Interactions and Use in the Attachment of Papain. *Biotechnology and Bioengineering* **1992**, 40, (11), 1319-1327.
78. Klibanov, A. M., Enzymes that Work in Organic-Solvents. *Chemtech* **1986**, 16, (6), 354-359.
79. Ryu, K.; Dordick, J. S., Free-Energy Relationships of Substrate and Solvent Hydrophobicities with Enzymatic Catalysis in Organic Media. *Journal of the American Chemical Society* **1989**, 111, (20), 8026-8027.
80. Reslow, M.; Adlercreutz, P.; Mattiasson, B., On the Importance of the Support Material for Bioorganic Synthesis - Influence of Water Partition Between Solvent, Enzyme and Solid Support in Water-Poor Reaction Media. *European Journal of Biochemistry* **1988**, 172, (3), 573-578.

81. Wang, P., Nanoscale biocatalyst systems. *Current Opinion in Biotechnology* **2006**, 17, (6), 574-579.
82. Chen, R. J.; Zhang, Y. G.; Wang, D. W.; Dai, H. J., Noncovalent sidewall functionalization of single-walled carbon nanotubes for protein immobilization. *Journal of the American Chemical Society* **2001**, 123, (16), 3838-3839.
83. Rege, K.; Raravikar, N. R.; Kim, D. Y.; Schadler, L. S.; Ajayan, P. M.; Dordick, J. S., Enzyme-polymer-single walled carbon nanotube composites as biocatalytic films. *Nano Letters* **2003**, 3, (6), 829-832.
84. Jia, H. F.; Zhu, G. Y.; Vugrinovich, B.; Kataphinan, W.; Reneker, D. H.; Wang, P., Enzyme-carrying polymeric nanofibers prepared via electrospinning for use as unique biocatalysts. *Biotechnology Progress* **2002**, 18, (5), 1027-1032.
85. Johnson, A. K.; Zawadzka, A. M.; Deobald, L. A.; Crawford, R. L.; Paszczynski, A. J., Novel method for immobilization of enzymes to magnetic nanoparticles. *Journal of Nanoparticle Research* **2008**, 10, (6), 1009-1025.
86. Vertegel, A. A.; Siegel, R. W.; Dordick, J. S., Silica nanoparticle size influences the structure and enzymatic activity of adsorbed lysozyme. *Langmuir* **2004**, 20, (16), 6800-6807.
87. Gasparac, R.; Kohli, P.; Mota, M. O.; Trofin, L.; Martin, C. R., Template synthesis of nano test tubes. *Nano Letters* **2004**, 4, (3), 513-516.
88. De, M.; Ghosh, P. S.; Rotello, V. M., Applications of Nanoparticles in Biology. *Advanced Materials* **2008**, 20, (22), 4225-4241.
89. Shim, M.; Kam, N. W. S.; Chen, R. J.; Li, Y. M.; Dai, H. J., Functionalization of carbon nanotubes for biocompatibility and biomolecular recognition. *Nano Letters* **2002**, 2, (4), 285-288.
90. Lundqvist, M.; Sethson, I.; Jonsson, B. H., Protein adsorption onto silica nanoparticles: Conformational changes depend on the particles' curvature and the protein stability. *Langmuir* **2004**, 20, (24), 10639-10647.
91. Roach, P.; Farrar, D.; Perry, C. C., Surface tailoring for controlled protein adsorption: Effect of topography at the nanometer scale and chemistry. *Journal of the American Chemical Society* **2006**, 128, (12), 3939-3945.
92. Karajanagi, S. S.; Vertegel, A. A.; Kane, R. S.; Dordick, J. S., Structure and function of enzymes adsorbed onto single-walled carbon nanotubes. *Langmuir* **2004**, 20, (26), 11594-11599.

93. Hong, R.; Fischer, N. O.; Verma, A.; Goodman, C. M.; Emrick, T.; Rotello, V. M., Control of protein structure and function through surface recognition by tailored nanoparticle scaffolds. *Journal of the American Chemical Society* **2004**, 126, (3), 739-743.
94. De, M.; Miranda, O. R.; Rana, S.; Rotello, V. M., Size and geometry dependent protein-nanoparticle self-assembly. *Chemical Communications* **2009**, (16), 2157-2159.
95. Escalante, M.; Zhao, Y. P.; Ludden, M. J. W.; Vermeij, R.; Olsen, J. D.; Berenschot, E.; Hunter, C. N.; Huskens, J.; Subramaniam, V.; Otto, C., Nanometer arrays of functional light harvesting antenna complexes by nanoimprint lithography and host-guest interactions. *Journal of the American Chemical Society* **2008**, 130, (28), 8892-+.
96. Ciesielski, P. N.; Scott, A. M.; Faulkner, C. J.; Berron, B. J.; Cliffel, D. E.; Jennings, G. K., Functionalized Nanoporous Gold Leaf Electrode Films for the Immobilization of Photosystem I. *ACS Nano* **2008**, 2, (12), 2465-2472.
97. Jonkheijm, P.; Weinrich, D.; Schroder, H.; Niemeyer, C. M.; Waldmann, H., Chemical Strategies for Generating Protein Biochips. *Angewandte Chemie-International Edition* **2008**, 47, (50), 9618-9647.
98. Farokhzad, O. C.; Langer, R., Impact of Nanotechnology on Drug Delivery. *Acs Nano* **2009**, 3, (1), 16-20.
99. Kam, N. W. S.; Liu, Z. A.; Dai, H. J., Carbon nanotubes as intracellular transporters for proteins and DNA: An investigation of the uptake mechanism and pathway. *Angewandte Chemie-International Edition* **2006**, 45, (4), 577-581.
100. Pantarotto, D.; Briand, J. P.; Prato, M.; Bianco, A., Translocation of bioactive peptides across cell membranes by carbon nanotubes. *Chemical Communications* **2004**, (1), 16-17.
101. Hirsch, L. R.; Stafford, R. J.; Bankson, J. A.; Sershen, S. R.; Rivera, B.; Price, R. E.; Hazle, J. D.; Halas, N. J.; West, J. L., Nanoshell-mediated near-infrared thermal therapy of tumors under magnetic resonance guidance. *Proceedings of the National Academy of Sciences of the United States of America* **2003**, 100, (23), 13549-13554.
102. Lambrianou, A.; Demin, S.; Hall, E. A. H., Protein engineering and electrochemical biosensors. In *Biosensing for the 21st Century*, Springer-Verlag Berlin: Berlin, 2008; Vol. 109, pp 65-96.
103. Kim, D. C.; Kang, D. J., Molecular Recognition and Specific Interactions for Biosensing Applications. *Sensors* **2008**, 8, (10), 6605-6641.

104. Wang, J., Nanomaterial-based electrochemical biosensors. *Analyst* **2005**, 130, (4), 421-426.
105. Chen, R. J.; Bangsaruntip, S.; Drouvalakis, K. A.; Kam, N. W. S.; Shim, M.; Li, Y. M.; Kim, W.; Utz, P. J.; Dai, H. J., Noncovalent functionalization of carbon nanotubes for highly specific electronic biosensors. *Proceedings of the National Academy of Sciences of the United States of America* **2003**, 100, (9), 4984-4989.
106. Wang, W. U.; Chen, C.; Lin, K. H.; Fang, Y.; Lieber, C. M., Label-free detection of small-molecule-protein interactions by using nanowire nanosensors. *Proceedings of the National Academy of Sciences of the United States of America* **2005**, 102, (9), 3208-3212.
107. Wang, J., Nanomaterial-based amplified transduction of biomolecular interactions. *Small* **2005**, 1, (11), 1036-1043.
108. Wang, J., Nanoparticle-based electrochemical bioassays of proteins. *Electroanalysis* **2007**, 19, (7-8), 769-776.
109. Norde, W., Driving forces for protein adsorption at solid surfaces. In *Biopolymers at Interfaces*, 2nd edn ed.; Marcel Dekker, Inc.: New York, 2003.
110. Unsworth, L. D.; van der Oost, J.; Koutsopoulos, S., Hyperthermophilic enzymes - stability, activity and implementation strategies for high temperature applications. *FEBS Journal* **2007**, 274, (16), 4044-4056.
111. Norde, W.; Zoungrana, T., Surface-induced changes in the structure and activity of enzymes physically immobilized at solid/liquid interfaces. *Biotechnology and Applied Biochemistry* **1998**, 28, 133-143.
112. Norde, W., My voyage of discovery to proteins in flatland ... and beyond. *Colloids and Surfaces B-Biointerfaces* **2008**, 61, (1), 1-9.
113. Kranz, B.; Burck, J.; Franzreb, M.; Koster, R.; Ulrich, A. S., Circular dichroism analysis of penicillin G acylase covalently immobilized on silica nanoparticles. *Journal of Colloid and Interface Science* **2007**, 316, (2), 413-419.
114. Yanagisawa, K.; Murakami, T. N.; Tokuoka, Y.; Ochiai, A.; Takahashi, M.; Kawashima, N., Immobilization and enzymatic activity of glucose oxidase on polystyrene surface modified with ozone aeration and UV irradiation in distilled water and/or aqueous ammonia solution. *Colloids and Surfaces B-Biointerfaces* **2006**, 48, (1), 67-71.

115. Unsworth, L. D.; Sheardown, H.; Brash, J. L., Protein resistance of surfaces prepared by sorption of end-thiolated poly(ethylene glycol) to gold: Effect of surface chain density. *Langmuir* **2005**, 21, (3), 1036-1041.
116. Koutsopoulos, S.; Tjeerdsma, A. M.; Lieshout, J. F. T.; van der Oost, J.; Norde, W., In situ structure and activity studies of an enzyme adsorbed on spectroscopically undetectable particles. *Biomacromolecules* **2005**, 6, (3), 1176-1184.
117. Koutsopoulos, S.; van der Oost, J.; Norde, W., Conformational studies of a hyperthermostable enzyme. *FEBS Journal* **2005**, 272, (21), 5484-5496.
118. Koutsopoulos, S.; Patzsch, K.; Bosker, W. T. E.; Norde, W., Adsorption of trypsin on hydrophilic and hydrophobic surfaces. *Langmuir* **2007**, 23, (4), 2000-2006.
119. Barrias, C. C.; Martins, C. L.; Miranda, C. S.; Barbosa, M. A., Adsorption of a therapeutic enzyme to self-assembled monolayers: effect of surface chemistry and solution pH on the amount and activity of adsorbed enzyme. *Biomaterials* **2005**, 26, (15), 2695-2704.
120. Giacomelli, C. E.; Norde, W., The adsorption-desorption cycle. Reversibility of the BSA-silica system. *Journal of Colloid and Interface Science* **2001**, 233, (2), 234-240.
121. Gun'ko, V. M.; Chuiko, A. A., Chemical Reactions at Fumed Silica Surfaces. In *Colloidal Silica: Fundamentals and Applications*, 1st ed.; Bergna, H. E.; Roberts, W. O., Eds. CRC Press: 2005; pp 467-496.
122. Gun'ko, V. M.; Zarko, V. I.; Turov, A. V.; Voronin, E. F.; Mironyuk, I. F.; Chuiko, A. A., Structural and Adsorptive Characteristics of Fumed Silicas in Different Media In *Colloidal Silica: Fundamentals and Applications*, 1st ed.; Bergna, H. E.; Roberts, W. O., Eds. CRC Press: 2005; pp 467-496.
123. Gun'ko, V. M.; Mironyuk, I. F.; Zarko, V. I.; Turov, V. V.; Voronin, E. F.; Pakhlov, E. M.; Goncharuk, E. V.; Leboda, R.; Skubiszewska-Zieba, J.; Janusz, W.; Chibowski, S.; Levchuk, Y. N.; Klyueva, A. V., Fumed silicas possessing different morphology and hydrophilicity. *Journal of Colloid and Interface Science* **2001**, 242, (1), 90-103.
124. Al-Malah, K., Modeling of Protein Adsorption Equilibrium at Hydrophobic Solid-Water Interfaces. In *Adsorption : Theory, Modeling, and Analysis*, Tóth, J., Ed. Marcel Dekker, Inc.: New York, 2002; pp 802-809.

125. Myers, J. K., The Origin and Measurement of Protein Conformational Stability. In *Conformational Stability, Size, Shape and Surface of Protein Molecules*, Uversky, V. N.; Permyakov, E. A., Eds. Nova Science Publishers, Inc.: New York, 2007.
126. Ross, J. B.; Laws, W. R.; Shea, M. A., Intrinsic Fluorescence in Protein Structure Analysis. In *Luminescence Spectroscopy and Circular Dichroism*, Uversky, V. N.; Permyakov, E. A., Eds. Nova Science Publishers, Inc.: New York, 2007.
127. Cooper, A., *Biophysical chemistry*. Royal Society of Chemistry: Cambridge, 2004.
128. Lees, J. G.; Miles, A. J.; Wien, F.; Wallace, B. A., A reference database for circular dichroism spectroscopy covering fold and secondary structure space. *Bioinformatics* **2006**, *22*, (16), 1955-1962.
129. Ganesan, A.; Moore, B. D.; Kelly, S. M.; Price, N. C.; Rolinski, O. J.; Birch, D. J. S.; Dunkin, I. R.; Halling, P. J., Optical Spectroscopic Methods for Probing the Conformational Stability of Immobilised Enzymes. *Chemphyschem* **2009**, *10*, (9-10), 1492-1499.
130. Kelly, S. M.; Jess, T. J.; Price, N. C., How to study proteins by circular dichroism. *Biochimica et Biophysica Acta-Proteins and Proteomics* **2005**, *1751*, (2), 119-139.
131. Greenfield, N. J., Using circular dichroism spectra to estimate protein secondary structure. *Nature Protocols* **2006**, *1*, (6), 2876-2890.
132. Barth, A., Infrared spectroscopy of proteins. *Biochimica et Biophysica Acta-Bioenergetics* **2007**, *1767*, (9), 1073-1101.
133. Barth, A.; Zscherp, C., What vibrations tell us about proteins. *Quarterly Reviews of Biophysics* **2002**, *35*, (4), 369-430.
134. Barth, A., Infrared Spectroscopy. In *Vibrational Spectroscopy*, Uversky, V. N.; Permyakov, E. A., Eds. Nova Science Publishers, Inc.: New York, 2007.
135. Byler, D. M.; Susi, H., Examination of the Secondary Structure of Proteins by Deconvolved FTIR Spectra. *Biopolymers* **1986**, *25*, (3), 469-487.

CHAPTER - 3 Immobilization of *Candida antarctica* Lipase B: Esterification of Geraniol in Hexane

3.1 Abstract

Enzymes are usually immobilized on solid supports or solubilized when they are to be used in organic solvents with poor enzyme solubility. We have reported previously on a novel immobilization method for *s. Carlsberg* on fumed silica with results that reached some of the best previously reported catalytic activities in hexane for this enzyme. Here we extend our method to *Candida antarctica* lipase B (CALB) as an attractive target due to the many potential applications of this enzyme in solvents. Our CALB/fumed silica preparations exceeded the catalytic activity of commercial Novozym 435® for a model esterification in hexane when an intermediate nominal surface coverage (%SC) of approximately 17% was approached. An intriguing observation was that the catalytic activity at first increases as more fumed silica was made available to the enzyme but then decreased precipitously below approximately 17%SC. This was not the case for *s. Carlsberg* where the catalytic activity leveled off at high relative amounts of fumed silica. We determined adsorption kinetics, performed variations of the pre-immobilization aqueous pH, determined the stability, and applied fluorescence microscopy to the preparations. A comparison with recent concepts by Gross et al. may point towards a rationale for an optimum intermediate surface coverage for some enzymes on solid supports.

3.2 Introduction

Enzyme based biocatalysts are an attractive option to perform the chemical synthesis of various compounds in non-aqueous media^{1, 2}. This approach has for example proven to be promising for the production of polymers^{3, 4}, anticancer and antiviral drugs⁵, aromas and fragrances^{6, 7}, and surfactants⁸. Performing biocatalysis in organic solvents is advantageous mainly because the solubility and stability of substrates and products are increased, thereby facilitating their transformation^{1, 9}, and because undesirable reactions, including hydrolysis, racemization, polymerization, and decomposition may be reduced when compared to aqueous systems^{1, 10}.

The catalytic activity of enzymes tends to decrease sharply when they are suspended in organic solvents compared to aqueous environments¹¹. Much effort has been focused on strategies to overcome this issue, including enzyme immobilization on porous and non-porous solid supports^{12, 13}, chemical modification of the enzymes' surfaces to improve compatibility with solvents¹⁴, protein engineering², and enzyme co-lyophilization with different types of excipients, such as cyclodextrins^{10, 15}, crown ethers¹⁵⁻¹⁷, and inorganic salts¹⁸⁻²⁰. Specifically, the co-lyophilization of enzymes with inorganic salts from aqueous solution, termed salt activation, has been remarkably successful. Salt activation has been reported to increase catalytic activity by three to four orders of magnitude compared to simply suspending the enzyme in the solvent²¹. We have recently reported a new immobilization technique based on co-lyophilization of an enzyme with commercial fumed silica (FS)^{22, 23}. The catalytic activity of *subtilisin Carlsberg* immobilized on fumed silica reached or even in some cases exceeded the best activities reported for salt activation while the immobilization process was somewhat simplified. Fumed silica is an amorphous material consisting of non-porous silica nanospheres fused into necklace-like structures, which is obtained by the hydrolysis of silicon tetra chloride in an O₂/H₂ flame^{24, 25}. Fumed silica possesses a large specific surface area and exhibits exceptional adsorptive affinity for various organic molecules in aqueous solution including proteins and polymers²⁶⁻³¹. The adsorption of proteins onto fumed silica has been reported to be essentially irreversible^{29, 32}. Adsorption is promoted by the formation of non-covalent interactions between the available groups on the surface of the fumed silica and the carbonyl or amino groups present in the enzyme molecules^{29, 32}. In general, these interactions are electrostatic in nature and driven by the net charges of the protein and the surface, therefore, they can be repulsive or attractive^{33, 34}. The main challenge when adsorbing enzymes on solid supports is to identify and predict the mechanisms that control these interactions, which are highly dependent on temperature, concentration, ionic strength and pH^{33, 34}. As enzymes exhibit a tremendous chemical and physical diversity, it is expected that multiple adsorption pathways may be significant. For instance, it has been reported that a pH change can increase enzyme adsorption and specific catalytic activity³⁵.

This work is aimed at extending the immobilization of enzymes on fumed silica for catalysis in hexane to Lipase B from *Candida antarctica* (CALB). Among lipases, CALB is one of the most recognized biocatalysts because of its high degree of selectivity in a broad range of

synthetic applications of industrial importance, including kinetic resolutions, aminolysis, esterification, and transesterification³⁶⁻³⁸. We benchmark our work against the commercial preparation Novozym 435 (Novozymes A/S), which consists of CALB physically adsorbed onto a macroporous acrylic polymer resin (Lewatit VP OC 1600, Bayer).

Gross and coworkers³⁹⁻⁴¹ have recently set out to further improve on the highly successful Novozym 435 by studying the protein-surface interactions. They discovered that catalytic activity improves with even distribution of the enzyme throughout the support and with increasing loadings/densities per area or volume of support material^{39, 40}. One concept put forth by Gross et al. is confirmed in the work with CALB presented here: optimum catalytic activity of an immobilized enzyme may be found not at low surface coverage but somewhat counter intuitively at an intermediate surface coverage.

Here we report a study of the immobilization of CALB on fumed silica by lyophilization, and the catalytic activity of the resulting preparations for a model esterification that we used previously^{6, 7, 42}. Adsorption of CALB on fumed silica pre-lyophilization from aqueous solution at different pH levels and silica-to-enzyme ratios was investigated by fluorescence microscopy. Catalytic competency, thermal stability, and stability during storage were examined.

The somewhat surprising maximum of catalytic activity at an intermediate surface loading of the enzyme on fumed silica is rationalized in light of recent similar results by Gross et al.³⁹⁻⁴¹ for the same enzyme on a different support.

3.3 Materials and Methods

3.3.1 Materials

Crude CALB (lyophilized; specific activity of 28U/mg solid) was obtained from Biocatalytics, Inc. (Pasadena, CA), stored at 4°C, and used as-received. Commercial Novozym 435® was purchased from Sigma, stored at 4°C, and used as-received. Novozym 435® is reported to be CALB immobilized on macroporous acrylic particles (0.3 - 0.9 mm diameter) with a reported catalytic activity of about 7,000 PLU/g (Propyl Laurate per gram).

Hexane (optima, as-received water content about 10 ppm), monobasic potassium phosphate (purity >99%), acetate buffer solution (pH 4.0, certified), sodium bicarbonate

(certified ACS), and glacial acetic acid (optima, purity >99.7%) were from Fisher Scientific (Pittsburgh, PA). Fumed silica (purity of 99.8%, specific surface area 258 m²/g, primary particle diameter ~7-50 nm, as reported by the manufacturer), geraniol (purity 98%), and geranyl acetate (purity 98%) were from Sigma-Aldrich (St. Louis, MO), and used as received. Glass vials (24 mL or 125 mL for low and high wt% fumed silica, respectively, screw-capped, flat-bottom) were used for lyophilization of the aqueous enzyme-fumed silica suspensions. Glass vials (24 mL or 2 mL, Teflon screw-capped, flat-bottom) were used to perform the batch activity assays.

3.3.2 Enzyme Immobilization

An overview of our immobilization procedure on fumed silica is given here with details available elsewhere ²². Crude CALB was weighed in a glass vial followed by aqueous buffer addition, and vortexing for about 30 seconds. Fumed silica was added, and the mixture was vortexed for 2-3 minutes resulting in a visually homogeneous suspension. This suspension was sonicated for ten minutes in a water bath (room temperature) and then placed in a refrigerator at -20°C for several hours until frozen. The frozen sample was then lyophilized (48h primary drying, 24h secondary drying, VirTis model 10-MR-TR; Gardiner, NY). Table 3.1 shows a summary of the amounts of fumed silica and buffer used to form our preparations at the various %SC of enzyme in the final CALB/fumed silica preparations. The %SC values in the final preparation are calculated from the mass of crude CALB and the mass of fumed silica initially weighted in (Table 3.1). The mass of buffer salts that may be contained in the final preparations is at most 10wt% of the final preparation and was neglected for calculation of the %SC in the final preparations.

3.3.3 Enzyme Adsorption Kinetics

CALB adsorption from the aqueous phase on fumed silica was followed for 9 minutes after vortexing for about 30 seconds. The aqueous pH was pre-adjusted to 4.0, 7.8 and 9.5 using 50 mM sodium acetate buffer, 10 mM monobasic phosphate buffer, or 50 mM sodium carbonate/bicarbonate buffer, respectively. The concentration in solution was measured spectrophotometrically at 595 nm (Bradford assay ⁴³). The amount of adsorbed CALB was then calculated by mass balance.

Table 3.1. Summary of the amount of fumed silica and buffer employed to prepare CALB supported nanobiocatalysts with different nominal surface coverages (%SC). In all cases, the amount of crude CALB was 5.83 mg.

Target preparations (Nominal Surface Coverage [%SC])	Aqueous buffer [mL]	Fumed Silica^a [mg]	Enzyme concentration [mg/mL]	Amount of preparation containing 35 U (mg of lyophilized preparation^b)
2	58.3	651.3	0.1	131.4
4	58.3	325.7	0.1	66.3
12	19.4	108.6	0.3	22.9
17	8.3	76.6	0.7	16.5
230	1.5	5.7	4.0	2.3
538	1.1	2.4	5.1	1.7
2087	0.9	0.6	6.3	1.3
N/A	0.9	0.0	6.7	1.2
Novozym 435®	-	-	-	5.0

^aThe required mass of fumed silica was calculated according to the following expressions:

$$(1) \text{ Area of FS} = (3.32 \text{ m}^2 / \%SC) * 100$$

where 3.32 m² is the projected area of enzyme (assuming a diameter of 6.4 nm for CALB) and %SC is the targeted nominal surface coverage.

$$(2) \text{ mgFS} = (\text{Area of FS} / 255 \text{ m}^2/\text{g}) * 1000$$

^bThe amount of preparation containing 35U of activity (mg 35U) is computed as follows:

$$(3) \text{ Units/mg preparation} = (\text{Units of weighed CALB}) / (\text{mgFS} + \text{mgCALB})$$

where mgFS are the milligrams of fumed silica and mgCALB the milligrams of crude CALB

$$(4) \text{ mg35U} = 35\text{U} / \text{Units/mg preparation}$$

3.3.4 Transmission Electron Microscopy (TEM) Analysis

An FEI CM100 Transmission Electron Microscope (100 kV) equipped with an AMT digital image capturing system was used. Only enzyme preparations obtained from adsorption at pH 7.8 were analyzed.

3.3.5 Imaging of Enzyme Distribution on Fumed Silica Surfaces by Confocal Laser Scanning Microscopy

CALB was labeled with Alexa Fluor® 488 carboxylic acid, TFP ester, bis (triethylammonium salt) (Ex:494 nm, Em:519 nm, MW~885) following the procedures provided by Molecular Probes. Briefly, 0.5 mL of CALB solution (2 mg/mL in Phosphate Buffered Saline (PBS)) was added to a vial of reactive dye. The mixture was then stirred in the dark for 1 hour at room temperature. Unbound Alexa Fluor® 488 was separated from the conjugated CALB by size exclusion chromatography (Bio-Rad Biogel P-6 size exclusion purification resin). The conjugated CALB fraction was collected and stored at 4°C in PBS buffer. Immobilization of Alexa Fluor conjugated CALB on fumed silica was then performed as described previously (see section 3.3.2). To determine the distribution of CALB immobilized on fumed silica, confocal laser scanning microscopy was employed (Zeiss Pascal 5 Laser Scanning Microscope). The fluorescence emission signal was obtained through a dichroic mirror (NFT 545) and a 535±30 nm band pass filter. Images were captured through a Plan Apochromat Objective 100x, 1.4NA, and oil immersion. The distribution analysis was performed only for enzyme preparations obtained from adsorption at pH 7.8.

3.3.6 Analytical Methods for Assays in Hexane

Gas chromatography was used to detect geranyl acetate (product) and geraniol (reactant) in the reaction mixtures. 1 µL of the reaction solution was injected into a Varian Model 3800 gas chromatograph (GC, FID, HP-5 crosslinked 5% HP ME siloxane column, 30 m, 0.25 mm i.d., 0.25 µm film thickness, column 120°C, injector and detector 250°C, split ratio 1/200, Hewlett Packard). Alternatively, a capillary column DB-WAX (30 m, 0.25 mm i.d., linear column temperature ramp 56-200°C at 30°C/min; J&W Scientific) was used.

3.3.7 Initial Reaction Rate Measurements and Kinetic Parameters

Initial reaction rates were measured in a solution of substrates (geraniol and acetic acid), and products formed (geranyl acetate (GerAc) and water) in hexane. The reaction rate remains essentially constant below about 20% of conversion. Thus, the initial reaction rates were determined by linear fitting of the data up to about 65 min. The reactions were carried out catalyzed by our preparations or the commercial Novozym 435 in 24-mL vials (reaction volume 5 ml, $30\pm 0.05^\circ\text{C}$). An equivalent of 35 PLU was always employed (Table 3.1). Fumed silica only showed no catalytic activity.

The apparent kinetic constants (maximum velocity, V_{mG} , and Michaelis-Menten constant, K_{mG} , where G stands for geraniol) at pH 7.8 were determined by carrying out the enzymatic reactions at initial geraniol concentrations ranging from 35–100 mM. The initial acid concentration was always maintained at 100mM. Lineweaver-Burk plots were used.

3.3.8 Thermal Stability Measurements

Temperature stability was investigated by measuring the initial reaction rates at 40, 55, and 70°C for our preparations prepared from pH 7.8 aqueous suspensions only. Novozym 435 was also evaluated for reference.

3.3.9 Storage Stability in Hexane

Enzyme preparations containing 17%SC, 12%SC, 4%SC, and 2%SC fumed silica were suspended in 5 mL of hexane and incubated at 30°C under shaker agitation (250 rpm). After selected incubation times, the substrates were added and the product formation followed as described previously. Only enzyme preparations obtained from adsorption at pH 7.8 were analyzed.

3.3.10 Long-Term Stability

The long-term stabilities were determined by measuring the initial reaction rate after storage of lyophilized preparations in closed vials at 4°C for 6 months. Only enzyme preparations obtained from adsorption at pH 7.8 were analyzed.

3.4 Results and Discussion

Würges et al. have recently reported on a highly active immobilizate of the protease *subtilisin Carlsberg* on fumed silica for biocatalysis in hexane²². This previous work is extended here to immobilization of the hydrolase CALB on fumed silica. CALB is an attractive enzyme for enzymatic catalysis in solvents^{3, 4, 37, 44-48}. Some aspects of the immobilization process and the physical characteristics of the immobilizate are discussed below before presenting results for enzymatic catalysis using the CALB/fumed silica immobilizate.

Fumed silica is generally thought to consist of solid spherical primary particles (several nm diameter) formed by a flame hydrolysis process^{24, 25, 49}. The primary particles fuse into necklace-like structures which then form entangled agglomerates with a size on the order of 100nm. Both the synthesis process and the resulting material are fundamentally different from silica gel^{49, 50}. A transmission electron micrograph of a CALB/fumed silica immobilizate reveals the expected size of the fumed silica aggregates (order of 100nm) with some indication of individual fumed silica particles in the expected necklace-like arrangement visible between the agglomerates (Figure 3.1). A schematic rendition of a fumed silica agglomerate is also shown.

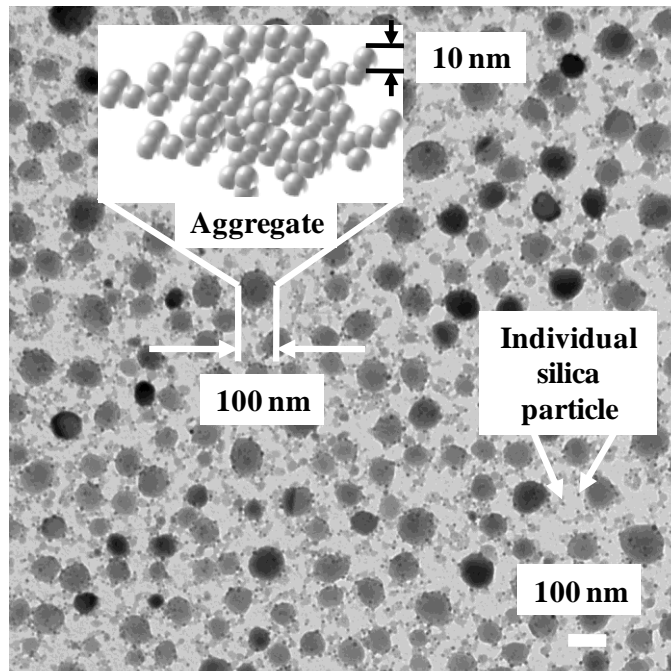


Figure 3.1. Transmission Electron Microscopy (TEM) image and schematic representation of a typical lyophilized fumed silica/enzyme preparation.

The initial interaction of CALB with fumed silica in aqueous suspension before freezing and lyophilization was explored by varying the pH of the aqueous phase using different buffers. Enzyme adsorption was tracked by difference using the Bradford assay of the liquid phase. Typical kinetic adsorption data in aqueous solution are shown in Figure 3.2. The data indicates that sorption equilibrium was reached or at least approached.

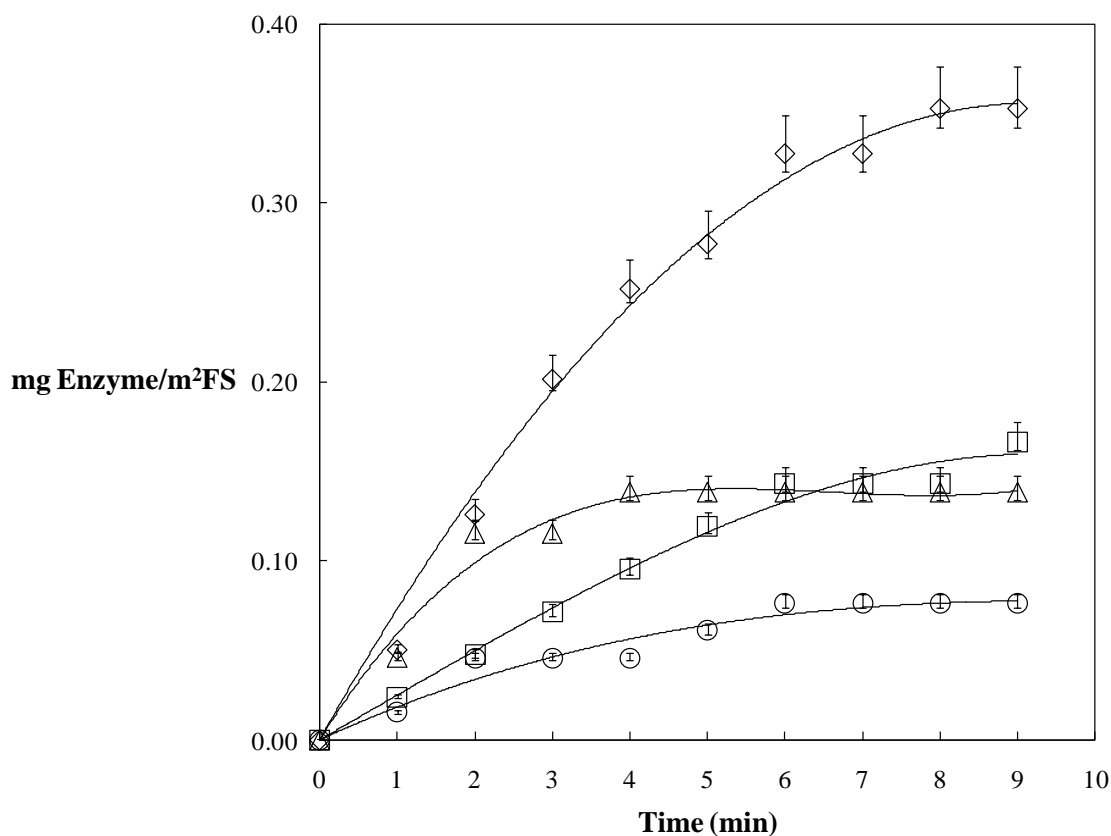


Figure 3.2. Adsorption kinetics of CALB on fumed silica in aqueous suspensions at pH7.8 (phosphate buffer, 0.1M; 25 °C). Surface coverage: (◇) 17%SC, (□) 12%SC, (△) 4%SC, (○) 2%SC (y-error bars represent the standard error of multiple analyses of identical samples).

Figure 3.3 shows the combined end points of the adsorption experiments at different pH values. From 2%SC to 12%SC (%SC = 100*(projected area of enzyme/nominal surface area of FS)) the adsorption proceeds to the maximum expected surface loading (indicated by the diagonal line), independent of pH. The values in the line were calculated by dividing the mass of enzyme by the nominal surface area of the mass of fumed silica weighed in as reported by the manufacturer. It appears that there are sufficient opportunities for all of the enzyme material to

adsorb on the fumed silica, both below and above the isoelectric point of CALB as long as the silica surface area is abundant.

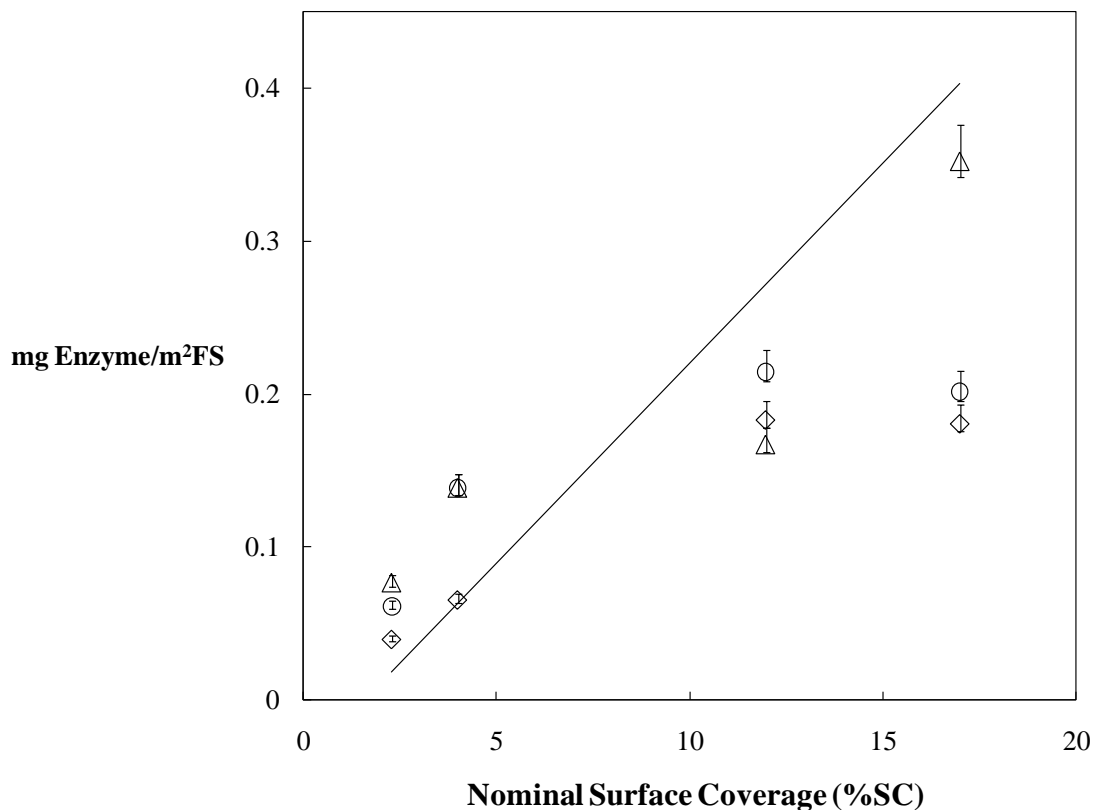


Figure 3.3. Surface loading of fumed silica with enzyme at different pH values as a function of the nominal surface coverage. (Δ) pH = 4.0, (\diamond) pH = 7.8, (\circ) pH = 9.5. Data obtained from the final steady-state of the adsorption kinetics experiments. The solid line is calculated by dividing the mass of enzyme weighed in by the nominal surface area of the fumed silica that was used. The impact of pH relative to the isoelectric point is only important when surface area availability start to be reduced (Above 12%SC).

When the surface area for interaction becomes more scarce, however (near 12%SC and above) the data seem to indicate that the strong expected electrostatic interaction between silica (negative) and enzyme (positive) below the isoelectric point becomes more important. This leads to lower adsorption above the isoelectric pH when the fumed silica area is scarcer. This situation is schematically shown in Figure 3.4. The catalytic experiments reported below were all performed with immobilizates originating from aqueous solution at pH 7.8.

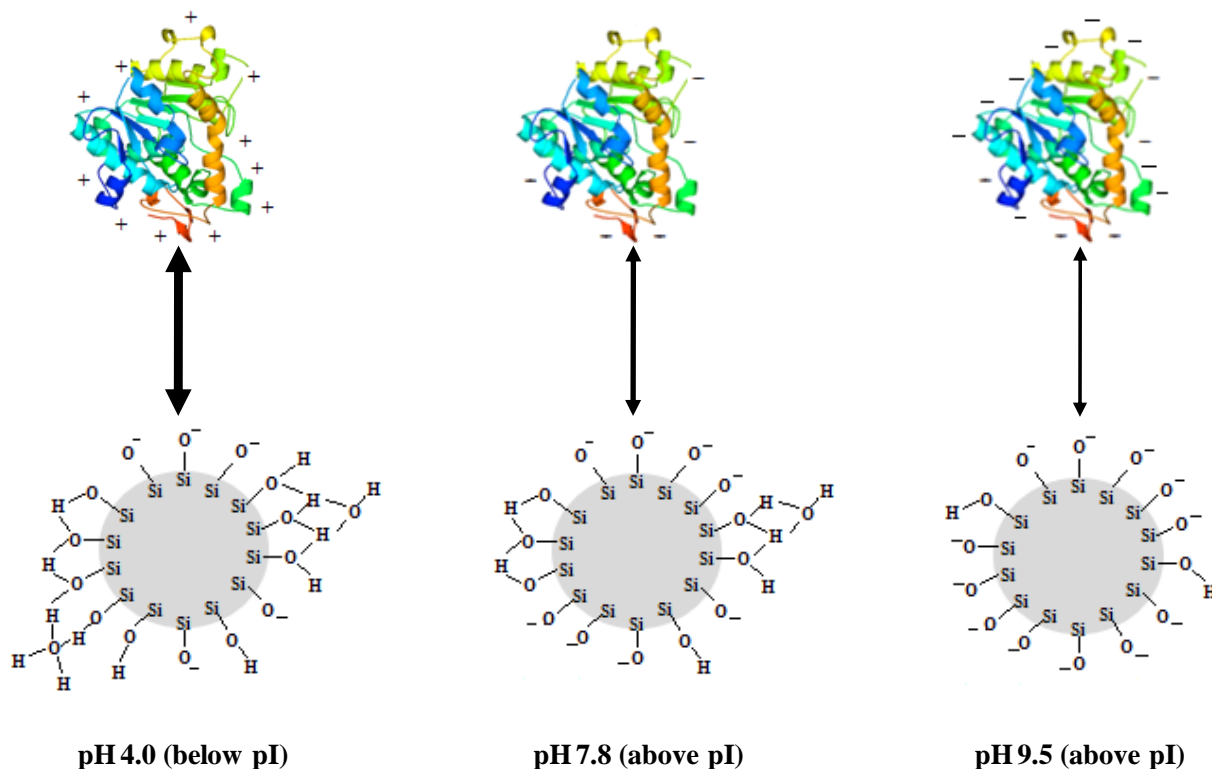


Figure 3.4. Schematic of surface charges for CALB and fumed silica nanoparticles in aqueous suspensions relative to the isoelectric point (pI). (Water molecules are not shown). Arrow widths illustrate the anticipated strength of the electrostatic interactions.

The question of how the enzyme is distributed on the fumed silica surfaces can be investigated using laser confocal microscopy of the immobilizate in hexane. The more uniform appearance in Figure 3.5 panel A compared to the more clustered appearance in panel B reflects our experience that the dispersion of the fumed silica/enzyme immobilizate in hexane is more uniform for preparations at lower %SC likely due to the surface properties of silica being more prominent at low %SC. The roughly doubled surface intensities from 2%SC to 4%SC fumed silica (Figure 3.5 panel A1 vs. panel B1) correspond to a theoretical estimate of an increased in surface loading (mg enzyme/m² fumed silica) of 34% when assuming the nominal surface area of fumed silica, and a known size of CALB (all protein assumed as CALB⁵¹). The reasonable correlation of the predicted increase in surface loading from simple mass balance and physical size of the molecule vs. the available nominal area, and the direct evidence by confocal microscopy also confirms that the enzyme largely remains with the immobilizate and is not lost elsewhere.

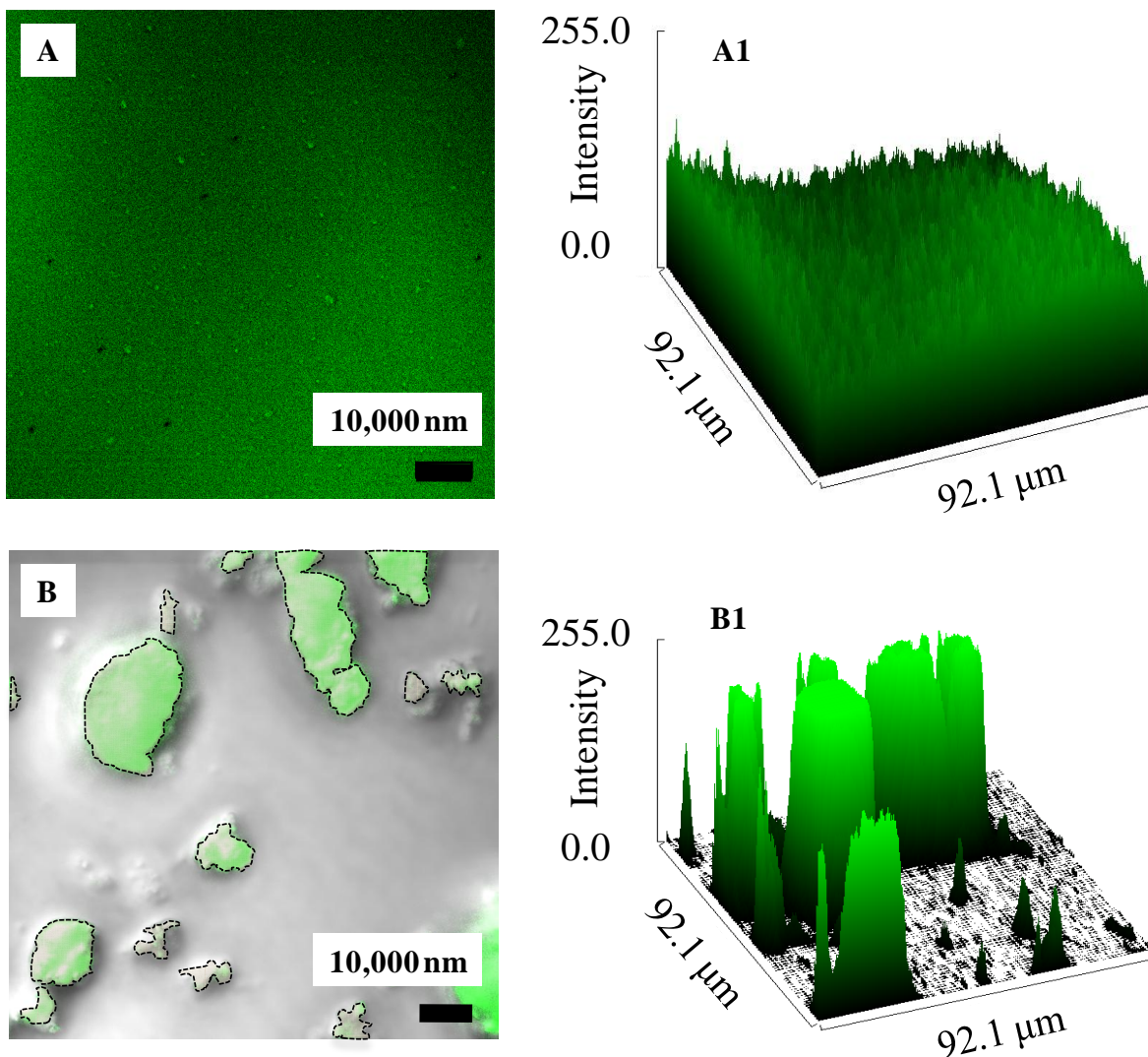


Figure 3.5. Confocal images of the distribution of CALB immobilized on fumed silica (FS). (A) 2%SC and (B) 4%SC. The corresponding surface fluorescence intensities are shown in panels A1 and B1. The doubling of the intensity corresponds roughly to a doubling of the enzyme loading per area of fumed silica (Figure 3.3, 4%SC and 2%SC, diamond symbols). The originally green fluorescence areas in panel B are emphasized by dashed contours.

The catalytic performance of our CALB/fumed silica preparations was first successfully benchmarked against our previous work with CALB where we used Novozym 435⁷ (data not shown).

The catalytic activity of CALB/fumed silica preparations significantly increased as the nominal surface coverage approached 17%SC (Figure 3.6). Our preparations exceeded the commercial Novozym 435 on an equivalent PLU basis.

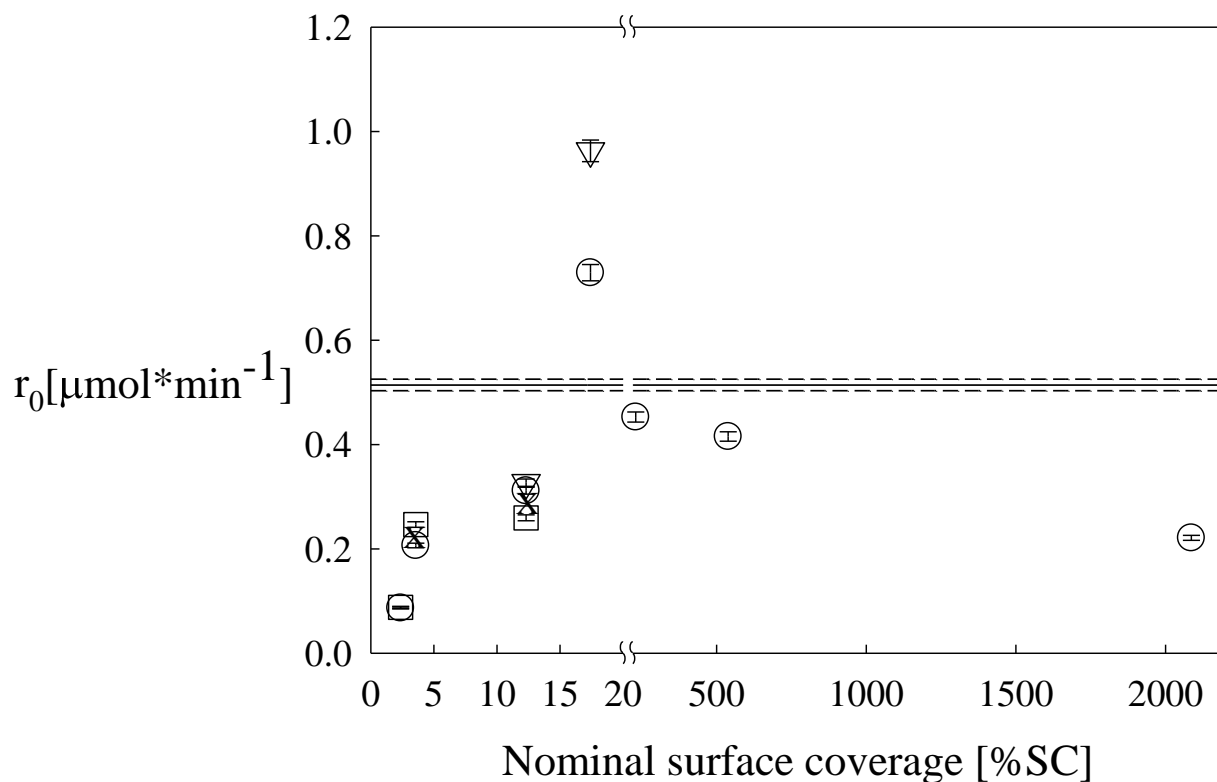


Figure 3.6. Catalytic activity of CALB immobilized on fumed silica as a function of the nominal surface coverage in the final preparation. Geraniol: 0.1 M. (○) Experiments over the entire domain of %SC. Experiments to confirm the surprising decrease in reaction rate at high fumed silica content: (▽) first replica of 17%SC and 12%SC fumed silica, (□) second replica of 12%SC, 4%SC and 2%SC, (×) test to rule out mass transfer limitations, reaction volume 15 mL, 12%SC and 4%SC. Solid line represents Novozym 435®; dashed lines and y-error bars represent the cumulative standard error from the calculation of conversion and the linear assumption of the initial reaction rate.

However, while the catalytic activity for *s. Carlsberg* immobilized on fumed silica in our previous work²² slowly increased further and essentially leveled off when even more fumed silica surface area was available for adsorption (i.e., at %SC below 17%) we found a precipitous drop in the activity for CALB at high fumed silica content. We successfully replicated this surprising result at high fumed silica content by testing two additional batches of each %SC referred to as first and second replicas in Figure 3.6. The possibility of mass transfer limitations causing the drop in activity at high fumed silica content was excluded through a reference test with 1/3 of the CALB/fumed silica preparation in the same amount of solution. The activity was not substantially different suggesting that mass transfer limitations are likely not responsible for

the drop in catalytic activity at high fumed silica content. We therefore conclude that the steep drop in catalytic activity at high fumed silica content for CALB preparations is indeed a real phenomenon that highlights the subtle differences between different enzymes even when they are immobilized with identical procedures on the same solid support. A possible rationale for the somewhat counterintuitive activity decrease as abundant area becomes available for enzyme immobilization is attempted below.

According to Gun'ko et al.³², the adsorption of proteins (e.g., Bovine Serum Albumin) on fumed silica in aqueous suspensions has many intricacies and depends on the morphology of the fumed silica, the protein type and concentration, pH, ionic strength, and fumed silica concentration, among other parameters. To form the preparations at the various %SC shown here, a rapidly increasing amount of fumed silica was required (Table 3.1). Prior to lyophilization, the area of fumed silica per mass of protein (enzyme plus any inactive proteins in our purchased crude enzyme) available for adsorption is significantly larger at low %SC. One might speculate that below 17%SC, the probability of strong surface/protein interactions as opposed to protein-protein interactions significantly increases. Confinement of the enzyme molecules by multipoint attachment of the enzyme to the fumed silica surface (for example in the “neck” regions of the fused spherical primary silica particle necklaces) may lead to detrimental structural changes of the enzyme. Enzyme molecules may also deactivate simply by strong interaction with silica at high silica surface availability.

Recently, Gross and coworkers have physically adsorbed CALB on a series of macroporous polymeric supports and have investigated catalytic activity in ring opening polymerizations and polycondensations in organic solvents³⁹⁻⁴¹. Gross et al. suggested that CALB molecules adsorbed in a more close-packed configuration are more likely to preserve their native structure and catalytic activity than when CALB molecules are adsorbed widely separated from one another^{39, 40}. In agreement with our findings, Gross et al. demonstrated that an intermediate enzyme loading can be found where no further improvement in activity is detected when more support material is provided per unit mass of enzyme. Their data suggest that this optimum enzyme/support ratio is highly dependent on the surface chemistry and morphology of the adsorbent. This research group has also reported that CALB molecules spread upon adsorption on their supports as has been suggested elsewhere for “soft” proteins⁵². This

effect is likely to be accentuated when excessive area is available for adsorption supporting the notion that structural changes are promoted at low %SC in our preparations (Figure 3.7).

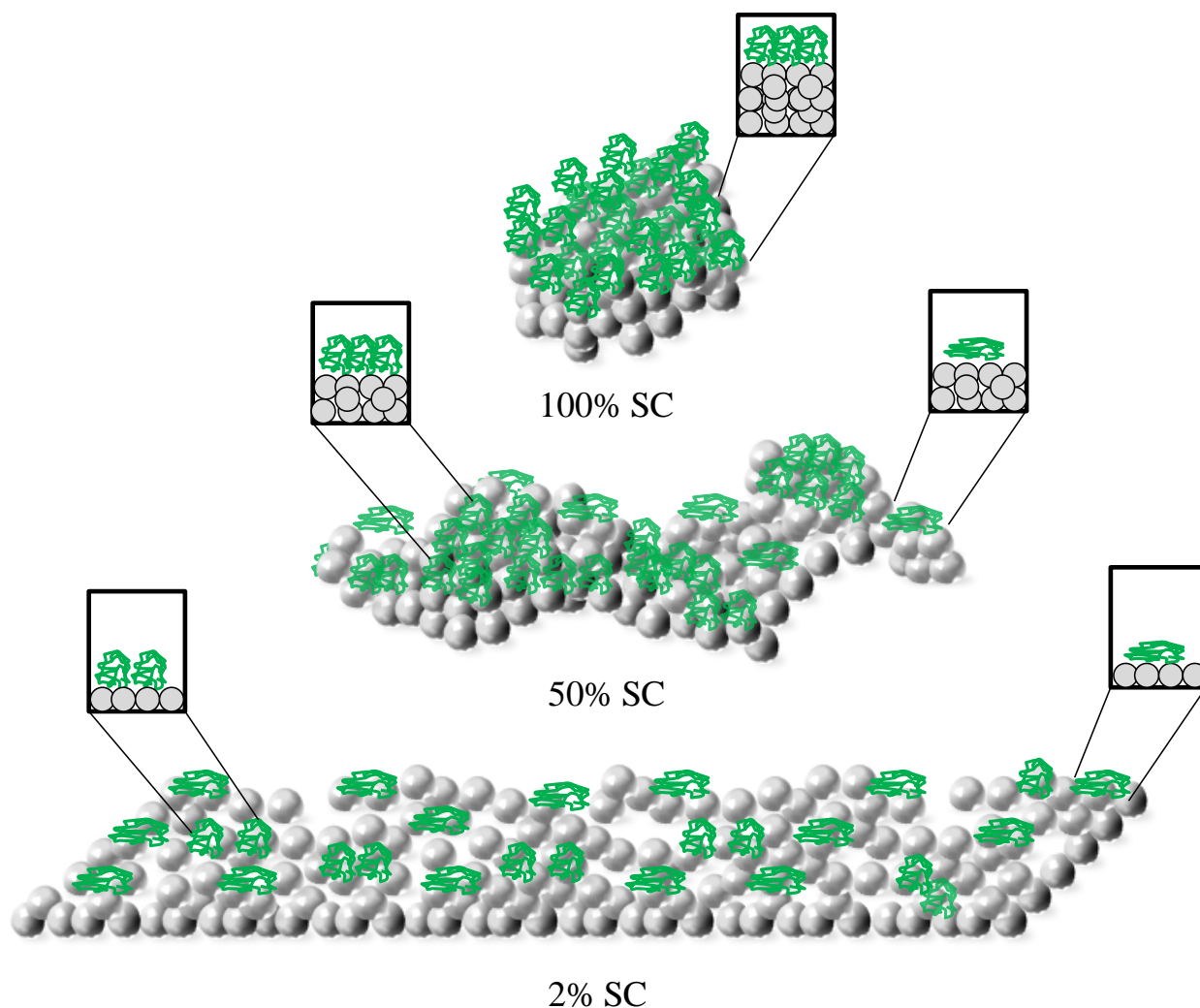


Figure 3.7. Schematic model for enzyme/fumed silica interactions at different surface loadings. The enzyme arrangement changes from a crowded surface to approximately single molecule adsorption as the surface availability increases. The opportunity for maximum interaction of the enzyme with fumed silica is perhaps enhanced by surface topography (availability of “neck” positions) may lead to detrimental deformation of the enzyme molecule. (Based on concepts put forth by Gross et al.^{39, 40}. The schematic is roughly to scale, primary fumed silica nanoparticle diameter ~10 nm; CALB molecular diameter ~6 nm⁵¹).

To benchmark our best preparations against Novozym 435® we compared the apparent kinetic constants K_m (ability to bind substrate) and V_m (max. rate of reaction with sufficient substrate) as well as the catalytic efficiency (V_m / K_m) (Table 3.2)⁵³. The catalytic efficiency for

our 17%SC preparation and Novozym 435® are of the same order of magnitude. In addition, Table 3.2 shows that the catalytic efficiency of our 17%SC preparation was about 90% higher compared to 2087%SC. This confirms the crucial role of fumed silica availability relative to adsorbing enzyme in enhancing the catalytic activity of the enzyme. The effectiveness factor (the ratio of the observed reaction rate and the reaction rate absent all diffusional limitations) is also shown in Table 3.2. The effectiveness factors for our preparations approach unity. This demonstrates the absence of diffusion limitations for adsorbed enzyme on the non-porous fumed silica nanoparticle aggregates. CALB molecules are confined to particle surfaces where their exposure to substrate molecules is maximized. In contrast, Novozym 435 shows an effectiveness factor of 0.2 likely due to diffusion limitations in the confined spaces of the porous support beads.

Table 3.2. Apparent kinetic constants and catalytic efficiency of CALB co-lyophilized with fumed silica (FS) compared to Novozym 435®

Preparation	V_{mG} ($\mu\text{mol}_{\text{GerAc}}/\text{min}$)	K_{mG} (mM)	Catalytic efficiency	Effectiveness
			V_{mG} / K_{mG} ($\mu\text{mol}_{\text{GerAc}} \text{min}^{-1} \text{mM}^{-1}$)	factor η
2087%SC	0.3	238	0.0014	0.9998
538%SC	3.6	781	0.0046	0.9614
230%SC	1.5	245	0.0063	0.9951
17%SC	1.8	161	0.0114	0.9928
Novozym 435®	2.7	204	0.0134	0.2144

Figure 3.8 shows the catalytic activity of our preparations up to 70°C. As the temperature is increased from 30°C to 40°C an Arrhenius-type activation is observed for all preparations. A clear and increasing loss of activity is however detected at 55°C and above. The 2%SC preparation is still somewhat active at 70°C where the other fumed silica preparations are almost completely deactivated. This appears consistent with the stabilization of adsorbed enzymes by solid supports^{33, 54}. The catalytic activity of Novozym 435 up to 70°C is also shown. A similar Arrhenius-type activation is observed but Novozym 435 is significantly more temperature stable than our preparations.

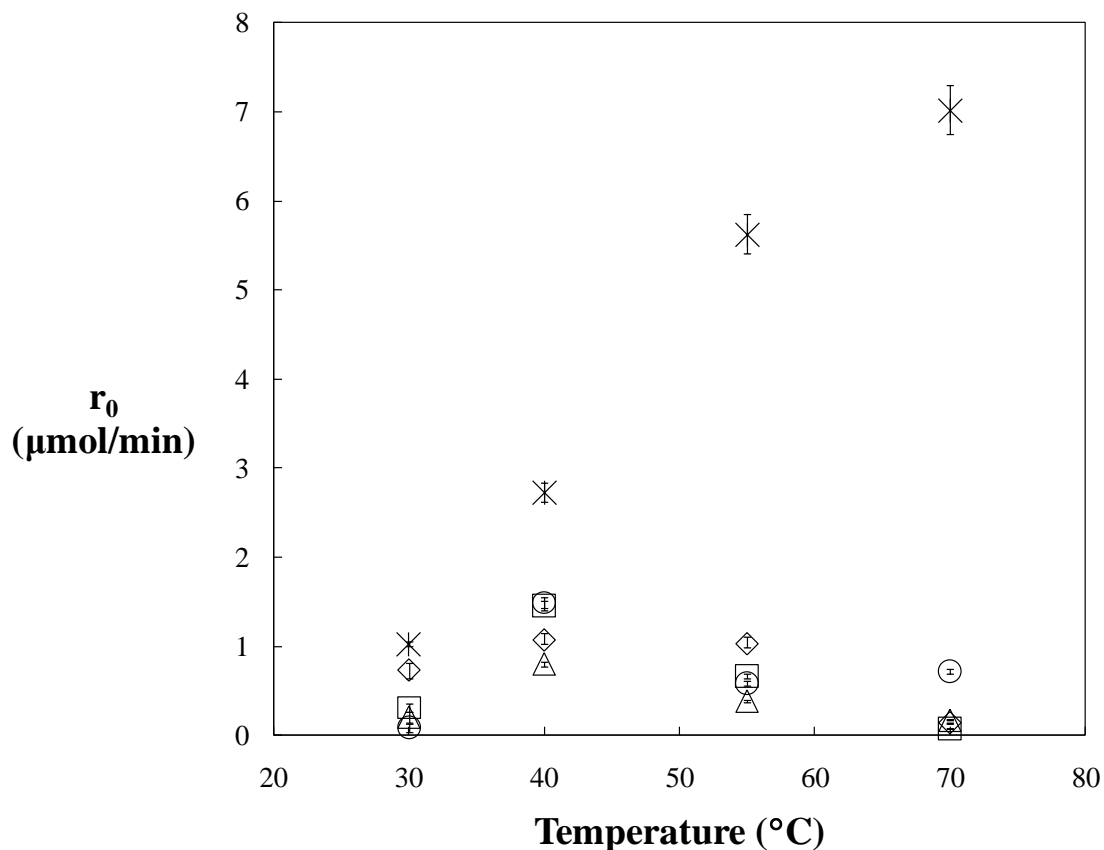


Figure 3.8. Effect of temperature on the catalytic activity of CALB immobilized on fumed silica at various %SC. (◇) 17%SC, (□) 12%SC, (Δ) 4%SC, (○) 2%SC. Effect of temperature on the catalytic activity of Novozym 435 (*). y-error bars represent the cumulative standard error from the calculation of conversion and the linear assumption of the initial reaction rate.

Figure 3.9 shows the initial reaction rates of our preparations in hexane up to four days. For comparison, the results for Novozym 435 are superimposed. The activity of the fumed silica preparations declines quickly in the first 24h and about 50% of the initial activity remains after 4 days of incubation while Novozym 435 retained about 60%. The data point at 48 hours for Novozym 435 is likely impacted by random error. The significant initial loss of activity has been attributed by others to events at the active site of the enzyme molecule, including the breakdown of the acid-base catalytic properties and changes in the protonation state of the involved residues⁵⁵. Gross et al. have recently speculated on desorption of the enzyme as a contributing cause of deactivation as seen in Figure 3.9⁴¹.

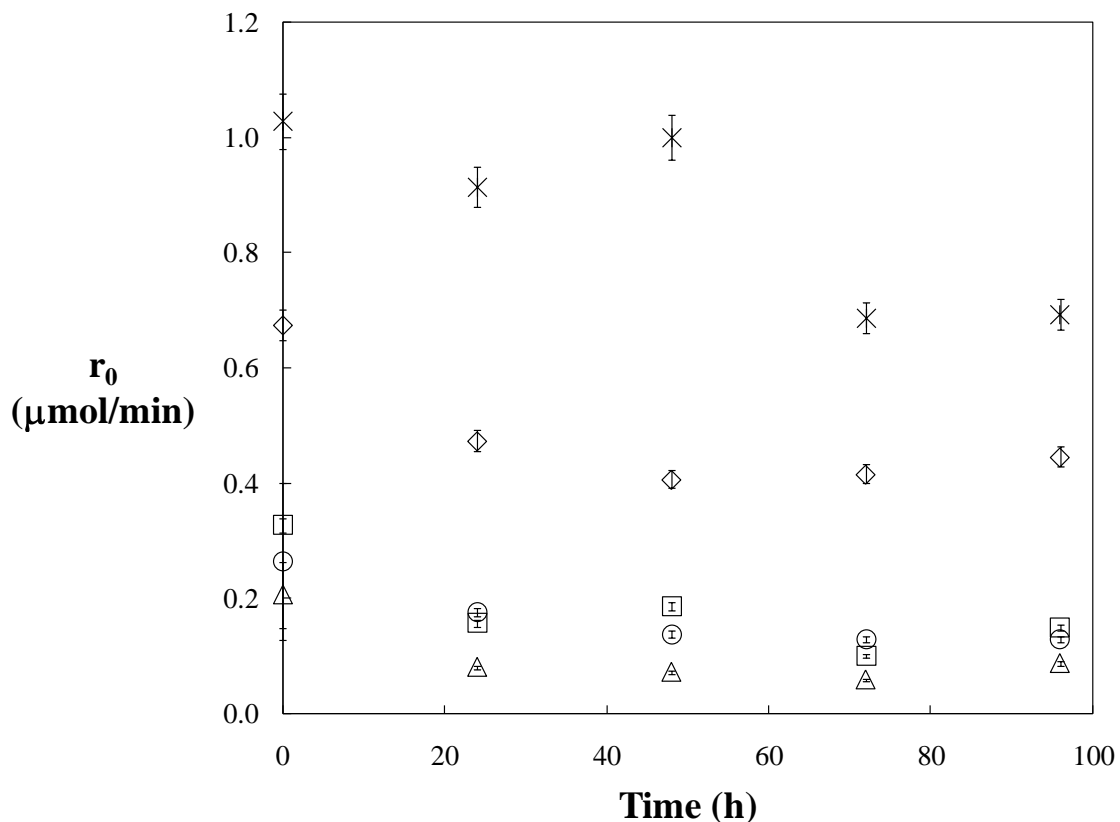


Figure 3.9. Storage stability of CALB immobilized on fumed silica (FS) in n-hexane. (◇) 17%SC, (□) 12%SC, (△) 4%SC, (○) 2%SC. (*) Novozym 435 shown for comparison. y-error bars represent the cumulative standard error from the calculation of conversion and the linear assumption of the initial reaction rate

The residual activity of our lyophilized preparations after 6 months of storage (4°C, closed container) is shown in Figure 3.10 along with data for fresh preparations. The 2%SC preparation maintained the same albeit low level of activity. This can be seen to support the stabilization due to the enzyme/support interactions discussed above.

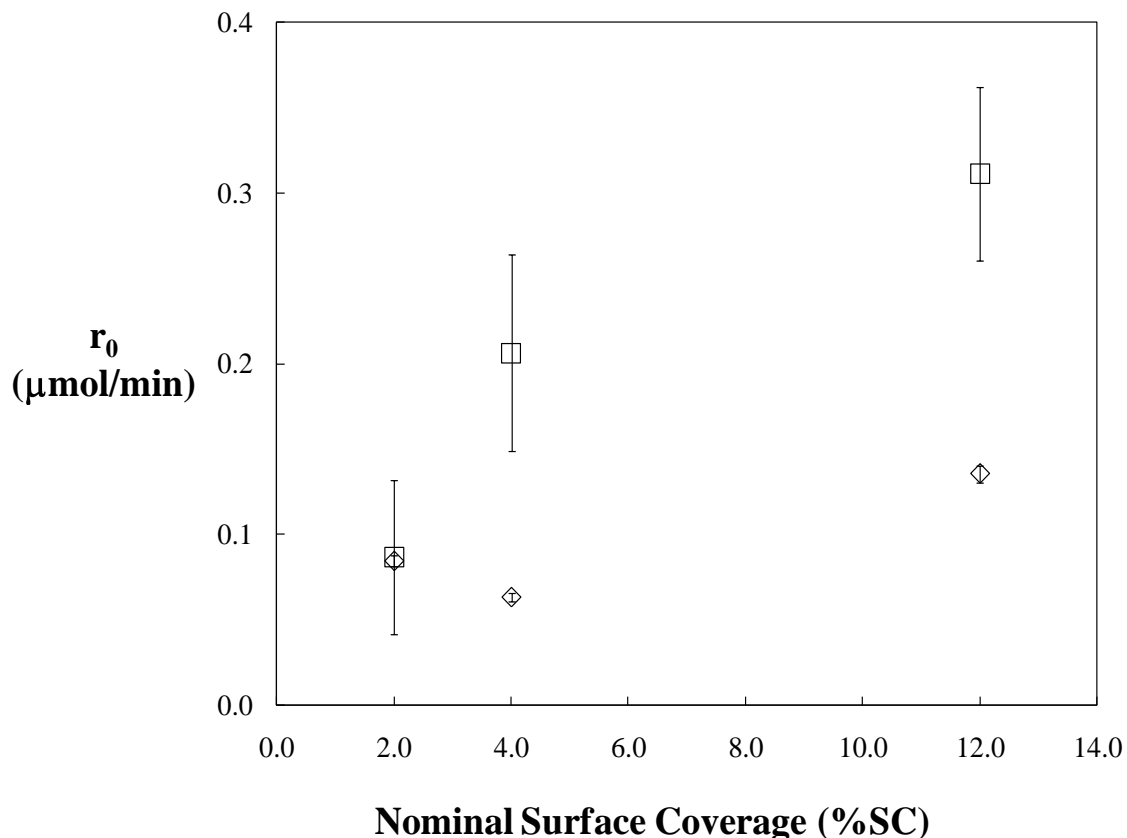


Figure 3.10. Long-term stability of CALB immobilized on fumed silica as a function of the fumed silica content: (\square) fresh preparation, (\diamond) 6 months-aged preparation (4°C, closed glass vials). y-error bars represent the cumulative standard error from the calculation of conversion and the linear assumption of the initial reaction rate.

3.5 Conclusions

We have extended our recently developed procedure (lyophilization in presence of fumed silica) to immobilize enzymes on fumed silica for catalysis in hexane from *s. Carlsberg* to *Candida antarctica* Lipase B (CALB). Adjustment of the aqueous pH relative to the isoelectric point of CALB (pre-lyophilization) at low fumed silica surface availability can reduce the adsorption of the enzyme on fumed silica likely due to a change in surface charge of the enzyme. The impact of pre-lyophilization pH adjustment is not significant for adsorption at high surface area availability.

The catalytic activity of our best CALB/fumed silica preparation exceeded the commercially available biocatalyst Novozym 435®. The surprising decrease of catalytic activity

of our preparations at very low %SC was confirmed by multiple reproductions and reference tests since our previous experience with *s. Carlsberg* showed no sign of this. An "optimum" surface coverage may be hypothesized to be due to excessive or multipoint enzyme/fumed silica interactions at high fumed silica surface availability leading to denaturation as has been proposed by Gross and co-workers^{39, 40}. This could be enzyme specific as our previous results with *s. Carlsberg* indicate. We confirmed that CALB is activated when the temperature is increased up to 55°C as has been observed for other enzymes. A clear loss of activity is observed at even higher temperatures. The fumed silica preparation with the highest fumed silica content (2%SC) is the most temperature-stable and shows the best long term stability while showing overall lower activity than our best (17%SC) preparations. This supports the argument of enhanced enzyme-fumed silica interactions at high fumed silica surface availability which may deactivate some enzyme molecules but confers stability on those still catalytically competent.

3.6 References

1. Klibanov, A. M., Improving enzymes by using them in organic solvents. *Nature* **2001**, 409, (6817), 241-246.
2. Hudson, E. P.; Eppler, R. K.; Clark, D. S., Biocatalysis in semi-aqueous and nearly anhydrous conditions. *Current Opinion in Biotechnology* **2005**, 16, (6), 637-643.
3. Gross, R. A.; Kumar, A.; Kalra, B., Polymer synthesis by in vitro enzyme catalysis. *Chemical Reviews* **2001**, 101, (7), 2097-2124.
4. Gross, R. A.; Kalra, B., Biodegradable polymers for the environment. *Science* **2002**, 297, (5582), 803-807.
5. Gotor, V., Biocatalysis applied to the preparation of pharmaceuticals. *Organic Process Research & Development* **2002**, 6, (4), 420-426.
6. Barahona, D.; Pfromm, P. H.; Rezac, M. E., Effect of water activity on the lipase catalyzed esterification of geraniol in ionic liquid [bmim]PF₆. *Biotechnology and Bioengineering* **2006**, 93, (2), 318-324.
7. Bartling, K.; Thompson, J. U. S.; Pfromm, P. H.; Czermak, P.; Rezac, M. E., Lipase-catalyzed synthesis of geranyl acetate in n-hexane with membrane-mediated water removal. *Biotechnology and Bioengineering* **2001**, 75, (6), 676-681.

8. Bruno, F. F.; Akkara, J. A.; Ayyagari, M.; Kaplan, D. L.; Gross, R.; Swift, G.; Dordick, J. S., Enzymatic modification of insoluble amylose in organic solvents. *Macromolecules* **1995**, *28*, (26), 8881-8883.
9. Carrea, G.; Riva, S., Properties and synthetic applications of enzymes in organic solvents. *Angewandte Chemie-International Edition* **2000**, *39*, (13), 2226-2254.
10. Ghanem, A., The utility of cyclodextrins in lipase-catalyzed transesterification in organic solvents: enhanced reaction rate and enantioselectivity. *Organic & Biomolecular Chemistry* **2003**, *1*, (8), 1282-1291.
11. Klibanov, A. M., Why are enzymes less active in organic solvents than in water? *Trends in Biotechnology* **1997**, *15*, (3), 97-101.
12. Persson, M.; Wehtje, E.; Adlercreutz, P., Factors governing the activity of lyophilised and immobilised lipase preparations in organic solvents. *Chembiochem* **2002**, *3*, (6), 566-571.
13. Long, J.; Hutcheon, G. A.; Cooper, A. I., Combinatorial discovery of reusable noncovalent supports for enzyme immobilization and nonaqueous catalysis. *Journal of Combinatorial Chemistry* **2007**, *9*, (3), 399-406.
14. Sheldon, R. A.; Schoevaart, R.; Van Langen, L. M., Cross-linked enzyme aggregates (CLEAs): A novel and versatile method for enzyme immobilization (a review). *Biocatalysis and Biotransformation* **2005**, *23*, (3-4), 141-147.
15. Mine, Y.; Fukunaga, K.; Itoh, K.; Yoshimoto, M.; Nakao, K.; Sugimura, Y., Enhanced enzyme activity and enantioselectivity of lipases in organic solvents by crown ethers and cyclodextrins. *Journal of Bioscience and Bioengineering* **2003**, *95*, (5), 441-447.
16. Secundo, F.; Barletta, G. L.; Dumitriu, E.; Carrea, G., Can an inactivating agent increase enzyme activity in organic solvent? Effects of 18-crown-6 on lipase activity, enantioselectivity, and conformation. *Biotechnology and Bioengineering* **2007**, *97*, (1), 12-18.
17. Santos, A. M.; Vidal, M.; Pacheco, Y.; Frontera, J.; Baez, C.; Ornellas, O.; Barletta, G.; Griebenow, K., Effect of crown ethers on structure, stability, activity, and enantioselectivity of subtilisin Carlsberg in organic solvents. *Biotechnology and Bioengineering* **2001**, *74*, (4), 295-308.
18. Lindsay, J. P.; Clark, D. S.; Dordick, J. S., Penicillin amidase is activated for use in nonaqueous media by lyophilizing in the presence of potassium chloride. *Enzyme and Microbial Technology* **2002**, *31*, (3), 193-197.

19. Lindsay, J. P.; Clark, D. S.; Dordick, J. S., Combinatorial formulation of biocatalyst preparations for increased activity in organic solvents: Salt activation of penicillin amidase. *Biotechnology and Bioengineering* **2004**, 85, (5), 553-560.
20. Ru, M. T.; Hirokane, S. Y.; Lo, A. S.; Dordick, J. S.; Reimer, J. A.; Clark, D. S., On the salt-induced activation of lyophilized enzymes in organic solvents: Effect of salt kosmotropicity on enzyme activity. *Journal of the American Chemical Society* **2000**, 122, (8), 1565-1571.
21. Ru, M. T.; Wu, K. C.; Lindsay, J. P.; Dordick, J. S.; Reimer, J. A.; Clark, D. S., Towards more active biocatalysts in organic media: Increasing the activity of salt-activated enzymes. *Biotechnology and Bioengineering* **2001**, 75, (2), 187-196.
22. Wurges, K.; Pfromm, P. H.; Rezac, M. E.; Czermak, P., Activation of subtilisin Carlsberg in hexane by lyophilization in the presence of fumed silica. *Journal of Molecular Catalysis B-Enzymatic* **2005**, 34, (1-6), 18-24.
23. Pfromm, P. H.; Rezac, M. E.; Wurges, K.; Czermak, P., Fumed silica activated subtilisin Carlsberg in hexane in a packed-bed reactor. *AIChE Journal* **2007**, 53, (1), 237-242.
24. Gun'ko, V. M.; Mironyuk, I. F.; Zarko, V. I.; Voronin, E. F.; Turov, V. V.; Pakhlov, E. M.; Goncharuk, E. V.; Nychiporuk, Y. M.; Vlasova, N. N.; Gorbik, P. P.; Mishchuk, O. A.; Mishchuk, O. A.; Chuiko, A. A.; Kulik, T. V.; Palyanytsya, B. B.; Pakhovchishin, S. V.; Skubiszewska-Zieba, J.; Janusz, W.; Turov, A. V.; Leboda, R., Morphology and surface properties of fumed silicas. *Journal of Colloid and Interface Science* **2005**, 289, (2), 427-445.
25. Gun'ko, V. M.; Mironyuk, I. F.; Zarko, V. I.; Turov, V. V.; Voronin, E. F.; Pakhlov, E. M.; Goncharuk, E. V.; Leboda, R.; Skubiszewska-Zieba, J.; Janusz, W.; Chibowski, S.; Levchuk, Y. N.; Klyueva, A. V., Fumed silicas possessing different morphology and hydrophilicity. *Journal of Colloid and Interface Science* **2001**, 242, (1), 90-103.
26. Gun'ko, V. M.; Voronin, E. F.; Nosach, L. V.; Pakhlov, E. M.; Guzenko, N. V.; Leboda, R.; Skubiszewska-Zieba, J., Adsorption and migration of poly(vinyl pyrrolidone) at a fumed silica surface. *Adsorption Science & Technology* **2006**, 24, (2), 143-157.
27. Gun'ko, V. M.; Zarko, V. I.; Voronin, E. F.; Goncharuk, E. V.; Andriyko, L. S.; Guzenko, N. V.; Nosach, L. V.; Janusz, W., Successive interaction of pairs of soluble organics with nanosilica in aqueous media. *Journal of Colloid and Interface Science* **2006**, 300, (1), 20-32.
28. Gun'ko, V. M.; Zarko, V. I.; Voronin, E. F.; Turov, V. V.; Mironyuk, I. F.; Gerashchenko, II; Goncharuk, E. V.; Pakhlov, E. M.; Guzenko, N. V.; Leboda, R.;

- Skubiszewska-Zieba, J.; Janusz, W.; Chibowski, S.; Levchuk, Y. N.; Klyueva, A. V., Impact of some organics on structural and adsorptive characteristics of fumed silica in different media. *Langmuir* **2002**, 18, (3), 581-596.
29. Mironyuk, I. F.; Gun'ko, V. M.; Turov, V. V.; Zarko, V. I.; Leboda, R.; Skubiszewska-Zieba, J., Characterization of fumed silicas and their interaction with water and dissolved proteins. *Colloids and Surfaces a-Physicochemical and Engineering Aspects* **2001**, 180, (1-2), 87-101.
30. Rugal, A. A.; Gun'ko, V. M.; Barvinchenko, V. N.; Turov, V. V.; Semeshkina, T. V.; Zarko, V. I., Interaction of fibrinogen with nanosilica. *Central European Journal of Chemistry* **2007**, 5, (1), 32-54.
31. Voronin, E. F.; Gun'ko, V. M.; Guzenko, N. V.; Pakhlov, E. M.; Nosach, L. V.; Leboda, R.; Skubiszewska-Zieba, J.; Malysheva, M. L.; Borysenko, M. V.; Chuiko, A. A., Interaction of poly(ethylene oxide) with fumed silica. *Journal of Colloid and Interface Science* **2004**, 279, (2), 326-340.
32. Gun'ko, V. M.; Mikhailova, I. V.; Zarko, V. I.; Gerashchenko, II; Guzenko, N. V.; Janusz, W.; Leboda, R.; Chibowski, S., Study of interaction of proteins with fumed silica in aqueous suspensions by adsorption and photon correlation spectroscopy methods. *Journal of Colloid and Interface Science* **2003**, 260, (1), 56-69.
33. Unsworth, L. D.; van der Oost, J.; Koutsopoulos, S., Hyperthermophilic enzymes - stability, activity and implementation strategies for high temperature applications. *FEBS Journal* **2007**, 274, (16), 4044-4056.
34. Norde, W., Driving forces for protein adsorption at solid surfaces. In *Biopolymers at Interfaces*, 2nd edn ed.; Marcel Dekker, Inc.: New York, 2003.
35. Barrias, C. C.; Martins, C. L.; Miranda, C. S.; Barbosa, M. A., Adsorption of a therapeutic enzyme to self-assembled monolayers: effect of surface chemistry and solution pH on the amount and activity of adsorbed enzyme. *Biomaterials* **2005**, 26, (15), 2695-2704.
36. Ghanem, A., Trends in lipase-catalyzed asymmetric access to enantiomerically pure/enriched compounds. *Tetrahedron* **2007**, 63, (8), 1721-1754.
37. Anderson, E. M.; Karin, M.; Kirk, O., One biocatalyst - Many applications: The use of *Candida antarctica* B-lipase in organic synthesis. *Biocatalysis and Biotransformation* **1998**, 16, (3), 181-204.

38. Schmid, R. D.; Verger, R., Lipases: Interfacial enzymes with attractive applications. *Angewandte Chemie-International Edition* **1998**, 37, (12), 1609-1633.
39. Chen, B.; Miller, M. E.; Gross, R. A., Effects of porous polystyrene resin parameters on *Candida antarctica* Lipase B adsorption, distribution, and polyester synthesis activity. *Langmuir* **2007**, 23, (11), 6467-6474.
40. Chen, B.; Miller, E. M.; Miller, L.; Maikner, J. J.; Gross, R. A., Effects of macroporous resin size on *Candida antarctica* lipase B adsorption, fraction of active molecules, and catalytic activity for polyester synthesis. *Langmuir* **2007**, 23, (3), 1381-1387.
41. Chen, B.; Hu, J.; Miller, E. M.; Xie, W. C.; Cai, M. M.; Gross, R. A., *Candida antarctica* lipase B chemically immobilized on epoxy-activated micro- and nanobeads: Catalysts for polyester synthesis. *Biomacromolecules* **2008**, 9, (2), 463-471.
42. Kang, I. J.; Pfromm, P. H.; Rezac, M. E., Real time measurement and control of thermodynamic water activities for enzymatic catalysis in hexane. *Journal of Biotechnology* **2005**, 119, (2), 147-154.
43. Bradford, M. M., Rapid and Sensitive Method for Quantitation of Microgram Quantities of Protein Utilizing Principle of Protein-Dye Binding. *Analytical Biochemistry* **1976**, 72, (1-2), 248-254.
44. Houde, A.; Kademi, A.; Leblanc, D., Lipases and their industrial applications - An overview. *Applied Biochemistry and Biotechnology* **2004**, 118, (1-3), 155-170.
45. Kirk, O.; Christensen, M. W., Lipases from *Candida antarctica*: Unique biocatalysts from a unique origin. *Organic Process Research & Development* **2002**, 6, (4), 446-451.
46. Kobayashi, T.; Adachi, S., Reaction equilibrium for lipase-catalyzed condensation in organic solvent systems. *Biotechnology Letters* **2004**, 26, (19), 1461-1468.
47. Lutz, S., Engineering lipase B from *Candida antarctica*. *Tetrahedron-Asymmetry* **2004**, 15, (18), 2743-2748.
48. Plou, F. J.; Cruces, M. A.; Ferrer, M.; Fuentes, G.; Pastor, E.; Bernabe, M.; Christensen, M.; Comelles, F.; Parra, J. L.; Ballesteros, A., Enzymatic acylation of di- and trisaccharides with fatty acids: choosing the appropriate enzyme, support and solvent. *Journal of Biotechnology* **2002**, 96, (1), 55-66.
49. Iler, R. K., *The Chemistry of Silica*. John Wiley & Sons, Inc.: 1979; p 896.

50. Barthel, H.; Heinemann, M.; Stintz, M.; Wessely, B., Particle sizes of fumed silica. *Particle & Particle Systems Characterization* **1999**, 16, (4), 169-176.
51. Sate, D.; Janssen, M. H. A.; Stephens, G.; Sheldon, R. A.; Seddon, K. R.; Lu, J. R., Enzyme aggregation in ionic liquids studied by dynamic light scattering and small angle neutron scattering. *Green Chemistry* **2007**, 9, (8), 859-867.
52. Koutsopoulos, S.; van der Oost, J.; Norde, W., Structural features of a hyperthermostable endo-beta-1,3-glucanase in solution and adsorbed on "invisible" particles. *Biophysical Journal* **2005**, 88, (1), 467-474.
53. Shuler, M. L.; Kargi, F., *Bioprocess Engineering : Basic Concepts*. Second ed.; Upper Saddle River: New Jersey, 2002; p 66-67.
54. Bailey, J. E.; Ollis., D. F., *Biochemical Engineering Fundamentals* Second ed.; McGraw-Hill: New York 1986.
55. Castillo, B.; Pacheco, Y.; Al-Azzam, W.; Griebenow, K.; Devi, M.; Ferrer, A.; Barletta, G., On the activity loss of hydrolases in organic solvents - I. Rapid loss of activity of a variety of enzymes and formulations in a range of organic solvents. *Journal of Molecular Catalysis B-Enzymatic* **2005**, 35, (4-6), 147-153.

CHAPTER - 4 Immobilization of *Candida antarctica* Lipase B on Fumed Silica: Enantioselective Transesterification of (RS)-1-Phenylethanol in Hexane

4.1 Abstract

Enzymatic catalysis to produce molecules such as perfumes, flavors, and fragrances has the advantage of allowing the products to be labeled “natural” for marketing in the U.S., in addition to the exquisite selectivity and stereoselectivity of enzymes that can be an advantage over chemical catalysis. Enzymatic catalysis in organic solvents is attractive if solubility issues of reactants or products, or thermodynamic issues (water as a product in esterification) complicate or prevent aqueous enzymatic catalysis. Immobilization of the enzyme on a solid support can address the generally poor solubility of enzymes in most solvents.

We have recently reported on a novel immobilization method for *Candida antarctica* Lipase B on fumed silica to improve the enzymatic activity in hexane. This research is extended here to study the enantioselective transesterification of (RS)-1-phenylethanol with vinyl acetate. The maximum catalytic activity for this preparation exceeded the activity (on an equal enzyme amount basis) of the commercial Novozyme® 435 significantly. The steady-state conversion for R-1-phenylethanol was about 75% as confirmed via forward and reverse reaction. The catalytic activity steeply increases with increasing nominal surface coverage of the support until a maximum is reached at a nominal surface coverage of 230%. We hypothesize that the physical state of the enzyme molecules at a low surface coverage is dominated in this case by detrimental strong enzyme-substrate interactions. Enzyme-enzyme interactions may stabilize the active form of the enzyme as surface coverage increases while diffusion limitations reduce the apparent catalytic performance again at multi-layer coverage. The temperature-, solvent-, and long-term stability for CALB/fumed silica preparations showed that these preparations can tolerate temperatures up to 70°C, continuous exposure to solvents, and long term storage.

4.2 Introduction

Non-aqueous enzymology is an attractive option for the synthesis of various molecules in non-aqueous media^{1,2}. Promising experiments for polymer synthesis^{3,4}, anticancer and antiviral drugs⁵, aromas and fragrances^{6,7}, and surfactants⁸ have been reported.

The performance of biocatalysis in organic solvents significantly extends the applications of biocatalysts. This is mainly because water is a poor solvent for many organic compounds of commercial interest⁹. Furthermore, undesirable side reactions such as hydrolysis, racemization, polymerization and decomposition are largely repressed in solvents when compared to aqueous solution^{2,9}.

Nevertheless, the catalytic activity of enzymes in organic solvents tends to be much lower than in aqueous environments^{2,9}.

To overcome this issue, different approaches have been developed. Immobilization of enzymes on porous and non-porous solid supports has been intensively explored^{10, 11}. The preferred matrices for immobilization include macroporous polypropylene particles¹², hydrophilic silicon wafers¹³, microemulsions and organogels¹⁴. Additional efforts include improving compatibility with the solvents by chemical modification of the enzymes' surface¹⁵, protein engineering¹, and co-lyophilization of the enzyme with various adjuvants, such as cyclodextrin^{16,17}, inorganic salts^{18,19}, and crown ethers^{17, 20, 21}.

The immobilization on organic and modified inorganic nano-structured supports is considered now as an attractive option for immobilization. A variety of these materials is available including epoxy-activated nanobeads, zirconia nanoparticles, and fumed silica. The main advantage is the large specific surface area provided by such materials²²⁻²⁴. We have recently reported on a new immobilization technique for the activation of two different enzymes on commercial fumed silica (FS): *Candida antarctica* Lipase B (CALB)²⁴ and *subtilisin Carlsberg*²⁴⁻²⁶. The enzyme is co-lyophilized from the aqueous phase with fumed silica. The significant activation of the enzyme reached or in some cases even exceeded the best activities reported for salt activation while the process is somewhat simplified^{24, 25}. The details can be found elsewhere²⁴⁻²⁶.

The main driving forces for protein adsorption on solids are thought to be of hydrophobic and electrostatic nature. These interactions are essentially driven by the net charge difference

between the protein and the surface^{24, 27}. An important issue associated with the adsorptive immobilization of enzymes is that conformational changes are sometimes observed^{12, 13, 27, 28}. These conformational changes may modify the native enzyme structure and promote fluctuations in activity at low enzyme loadings (in this work, referred as low nominal surface coverage). Thus, a large excess of surface area maximizes the interactions of the lipase with the surface, which can result in the above described structural changes and in reduced activity^{12, 27}.

To retain more lipase molecules in the active conformations after adsorption, one may consider mechanisms to suppress the tendency of the enzyme to deform when sufficient surface area is provided. This might be achieved by increasing the presence of neighboring molecules at increased surface coverages^{12, 13, 27}. Mass-transfer limitations may start to be significant at multi-layer coverages thereby, potentially leading to reduced apparent activity. The overall result is low apparent activity at low surface coverage, maximum apparent activity at an intermediate coverage, and again low activity at high or multi-layer coverages^{12, 27}.

This work reports on the performance of *Candida antarctica* Lipase B immobilized on fumed silica in an enantioselective transesterification reaction in hexane. Our findings reproduce the maximum of catalytic activity at an intermediate surface loading, reported previously for a non-stereoselective reaction²⁴. We also investigated the steady-state conversion, the thermal stability, the solvent stability, and the long-term stability at 4°C for preparations with various surface coverages.

4.3 Materials and Methods

4.3.1 Enzymes

Crude CALB (E.C. 3.1.1.3; lyophilized; specific activity of 30 U/mg solid) was purchased from Biocatalytics, Inc. (Pasadena, CA), stored at 4°C, and used as-received. Commercial Novozym 435® was purchased from Sigma, stored at 4°C, and used as-received. Novozym 435® is a preparation of the lipase B from *Candida antarctica* adsorbed on macroporous acrylic particles (0.3-0.9 mm diameter) reported to have about 7000 PLU/g (Propyl Laurate Units per gram preparation).

4.3.2 *Chemicals and Materials*

Monobasic potassium phosphate (>99.9%), potassium hydroxide, hexane (98.5%, Acros Organics), isopropanol (99.9%, Fisher, Sigma-Aldrich), vinyl acetate (99%, Alfa Aesar), acetaldehyde (99.5%, Acros Organics, stored at 4°C) were purchased from Fisher Scientific (Pittsburg, PA).

The chemicals for calibration, enzymatic reactions, immobilization, and Karl Fischer titration, α -methylbenzyl acetate (98+%, SAFC sampling solutions), S-1-phenylethanol (97%, Sigma-Aldrich), 1-phenylethanol (98%, Sigma-Aldrich), HYDRANAL®-Coulomat AK anolyte (Fluka), HYDRANAL®-Coulomat CG-K catholyte (Fluka), and Fumed Silica (99.8%, specific surface area 255m²/g, primary particle diameter \cong 7-50 nm, as reported by the manufacturer) were purchased from Sigma-Aldrich (St. Louis, MO). A chiral High Performance Liquid Chromatography (HPLC) column (Chiralcel OD-H, 0.46 cm inner diameter, 25 cm length; Daicel Chemical Industries, Tokyo, Japan) and a Shimadzu HPLC system (Shimadzu, Kyoto, Japan) were used (Pumps LCD-10ATvp liquid chromatography, degasser DGU-14A, auto injector SIL-10ADvp, system controller SCL-10Avp, column oven CTO-10Avp, diode array detector SPD-M10Avp, Shimadzu Chromatography Laboratory Automated Software System Version 7).

A 20 μ L-200 μ L and a 100 μ L-1000 μ L Finnpiptette (Fisher Scientific) were used for pipetting. 1.5 mL glass vials and caps with pre-assembled septa for HPLC sampling were from Sun Sri. For storage the septum caps were replaced with solid caps (Fisherbrand, Fisher Scientific).

To carry out the enzymatic reactions a PsyCro Term Controlled Environment Incubator Shaker (New Brunswick Scientific) was used. Reactions were performed in 12 mL glass vials with open top caps and septa from National Scientific. Solvent and temperature stability experiments were performed using solid caps (Kimble). 4 oz glass jars with plastic screw caps were used for conversion experiments (Wheaton). A 1 mL gastight syringe with Luer Lock head and 3 inch needles (Hamilton, Reno, NV) was used for sampling. Samples were filtered with 0.2 μ m PTFE syringe filters (Whatman Inc.).

4.3.3 Enzyme Surface Coverage of the Support

The surface coverage of the solid support (fumed silica) by the immobilized enzyme is tracked here by calculating a nominal surface coverage based on the projected surface area of a CALB molecule of 28.27nm² determined via x-ray crystallography resulting in a spherical CALB molecule of 6nm diameter²⁹. The surface coverage is determined according to:

$$\%SC = 100 \frac{nA_E}{A_S} \quad \text{Equation 4.1}$$

where %SC is the nominal surface coverage in %, n is the number of moles of enzyme, A_E is the projected surface area of an enzyme molecule in m², and A_S is the surface area of the fumed silica support in m² as reported by the manufacturer. Both the spherical shape of the enzyme and the surface curvature of the support cause actual 100% monolayer surface coverage to likely occur below 100%SC nominal surface coverage. This is exacerbated if the enzyme molecules deform to maximize enzyme-support interactions. In summary, actual monolayer coverage is expected below a calculated nominal 100%SC. Multi layer coverage will lead to nominal surface coverages calculated above 100%SC.

4.3.4 Enzyme Immobilization

Details for this process can be found elsewhere^{24, 26}. In a glass vial crude CALB and aqueous buffer were mixed under vortexing for about 30 s. After adding fumed silica the preparations were homogenized by vortexing followed by sonication for 10 min. The suspension was then stored at -20°C in a refrigerator until frozen. The frozen samples were lyophilized (48 h primary drying, 24 h secondary drying, VirTis model 10-MR-TR: Gardiner, NY).

Table 4.1 shows the amounts of aqueous buffer and fumed silica needed for the various % SC-preparations.

Our preparations and Novozym 435® are compared here on an equal PLU basis. As reported elsewhere²², the fraction of active enzyme in the Novozym 435® immobilizate is about 50.3% (active site titration in organic media). The measured initial reaction rates for Novozyme 435® were corrected to compare with our preparations using the relationship

Table 4.1. Summary of the amount of fumed silica and aqueous buffer for the various enzyme preparations. In all cases, the amount of crude CALB was 5.83 mg.

Target preparations (% nominal surface coverage)	Aqueous buffer [mL]	Fumed silica ^a [mg]	Enzyme concentration [mg/mL]	Amount of preparation containing 35 U ^b (mg of lyophilized preparation)
2	58.3	651.3	0.1	131.4
4	58.3	325.7	0.1	66.3
12	19.4	108.6	0.3	22.9
17	8.3	76.6	0.7	16.5
50	2.1	26.1	2.7	6.4
100	1.7	13.0	3.5	3.8
150	1.5	8.7	3.9	2.9
230	1.5	5.7	4.0	2.3
300	1.2	4.3	4.7	2.0
400	1.2	3.3	5.0	1.8
538	1.1	2.4	5.1	1.7
1250	0.9	1.0	6.3	1.4
2087	0.9	0.6	6.3	1.3
Novozym 435®	-	-	-	5.0

^a the required amount of FS was calculated as follows:

$$\text{area FS} = 3.32 \text{ m}^2 / \% \text{ SC} \quad (1)$$

$$\text{amount FS} = \text{area FS} * (\text{g} / 255 \text{ m}^2) \quad (2)$$

where 3.32 m² is the area of 1.17mg enzyme regarding an area of 3.12 x 10⁻¹⁷ m²/molecule

^b the amount of preparation was calculated as follows:

$$\chi_{g \text{ prep}} = \frac{\text{Units CALB in preparation}}{\text{Units/g preparation}} = \frac{35U}{\text{Units/g preparation}} \quad (3)$$

$$\text{Units/g preparation} = \frac{\text{Units weighed CALB}}{\text{g CALB} + \text{g FS}} \quad (4)$$

$$r_{0\text{plotted}} = r_{0\text{measured}} * 0.503$$

Equation 4.2

where r_0 is the initial reaction rates in $\mu\text{mol/s}$.

4.3.5 Mobile Phase

The mobile phase used for HPLC was a hexane/isopropanol mixture (9:1, v/v). The stock solution was composed of 3600 mL of hexane and 400 mL of isopropanol and stored in amber glass vessels sealed against the open atmosphere.

4.3.6 Analytical Methods for Reactions in Hexane

Substrates (1-phenylethanol, vinyl acetate) and products (R-1-phenylethyl acetate, S-1-phenylethanol) were tracked in the reaction mixture by HPLC. Kinetic parameters are based on the appearance of R-1-phenylethyl acetate. The conversion is defined in terms of a fractional conversion c as ³⁰:

$$c = 1 - \frac{[R] + [S]}{[R]_0 + [S]_0}$$

Equation 4.3

where $[R]$ is moles of R-1-phenylethanol from analysis, $[S]$ is moles of S-1-phenylethanol from analysis, $[R]_0$ is the initial amount of R-1-phenylethanol in moles, and $[S]_0$ is the initial amount of S-1-phenylethanol in moles.

4.3.7 Initial Reaction Rates

The enzyme preparation was weighed into 12 mL glass vials. Table 4.1 shows the needed weights for the different preparations. 6 mL hexane were then added. As substrates 42.4 mg vinyl acetate and 60 mg (RS)-1-phenylethanol were finally added and the time of adding the reactants was defined as time zero.

The vials were then placed in the incubator (30°C, 280 rpm). 400 μL samples are taken every 20 min with 1 mL gastight syringes and are afterwards directly filtered with syringe filters pre-purged with hexane. 200 μL are pipetted into 1.5 mL HPLC vials with 1100 μL mobile phase. These HPLC vials are refrigerated until used.

4.3.8 Thermal Stability

Temperature stability experiments were carried out with enzyme preparations of 230 %SC, 100 %SC, 12 %SC, and 2 %SC nominal surface coverage and for Novozyme 435® by measuring the initial reaction rates at 45°C, 60°C, and 70°C.

4.3.9 Steady-State Conversion

To determine the steady-state conversion forward reactions with a reaction mixture volume of 48 mL were performed. The amounts of preparations and substrates were properly scaled-up. Preparations with a range of nominal surface coverages between 400 %SC and 4 %SC were tested. The reactions were tracked by measuring the RS-1-phenylethanol consumption. The reverse reaction with the 230%SC preparation was performed to check the accuracy of the steady-state condition and the experimental procedures.

4.3.10 Hexane Storage Stability

Preparations were suspended in 6 mL hexane and incubated (280 rpm, 30°C) for up to 4 days. The substrates were then added and initial reaction rate experiments were carried.

4.3.11 Long-term Stability for Storage at 4 °C

Initial reaction rates of enzyme preparations (17, 4, and 2 %SC) that had been stored dry for one year at 4°C in glass vials closed with screw caps were determined (see procedure above).

4.3.12 Water Content Analysis

The water content of our reaction mixture was measured by coulometric Karl Fischer titration (Denver Model 275 KF titration module, Model 270 controller, Denver Instruments) of about 1 mL samples taken with a gas tight syringe (5mL, Hamilton).

Due to the presence of the keto group ($=C=O$) in the vinyl acetate, it is likely that interference with standard Karl Fischer reagents occurs³¹. Karl Fischer reagents HYDRANAL®-Coulomat AK and HYDRANAL®-Coulomat CG-K (both Fluka purchased from Sigma-Aldrich) were therefore used. Titration of a HYDRANAL® Water Standard (Riedel-de Haën, 100mg water/g) in six independent titrations in the same titration module resulted in an average of 99.6 ppm H₂O (standard deviation 4.4 ppm).

Syringes were carefully cleaned and always stored in a dessicator. The water concentration in our reaction mixture (6 mL hexane, 60 μ L (RS)-1-phenylethanol, 45 μ L vinyl acetate, appropriate amount of CALB/FS preparation) was determined after filtering (0.2 μ m syringe filters) the homogenized mixtures three times.

4.4 Results and Discussion

We report the enantioselective catalytic activity of CALB in hexane immobilized on a non-porous inorganic support that consists of nano-scale spherical silica particles fused into necklace-like arrangements (fumed silica)³².

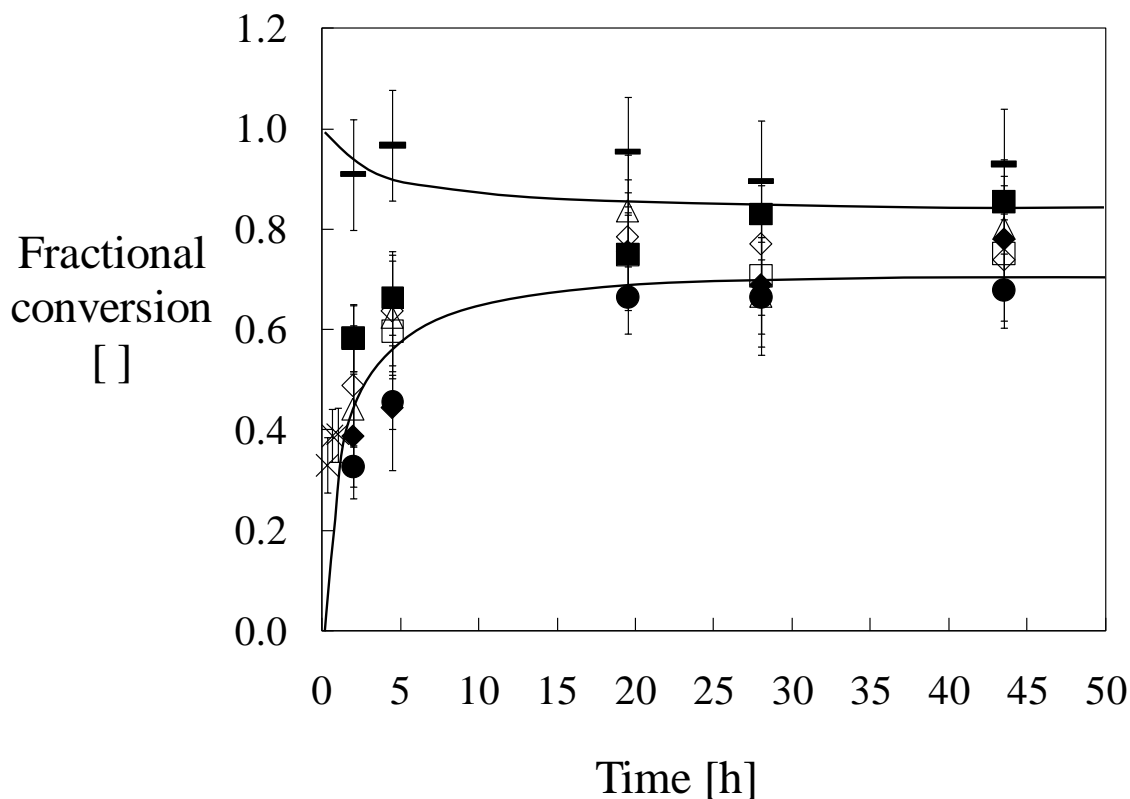


Figure 4.1. Time evolution of the fractional conversion of R-1-phenylethanol during the transesterification with vinyl acetate for CALB/FS preparations with different nominal surface coverages %SC (30°C, 48 ml reaction volume, 35U of enzyme per preparation): 4 %SC (●), 12 %SC (□), 17 %SC (■), 100 %SC (△), 230 %SC (◇), 400 %SC (◆).Novozym 435® during the initial 1.33 hours of reaction (X). Reverse reaction carried out with 230 %SC preparations (-); Solid lines added to guide the eye; y-error bars show the cumulative standard errors and are obtained from the kinetic parameter calculations.

The simplicity of the procedure to produce the preparation, the low cost and availability of the fumed silica (commercially available both native and with surface modifications), and the proven ability to operate the preparation in a packed bed continuous reactor are attractive^{25, 26}.

The good match of the conversion (about 75%, Figure 4.1) of the forward and reverse reactions for the transesterification of (R)-1-phenylethanol with vinyl acetate as acyl donor catalyzed by CALB immobilized on fumed silica in hexane indicates that our experimental and analytical procedures appear consistent. Comparison with the literature confirms this in hexane³³ and other organic solvents^{34, 35}. The water content in our reaction mixtures was on average 33 ± 5.5 ppm. This corresponds to a thermodynamic water activity a_w of 0.38 ± 0.06 assuming a saturation level of 89.4ppm of water in hexane at the reaction conditions³⁶.

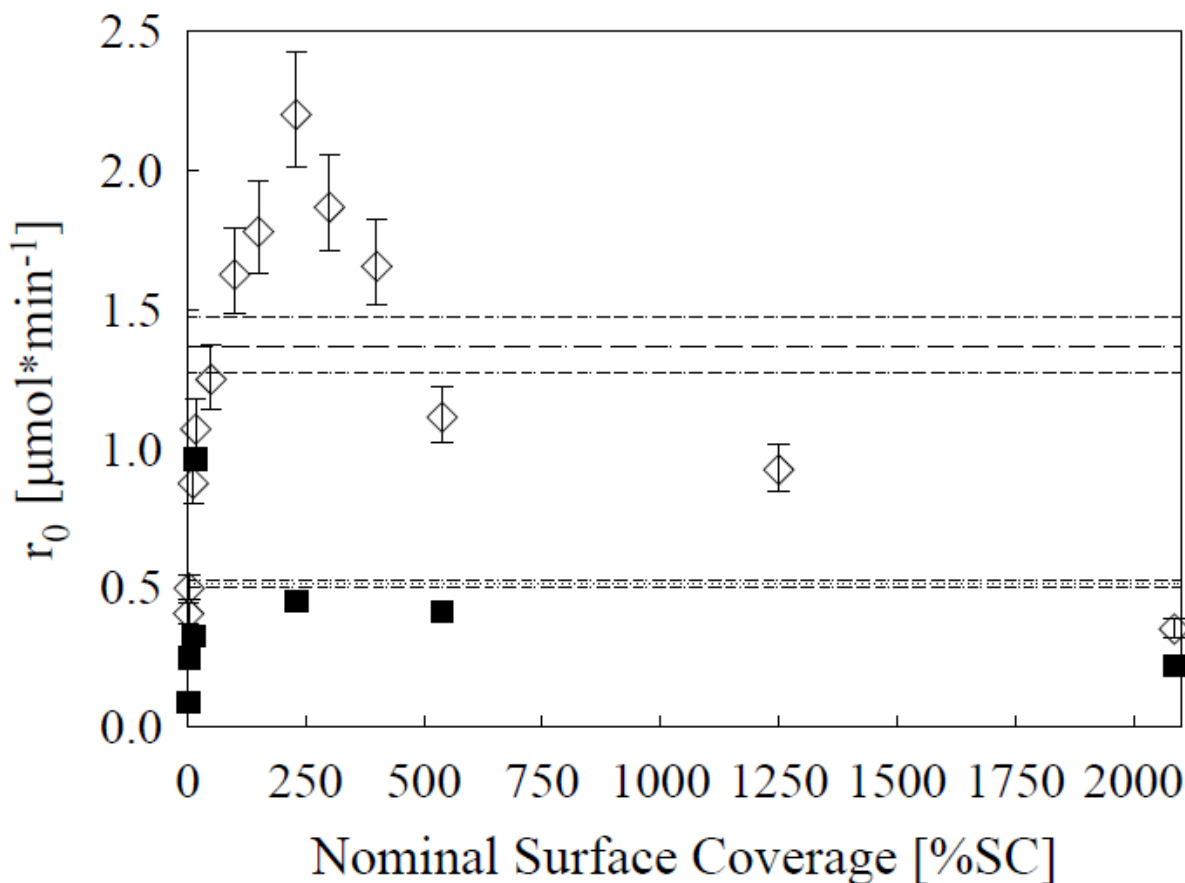


Figure 4.2. Catalytic activity of CALB/FS preparations as a function of the nominal surface coverage %SC. (\diamond) Enantioselective transesterification of (RS) 1-phenylethanol in n-hexane. (\blacksquare) Esterification of geraniol with acetic acid in n-hexane. (---) Reaction rate for Novozyme435® in the enantioselective transesterification of (RS) 1 phenylethanol; (···) represents Novozyme435® in geraniol system. y-error-bars and short dashed lines represent the cumulative standard error from the calculation of the initial reaction rates. (30°C, 6 mL reaction volume, 35U of enzyme per preparation).

The initial reaction rates (2 hrs) for different nominal surface coverages show a maximum at an intermediate nominal surface coverage of about 230%SC (Figure 4.2). This indicates multi-layer coverage if the geometry of the enzyme molecule and the available fumed silica surface assumed in the calculation of %SC is correct. This is similar to previous observations^{12, 24, 26} although the maximum occurs at different nominal surface coverages (discussion below). The best reaction rate doubles that of commercial Novozym 435® on an equal PLU basis. The different CALB immobilizates on fumed silica all showed the same high enantioselectivity; >99% (data not shown) as reported by others³⁴.

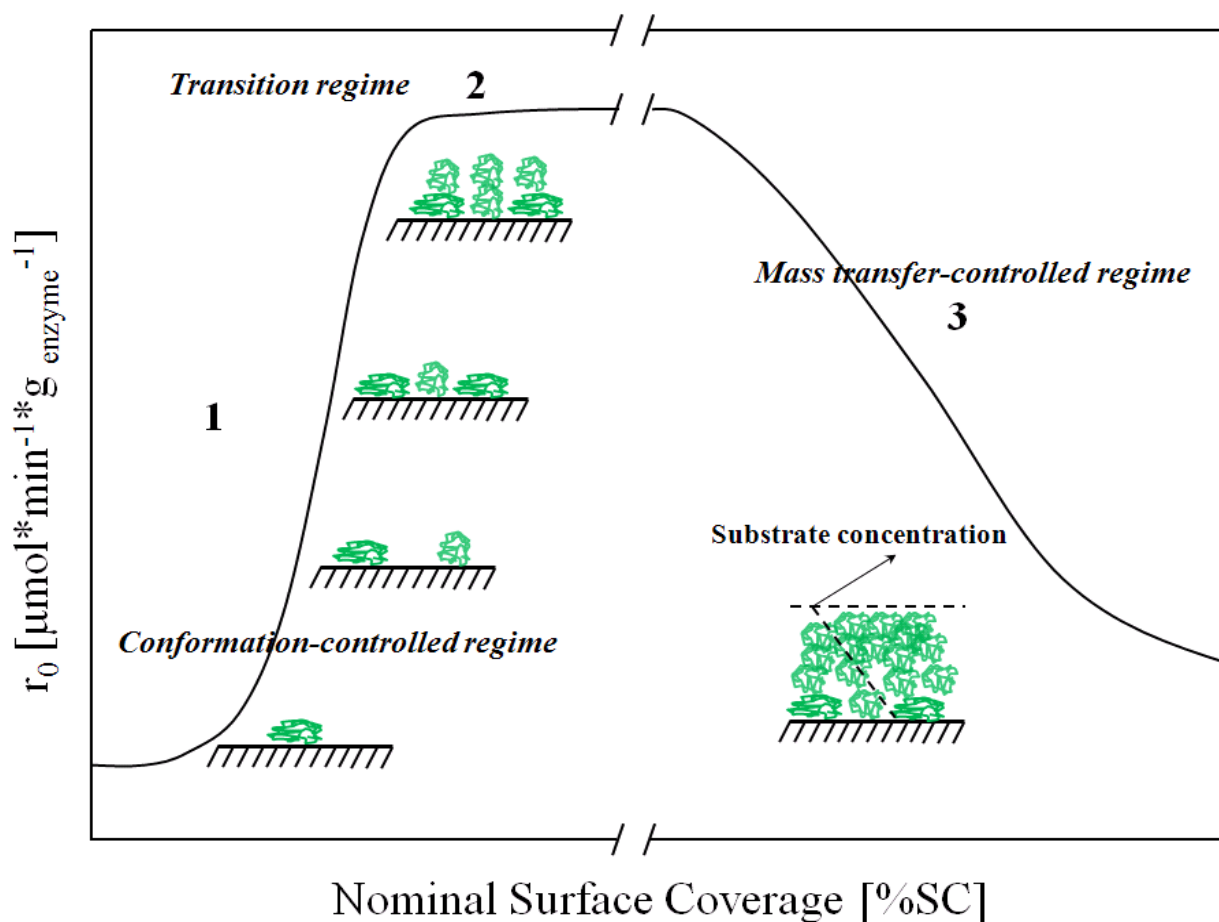


Figure 4.3. Schematic of the three regimes controlling the catalytic activity per enzyme molecule of FS/CALB preparations in hexane: 1. at low surfaces coverages, interactions with the surface are maximized leading to detrimental conformational changes. 2. at intermediate surface coverages, a transitional regime where enzyme structure is more generally maintained. 3. at high surface coverages multi-layer coverage leads to mass-transfer resistance and low apparent catalytic activity per enzyme molecule.

Based on the literature and our results^{12, 24, 27, 37, 38}, we postulate here that three phenomena contribute to the observed catalytic activity maximum: 1. detrimental conformational changes of enzyme molecules upon adsorption on a solid^{12, 27}, 2. beneficial interaction of adsorbed enzymes with neighboring enzyme molecules at increasingly "crowded" conditions, and 3. reactant and/or product diffusional limitations due to multi-layer deposition of the enzyme^{27, 37, 38}. A more detailed mechanistic explanation of each situation is given below and schematically shown in Figure 4.3

Figure 4.2 can be interpreted in light of the three effects above. The possible detrimental structural changes of the enzyme after adsorption on the solid may impact the more sensitive stereoselective reaction more severely than the simple esterification of geraniol. More stabilization may therefore be needed to reach the maximum reactivity for the more complex stereoselective catalytic process. This corresponds to a higher nominal surface coverage needed to reach the maximum reactivity, pointing towards more protein/protein interactions. The decline in reactivity then follows when increasing multi layer coverage causes mass transfer limitations. This is schematically shown in Figure 4.3 where three regimes of surface loading are proposed:

1. Low nominal surface coverage where most enzyme molecules adsorb isolated from each other thereby promoting conformational changes (by deformation upon multipoint attachment to the surface). Few active enzyme molecules are responsible for catalysis, which explains the considerable loss of activity per enzyme molecule in this regime. The presence of this conformation-controlled regime has been previously suggested by others³⁷.

2. High catalytic activity per enzyme molecule at intermediate surface coverage where enzymes are likely adsorbed on a previously formed enzyme monolayer and stabilized by enzyme-enzyme interactions.

3. A high nominal surface coverage regime with multiple layers where diffusional mass transfer barriers result in a low apparent catalytic activity per enzyme molecule. The existence of this mass transfer-controlled regime was also suggested previously³⁷.

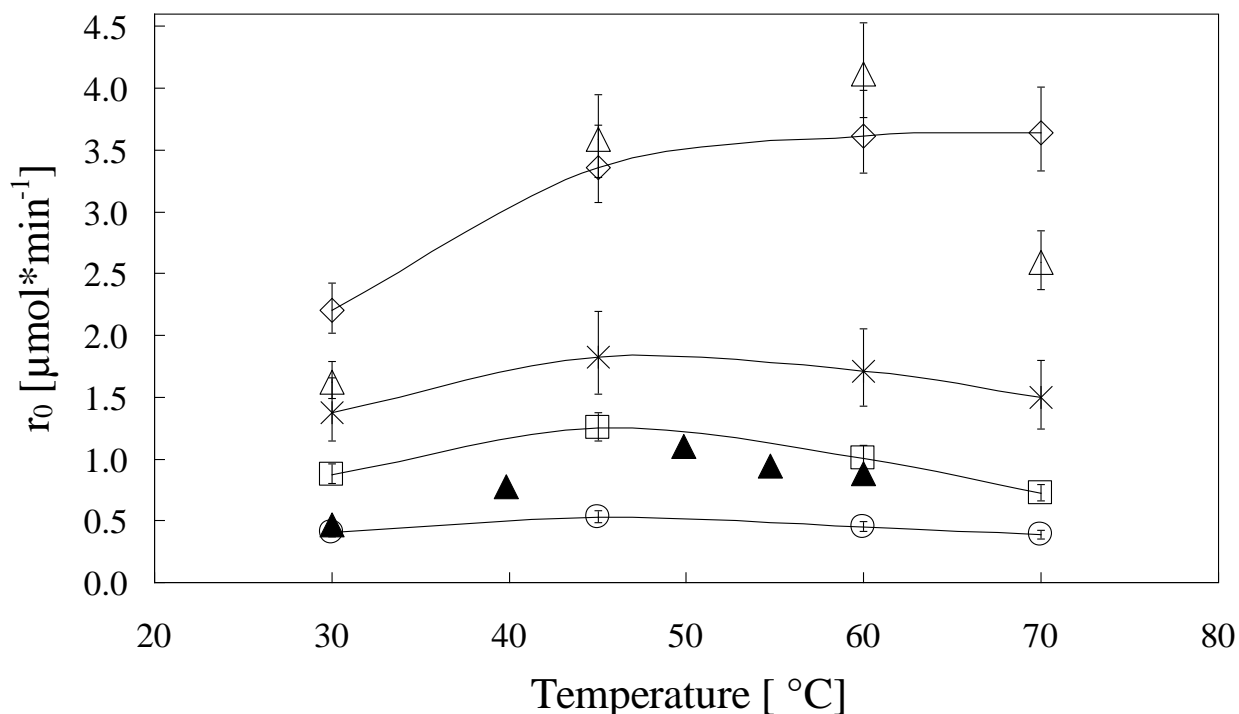


Figure 4.4. Temperature stability of CALB/FS preparations with various surface coverages (%SC): 2 %SC (○), 12 %SC (□), 100 %SC (△), 230 %SC (◇). Temperature Novozym 435® preparations (X). (▲) *R. miehei* lipase immobilized in agar organogels based on lecithin, isooctane as solvent, shown for comparison (Zoumpantioti et al. 2008) Solid lines added to guide the eye; y-error bars show the cumulative standard errors from the kinetic parameter calculation. (Various temperature, 6 mL reaction volume, 35U of enzyme per preparation)

Figure 4.4 shows the impact of temperature on the catalytic activity of our preparations. All enzyme preparations show Arrhenius-type activation from 30°C to 45°C. The 2 %SC preparation remains at the same albeit low level of activity for all temperatures. This can be interpreted to support the notion that the enzyme molecules in this preparation may have strong interactions with the support due to the large surface area provided. This enhanced contact is likely to lead to detrimental impact on the structure (resulting in low activity) but on the other hand helps to maintain the integrity of the still active molecules at higher temperatures²⁷. The 12 %SC preparation shows a similar progression, however, the denaturing effect of increased temperature is more pronounced. Thus, after reaching a maximum at 45°C the activity decays continuously.

Higher activity values for the 100 %SC and 230 %SC preparations were observed at all temperatures exceeding those of Novozym 435®. Additionally, the 100 %SC shows a 2.5-fold

increase in activity from 30°C to 60°C and a precipitous decrease from 60°C to 70°C. The activity of the 230 %SC preparation, however, increased 1.5-fold from 30°C to 45°C and remained at the same high level above 60°C indicating that the enzyme localization on the surface largely prevents thermal damage and the subsequent break down of the catalytic machinery.

In summary, when superimposed; the three effects of denaturation by enzyme-solid interaction, stabilization by enzyme-enzyme interaction, and mass transfer limitation at multi layer coverage lead not only to a maximum in the activity as a function of coverage but to very stable conformations that can tolerate relatively high temperatures. This represents a tremendous advantage from the processing stand point as a number of processes of industrial importance are preferentially performed at temperatures above the ambient condition.

The temperature dependence of *R. miehei* lipase immobilized in lecithin based microemulsion-based organogels is superimposed in Figure 4.4 for comparison¹⁴. Figure 4.4 shows that these lipase preparations are behaving similarly as the temperature is raised from 30°C to 70°C. This confirms that our system exhibits a similar temperature dependency as those reported elsewhere¹⁴. This further supports that our preparations can activate to a level that is commonly obtained for the same enzyme immobilized on supports with different chemical and physical properties.

Figure 4.5 shows the storage stability in hexane in terms of the initial reaction rates for up to 4 days. The results for Novozym 435® are superimposed. Lower activities for the fresh preparations are explained by the fact that separately prepared batches with batch-to-batch fluctuations in catalytic activity were used for the remaining data points. The data clearly shows that the solvent appears not to affect the subtle enzymatic catalysis for this stereoselective reaction substantially over the time investigated here. Unlike our previous work, where the catalytic mechanism does not require specific active site geometries; the active site's binding affinity is likely to remain unaffected during catalysis^{24, 37}.

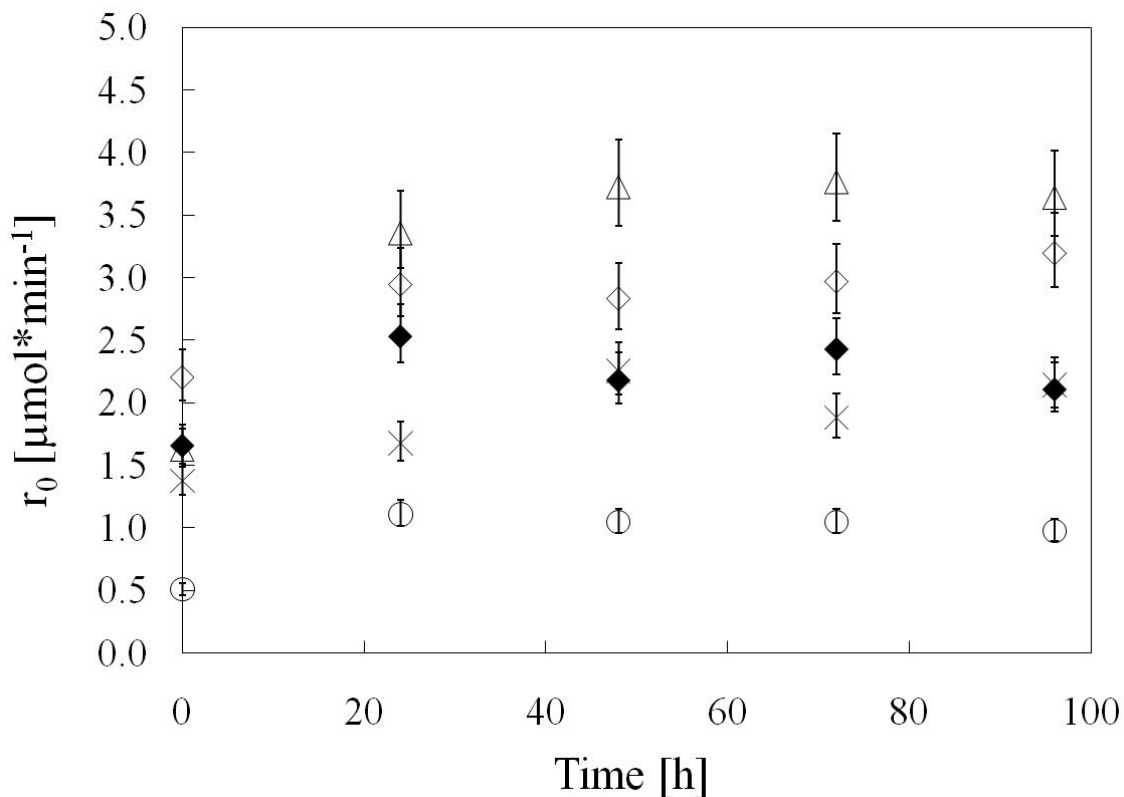


Figure 4.5. Solvent stability of CALB/FS preparations with various surface coverages %SC. After 4 days exposure to the solvent, the catalytic activity remains almost unaffected: 400 %SC (◆), 230 %SC (◇), 100 %SC (△), 2 %SC (○). Storage stability of Novozym 435® in n-hexane (X). y-error bars represent the cumulative standard error and are obtained from the initial reaction rate calculation. (30°C, 6 mL reaction volume, 35U of enzyme per preparation).

Table 4.2. Long-term stability (reaction conditions: 30°C, 6 mL reaction volume, 35U of enzyme per preparation) of various CALB/fumed silica preparations (storage at 4°C, closed glass vials).

Preparation [%SC]	r_0 fresh preparation [$\mu\text{mol}\cdot\text{min}^{-1}$]	r_0 one year-aged [$\mu\text{mol}\cdot\text{min}^{-1}$]	Activity retained after one year storage
2	0.41	0.37	90 %
4	0.50	0.35	70 %
12	0.88	0.64	73 %

Figure 4.6 shows the initial and residual activity of our CALB preparations after one year of storage at 4°C (glass vial, Teflon-lined screw cap). The activity of the 12 %SC and 4 %SC preparations is about 70% of the initial values (Table 4.2). The one year-stored 2 %SC preparation maintained over 90% of the same albeit low activity level of the fresh preparation (Table 4.2). As reported by ²⁴ this can be interpreted as evidence for stabilization due to enzyme-support interactions. The long term stability is encouraging in regard to practical application of the preparations.

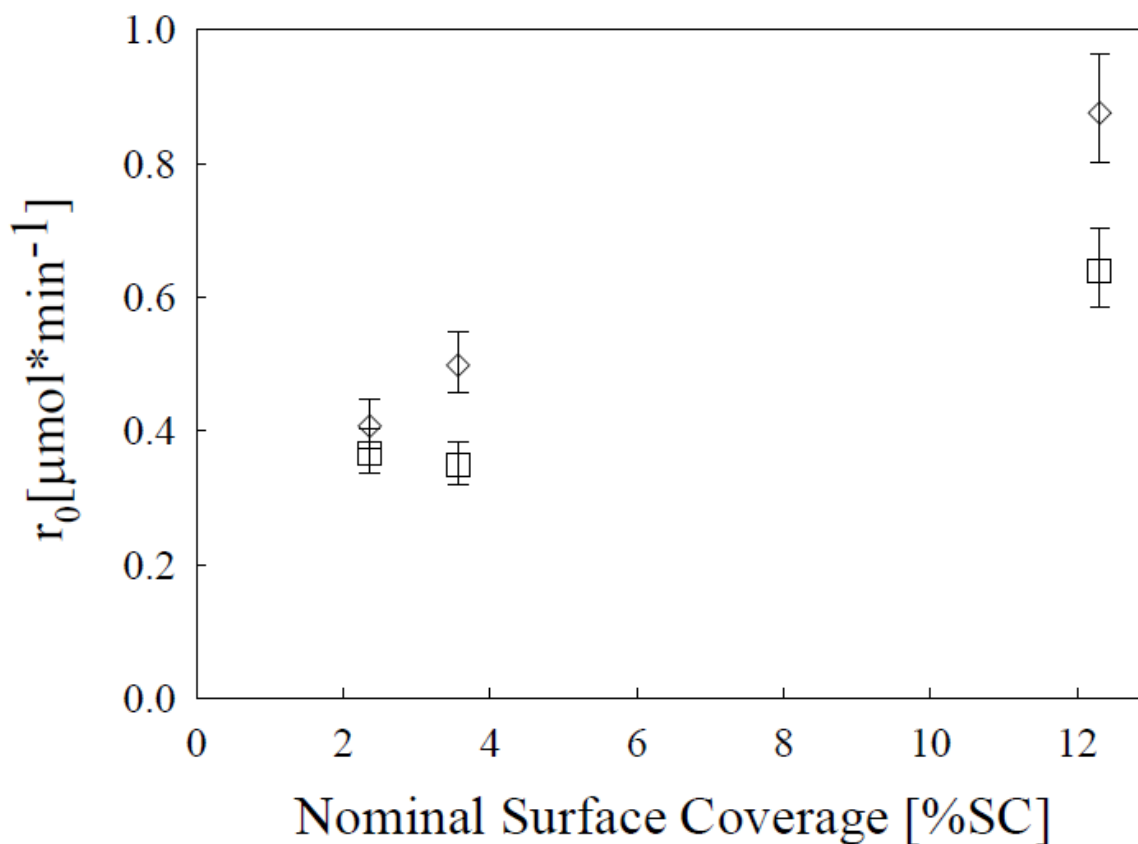


Figure 4.6. Long-term stability of CALB/FS preparations with various surface coverages %SC: (\diamond) fresh preparations, (\square) one year-aged preparations (storage at 4°C, closed glass vials). Cumulative standard errors are obtained from the kinetic parameter calculation and are shown as y-error bars. (30°C, 6 mL reaction volume, 35U of enzyme per preparation).

4.5 Conclusions

We extended the applicability of CALB biocatalysts immobilized on fumed silica to an enantioselective reaction in hexane. The catalytic activity of the biocatalysts is a function of the nominal surface coverage %SC by the immobilized enzyme molecules. A maximum in activity was found at a nominal surface coverage of approximately 230%SC, which confirms previous results for a conventional esterification. We hypothesize three different and to some extent overlapping enzyme surface loading regimes: 1. low nominal surface coverage where the surface-protein interactions dominate and deactivate many enzyme molecules; 2. intermediate nominal surface coverage where protein-protein interactions protect the catalytic activity of the enzyme molecules while access to the individual active sites is relatively unfettered; and 3. multi layer nominal surface coverage where enzymes are mass transfer limitations prevail. The preparation with nominal surface coverages of %SC 100 and %SC 230 showed better thermal stability at low specific catalytic activity which is perhaps due to the remaining active enzyme molecules' stabilization by strong surface-enzyme interactions. The enzyme/fumed silica preparation showed very good stability during prolonged exposure to hexane. Refrigerated storage of the preparation for one year caused only a 25% of reduction in the catalytic activity.

4.6 References

1. Hudson, E. P.; Eppler, R. K.; Clark, D. S., Biocatalysis in semi-aqueous and nearly anhydrous conditions. *Current Opinion in Biotechnology* **2005**, 16, (6), 637-643.
2. Klibanov, A. M., Improving enzymes by using them in organic solvents. *Nature* **2001**, 409, (6817), 241-246.
3. Gross, R. A.; Kalra, B., Biodegradable polymers for the environment. *Science* **2002**, 297, (5582), 803-807.
4. Gross, R. A.; Kumar, A.; Kalra, B., Polymer synthesis by in vitro enzyme catalysis. *Chemical Reviews* **2001**, 101, (7), 2097-2124.
5. Gotor, V., Biocatalysis applied to the preparation of pharmaceuticals. *Organic Process Research & Development* **2002**, 6, (4), 420-426.

6. Barahona, D.; Pfromm, P. H.; Rezac, M. E., Effect of water activity on the lipase catalyzed esterification of geraniol in ionic liquid [bmim]PF₆. *Biotechnology and Bioengineering* **2006**, 93, (2), 318-324.
7. Bartling, K.; Thompson, J. U. S.; Pfromm, P. H.; Czermak, P.; Rezac, M. E., Lipase-catalyzed synthesis of geranyl acetate in n-hexane with membrane-mediated water removal. *Biotechnology and Bioengineering* **2001**, 75, (6), 676-681.
8. Bruno, F. F.; Akkara, J. A.; Ayyagari, M.; Kaplan, D. L.; Gross, R.; Swift, G.; Dordick, J. S., Enzymatic modification of insoluble amylose in organic solvents. *Macromolecules* **1995**, 28, (26), 8881-8883.
9. Ghanem, A., Trends in lipase-catalyzed asymmetric access to enantiomerically pure/enriched compounds. *Tetrahedron* **2007**, 63, (8), 1721-1754.
10. Long, J.; Hutcheon, G. A.; Cooper, A. I., Combinatorial discovery of reusable noncovalent supports for enzyme immobilization and nonaqueous catalysis. *Journal of Combinatorial Chemistry* **2007**, 9, (3), 399-406.
11. Persson, M.; Wehtje, E.; Adlercreutz, P., Factors governing the activity of lyophilised and immobilised lipase preparations in organic solvents. *Chembiochem* **2002**, 3, (6), 566-571.
12. Bosley, J. A.; Peilow, A. D., Immobilization of lipases on porous polypropylene: Reduction in esterification efficiency at low loading. *Journal of the American Oil Chemists Society* **1997**, 74, (2), 107-111.
13. van der Veen, M.; Stuart, M. C.; Norde, W., Spreading of proteins and its effect on adsorption and desorption kinetics. *Colloids and Surfaces B-Biointerfaces* **2007**, 54, (2), 136-142.
14. Zoumpantioti, M.; Parmaklis, P.; de Maria, P. D.; Stamatis, H.; Sinisterra, J. V.; Xenakis, A., Esterification reactions catalyzed by lipases immobilized in organogels: effect of temperature and substrate diffusion. *Biotechnology Letters* **2008**, 30, (9), 1627-1631.
15. Sheldon, R. A.; Schoevaart, R.; Van Langen, L. M., Cross-linked enzyme aggregates (CLEAs): A novel and versatile method for enzyme immobilization (a review). *Biocatalysis and Biotransformation* **2005**, 23, (3-4), 141-147.
16. Ghanem, A., The utility of cyclodextrins in lipase-catalyzed transesterification in organic solvents: enhanced reaction rate and enantioselectivity. *Organic & Biomolecular Chemistry* **2003**, 1, (8), 1282-1291.

17. Mine, Y.; Fukunaga, K.; Itoh, K.; Yoshimoto, M.; Nakao, K.; Sugimura, Y., Enhanced enzyme activity and enantioselectivity of lipases in organic solvents by crown ethers and cyclodextrins. *Journal of Bioscience and Bioengineering* **2003**, 95, (5), 441-447.
18. Lindsay, J. P.; Clark, D. S.; Dordick, J. S., Penicillin amidase is activated for use in nonaqueous media by lyophilizing in the presence of potassium chloride. *Enzyme and Microbial Technology* **2002**, 31, (3), 193-197.
19. Lindsay, J. P.; Clark, D. S.; Dordick, J. S., Combinatorial formulation of biocatalyst preparations for increased activity in organic solvents: Salt activation of penicillin amidase. *Biotechnology and Bioengineering* **2004**, 85, (5), 553-560.
20. Santos, A. M.; Vidal, M.; Pacheco, Y.; Frontera, J.; Baez, C.; Ornellas, O.; Barletta, G.; Griebenow, K., Effect of crown ethers on structure, stability, activity, and enantioselectivity of subtilisin Carlsberg in organic solvents. *Biotechnology and Bioengineering* **2001**, 74, (4), 295-308.
21. Secundo, F.; Barletta, G. L.; Dumitriu, E.; Carrea, G., Can an inactivating agent increase enzyme activity in organic solvent? Effects of 18-crown-6 on lipase activity, enantioselectivity, and conformation. *Biotechnology and Bioengineering* **2007**, 97, (1), 12-18.
22. Chen, B.; Hu, J.; Miller, E. M.; Xie, W. C.; Cai, M. M.; Gross, R. A., *Candida antarctica* lipase B chemically immobilized on epoxy-activated micro- and nanobeads: Catalysts for polyester synthesis. *Biomacromolecules* **2008**, 9, (2), 463-471.
23. Chen, Y. Z.; Yang, C. T.; Ching, C. B.; Xu, R., Immobilization of lipases on hydrophobized zirconia nanoparticles: Highly enantioselective and reusable biocatalysts. *Langmuir* **2008**, 24, (16), 8877-8884.
24. Cruz, J. C.; Pfromm, P. H.; Rezac, M. E., Immobilization of *Candida antarctica* Lipase B on fumed silica. *Process Biochemistry* **2009**, 44, (1), 62-69.
25. Pfromm, P. H.; Rezac, M. E.; Wurges, K.; Czermak, P., Fumed silica activated subtilisin Carlsberg in hexane in a packed-bed reactor. *AIChE Journal* **2007**, 53, (1), 237-242.
26. Wurges, K.; Pfromm, P. H.; Rezac, M. E.; Czermak, P., Activation of *subtilisin Carlsberg* in hexane by lyophilization in the presence of fumed silica. *Journal of Molecular Catalysis B-Enzymatic* **2005**, 34, (1-6), 18-24.

27. Koops, B. C.; Papadimou, E.; Verheij, H. M.; Slotboom, A. J.; Egmond, M. R., Activity and stability of chemically modified *Candida antarctica* lipase B adsorbed on solid supports. *Applied Microbiology and Biotechnology* **1999**, 52, (6), 791-796.
28. Unsworth, L. D.; van der Oost, J.; Koutsopoulos, S., Hyperthermophilic enzymes - stability, activity and implementation strategies for high temperature applications. *Febs Journal* **2007**, 274, (16), 4044-4056.
29. Uppenberg, J., Sequence, Crystal-Structure Determination and Refinement of 2 Crystal Forms of Lipase-B from *Candida antarctica*. *Structure* **1994**, 2, (4), 293-308.
30. Chen, C. S.; Fujimoto, Y.; Girdaukas, G.; Sih, C. J., Quantitative-Analyses of Biochemical Kinetic Resolutions of Enantiomers. *Journal of the American Chemical Society* **1982**, 104, (25), 7294-7299.
31. Vantol, J. B. A.; Kraayveld, D. E.; Jongejan, J. A.; Duine, J. A., The Catalytic Performance of Pig Pancreas Lipase in Enantioselective Transesterification in Organic-Solvents. *Biocatalysis and Biotransformation* **1995**, 12, (2), 119-136.
32. Iler, R. K., *Chemistry of Silica - Solubility, Polymerization, Colloid and Surface Properties and Biochemistry*. **1979**.
33. Sriappareddy, T. A.; Shinji, H. C.; Takanori, T. A.; Mahabubur, R. T. D.; Kondo, A.; Fukuda, H., Immobilized recombinant *Aspergillus oryzae* expressing heterologous lipase: An efficient whole-cell biocatalyst for enantioselective transesterification in non-aqueous medium. *Journal of Molecular Catalysis B-Enzymatic* **2007**, 48, (1-2), 33-37.
34. Han, Y.; Lee, S. S.; Ying, J. Y., Pressure-driven enzyme entrapment in siliceous mesocellular foam. *Chemistry of Materials* **2006**, 18, (3), 643-649.
35. Kamori, M.; Yamashita, Y.; Naoshima, Y., Enzyme immobilization utilizing a porous ceramics support for chiral synthesis. *Chirality* **2002**, 14, (7), 558-561.
36. Kang, I. J.; Pfromm, P. H.; Rezac, M. E., Real time measurement and control of thermodynamic water activities for enzymatic catalysis in hexane. *Journal of Biotechnology* **2005**, 119, (2), 147-154.
37. Cao, L., Adsorption-based Immobilization. In *Carrier-bound Immobilized Enzymes: Principles, Applications and Design*, Wiley-VCH Verlag GmbH & Co. KGaA, Germany: Weinheim, **2005**; Vol. 1, pp 53-168.

38. Janssen, M. H. A.; van Langen, L. M.; Pereira, S. R. M.; van Rantwijk, F.; Sheldon, R. A., Evaluation of the performance of immobilized penicillin G acylase using active-site titration. *Biotechnology and Bioengineering* **2002**, 78, (4), 425-432.

CHAPTER - 5 Conformational Changes and Catalytic Competency of Hydrolases Adsorbing on Fumed Silica: I.

Tertiary Structure

5.1 Abstract

We have recently introduced an immobilization protocol for preparations of enzymes on fumed silica for catalysis in organic solvents. The observation of a maximum in apparent catalytic activity at intermediate surface coverage for one enzyme while another enzyme showed continuously increasing apparent catalytic activity with decreasing surface coverage led to speculation on the impact of surface coverage on apparent catalytic activity through different relative surface-protein and protein-protein interactions, combined with different “hardness” or resistance towards unfolding by the enzymes. The kinetics of tertiary unfolding of *Candida antarctica* Lipase B (CALB), *subtilisin Carlsberg*, and the Lipase from *Thermomyces lanuginosus* (TLL) adsorbing on fumed silica nanoparticles were inferred here from tryptophan fluorescence for 2%SC to 1250%SC, 0.5 mg/mL to 4.70 mg/mL enzyme concentration in aqueous buffer solution, and in the presence of the structural modifiers 2,2,2-trifluoroethanol (TFE) and Dithiothreitol (DTT). The results shown here confirm the earlier speculation that “hard” enzymes can perform well at low and intermediate surface coverage of the solid fumed silica particles until multi-layer packing imposes mass transfer limitations, while “soft” enzymes unfold at low surface coverage and therefore show a maximum in catalytic competency at intermediate surface coverage before declining apparent activity is caused by multi-layer packing.

5.2 Introduction

The synthesis of organic compounds often requires non-aqueous media due to solubility and stability issues, and undesirable side reactions in the presence of water¹⁻⁷. Many chemical synthesis schemes require multiple steps and may involve toxic inorganic catalysts as well as generate undesirable by-products^{8,9}. One avenue to overcome the issues with chemical synthesis has been the extension of enzymatic catalysis in aqueous media to non-aqueous media exploiting the exquisite regio- and stereo- selectivity of enzymes^{2,5,10} in addition to the fact that enzymatic

catalysts are generally renewable and non-toxic. However, poor enzyme solubility in solvents¹¹ generally requires to either solubilize the enzyme or immobilize it on a solid support¹²⁻¹⁸ to avoid mass transfer limitations for the desired reaction. There has been an increasing interest in the immobilization of enzymes on nanoparticles due to their unique properties including the extremely large surface area per mass¹⁹.

We have recently introduced an immobilization protocol with an inexpensive nanostructured support¹⁶⁻¹⁸. Fumed silica is a fractal aggregate that consists of individual spherical non-porous nanoparticles linked in necklace-like structures²⁰⁻²². This material has proven to be an exceptional adsorbent for proteins and polymers²³⁻²⁵. In our two-step immobilization protocol, the enzyme molecules are first physically adsorbed on fumed silica in an aqueous buffer. The adsorbate is then lyophilized. We have previously considered *subtilisin Carlsberg* and *Candida antarctica* Lipase B (CALB) to assess our immobilization protocol, alterations in physical properties, and the impact on the catalytic competency. These enzymes were chosen due to their wide range of applications in nonaqueous media. The maximum observed catalytic activity in hexane reached or even exceeded commercial immobilizates of CALB¹³⁻¹⁵ and what has been termed “salt-activated” preparations for *s. Carlsberg*^{26, 27}. CALB is a monomeric 317 residue protein²⁸ with five tryptophan (Trp52, Trp65, Trp104, Trp113 and Trp155) nine tyrosine, and ten phenylalanine residues, which can be monitored to follow conformational changes²⁸. CALB’s structure is stabilized by four disulfide bridges²⁸. The *s. Carlsberg* protein is a single polypeptide chain consisting of 274 amino acid residues²⁹ including one surface exposed tryptophan (Trp117) and thirteen tyrosine residues^{30, 31}. The Trp fluorescence of *s. Carlsberg*, however, dominates mainly due to quenching and energy transfer mechanisms^{30, 31}.

We have previously reported on the relationship of surface coverage to apparent catalytic activity of enzymes immobilized on fumed silica¹⁶⁻¹⁸. The *s. Carlsberg* exhibited a constant increase in apparent catalytic activity as more surface area is provided per enzyme molecule for immobilization. This enzyme increase levels off after sufficient area is available for a nominally “sparse” surface population. CALB, however, showed a maximum in apparent catalytic activity with steep decreases at both higher and lower surface coverage. In accordance with previously reported observations¹²⁻¹⁵, we postulated that this maximum in apparent catalytic activity corresponds to a surface loading regime at intermediate surface coverage that results from the

overlapping of two other surface regimes at high and low coverages: I. low surface coverage with opportunities for multi-point attachment of the enzyme on the support promoting detrimental conformational changes, II. an intermediate surface coverage where some interactions with neighboring enzyme molecules in addition to interactions with the support surface help to maintain a higher population of catalytically competent enzyme molecules, and III. increasingly multi-layer coverage where mass transfer limitations reduce the apparent catalytic activity with increasing enzyme loading per support area.

The multi-point attachment and deformation under regime I. appears to promote substantial conformational changes and consequently loss of catalytic activity for CALB. Previous investigations have demonstrated that proteins can either deform or maintain their structure upon adsorption on nanomaterials³²⁻³⁵ depending on the chemistry, size, and curvature of the nanomaterials³⁶, the intricate intermolecular forces between the surface and the protein³⁷, and the conformational stability of the protein^{38, 39}. A more complete understanding of these phenomena appears crucial not only for enzyme based biocatalysis but for a number of emerging fields including nanobiophotonics^{40, 41} and nanobioelectronics^{42, 43}.

Hitherto, information regarding in-situ conformation/structure of immobilized enzyme molecules remains scarce⁴⁴. A characterization of the folding/unfolding tendencies for enzymes interacting with surfaces will help to engineer strategies for the development of structurally stable and highly active biocatalysts for use in solvents^{39, 44-46}. Fourier Transform Infrared- (FTIR), Circular Dichroism- (CD), Intrinsic Fluorescence-, Raman optical activity- and Nuclear Magnetic Resonance (NMR) spectroscopy techniques are the preferred techniques for conformational assessment of proteins^{39, 44-49}. The intrinsic tryptophan fluorescence has been described as particularly well suited for characterizing tertiary conformational changes of adsorbed proteins on nanomaterials^{39, 45, 46, 50}. Fluorescence spectroscopy is applied here to probe the kinetics of tertiary conformational changes of enzymes adsorbing on fumed silica nanoparticles from the aqueous phase for CALB, *s. Carlsberg* and the Lipase from *Thermomyces lanuginosus* (TLL). TLL was added as an external control representing high intrinsic conformational stability.

We show evidence that for CALB in hexane the previously observed maximum in apparent catalytic activity, at an intermediate surface coverage of fumed silica nanoparticles, is most likely related to the low conformational stability of this enzyme. Conversely, the *s.*

Carlsberg and TLL enzymes appear to be conformationally more stable. The time-course of unfolding during and after adsorption on fumed silica followed for about 40 minutes clearly shows that CALB undergoes some unfolding and refolding until a steady-state is reached as would be expected for a “soft” enzyme⁵¹. Structurally “hard” *s. Carlsberg* and TLL, however, unfold gradually before reaching steady-state on fumed silica at both low and high surface coverages. At equilibrium, all three enzymes exhibited distinctly different regions of conformational stability. Comparison with the apparent catalytic activity of the lyophilized enzyme adsorbates in hexane demonstrates that the postulated impact of changing surface coverage on the stabilization of adsorbed molecules is corroborated by the spectroscopic unfolding measurements. Finally, we will also discuss the impact of structure modifiers on the conformational stability conditions and thereby on immobilization on fumed silica.

5.3 Materials and Methods

5.3.1 Materials

Crude CALB (lyophilized; specific activity of 28U/mg solid) and TLL (lyophilized; specific activity of 1400U/mg solid) were obtained from Codexis, Inc. (Pasadena, CA), stored at 4°C, and used as-received. TLL is a glycosylated monomeric protein with 269 amino acid residues, among them four tryptophans (Trp89, Trp117, Trp221, Trp260)⁵²⁻⁵⁵. TLL is used for the interesterification and hydrolysis of vegetable oils and animal fats⁵⁶. *Subtilisin Carlsberg* (EC 3.4.21.14; proteinase from *Bacillus licheniformis*; specific activity of 8 U/mg solid), fumed silica (purity of 99.8 wt.%, specific surface area 255 m²/g, primary particle diameter ~7-50 nm, as reported by the manufacturer), ultrapure Guanidine Hydrochloride (GdmCl), 2,2,2-trifluoroethanol (TFE), and dithiothreitol (DTT) were from Sigma-Aldrich (St. Louis, MO), and used as received. Glass vials (24 mL screw-capped, flat-bottom) were used to prepare the enzyme-fumed silica suspensions.

5.3.2 Unfolding of Enzymes by GdmCl in Aqueous Buffer

The intrinsic fluorescence spectroscopy method to detect unfolding was tested for reference with the powerful denaturant GdmCl in aqueous buffer solution. Unfolding relocates Trp residues^{45, 46, 55, 57} which is detectable by fluorescence spectroscopy. Crude enzyme was weighed in a glass vial and 10 mM monobasic phosphate buffer (0.5 to 4.7 mg enzyme/mL,

adjusted to pH 7.8 by KOH) containing GdmCl with final concentrations in the range of 1M to 8M was added followed by vortexing for about 30 seconds. Trp is excited at 288 nm. At least five scans were performed and averaged for each sample. Unfolding was monitored in a quartz cuvette (3mm pathlength; Starna Cells, Atascadero CA) by collecting the emission spectrum from 300 to 500 nm (Cary Eclipse spectrofluorimeter, Varian, Cary, NC, 25°C). Excitation and emission bandpasses were set at 5 nm. Maximum emission intensity ($I_{\max/em}$) and maximal emission wavelength ($\lambda_{\max/em}$) were extracted from the spectra.

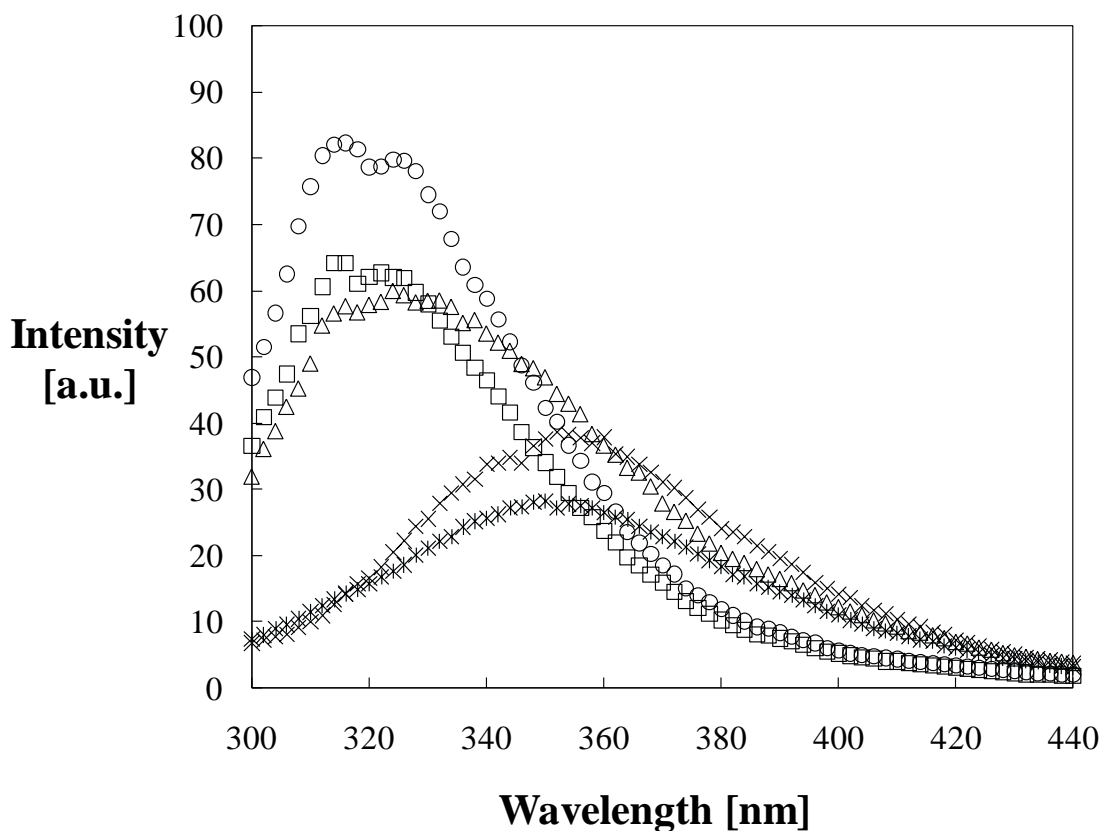


Figure 5.1. Tryptophan fluorescence spectrum of the unfolding of CALB induced by GdmCl in aqueous buffer solution. (○) Native, (□) 1M GdmCl, (Δ) 2M GdmCl, (×) 4M GdmCl and (*) 8M GdmCl. Enzyme concentration of 0.5 mg/mL and pH 7.8.

Two phenomena have been identified for globular proteins undergoing unfolding initiated by changing from low to high concentrations of GdmCl: 1. Decrease in $I_{\max/em}$ and 2. shifting of $\lambda_{\max/em}$ towards the red through exposure of the Trp residues to the buffer^{54, 55, 58}. Figure 5.1 shows typical tryptophan emission spectra for the unfolding of CALB in aqueous buffer solution by GdmCl from zero to 8M about 30 seconds after the denaturant was added to the enzyme solution. The spectra are assumed to be at equilibrium since no further changes after this

measurement were detected over 40 minutes. The decrease in the maximum intensity is attributed to a significant reduction in the quantum yield of the now increasingly exposed Trp residues^{54, 55, 58}, while the red (right) shifting is attributed to the increased hydrophilicity of the environment surrounding the Trp residues^{54, 55, 58}.

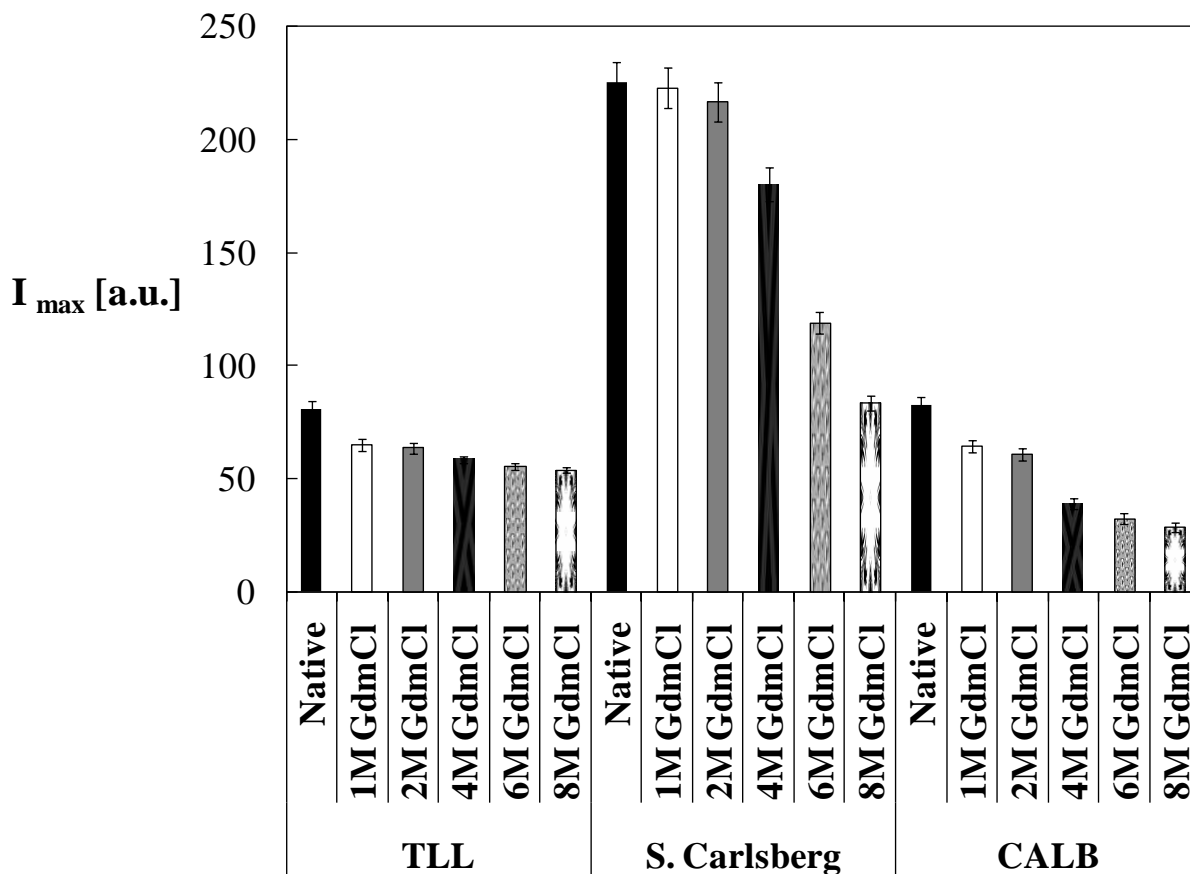


Figure 5.2. Decrease in the maximum emission intensity of Tryptophan residues due to GdmCl induced unfolding. Enzyme concentration was maintained at 0.5 mg/mL and pH 7.8 in all cases. CALB unfolds to a larger extent when compared with *s. Carlsberg* and TLL which have tightly packed structures. y -error bars represent the standard error of multiple analyses of identical samples.

Figure 5.2 confirms how a denaturant's action can be tracked by the $I_{\max/em}$ as was reported in the literature. The impact on CALB is strongest likely due to its low conformational stability while *s. Carlsberg* and TLL are less impacted due to their rigid structures. This data confirms that under the conditions of our aqueous buffer solutions, unfolding for the test enzymes can be monitored by tracking subtle changes in the emission intensity of the Trp residues. Furthermore, it allowed us to qualitatively rank the test enzymes in order of increasing conformational stability: CALB, *s. Carlsberg*, TLL.

5.3.3 Unfolded Fraction Inference for GdmCl Unfolding in Aqueous Buffer Solution

The unfolding data in the presence of GdmCl can be normalized to define an unfolded fraction (ϕ) as follows^{45, 46}:

$$\phi_{GdmCl} = 1 - \left(\frac{I_{\lambda}^S - I_{\lambda}^{8M\ GdmCl}}{I_{\lambda}^N - I_{\lambda}^{8M\ GdmCl}} \right) \quad \text{Equation 5.1}$$

where ϕ_{GdmCl} is the unfolded fraction (0, native; 1, completely unfolded).

I_{λ}^S is the emission intensity at a fixed wavelength for enzyme molecule ensembles at any state of unfolding, I_{λ}^N is the emission intensity at a fixed wavelength for ensembles of native enzyme molecules, and $I_{\lambda}^{8M\ GdmCl}$ is the emission intensity at a fixed wavelength for fully unfolded enzyme ensembles all in aqueous buffer and in arbitrary units (a.u.).

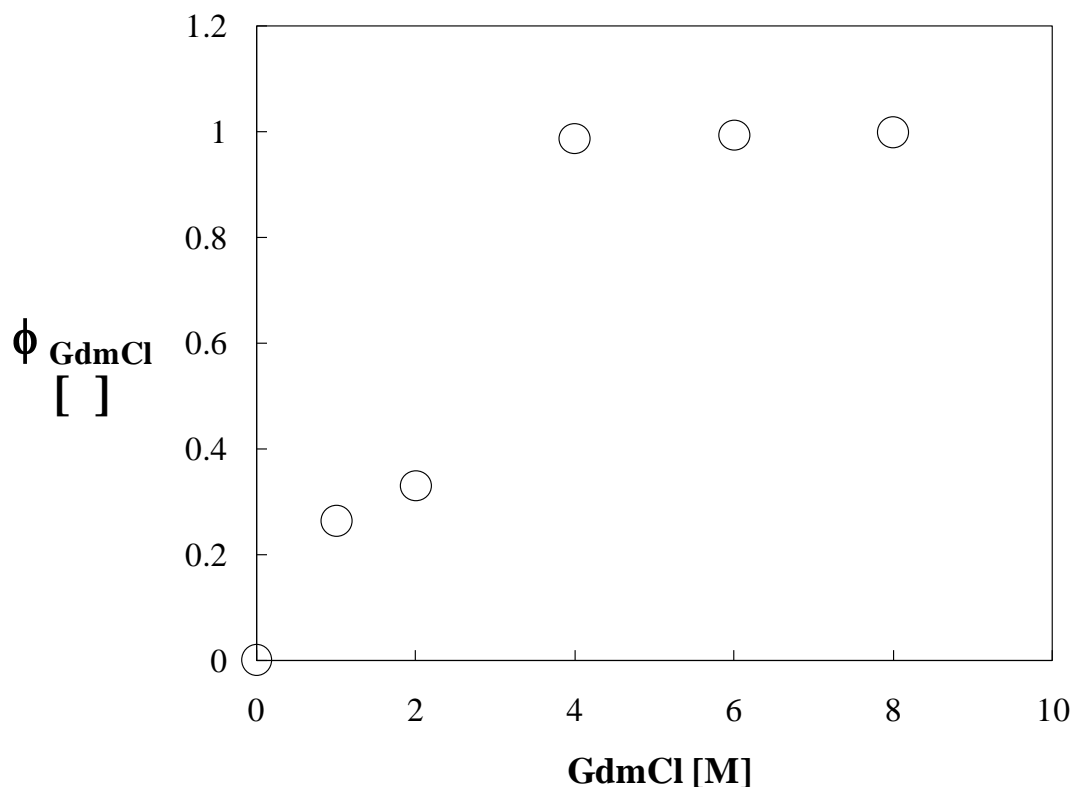


Figure 5.3. Normalized fluorescence intensity for the GdmCl induced unfolding of CALB in aqueous buffer. The tryptophan emission was monitored at 330 nm. Measurements were carried out at enzyme concentration of 0.5 mg/mL and pH 7.8. Similar calibration curves were obtained for *s. Carlsberg* and TLL (data not shown).

TLL shows the highest resistance to unfolding followed by *s. Carlsberg* and then CALB based on the relative loss of $I_{\max/\text{em}}$ from native enzyme to 8M GdmCl. This is corroborated by CALB's plasticity and molecular dynamism⁵⁹ as opposed to the rigidity of structurally "hard" *s. Carlsberg* and TLL^{31, 60}. Similar plots were obtained for other enzyme concentrations (data not shown). In all cases, the enzyme most resistant to denaturation by GdmCl is TLL with CALB being denatured most easily.

The wavelength was selected as 330 nm for CALB and TLL and as 305 nm for *s. Carlsberg*. These wavelengths were found to produce the best resolution for detecting different unfolding levels. The ϕ_{GdmCl} values showed a linear dependency on the GdmCl concentration^{45, 46} and served as reference to determine the extent of tertiary unfolding in the presence of fumed silica nanoparticles (Figure 5.3). Similar calibration curves were prepared for other enzyme concentrations as well as for the other enzymes under study.

No significant changes in $\lambda_{\max/\text{em}}$ were detected for *s. Carlsberg*, which limits the application of this approach for monitoring unfolding under the conditions of our buffer solutions (data not shown).

5.3.4 Baseline for Kinetic Experiments

Buffer only (no enzyme) and nanoparticles in buffer (no enzyme), as well as enzymes in buffer were served as the controls at typical concentrations. These solutions showed no time-dependent change in intensity over 40 minutes as expected^{45, 46} leading to the conclusion that all changes with time were attributable to changes in the enzyme molecules introduced by interaction of enzymes, nanoparticles, and added chemicals.

5.3.5 Kinetics of Tertiary Conformational Changes of Enzymes Adsorbing/Desorbing on Fumed Silica

The time evolution of the tertiary conformational changes of enzymes interacting with fumed silica nanoparticles were monitored by following the emission intensity of Trp residues at a fixed wavelength. Crude enzymes (i.e., CALB, *s. Carlsberg* and TLL) were weighed in a glass vial and 10 mM monobasic phosphate (adjusted to pH 7.8 by KOH) was added followed by vortexing for about 30 seconds. Fumed silica was then added and vortexed until visually homogeneous suspensions were formed (about 30 seconds) as described elsewhere¹⁶⁻¹⁸. Table 5.1

shows a summary of the amounts of fumed silica and enzyme used to form the suspensions at the various nominal surface coverages %SC of enzyme in the final enzyme/fumed silica adsorbates.

The suspensions were transferred to quartz cuvettes and placed in the spectrofluorimeter which was set at 25°C. The excitation was set at 288 nm and the emission collected at 330 nm for CALB and TLL and at 305 nm for *s. Carlsberg*.

Table 5.1. Summary of the amounts of fumed silica and enzyme employed to form the suspensions with different nominal surface coverages. The enzyme concentration for each suspension was varied from 0.5 mg/mL to 4.70 mg/mL.

Enzyme	Enzyme mass (mg)	Mass fumed silica (g)					
		2%SC*	17%SC	100%SC	230%SC	400%SC	1250%SC
CALB	7	0.718	0.092	0.016	0.0068	0.0039	0.0013
TLL	5	0.350	0.040	0.010	0.0030	0.0018	0.0006
<i>s. Carlsberg</i>	5	0.315	0.036	0.009	0.0027	0.0016	0.0005

* The Nominal Surface Coverage (% SC) was calculated as follows:

$$\%SC = \frac{\text{Projected area of enzyme molecule}}{\text{Nominal surface area of Fumed Silica}} * 100 \quad \text{Equation 5.2}$$

The projected area of enzyme is calculated assuming a spherical shape for the enzyme molecules. The diameter of the enzyme molecules from crystallographic data were 6.4 nm²⁸, 5.0 nm⁶³, and 4.2 nm²⁹ for CALB, TLL and *s. Carlsberg*, respectively. The nominal surface area of fumed silica is as provided by the manufacturer: 255m²/g.

5.3.6 Unfolded Fraction Inference for Kinetic Experiments with Fumed Silica in Aqueous Solution

The kinetics of tertiary unfolding of the enzymes in the presence of fumed silica were normalized according to Equation 5.3^{45, 46}:

$$\phi_{FS} = 1 - \left(\frac{I_{FS}^S_{\lambda} - I^{8M GdmCl}_{\lambda}}{I^N_{\lambda} - I^{8M GdmCl}_{\lambda}} \right) \quad \text{Equation 5.3}$$

where ϕ_{FS} is the instantaneous unfolded fraction for enzymes in the presence of fumed silica nanoparticles (0, native; 1, completely unfolded).

$I_{FS}^S_{\lambda}$ is the net average emission intensity at a fixed wavelength of enzyme molecule ensembles interacting with fumed silica at any instantaneous state of unfolding (obtained by subtracting the corresponding instantaneous contribution of buffer and nanoparticles), I^N_{λ} is the average

emission intensity at a fixed wavelength for the ensembles of native enzyme molecules, and $I^{\text{8M GdmCl}}_{\lambda}$ is the average emission intensity at a fixed wavelength for fully unfolded enzyme ensembles all in aqueous buffer and in arbitrary units (a.u.).

5.3.7 Regions of Conformational Stability: 3D Filled Contour Plots

Enzyme solutions of CALB and *s. Carlsberg* at concentrations of 0.5, 0.7, 3.30, and 4.70 mg/mL were mixed with nanoparticles to form adsorbates with different %SC according to Table 5.1. For TLL 0.5, 0.7, and 3.30 mg/mL were explored. Each suspension was monitored over about 40 minutes for changes in the tertiary structure via spectrofluorimetry (above). The final equilibrium values for deformation (as a function of total enzyme molecules present) for each enzyme are plotted as the elevation (*z*-direction) of contour plots where the *y*-axis is the concentration of enzyme in the solution at the beginning of preparing the adsorbate and the horizontal *x*-axis represents the expected %SC by the enzyme molecules in the obtained adsorbates (Table 5.1). Figure 5.4 shows the deformation data for CALB on fumed silica as an example to introduce this type of plot. A total of 20 data points for CALB and *s. Carlsberg*, and 15 points for TLL were used to develop contour plots (see below). An inverse-distance algorithm (SigmaPlot®) was used to interpolate. Figure 5.4 indicates that at low surface coverage deformation becomes very significant, no matter what the initial concentration to prepare the adsorbate was. Detailed discussions follow below.

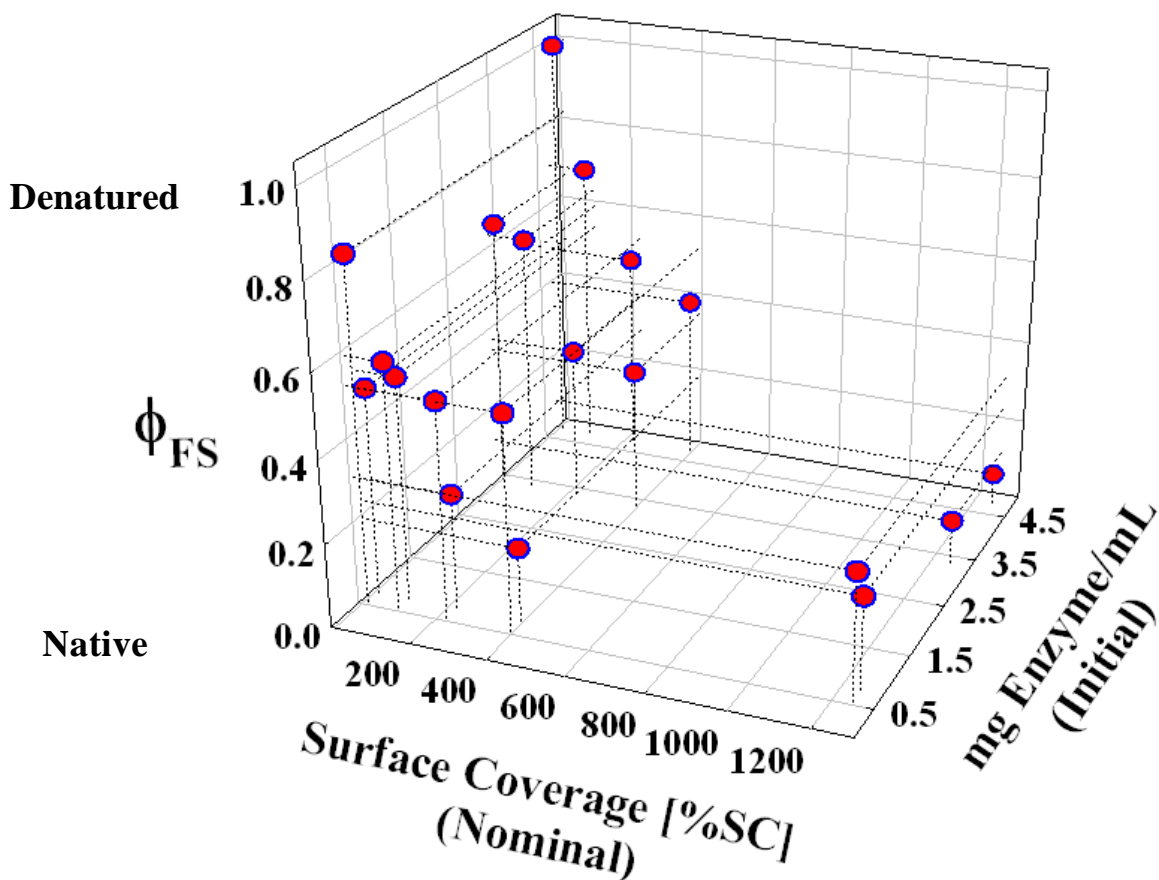


Figure 5.4. Unfolding data for CALB on fumed silica (z-axis) as a function of initial enzyme concentration (y-axis) and nominal surface coverage (x-axis). These data will be shown in 3D contour plots to identify regions of conformational stability and to subsequently correlate them with the surface loading regimes previously postulated for the lyophilized adsorbates.

5.4 Results and Discussion

5.4.1 Deformation of Enzymes during Adsorption/Desorption on Fumed Silica in Aqueous Solution

Time-dependent fluorescence intensity changes from the Trp residues were used to monitor the structural alteration kinetics of enzymes interacting with fumed silica. Only events after ~30 s could be monitored due to the time needed to mix and vortex suspensions. Baselines for nanoparticle suspensions as well as for the enzyme solutions remained approximately constant as a function of time with a combined error of 7%. Error propagation analysis for the unfolded fraction function (ϕ_{FS}) (Equation 5.3) indicates an error of ~2% or equivalently $\phi_{FS} \pm$

0.02. Deviations from the linear behavior and beyond this error limit can be, therefore, attributed to structural changes.

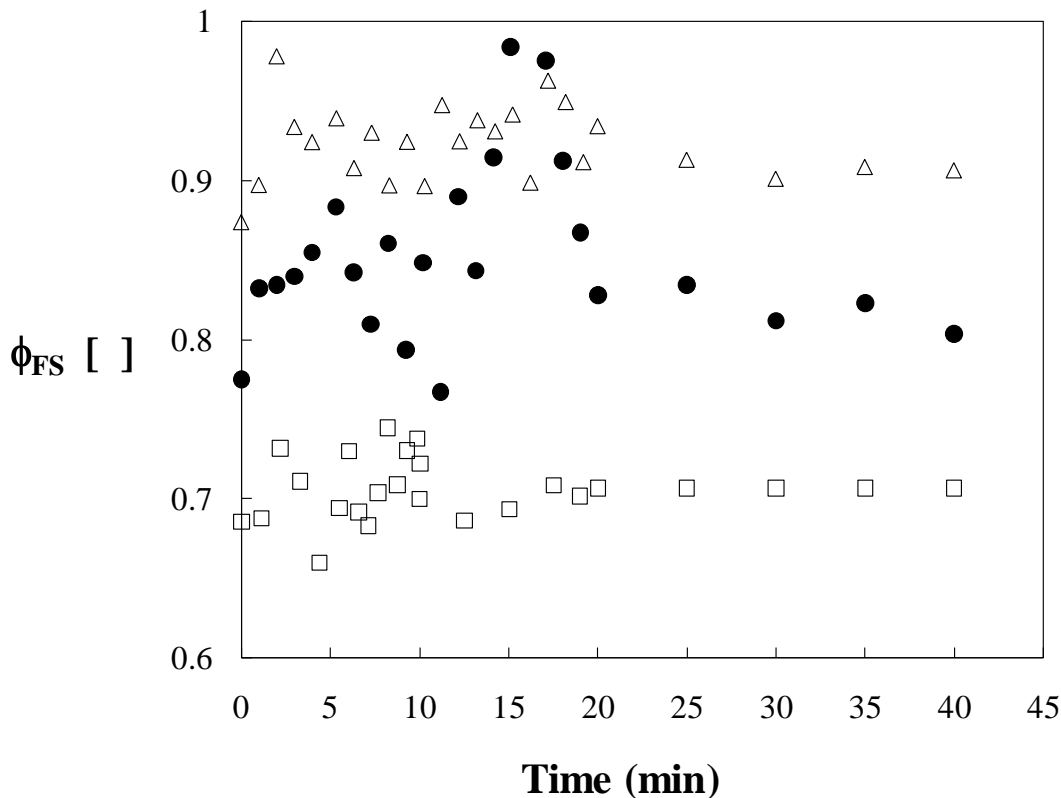


Figure 5.5. Unfolding kinetics of (●) CALB, (□) *s. Carlsberg* and (Δ) TLL adsorbing on fumed silica nanoparticles to form adsorbates with a nominal surface coverage of 2%SC. Data is normalized with the corresponding calibration curves and subsequently expressed as unfolded fraction. Enzyme concentration was maintained at 0.5 mg/mL and pH at 7.8.

Figure 5.5 compares the time evolution of the unfolding of CALB, *s. Carlsberg* and TLL in the presence of fumed silica. Here, we explore tertiary structural changes of enzymes adsorbing on fumed silica that occur at long time scales (order of several minutes). This time framework encompasses adsorption events that lead to surface saturation as reported previously¹⁶. In this case, adsorbates forming a low surface coverage of 2%SC are shown. The three enzymes underwent an initial rapid structural change (high initial ϕ_{FS} values). Those initial events are thought to occur within a very short time scale on the order of milliseconds⁴⁶ and consequently cannot be tracked with the techniques used in this study.

Unfolding studies by others for proteins adsorbing on colloidal silica nanoparticles revealed rapid initial unfolding for both β lactoglobulin (1200 min)⁴⁵ and Cytochrome c (10 min)³⁹ followed by slower unfolding. For lysozyme (600 min)⁴⁶, on the other hand, three events

were detected: an initial rapid unfolding followed by a slower refolding, and finally a slow unfolding leading to apparent equilibrium.

Over the initial 20 minutes, CALB molecules undergo both unfolding and refolding until an apparent equilibrium is reached. This might be attributed to the already demonstrated plasticity/dynamism of this enzyme⁵⁹. CALB's structure is composed of seven central β strands flanked by ten α helices⁵⁹. The $\alpha 5$ and $\alpha 10$ are highly mobile regions thought to be involved in CALB's molecular dynamism also demonstrated by CALB's catalytic promiscuity⁶¹. Trp 113 (detected by our technique) is in close proximity to a mobile $\alpha 5$ region.

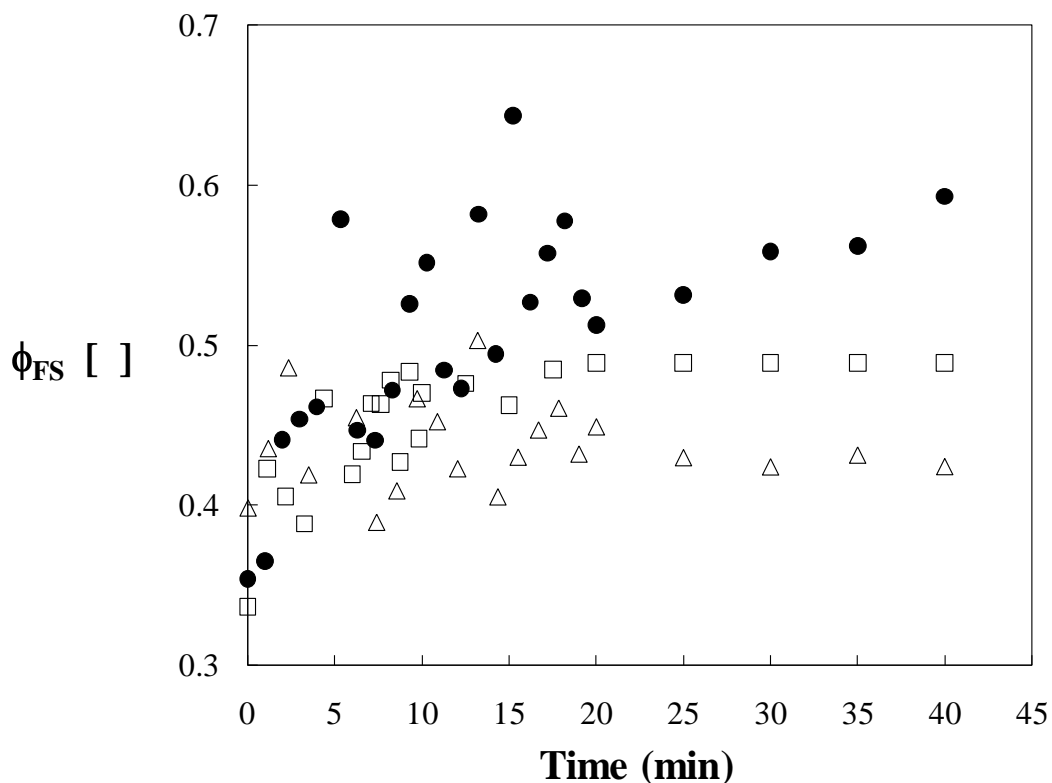


Figure 5.6. Unfolding kinetics of (●) CALB, (□) *s. Carlsberg* and (Δ) TLL adsorbing of fumed silica nanoparticles to form adsorbates with a nominal surface coverage of 100%SC. Data is normalized with the corresponding calibration curves and subsequently expressed as unfolded fraction using Equation 5.3. Enzyme concentration was maintained at 0.5 mg/mL and pH at 7.8.

An alternative explanation of the unfolding/refolding of CALB is reorientation of CALB molecules on the surface of the nanoparticles towards a low energy state as suggested in the literature (^{46 51}). As opposed to CALB, both TLL and *s. Carlsberg*, showed no significant further conformational changes as indicated by essentially constant ϕ_{FS} values. This is most likely a

consequence of the stable structures of these two enzymes. In all cases, no significant net conformational change was observed beyond the initial value.

Figure 5.6 shows that decreasing the amount of nanoparticles to form adsorbates with 100%SC leads to both lower initial and equilibrium deformation for all three enzymes as reported by others⁴⁶ for lysozyme adsorbed on colloidal silica nanoparticles at high protein surface concentrations. The lower extent of denaturation was attributed to the higher crowding regime where protein-protein interactions become more dominant and help to stabilize the protein conformation.

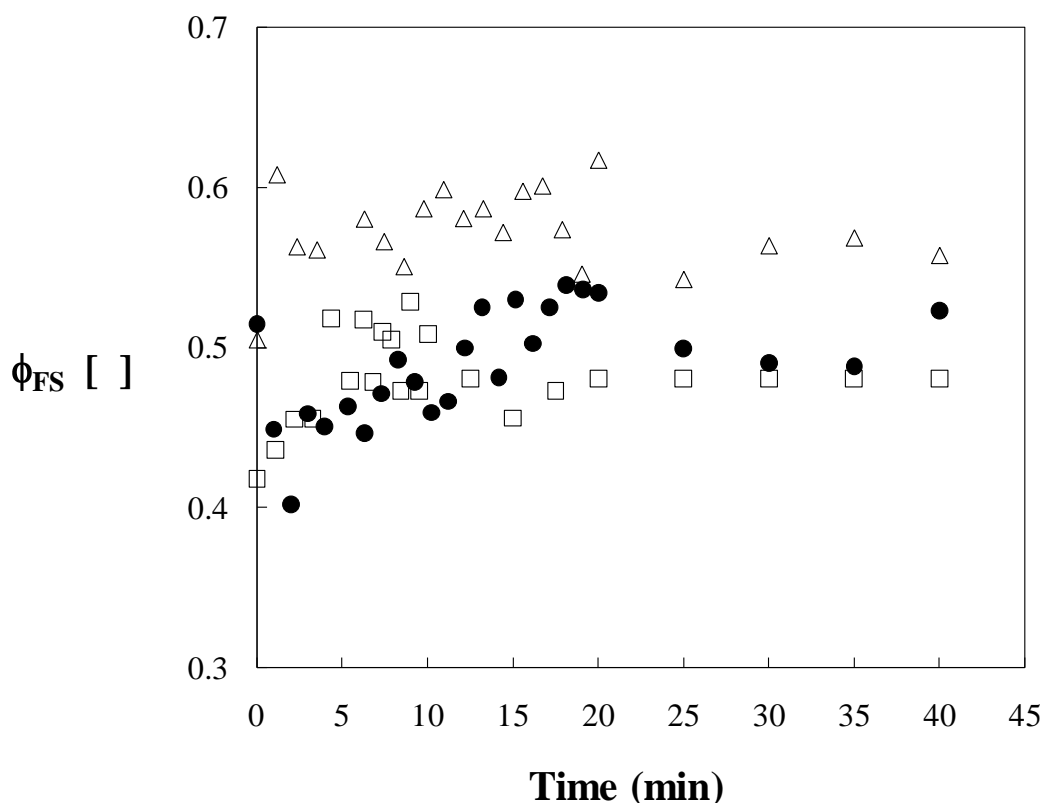


Figure 5.7. Unfolding kinetics of (●) CALB, (□) *s. Carlsberg* and (Δ) TLL adsorbed on fumed silica nanoparticles to obtain a nominal surface coverage of 400%SC. Data is normalized with the corresponding calibration curves and subsequently expressed as unfolded fraction using Equation 5.3. Enzyme concentration was maintained at 0.5 mg/mL and pH at 7.8.

The dramatic changes of ϕ_{FS} can be rationalized again by the continuous reorientation/reorganization of the flexible unfolded state of CALB molecules on the surface of

the nanoparticles. In this case, however, rapid initial unfolding followed by a slower phase was observed as reported for β lactoglobulin⁴⁵. A significant net unfolding above the initial value was also observed for *s. Carlsberg*. No significant net unfolding for TLL was observed. The equilibrium values of unfolding correlated with the conformational stability or “hardness” of the enzymes. “Hard” TLL unfolded the least while “soft” CALB unfolded the most.

The amount of fumed silica added was decreased even further to form adsorbates with nominal 400%SC (Figure 5.7). The equilibrium unfolding values for the three enzymes are quite similar. This further supports the notion that protein-protein interaction precludes structural perturbations. The unfolding pathways for CALB and *s. Carlsberg* show logarithmic trends over time. This can be attributed to a two-stage model of unfolding³⁹. The unfolding trace for TLL is essentially horizontal and consequently reflects no significant net unfolding with respect to the initial value.

5.4.2 Regions of Conformational Stability for Enzyme/Fumed Silica Adsorbates

A general view of conformational stability for the three hydrolases adsorbing on fumed silica was obtained by conducting multiple unfolding experiments for various surface coverages and enzyme concentrations according to Table 5.1.

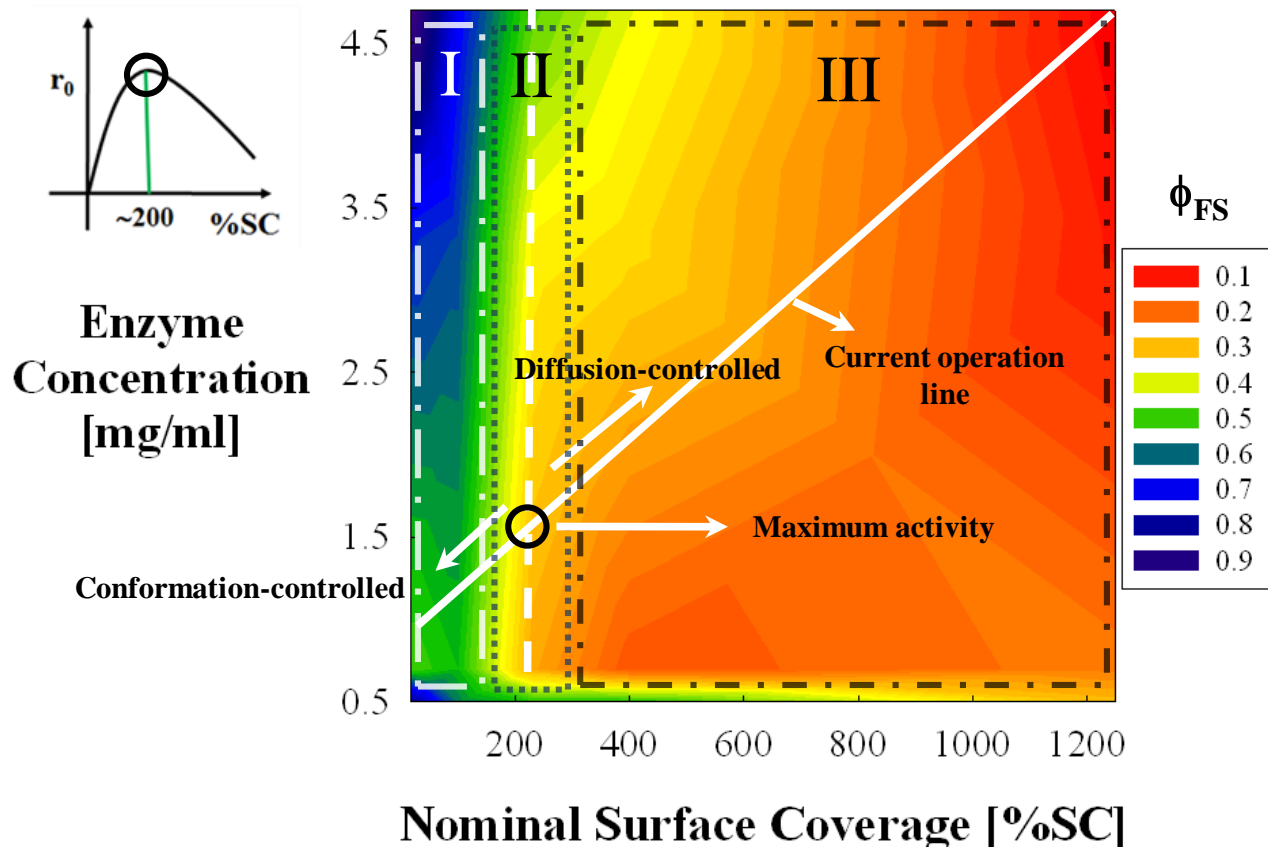


Figure 5.8. Regions of conformational stability for CALB/Fumed Silica adsorbates. The dotted vertical line at $\sim 200\%$ SC separates two different regions of conformational stability: Region I delimited by a long-dash-dot line where adsorbates exhibit low conformational stability, and Region III delimited by a short-dash-dot line where adsorbates have highly stable conformations. The presence of these two regions is likely to be responsible for the observed catalytic activity (r_0) of the lyophilized adsorbates in hexane (inset). The low catalytic activity observed at low %SC can be linked to Region I. Even though the structure is well preserved in Region III, multi-layer packing is likely responsible for diffusional limitations of catalysis. The maximum in activity between those two regions can be attributed to an optimal arrangement on the surface where the structure is relatively well maintained without excessive clustering (Region II, delimited by a dotted line).

Figure 5.8 combines the equilibrium values of deformation for CALB. Two different regions of conformational stability are observed at surface coverage values above and below approximately 200%SC (vertical dotted line). Adsorbates obtained at high surface coverages (i.e., above 200%SC) exhibit highly stable conformations (region III). The tertiary structure remains essentially intact in this region (lighter shading). Below 200%SC (region I), however, the adsorbed enzymes deform significantly (darker areas). Some may even appear to be completely denatured at very low surface coverages as indicated by ϕ_{FS} values near unity.

Region II is a transitional region. Adsorbates with different %SC have been previously obtained along the diagonal line (Figure 5.8).

The catalytic competency of these lyophilized adsorbates in hexane¹⁶ are schematically shown in the inset (Figure 5.8). The three regimes of surface loading and the catalytic competency can be linked: 1. (enzyme conformation controlled, region I) low surface coverages where the enzyme molecules have enough space to maximize their contact with the surface. This can alter the native conformation especially for “soft” enzymes thereby leading to reduced catalytic activity while “hard” enzymes suffer less impact¹⁷, 2. intermediate surface coverages (Region II) have active enzyme conformations where enzyme-enzyme interactions stabilize even “soft” enzymes and prevent excessive surface interactions, and 3. (reactions are diffusion controlled, Region III) high surface coverages where the enzyme molecules are densely packed in multi-layers on the surface leading to mass transfer limitation of catalysis⁶².

Unfolding for “hard” (relative to CALB) *s. Carlsberg* is shown in Figure 5.9. As in the case of CALB, Figure 5.9 shows the presence of three zones of conformational stability but *s. Carlsberg* shows more resilience against denaturation in region I where the “soft” CALB denatures strongly. Catalytic competency of *s. Carlsberg* along the diagonal in Figure 5.9 is shown in the inset (Figure 5.9), demonstrating that the “hard” *s. Carlsberg* shows high catalytic competency at low surface coverage which would denature the “soft” CALB.

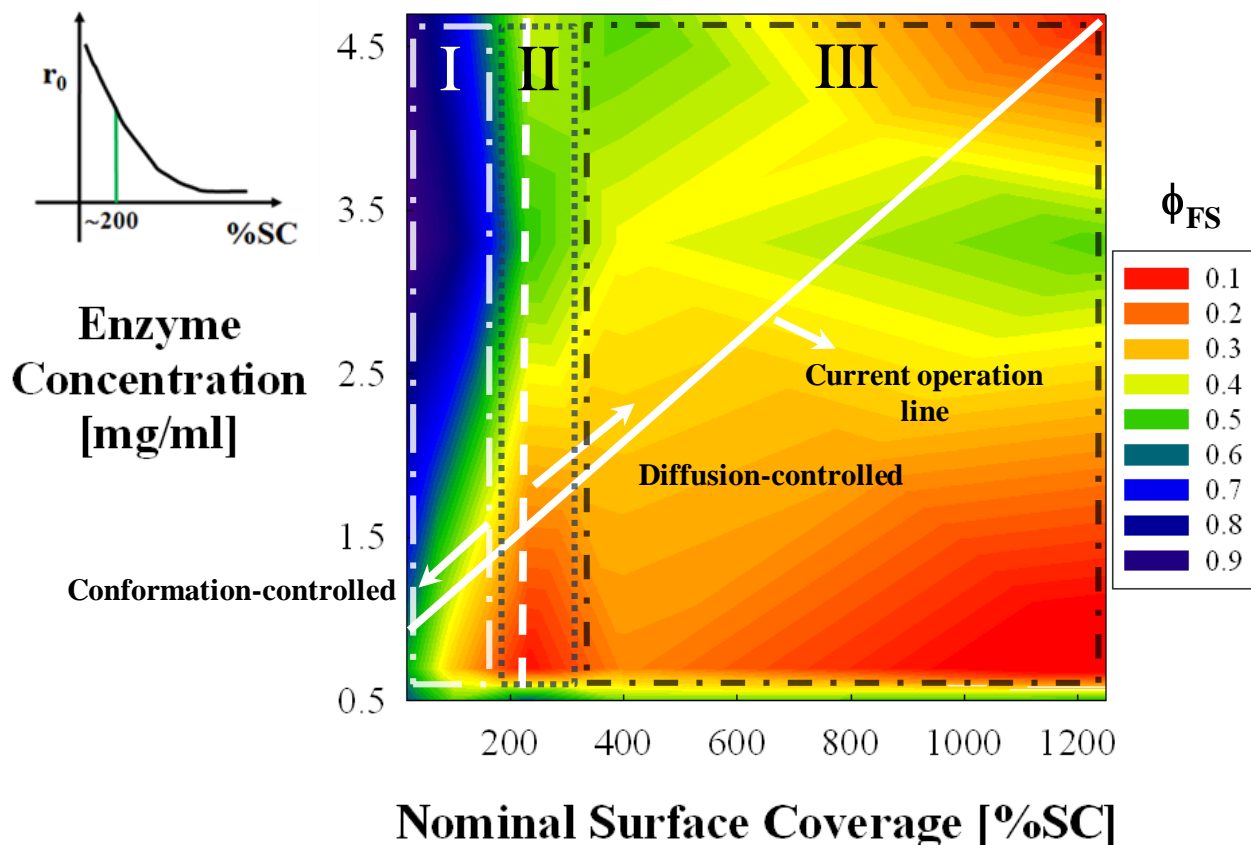


Figure 5.9. Regions of conformational stability for *s. Carlsberg*/Fumed Silica adsorbates. The dotted vertical line at ~200%SC separates two different regions of conformational stability: Region I and III of low and high conformational stability, respectively. In this case, the catalytic activity (r_0) of the lyophilized adsorbates in hexane (inset) is constantly increasing. As opposed to CALB, only partially unfolded enzyme molecules are present in the lower part of Region I at low initial enzyme concentrations. This resilience to denaturation could explain the higher activities observed for lyophilized adsorbates of *s. Carlsberg* at low surface coverages. The same type of lines as those in Figure 5.8 were used to delimit the regions of conformational stability.

A similar diagram for TLL is shown in Figure 5.10. TLL exhibits three regions of conformational stability similar to the enzymes discussed above. In the TLL case, however, region I has only partially altered enzyme conformations as evident from a maximum ϕ_{FS} value of 0.6. This finding further supports the proposed relationship between the inherent conformational stability of enzyme molecules and their tendency to undergo conformational changes upon contact with solid surfaces.

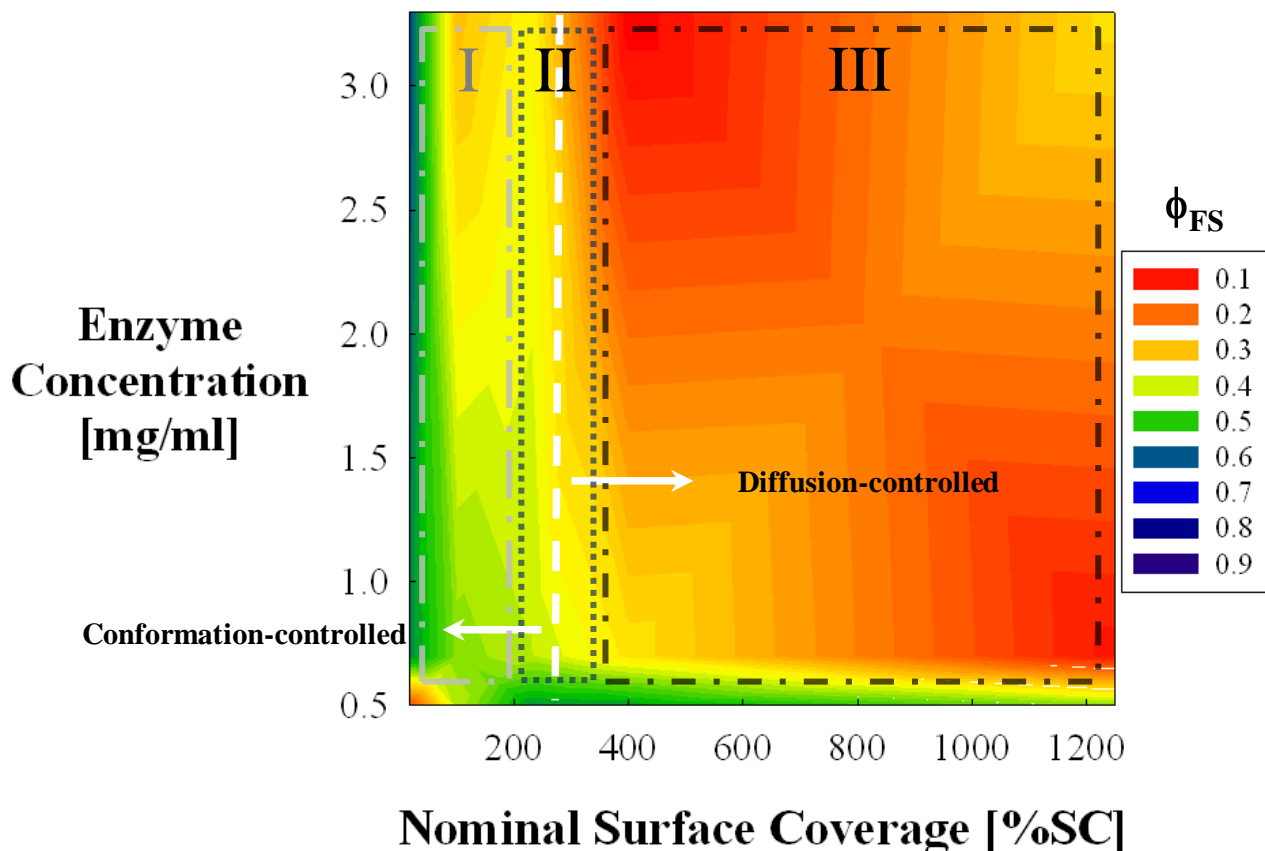


Figure 5.10. Regions of conformational stability for TLL/Fumed Silica adsorbates. The dotted vertical line at $\sim 250\%SC$ separates two different regimes of conformational stability: Region I and III of low and high conformational stability, respectively. Across the whole Region I only partially unfolded conformations ($\phi_{FS} \sim 0.6$) were identified, which confirms the resilience of highly stable enzymes to denature at low surface coverages. The same type of lines as those in Figure 5.8 were used to delimit the regions of conformational stability.

In summary, our findings confirm the critical role that the surface area availability plays by defining the physical arrangement of the enzyme molecules on the surface of the nanoparticles. Additionally, the conformational diagrams introduced here are useful tools that can be used to design highly active and stable adsorbates. While “soft” enzymes require intermediate surface coverage to stabilize them and optimize the catalytic productivity, “hard” enzymes perform well already at low surface coverage and only suffer when multi-layers are formed that impede diffusion.

5.4.3 Impact of Tertiary Structure Modifiers for Enzymes Adsorbing/Desorbing on Fumed Silica in Aqueous Solution

Tertiary structure modifiers (2,2,2-trifluoroethanol (TFE) and Dithiothreitol (DTT)) can be added prior to adsorption on fumed silica to gain more insight into the type of interactions predominating during the adsorption process. TFE induces structural changes in hydrophobic protein segments while DTT reduces disulfide bonds to the unbounded thiols. The time dependent conformational changes of the three enzymes in the presence of 30% (v/v) TFE for adsorbates with a 100%SC is shown in Figure 5.11 panel A. Addition of TFE to both *s. Carlsberg* and TLL resulted in increased initial values of deformation (data in the absence of TFE is superimposed in Figure 5.11 panel A). The shape of the absorbance changes for these two enzymes were similar to those in the absence of TFE, i.e., logarithmic for *s. Carlsberg* and linear for TLL. Overall, the extent of denaturation substantially increased over the initial values (40% and 30% for *s. Carlsberg* and TLL, respectively). This most likely indicates that the disrupting intramolecular contacts hasten denaturation, suggesting that these contact regions are responsible for stabilizing the structures of these two enzymes.

The initial impact of TFE on CALB unfolding was essentially negligible and some refolding is observed, likely due to the different content of groups in CALB that interact strongly with TFE.

The presence of DTT showed no significant impact on the time-course and extent of unfolding for *s. Carlsberg* and TLL (Figure 5.11 panel B). This is most likely due to the absence of thiol sensitive disulfide bonds. CALB, on the other hand, contains DTT-sensitive disulfide bridges and showed decreased initial and equilibrium unfolding values (Figure 5.11 panel B). The exposed residues are then available for interaction with the nanoparticles. This further supports the notion that increased interactions lead to repression of dynamism and ultimately to less opportunities for continued unfolding. This could also explain why the observed DTT-disrupted CALB unfolding pathway resembles those of the “hard” enzymes. The exposure of regions suitable for interaction with the surface is therefore likely to occur more gradually in the presence of DTT.

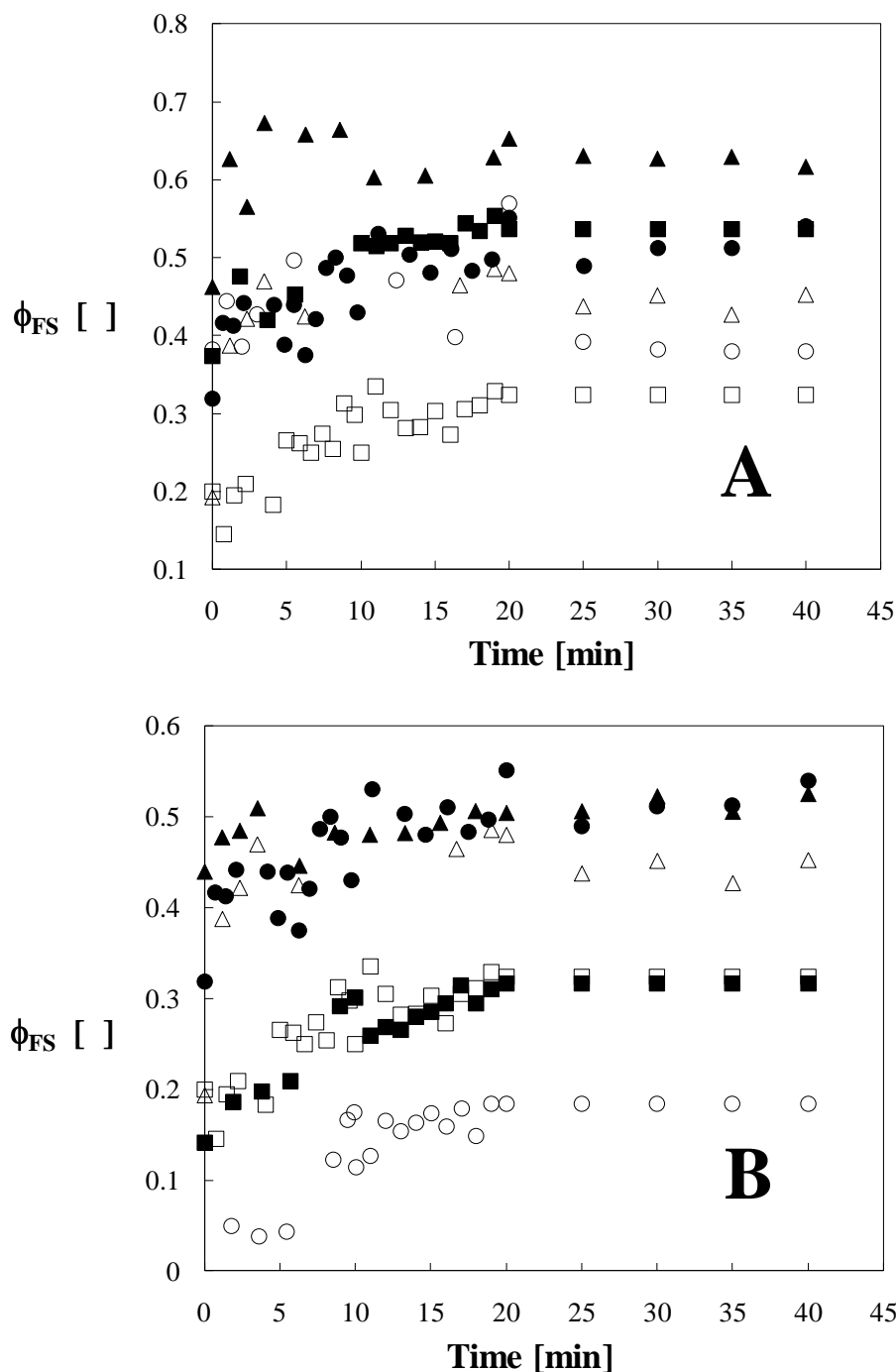


Figure 5.11. Unfolding kinetics of hydrolases adsorbing on fumed silica nanoparticles in the presence of tertiary structure modifiers: (A) 30% (v/v) TFE and (B) 0.5 mg/mL DTT: (O) CALB, (■) *s. Carlsberg* and (▲) TLL. Data for unfolding in the absence of modifiers is superimposed for comparison: (●) CALB, (□) *s. Carlsberg* and (Δ) TLL. Components were mixed to form a nominal surface coverage of 100%SC. Data is normalized with the corresponding calibration curves and subsequently expressed as unfolded fraction. Enzyme concentration was maintained at 0.7 mg/mL and pH at 7.8.

5.4.4 Regions of Conformational Stability for Enzyme/Fumed Silica Adsorbates in the Presence of Structure Modifiers

Figure 5.12 panel A shows that the region III originally observed for CALB was destabilized by TFE. It is likely that groups exposed by TFE facilitated additional opportunities for unfolding by increasing the affinity towards the hydrophilic solid surface. The unfolding extent in this region increased by nearly 50% with respect to the absence of TFE (Figure 5.8).

Figure 5.12 panel B summarizes the impact of DTT on CALB's tertiary structure. Once disulfide bridges are disrupted, CALB's structure is destabilized and some previously occluded regions are exposed. The extent of unfolding in the lower part of regions II and III (i.e., below 2.5 mg/mL and surface coverages above 100%SC) remains low. This could support the argument that the DTT-induced destabilization of CALB may possibly be compensated by interactions with the neighboring molecules. This further supports the idea that protein-protein interactions outweigh protein-surface interactions in region III.

As the enzyme concentration increases, the extent of unfolding also increases at both low and high surface coverages (upper part of regions I and III in Figure 5.12 panel B). The accessibility of DTT to the enzyme at high enzyme concentrations is likely to be compromised by the crowding of enzyme molecules. This leads to a behavior resembling that of the enzyme molecules in the absence of DTT.

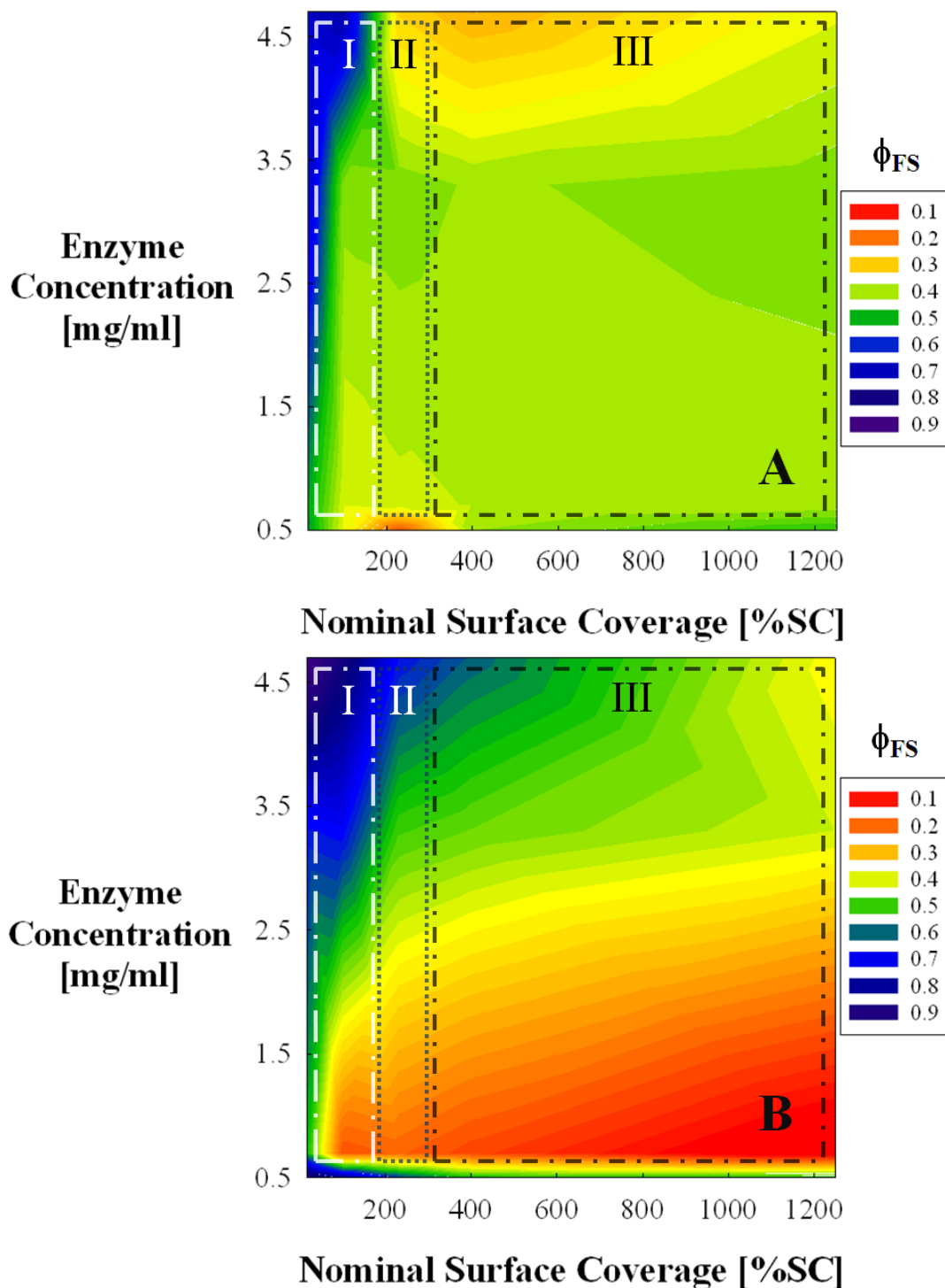


Figure 5.12. Impact of tertiary structure modifiers on conformational regions of CALB/FS adsorbates. This was tested by forming buffered suspensions with (A) 30%(v/v) TFE and (B) 0.5 mg/mL DTT. The previously identified Region III exhibits a higher unfolding in the presence of TFE. The extent of unfolding in Region I decreased in the presence of TFE. The addition of DTT resulted in a substantially large Region III for low %SC and low concentrations. The same type of lines as those in Figure 5.8 were used to delimit the regions of conformational stability.

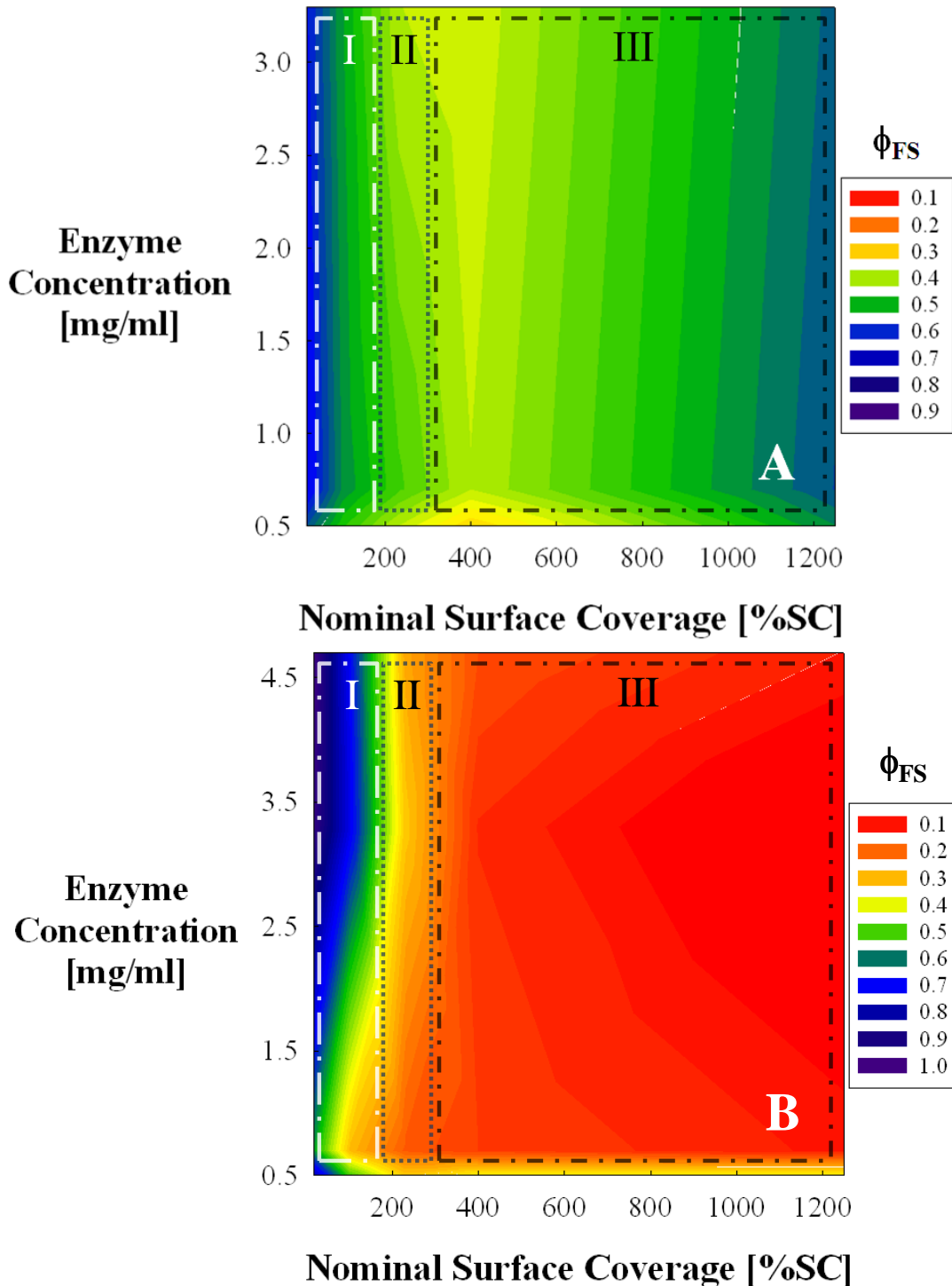


Figure 5.13. Impact of tertiary structure modifiers on conformational regions of *s. Carlsberg*/FS adsorbates. This was tested by forming buffered suspensions with (A) 30%(v/v) TFE and (B) 0.5 mg/mL DTT. As in the case of CALB, TFE promoted a higher unfolding in the previously identified Region III. The maximum extent of unfolding in Region I decreased too. The addition of DTT showed no significant impact on the tertiary structure of *s. Carlsberg*. The same type of lines as those in Figure 5.8 were used to delimit the regions of conformational stability.

A similar study with structural modifiers was conducted for *s. Carlsberg*. Figure 5.13 panel A shows that as in the case of CALB, the exposure of hydrophobic groups leads to a substantial loss of conformational stability for *s. Carlsberg* in region III. Due to the tightly packed and “hard” structure of *s. Carlsberg*, the exposure of hydrophobic groups is rapid. This led to a relatively higher net unfolding than that observed for CALB in this region. Below 100%SC in region I, unfolding was reduced when compared with the enzyme in the absence of TFE. This could be also a direct consequence of the rapid initial unfolding. Once fully extended binding is promoted at the outset of the experiment, the unfolded enzyme molecule’s structure is rapidly attached to the abundant solid surface area provided in this region. No additional opportunities are present that would allow for further unfolding. The case of DTT-induced conformational changes for *s. Carlsberg* is very different. Due to the lack of open moieties on the structure suitable for reduction, no major changes are observed in the presence of DTT and the regions of stability remained essentially unaffected (Figure 5.13 panel B).

5.5 Conclusions

We have shown evidence that the extent of tertiary conformational changes of three hydrolases adsorbed on fumed silica is mainly dependent on the density of the surface covered by the enzyme molecules, which is described here as a nominal surface coverage (%SC), and the inherent conformational stability and dynamics of the enzyme molecules (“hardness”). At low %SC, the unfolding pathway of CALB, a “soft” enzyme, on fumed silica showed continuous unfolding/refolding events. This was attributed to CALB’s conformationally dynamic and fluctuating structure. “Hard” *s. Carlsberg* and TLL, in contrast, exhibited approximately linear unfolding with time which was attributed to their higher inherent conformational stabilities. When moving to high %SC, the unfolding pathways exhibited fewer fluctuations due to stabilizing protein-protein interactions.

Three regions of conformational stability were identified for the three hydrolases at steady-state with the aid of 3D conformational diagrams: I. a region at low % SC where adsorbates of “soft” CALB exhibited low conformational stability most likely due to multi-point attachment to the surface, II. a region of transitional stability at an intermediate %SC (~200%SC), and III. a region of high stability at high %SC where protein-protein interactions exert a stabilizing effect. These regions correlated well the observed apparent catalytic activity in

hexane. The low stability region correlated well with poorly active preparations due to denaturation for “soft” CALB, the transitional region with an optimal in activity, and the high stability region with low CALB catalytic activity due to mass-transfer limitations. In the case of “hard” *s. Carlsberg*, resilience to denaturation at low %SC when compared to CALB explained the constantly increasing apparent catalytic activity observed in this surface loading regime.

Details of the structural interactions were further resolved by adding TFE and DTT to the adsorbing mixtures. TFE exposed hydrophobic segments that for all enzymes appeared to help to stabilize the structure in the “crowded surface” Region III. In the sparsely populated surface Region I, the maximum extent of unfolding for both CALB and *s. Carlsberg* was reduced. This was explained by lower content of interacting groups for CALB and by a rapid attachment of the rigid unfolded state for *s. Carlsberg*. The addition of DTT to CALB’s adsorbing mixtures showed no significant impact in the unfolding levels in the lower part of region III, which confirmed that protein-protein interactions outweigh surface-protein interactions in this region. Upon DTT-induced disruption, Region I showed less unfolding most likely due to a gradual attachment of the very flexible unfolded state of CALB. This was corroborated with unfolding pathways that resemble those of “hard” enzymes.

The complex enzyme/solid interactions in regard to catalytic activity that were investigated here can be used to rationalize and optimize catalysis with enzymes in solvents. The conclusion that for “soft” enzymes there is an optimum enzyme/surface area ratio for immobilization while there is not for “hard” enzymes appears not obvious.

5.6 References

1. Gupta, M. N., Enzyme Function in Organic-Solvents. *European Journal of Biochemistry* **1992**, 203, (1-2), 25-32.
2. Zaks, A.; Russell, A. J., Enzymes in Organic-Solvents - Properties and Applications. *Journal of Biotechnology* **1988**, 8, (4), 259-270.
3. Kise, H., Ester and Peptide-Synthesi by Proteases in Organic-Solvents. *Journal of Synthetic Organic Chemistry Japan* **1991**, 49, (1), 42-51.
4. Fernandezlafuente, R.; Rosell, C. M.; Guisan, J. M., Enzyme Reaction-Engineering - Synthesis of Antibiotics Catalyzed by Stabilized Penicillin-G Acylase in the Presence of Organic Cosolvents. *Enzyme and Microbial Technology* **1991**, 13, (11), 898-905.

5. Khmelnitsky, Y. L.; Rich, J. O., Biocatalysis in nonaqueous solvents. *Current Opinion in Chemical Biology* **1999**, 3, (1), 47-53.
6. Rich, J. O.; Khmelnitsky, Y. L., Phospholipase D-catalyzed transphosphatidylation in anhydrous organic solvents. *Biotechnology and Bioengineering* **2001**, 72, (3), 374-377.
7. Klibanov, A. M., Asymmetric enzymatic oxidoreductions in organic solvents. *Current Opinion in Biotechnology* **2003**, 14, (4), 427-431.
8. Antczak, M. S.; Kubiak, A.; Antczak, T.; Bielecki, S., Enzymatic biodiesel synthesis - Key factors affecting efficiency of the process. *Renewable Energy* **2009**, 34, (5), 1185-1194.
9. Puskas, J. E.; Sen, M. Y.; Seo, K. S., Green Polymer Chemistry Using Nature's Catalysts, Enzymes. *Journal of Polymer Science Part a-Polymer Chemistry* **2009**, 47, (12), 2959-2976.
10. Klibanov, A. M., Improving enzymes by using them in organic solvents. *Nature* **2001**, 409, (6817), 241-246.
11. Klibanov, A. M., Why are enzymes less active in organic solvents than in water? *Trends in Biotechnology* **1997**, 15, (3), 97-101.
12. Bosley, J. A.; Peilow, A. D., Immobilization of lipases on porous polypropylene: Reduction in esterification efficiency at low loading. *Journal of the American Oil Chemists Society* **1997**, 74, (2), 107-111.
13. Chen, B.; Hu, J.; Miller, E. M.; Xie, W. C.; Cai, M. M.; Gross, R. A., Candida antarctica lipase B chemically immobilized on epoxy-activated micro- and nanobeads: Catalysts for polyester synthesis. *Biomacromolecules* **2008**, 9, (2), 463-471.
14. Chen, B.; Miller, E. M.; Miller, L.; Maikner, J. J.; Gross, R. A., Effects of macroporous resin size on Candida antarctica lipase B adsorption, fraction of active molecules, and catalytic activity for polyester synthesis. *Langmuir* **2007**, 23, (3), 1381-1387.
15. Chen, B.; Miller, M. E.; Gross, R. A., Effects of porous polystyrene resin parameters on Candida antarctica Lipase B adsorption, distribution, and polyester synthesis activity. *Langmuir* **2007**, 23, (11), 6467-6474.
16. Cruz, J. C.; Pfromm, P. H.; Rezac, M. E., Immobilization of Candida antarctica Lipase B on fumed silica. *Process Biochemistry* **2009**, 44, (1), 62-69.
17. Wurges, K.; Pfromm, P. H.; Rezac, M. E.; Czermak, P., Activation of subtilisin Carlsberg in hexane by lyophilization in the presence of fumed silica. *Journal of Molecular Catalysis B-Enzymatic* **2005**, 34, (1-6), 18-24.

18. Pfromm, P. H.; Rezac, M. E.; Wurges, K.; Czermak, P., Fumed silica activated subtilisin Carlsberg in hexane in a packed-bed reactor. *AIChE Journal* **2007**, 53, (1), 237-242.
19. Wang, P., Nanoscale biocatalyst systems. *Current Opinion in Biotechnology* **2006**, 17, (6), 574-579.
20. Iler, R. K., *The Chemistry of Silica*. John Wiley & Sons, Inc.: 1979; p 896.
21. Gun'ko, V. M.; Mironyuk, I. F.; Zarko, V. I.; Turov, V. V.; Voronin, E. F.; Pakhlov, E. M.; Goncharuk, E. V.; Leboda, R.; Skubiszewska-Zieba, J.; Janusz, W.; Chibowski, S.; Levchuk, Y. N.; Klyueva, A. V., Fumed silicas possessing different morphology and hydrophilicity. *Journal of Colloid and Interface Science* **2001**, 242, (1), 90-103.
22. Gun'ko, V. M.; Mironyuk, I. F.; Zarko, V. I.; Voronin, E. F.; Turov, V. V.; Pakhlov, E. M.; Goncharuk, E. V.; Nychiporuk, Y. M.; Vlasova, N. N.; Gorbik, P. P.; Mishchuk, O. A.; Mishchuk, O. A.; Chuiko, A. A.; Kulik, T. V.; Palyanytsya, B. B.; Pakhovchishin, S. V.; Skubiszewska-Zieba, J.; Janusz, W.; Turov, A. V.; Leboda, R., Morphology and surface properties of fumed silicas. *Journal of Colloid and Interface Science* **2005**, 289, (2), 427-445.
23. Gun'ko, V. M.; Voronin, E. F.; Nosach, L. V.; Pakhlov, E. M.; Guzenko, N. V.; Leboda, R.; Skubiszewska-Zieba, J., Adsorption and migration of poly(vinyl pyrrolidone) at a fumed silica surface. *Adsorption Science & Technology* **2006**, 24, (2), 143-157.
24. Gun'ko, V. M.; Zarko, V. I.; Voronin, E. F.; Goncharuk, E. V.; Andriyko, L. S.; Guzenko, N. V.; Nosach, L. V.; Janusz, W., Successive interaction of pairs of soluble organics with nanosilica in aqueous media. *Journal of Colloid and Interface Science* **2006**, 300, (1), 20-32.
25. Gun'ko, V. M.; Zarko, V. I.; Voronin, E. F.; Turov, V. V.; Mironyuk, I. F.; Gerashchenko, II; Goncharuk, E. V.; Pakhlov, E. M.; Guzenko, N. V.; Leboda, R.; Skubiszewska-Zieba, J.; Janusz, W.; Chibowski, S.; Levchuk, Y. N.; Klyueva, A. V., Impact of some organics on structural and adsorptive characteristics of fumed silica in different media. *Langmuir* **2002**, 18, (3), 581-596.
26. Ru, M. T.; Hirokane, S. Y.; Lo, A. S.; Dordick, J. S.; Reimer, J. A.; Clark, D. S., On the salt-induced activation of lyophilized enzymes in organic solvents: Effect of salt kosmotropicity on enzyme activity. *Journal of the American Chemical Society* **2000**, 122, (8), 1565-1571.
27. Ru, M. T.; Wu, K. C.; Lindsay, J. P.; Dordick, J. S.; Reimer, J. A.; Clark, D. S., Towards more active biocatalysts in organic media: Increasing the activity of salt-activated enzymes. *Biotechnology and Bioengineering* **2001**, 75, (2), 187-196.

28. Uppenberg, J.; Hansen, M. T.; Patkar, S.; Jones, T. A., Sequence, Crystal-Structure Determination and Refinement of 2 Crystal Forms of Lipase-B From *Candida antarctica*. *Structure* **1994**, 2, (4), 293-308.
29. Neidhart, D. J.; Petsko, G. A., The Refined Crystal-Structure of Subtilisin Carlsberg at 2.5 Å Resolution. *Protein Engineering* **1988**, 2, (4), 271-276.
30. Kamal, J. K. A.; Xia, T. B.; Pal, S. K.; Zhao, L.; Zewail, A. H., Enzyme functionality and solvation of Subtilisin Carlsberg: from hours to femtoseconds. *Chemical Physics Letters* **2004**, 387, (4-6), 209-215.
31. Shaw, A. K.; Pal, S. K., Activity of Subtilisin Carlsberg in macromolecular crowding. *Journal of Photochemistry and Photobiology B-Biology* **2007**, 86, (3), 199-206.
32. Asuri, P.; Bale, S. S.; Karajanagi, S. S.; Kane, R. S., The protein-nanomaterial interface. *Current Opinion in Biotechnology* **2006**, 17, (6), 562-568.
33. Asuri, P.; Bale, S. S.; Pangule, R. C.; Shah, D. A.; Kane, R. S.; Dordick, J. S., Structure, function, and stability of enzymes covalently attached to single-walled carbon nanotubes. *Langmuir* **2007**, 23, (24), 12318-12321.
34. Asuri, P.; Karajanagi, S. S.; Vertegel, A. A.; Dordick, J. S.; Kane, R. S., Enhanced stability of enzymes adsorbed onto nanoparticles. *Journal of Nanoscience and Nanotechnology* **2007**, 7, (4-5), 1675-1678.
35. Singh, P.; Rao, A.; Dutta, V.; Gupta, M.; Raghava, S., Nanoparticles of unmodified titanium dioxide facilitate protein refolding. *Journal of materials chemistry* **2009**, 19, (18), 2830-2834.
36. Kane, R. S.; Stroock, A. D., Nanobiotechnology: Protein-nanomaterial interactions. *Biotechnology Progress* **2007**, 23, (2), 316-319.
37. Norde, W.; Favier, J. P., Structure of Adsorbed and Desorbed Proteins. *Colloids and Surfaces* **1992**, 64, (1), 87-93.
38. Shang, W.; Nuffer, J. H.; Dordick, J. S.; Siegel, R. W., Unfolding of ribonuclease A on silica nanoparticle surfaces. *Nano Letters* **2007**, 7, (7), 1991-1995.
39. Shang, W.; Nuffer, J. H.; Muniz-Papandrea, V. A.; Colon, W.; Siegel, R. W.; Dordick, J. S., Cytochrome c on Silica Nanoparticles: Influence of Nanoparticle Size on Protein Structure, Stability, and Activity. *Small* **2009**, 5, (4), 470-476.

40. West, J. L.; Halas, N. J., Engineered nanomaterials for biophotonics applications: Improving sensing, imaging, and therapeutics. *Annual Review of Biomedical Engineering* **2003**, *5*, 285-292.
41. Lewerenz, H. J., Enzyme-semiconductor interactions: Routes from fundamental aspects to photoactive devices. *Physica Status Solidi B-Basic Solid State Physics* **2008**, *245*, (9), 1884-1898.
42. Su, H. L.; Yuan, R.; Chai, Y. Q.; Zhuo, Y.; Hong, C. L.; Liu, Z. Y.; Yang, X., Multilayer structured amperometric immunosensor built by self-assembly of a redox multi-wall carbon nanotube composite. *Electrochimica Acta* **2009**, *54*, (17), 4149-4154.
43. Chopra, N.; Gavalas, V. G.; Hinds, B. J.; Bachas, L. G., Functional one-dimensional nanomaterials: Applications in nanoscale biosensors. *Analytical Letters* **2007**, *40*, (11), 2067-2096.
44. Ganesan, A.; Moore, B. D.; Kelly, S. M.; Price, N. C.; Rolinski, O. J.; Birch, D. J. S.; Dunkin, I. R.; Halling, P. J., Optical Spectroscopic Methods for Probing the Conformational Stability of Immobilised Enzymes. *Chemphyschem* **2009**, *10*, (9-10), 1492-1499.
45. Wu, X.; Narsimhan, G., Characterization of secondary and tertiary conformational changes of beta-lactoglobulin adsorbed on silica nanoparticle surfaces. *Langmuir* **2008**, *24*, (9), 4989-4998.
46. Wu, X. Y.; Narsimhan, G., Effect of surface concentration on secondary and tertiary conformational changes of lysozyme adsorbed on silica nanoparticles. *Biochimica et Biophysica Acta-Proteins and Proteomics* **2008**, *1784*, (11), 1694-1701.
47. Ganesan, A.; Price, N. C.; Kelly, S. M.; Petry, I.; Moore, B. D.; Halling, P. J., Circular dichroism studies of subtilisin Carlsberg immobilised on micron sized silica particles. *Biochimica et Biophysica Acta-Proteins and Proteomics* **2006**, *1764*, (6), 1119-1125.
48. Hidajat, K.; Uddin, M.; Peng, Z., Conformational change of adsorbed and desorbed bovine serum albumin on nano-sized magnetic particles. *Colloids and Surfaces B: Biointerfaces* **2004**, *33*, (1), 15-21.
49. Shamim, N.; Liang, H.; Hidajat, K.; Uddin, M. S., Adsorption, desorption, and conformational changes of lysozyme from thermosensitive nanomagnetic particles. *Journal of Colloid and Interface Science* **2008**, *320*, (1), 15-21.

50. Kondo, A.; Oku, S.; Higashitani, K., Structural-Changes in Protein Molecules Adsorbed on Ultrafine Silica Particles. *Journal of Colloid and Interface Science* **1991**, 143, (1), 214-221.
51. Tokuriki, N.; Tawfik, D. S., Protein Dynamism and Evolvability. *Science* **2009**, 324, (5924), 203-207.
52. Hoyrup, P.; Patkar, S.; Vind, J.; Svendsen, A.; Hult, K.; Hedin, E., Implications of surface charge and curvature for the binding orientation of *Thermomyces lanuginosus* lipase on negatively charged or zwitterionic phospholipid vesicles as studied by ESR spectroscopy. *Biochemistry* **2005**, 44, (50), 16658-16671.
53. Jutila, A.; Zhu, K.; Patkar, S. A.; Vind, J.; Svendsen, A.; Kinnunen, P. K. J., Detergent-induced conformational changes of *Humicola lanuginosa* lipase studied by fluorescence spectroscopy. *Biophysical Journal* **2000**, 78, (3), 1634-1642.
54. Jutila, A.; Zhu, K.; Tuominen, E. K. J.; Kinnunen, P. K. J., Fluorescence spectroscopic characterization of *Humicola lanuginosa* lipase dissolved in its substrate. *Biochimica Et Biophysica Acta-Proteins and Proteomics* **2004**, 1702, (2), 181-189.
55. Zhu, K.; Jutila, A.; Kinnunen, P. K. J., Steady state and time resolved effects of guanidine hydrochloride on the structure of *Humicola lanuginosa* lipase revealed by fluorescence spectroscopy. *Protein Science* **2000**, 9, (3), 598-609.
56. Schafer, T.; Borchert, T. W.; Nielsen, V. S.; Skagerlind, P.; Gibson, K.; Wenger, K.; Hatzack, F.; Nilsson, L. D.; Salmons, S.; Pedersen, S.; Heldt-Hansen, H. P.; Poulsen, P. B.; Lund, H.; Oxenboll, K. M.; Wu, G. F.; Pedersen, H. H.; Xu, H., Industrial enzymes. In *White Biotechnology*, Springer-Verlag Berlin: Berlin, 2007; Vol. 105, pp 59-131.
57. Acharya, P.; Rao, N. M., Stability studies on a lipase from *Bacillus subtilis* in guanidinium chloride. *Journal of Protein Chemistry* **2003**, 22, (1), 51-60.
58. De Diego, T.; Lozano, P.; Gmouh, S.; Vaultier, M.; Iborra, J. L., Understanding structure - Stability relationships of *Candida antarctica* lipase B in ionic liquids. *Biomacromolecules* **2005**, 6, (3), 1457-1464.
59. Skjot, M.; De Maria, L.; Chatterjee, R.; Svendsen, A.; Patkar, S. A.; Ostergaard, P. R.; Brask, J., Understanding the Plasticity of the alpha/beta Hydrolase Fold: Lid Swapping on the *Candida antarctica* Lipase B Results in Chimeras with Interesting Biocatalytic Properties. *ChemBiochem* **2009**, 10, (3), 520-527.

60. Sonesson, A. W.; Callisen, T. H.; Brismar, H.; Elofsson, U. M., Lipase surface diffusion studied by fluorescence recovery after photobleaching. *Langmuir* **2005**, 21, (25), 11949-11956.
61. Carboni-Oerlemans, C.; de Maria, P. D.; Tuin, B.; Bargeman, G.; van der Meer, A.; van Gemert, R., Hydrolase-catalysed synthesis of peroxy-carboxylic acids: Biocatalytic promiscuity for practical applications. *Journal of Biotechnology* **2006**, 126, (2), 140-151.
62. Cao, L., Adsorption-based Immobilization. In *Carrier-bound Immobilized Enzymes: Principles, Applications and Design*, Wiley-VCH Verlag GmbH & Co. KGaA, Germany: Weinheim, 2005; Vol. 1, pp 53-168.
63. Derewenda, U.; Swenson, L.; Green, R.; Wei, Y.; Yamaguchi, S.; Joerger, R.; Haas, M. J.; Derewenda, Z. S., Current Progress in Crystallographic Studies of New Lipases from Filamentous Fungi. *Protein Engineering* **1994**, 7, (4), 551-557.

CHAPTER - 6 Conformational Changes and Catalytic Competency of Hydrolases Adsorbing on Fumed Silica: II.

Secondary Structure

6.1 Abstract

Secondary conformational analysis via Circular Dichroism (CD) and Amide-I FTIR was applied to preparations of *Candida antarctica* Lipase B (CALB), *subtilisin Carlsberg*, and the Lipase from *Thermomyces lanuginosus* (TLL) on fumed silica to confirm that the “hardness” and packing density of the enzymes on the solid silica nanoparticle surface can be used to rationalize the surprising enzyme-dependent changes of catalytic competency with surface coverage. “Soft” enzymes should be immobilized at a surface coverage where enzyme-enzyme interactions prevent detrimental structural changes caused by enzyme-support interactions, while “hard” enzymes can be immobilized at low to intermediate surface coverage with good catalytic performance. Multi-layer coverage reduces the superficial average catalytic performance in all cases due to mass transfer limitations.

6.2 Introduction

Enzymes in non-aqueous media are an alternative avenue to conventional chemistry for the production of numerous compounds of commercial interest¹⁻¹¹. The exquisite selectivity and stereoselectivity of enzymes is well recognized. Some additional advantages of enzymatic catalysis in non-aqueous media include increased solubility and stability of reactants and products¹²⁻²², reduced complexity for downstream recovery of products and enzyme¹²⁻²², and improved sterility¹²⁻²². However, enzymes are essentially insoluble in organic solvents that do not denature them²³⁻²⁶. Various strategies have been attempted to overcome this major limitation including the incorporation of lyo- and cryo-protectants^{27, 28}, encapsulation in reverse micelles^{29, 30}, lyophilization in the presence of non-buffer salts (termed salt-activation)^{7, 31}, and immobilization on micro- and nano-sized organic and inorganic materials^{23, 24, 26, 32, 33}. These immobilizates are often costly due in part to expensive solid supports which ultimately limits industrial applications of non-aqueous enzymatic catalysis^{34, 35}.

We have immobilized enzymes on fumed silica, an inexpensive nanostructured support²⁴⁻²⁶ to tackle the cost issue while maintaining or increasing catalytic efficiency. Fumed silica is a fractal aggregate with large specific surface area (up to 500 m²/g) formed by the fusion of individual nanoparticles of approximately 10-50 nm in diameter³⁶⁻³⁸. Fumed silica has been successfully used for adsorbing a wide variety of compounds ranging from polymers to proteins³⁹⁻⁴². Our protocol exploits these unique adsorptive properties using a two-step immobilization strategy. The enzyme molecules are first adsorbed on the nanoparticles from aqueous solution and then lyophilized to obtain the adsorbates. The lyophilized nanobiocatalysts are then ready-to-use in non-aqueous media. Our protocol has been successfully applied to *subtilisin Carlsberg*^{25, 26} and *Candida antarctica* Lipase B (CALB)²⁴, due to their importance as biocatalysts in industry.

The maximum observed apparent catalytic activity in hexane reached or even exceeded those obtained with commercial preparations of CALB, and what has been termed salt-activated for *s. Carlsberg*. CALB a monomeric protein with 317 amino acid residues and belongs to the family of globular α/β -hydrolase-like fold enzymes^{43, 44}. CALB's structure contains 7 central β -strands flanked by 10 α -helices^{43, 44}. In particular, $\alpha 5$ and $\alpha 10$ are found to be extremely mobile regions that are loosely associated with the rest of the structure⁴⁵. This confers a plasticity and dynamism thought to be responsible for broadening its substrate specificity^{46, 47}. Four disulfide bridges help to stabilize CALB's structure⁴³. The *s. Carlsberg* enzyme is a single polypeptide chain enzyme with 274 amino acid residues and two α/β domains that are composed of 7 central β -parallel strands flanked by 5 α -helices⁴⁸.

The apparent catalytic activity in hexane for our preparations was found to depend strongly on the nominal surface coverage (%SC) of the enzyme molecules^{24, 26}. Surprisingly, enzyme activity levels are dissimilar for *s. Carlsberg* and CALB at comparable surface coverage. Apparent catalytic activity increases with increasing %SC for both enzymes. CALB's apparent catalytic activity attains a maximum at an intermediate %SC and then steeply decreases with decreasing %SC. On the other hand, *s. Carlsberg*'s remains high even at low %SC. This behavior has been explained by us and others in light of three regimes of surface loading as follows: I. a low surface coverage regime where enough surface area is provided for the enzyme molecules, therefore, maximizing the opportunities for multi-point attachment and detrimental spreading. This will promote substantial conformational changes and a decrease in flexibility

which in turn leads to loss of activity, II. an intermediate surface coverage regime where the enzyme molecules are less dispersed thus affording beneficial interactions with neighboring molecules along with surface interactions to maintain a high population of active conformations, and III. a multi layer coverage regime where the enzyme molecules are aggregated but mass transfer limitations reduce the availability of substrate molecules to the catalytic sites.

Integrating proteins with nanomaterials has gained popularity as this approach provides an avenue for developing new materials with applications in fields as diverse as biomedicine⁴⁹⁻⁵¹, biosensors and bioelectronics^{50, 52-55}, and bioelectrochemistry⁵⁶. One of the major challenges is to preserve protein functionality in the final biomaterial^{49, 57}. This can be achieved by developing strategies to enhance the conformational stability of the adsorbed proteins^{58, 59}. Numerous studies have described the crucial role of surface chemistry, size, and curvature of the nanomaterials in the conformational stability of the immobilized proteins^{49, 58-63}. Recent reports have proposed that considerable attention should also be given to characterizing the different intricate surface-protein interactions during the adsorption process^{61, 64, 65}.

Quantifying conformational perturbations for proteins immobilized on solid supports is challenging due to the scarcity of tools for direct interrogation of the molecular rearrangements associated with structural fluctuations⁶⁶. The most popular approaches include Fourier Transform Infrared- (FTIR), Circular Dichroism- (CD), Intrinsic Fluorescence-, Raman optical activity- and Nuclear Magnetic Resonance- (NMR) spectroscopies. CD and FTIR have been particularly useful to collect secondary structural information for both proteins in solution and immobilized on solid materials^{62, 63, 66-74}. CD spectroscopy relies on the different response of chiral secondary structural components to circularly polarized light^{75, 76}. Therefore, CD can be successfully applied to estimate the individual contributions of α -helical, β -sheet, and less ordered secondary structural components. FTIR can be also exploited for the analysis of secondary structure of proteins, principally, by observing changes in the amide absorptions⁶⁷. The amide group exhibits 9 vibrational modes that give rise to amide bands A, B, and I-VII^{77, 78}. The preferred spectral components for secondary analysis are, however, amide I⁷⁹, amide II^{79, 80}, and amide III^{79, 81-83} due to the simplicity for analysis. Amide I has attracted the most attention due to its increased sensitivity towards conformational changes in the secondary arrangement of the protein backbone^{84, 85}. This has allowed extensive use for secondary structural analyses of proteins including folding, unfolding, and aggregation⁸⁶⁻⁹⁶. The main challenge for the analysis is posed

by the overlapping of the individual structural components⁹⁷. Two strategies have been applied to overcome this issue, thereby allowing the extraction of quantitative information from the spectrum: (i) resolution enhancement (also called band-narrowing)⁹⁸⁻¹⁰¹ followed by curve-fitting^{102, 103} and (ii) deconstruction into basis spectra with a reference calibration set^{104, 105}. Here we applied second derivative of the amide I band as resolution enhancement method to identify the dominant secondary structural components.

Secondary conformational stability studies of hydrolases with different native “hardness” on solid fumed silica nanoparticles are performed here for both enzyme adsorbates prepared from aqueous solution, and the resulting preparations after lyophilization. In both cases, the impact of varying the surface coverage by the enzyme molecules is evaluated. Perturbation on the intramolecular hydrogen bonding sustaining the secondary structure by attachment of the enzymes to the nanoparticles was inferred from CD spectral information after normalizing with respect to the native state in solution. Three regions of secondary conformational stability were visualized as a function of the surface coverage which correlated well with those observed previously from tertiary structural analyses. The analysis confirmed also that as opposed to “hard” enzymes, “soft” enzymes show a marked tendency to denature when sufficient opportunities for surface interaction are provided. This can however be counteracted by providing enzyme-enzyme interactions at higher surface coverages. Structure modifiers were added to further probe the types of interactions prevailing in each region of conformational stability of immobilized enzymes. The amide I-FTIR analyses in the lyophilized state confirmed alteration on the secondary structure in the low surface coverage regime and showed that applying our protocol apparently does not introduce additional perturbations in the secondary structure relative to those already present in the native lyophilized preparation. The FTIR analysis for lyophilized preparations obtained under crowding conditions of surface coverages below 100%SC and initial enzyme concentrations above 3.0 mg/mL revealed major conformational changes apparently triggered by association-induced structural transitions. Emerging applications in nanobiotechnology where preserving protein conformational stability is a major issue are expected to be highly benefited from the approach discussed here.

6.3 Materials and Methods

6.3.1 Materials

Crude CALB (lyophilized; specific activity of 28U/mg solid) and TLL (lyophilized; specific activity of 1400U/mg solid) were obtained from Codexis, Inc. (Pasadena, CA), stored at 4°C, and used as-received. TLL is a glycosylated monomeric protein with 269 amino acid residues, containing eight central β -sheets (predominantly parallel) flanked by 5 interconnecting α -helices^{74, 106-108}. TLL is used for the interesterification and hydrolysis of vegetable oils and animal fats¹⁰⁹. *Subtilisin Carlsberg* (EC 3.4.21.14; proteinase from *Bacillus licheniformis*; specific activity of 8 U/mg solid), fumed silica (purity of 99.8 wt.%, specific surface area 255 m²/g, primary particle diameter ~7-50 nm, as reported by the manufacturer), ultrapure Guanidine Hydrochloride (GdmCl), 2,2,2- trifluoroethanol (TFE), and dithiothreitol (DTT) were from Sigma-Aldrich (St. Louis, MO), and used as received. Glass vials (24 mL screw-capped, flat-bottom) were used to prepare the enzyme-fumed silica suspensions.

6.3.2 Circular Dichroism Conditions to Monitor Unfolding

Unfolding was monitored in a cylindrical quartz cuvette (1 cm pathlength) by collecting the far-UV CD spectrum from 190 nm to 300 nm every 0.2 nm with 2 nm bandwidth and at a scan speed of 50 nm/min (Jasco J-720 spectropolarimeter, Jasco Spectroscopic Co., Hachioji, Japan, room temperature). The simple point-by-point average of three consecutive full wavelength scans is reported here. A baseline for the buffer was electronically subtracted from each enzyme spectrum (after averaging). The CD signal at 222 nm was extracted from the spectra.

6.3.3 Enzyme in Aqueous Buffer Solution: Unfolding by GdmCl/Urea and Unfolded Fraction Tracking by CD

When proteins undergo unfolding, the α -helical content decreases, which can be monitored by tracking the CD signal loss at 222 nm^{62, 63}. The GdmCl/Urea-induced unfolding of the three hydrolases in aqueous buffer solution was normalized based on the degree of signal loss at 222 nm according to^{62, 63}:

$$\phi_{GdmCl} = \left(\frac{CD^S_{222} - CD^N_{222}}{-CD^N_{222}} \right) \quad \text{Equation 6.1}$$

where ϕ_{GdmCl} is the unfolded fraction (0, native; 1, completely unfolded).

CD^S_{222} is the CD signal at 222 nm for enzyme molecule ensembles at any state of unfolding, and CD^N_{222} is the CD signal at 222 nm for ensembles of native enzyme molecules both in aqueous buffer solution and in millidegrees (mdeg).

The ability of Circular Dichroism spectroscopy (CDS) to detect unfolding was tested for reference in aqueous buffer with the powerful denaturants GdmCl and Urea. Typically, the α -helical content decreases upon exposure of the enzyme to these denaturants while both the β -sheet and random coil contents increase^{72, 73}, which is detected by CDS due to its sensitivity to subtle changes in the secondary structure.

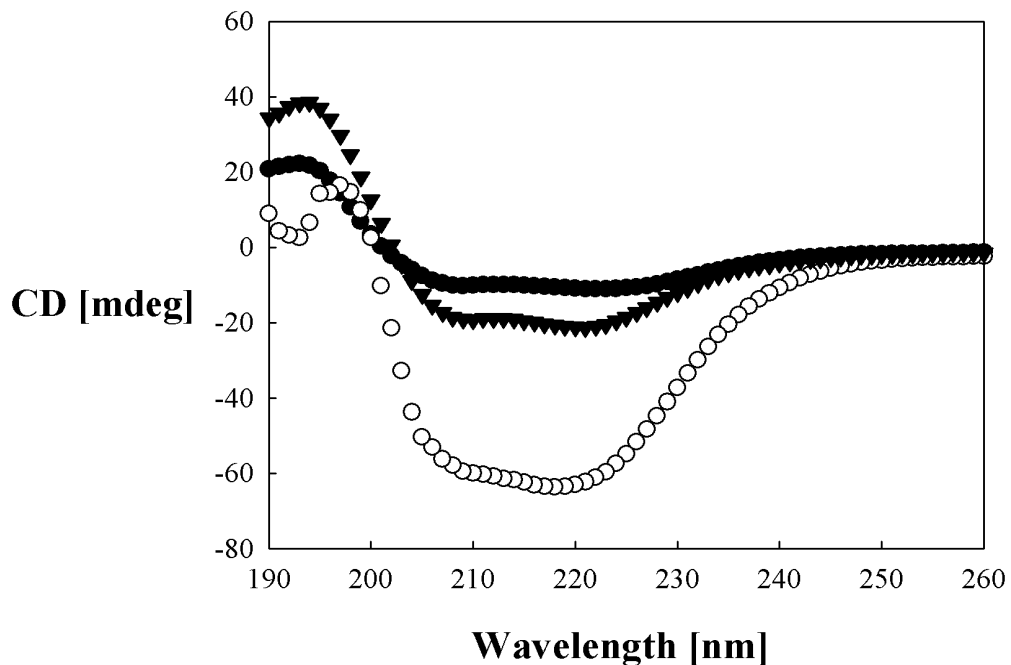


Figure 6.1. CD spectra for native enzymes in aqueous buffer at an enzyme concentration of 0.7 mg/mL. CALB (●), *s. Carlsberg* (○), TLL (▼). The signal at 222 nm can be used as baseline to estimate the α -helical content in the presence of denaturants. Similar plots were obtained for enzyme solutions with other concentrations.

Crude enzyme solution was made (0.5 to 4.7 mg enzyme/mL in 10 mM monobasic phosphate buffer, adjusted to pH 7.8 by KOH). GdmCl with final concentrations in the range of 1M to 6M was added followed by vortexing for about 30 seconds. Buffer solutions with final Urea concentrations from 1M to 10 M were produced and analyzed in the same manner. The solutions were transferred to the CD instrument for analysis. Figure 6.1 shows typical CD spectra for the three hydrolases in aqueous buffer solution about 30 seconds after the denaturant was added.

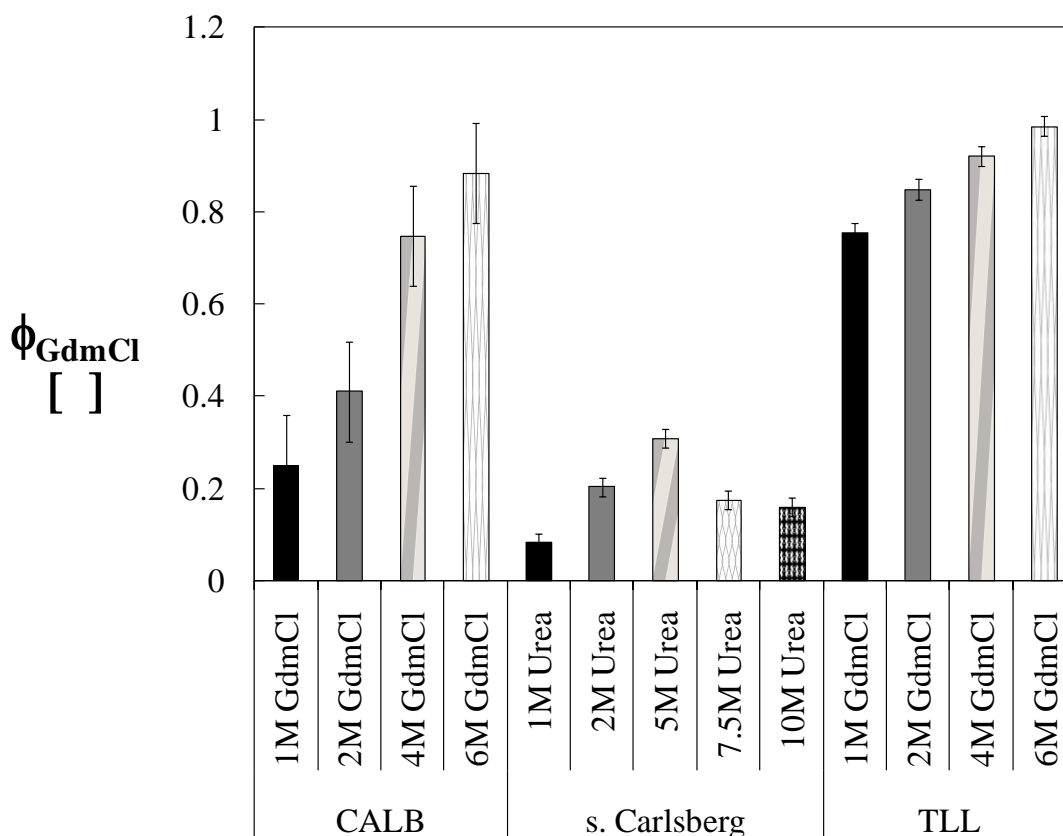


Figure 6.2. Chemically-induced unfolding of enzymes. Equation 6.1 was employed to compute the unfolded fraction based on signal loss at 222 nm. The unfolding pathways in the presence of denaturants are similar to those reported previously based on intrinsic fluorescence spectroscopy. The relatively modest unfolding for *s. Carlsberg* and TLL after an initial unfolding can be attributed to their high conformational stabilities.

TLL and CALB show unfolding with increasing concentration of the denaturant (Figure 6.2). The much more pronounced magnitude of unfolding for TLL compared to CALB at low GdmCl concentrations may be attributed to TLL's 5 α -helices vs. CALB's 10 α -helices. Thus, more denaturant is initially required per CALB molecule to promote unfolding. The modest

increase in TLL's unfolding at higher GdmCl concentrations, however, could be correlated with its high conformational stability. *S. Carlsberg* shows significant resistant to unfolding (low magnitude) and a reversal of the trend at high denaturant concentrations perhaps due to the higher energy penalty associated with introducing the urea into a very rigid "hard" enzyme¹¹⁰. Similar experiments for different enzyme concentrations (not shown) confirm trends and magnitudes in Figure 6.2.

6.3.4 *Enzyme Adsorbed: Secondary Conformational Changes of Enzymes Interacting with Fumed Silica Nanoparticles in Aqueous Buffer Solution*

Secondary conformational changes of enzymes interacting with fumed silica nanoparticles were monitored by following the loss of CD signal at 222 nm. Previous studies have shown that the CD signal is not significantly scattered by the presence of nanoparticles^{63, 72, 73}.

CD data at 222 nm (or alternatively 235 nm for *s. Carlsberg* adsorbates at initial enzyme concentrations of 3.3 mg/mL and above, see discussion for explanation) were normalized based on the degree of signal loss according to^{62, 63}:

$$\phi_{FS} = \left(\frac{CD_{FS\ 222}^S - CD_{222}^N}{-CD_{222}^N} \right) \quad \text{Equation 6.2}$$

where ϕ_{FS} is the average unfolded fraction for enzyme ensembles in the presence of fumed silica nanoparticles (0, native; 1, completely unfolded).

$CD_{FS\ 222}^S$ is the net average CD signal at 222 nm of enzyme molecule ensembles interacting with fumed silica at any state of unfolding in millidegrees, and CD_{222}^N is the average CD signal at 222 nm for ensembles of native enzyme molecules both in aqueous buffer and in millidegrees (mdeg).

Crude enzymes (i.e., CALB, *s. Carlsberg* and TLL) were weighed in a glass vial and 10 mM monobasic phosphate buffer (adjusted to pH 7.8 by KOH) was added followed by vortexing for about 30 seconds. Fumed silica was then added followed by vortexing until visually homogeneous suspensions were formed (about 30 seconds) as described elsewhere^{24, 26}. Table 6.1 shows a summary of the amounts of fumed silica and enzyme used to form our suspensions

at the various nominal surface coverages %SC of enzyme in the final enzyme/fumed silica adsorbates. The suspensions were transferred to the CD instrument for analysis.

Table 6.1. Summary of the amounts of fumed silica and enzyme employed to form the suspensions with different nominal surface coverages. The enzyme concentration for each suspension was varied from 0.5 mg/mL to 4.70 mg/mL.

Enzyme	Enzyme mass (mg)	Mass fumed silica (g)					
		2%SC*	17%SC	100%SC	230%SC	400%SC	1250%SC
CALB	7	0.718	0.092	0.016	0.0068	0.0039	0.0013
TLL	5	0.350	0.040	0.010	0.0030	0.0018	0.0006
<i>s. Carlsberg</i>	5	0.315	0.036	0.009	0.0027	0.0016	0.0005

* The Nominal Surface Coverage (% SC) was calculated as follows:

$$\%SC = \frac{\text{Projected area of enzyme molecule}}{\text{Nominal surface area of Fumed Silica}} * 100 \quad \text{Equation 6.3}$$

The projected area of enzyme is calculated assuming a spherical shape for the enzyme molecules. The diameter of the enzyme molecules from crystallographic data were 6.4 nm²⁸, 5.0 nm⁵⁸, and 4.2 nm²⁹ for CALB, TLL and *s. Carlsberg*, respectively. The nominal surface area of fumed silica is as provided by the manufacturer: 255m2/g.

6.3.5 Regions of Secondary Conformational Stability: 3D Filled Contour Plots

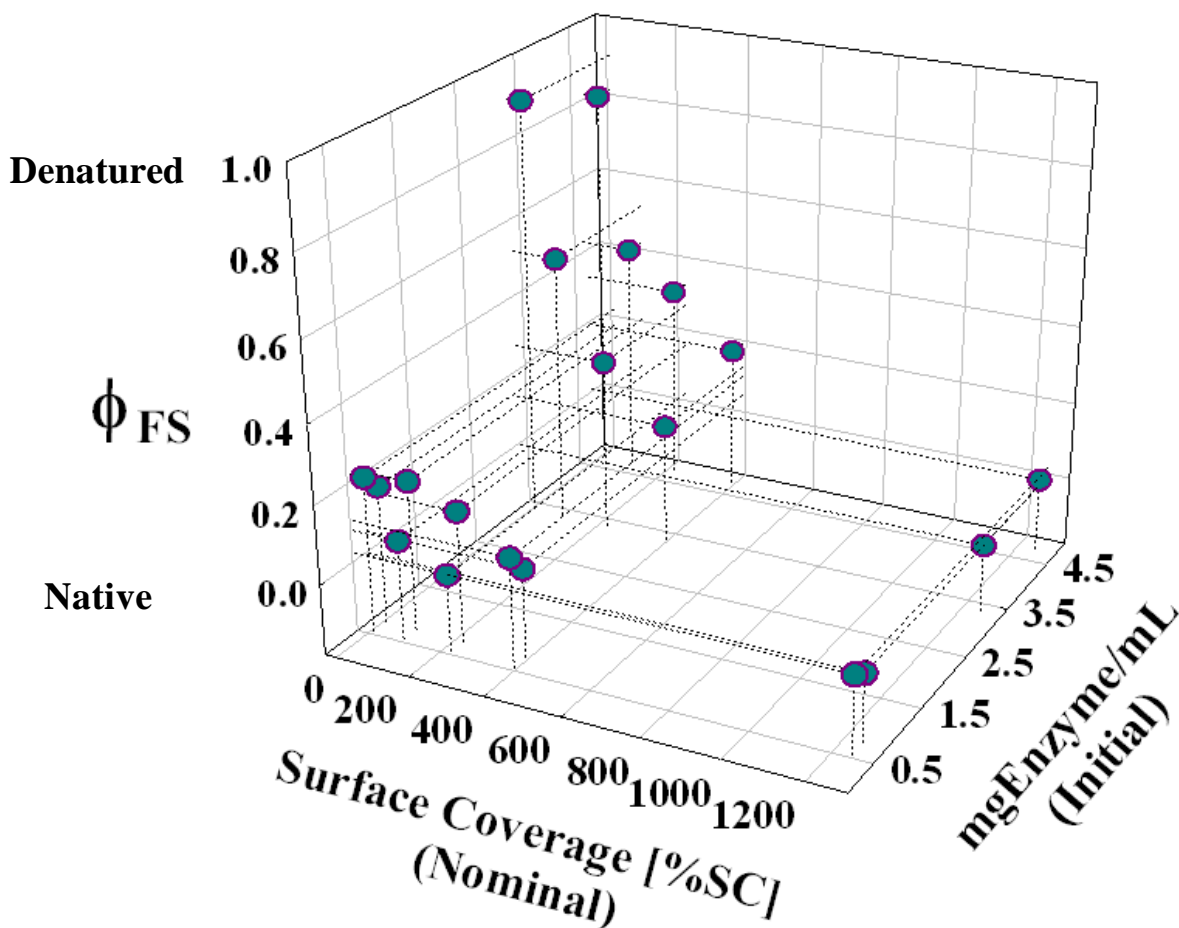


Figure 6.3. Unfolding data for CALB on fumed silica (z -axis) as a function of initial enzyme concentration (y -axis) and nominal surface coverage (x -axis). These data will be shown in 3D contour plots to identify regions of conformational stability and to subsequently correlate them with surface loading regimes previously postulated for the lyophilized adsorbates. This approach was introduced in the previous chapter using tertiary unfolding data.

The values of unfolding tracked by changes in the CD signal at 222 nm (as a function of total enzyme molecules present, compositions see Table 6.1) for each enzyme are plotted as the elevation (z -direction) of contour plots where the y -axis is the concentration of enzyme in the solution at the beginning of preparing the adsorbate and the horizontal x -axis represents the expected %SC by the enzyme molecules in the obtained adsorbates (Table 6.1). Figure 6.3 shows the unfolding data for CALB on fumed silica as an example to introduce this type of plot. A total of 20 data points were used to develop contour plots (see below). An inverse-distance algorithm (SigmaPlot®) was used to interpolate. Figure 6.3 indicates that at low surface coverage

unfolding becomes very significant, no matter what the initial concentration to prepare the adsorbate was. Detailed discussions follow below.

6.3.6 FTIR Analysis of Lyophilized Adsorbates

The adsorbates at the various %SC were placed in a refrigerator at -20°C for several hours until frozen. These preparations were then transferred to a lyophilizer where most of the water is removed by sublimation over approximately 72h as described elsewhere^{24, 26}. The lyophilized powders are removed and stored at 4°C for secondary structure analysis with FTIR. Samples of approximately 0.5 mg were placed in a Spectrum 100 Fourier Transform Infrared Spectrometer (FTIR) (PerkinElmer, Waltham, MA). Absorbance IR spectra were collected from 2000 cm^{-1} to 700 cm^{-1} . The reported spectra were an average of 10 scans at 2 cm^{-1} resolution. All spectra were corrected by the automatic subtraction of water vapor and carbon dioxide using the Atmospheric Vapor Compensation (AVC) algorithm incorporated in the instrument.

6.3.7 Second Derivative Spectral Analysis of Lyophilized Adsorbates

The conformational state of the immobilized enzyme molecules previous to their incorporation in the reaction media was accomplished here by deconstructing the information contained under the amide I region of the IR spectrum. The resolution of the original IR spectra was enhanced by taking the second derivative. This approach has been reported to narrow the half-bandwidth of the Amide I without losing the band frequencies and relative contributions of the structural components^{99, 101, 111-113}. The generated peaks were then assigned to secondary structural components according to Table 6.2^{67, 113-117}. The derivative was calculated with the Savitsky–Golay method (4th grade polynomial, 13 smoothing points) and baseline corrected using EssentialFTIR® v.150.250.

Table 6.2. Band assignments for proteins in the infrared amide I region of the spectrum¹¹⁸

Wavenumber [cm ⁻¹]	Assignment
1620-1628	Intermolecular β aggregates
1629-1632	β -sheet
1636-1640	β -sheet, antiparallel β -sheet
1645-1657	Disordered
1648-1652	α -helix
1655-1658	α -helix
1668-1674	Turns
1681-1683	Turns
1684-1696	β -sheet

Table 6.3. Band assignments for CALB in the infrared amide I region of the spectrum¹¹⁸

Wavenumber [cm ⁻¹]	Assignment
1622 \pm 3	Intermolecular β aggregates
1627 \pm 3	β -sheet
1636 \pm 3	β -sheet, antiparallel β -sheet
1643 \pm 3	Disordered
1660 \pm 3	α -helix
1677 \pm 3	Turns
1690 \pm 3	β -sheet

To determine the major secondary structural components for CALB and its preparations, a sample of crude lyophilized enzyme was interrogated with the FTIR. The spectrum was collected 3 times and the second derivative calculated as described above. This analysis revealed that 1660 \pm 3 cm⁻¹ and 1635 \pm 3 cm⁻¹ were the dominant bands. Less intense bands were also detected at 1690 \pm 3 cm⁻¹, 1677 \pm 3 cm⁻¹, 1642 \pm 3 cm⁻¹, 1627 \pm 3 and 1622 \pm 3 cm⁻¹. The assignment to secondary structural components was prepared with the reported values of Table 6.2 and is

summarized in Table 6.3. These assignments agree well with a recent report for CALB immobilized on titania¹¹⁸.

6.4 Results and Discussion

6.4.1 *Unfolding of Enzymes Interacting with Fumed Silica in Aqueous Solution*

Figure 6.4 panel A shows a comparison of the CD spectrum in aqueous buffer solution of native CALB with those of the enzyme in the presence of fumed silica nanoparticles at different surface coverages (%SC). The results indicate that, at lower loading values, the α -helical content decreased as evidenced from the loss of signal at 222 nm. Based on secondary structure analysis with CD, Wu and Narsimhan⁷³ recently reported a similar loss of α -helical content when lysozyme was absorbed on 90 nm diameter colloidal silica nanoparticles at low surface concentrations. This is also consistent with the findings of Vertegel et al.¹¹⁹ for lysozyme adsorbing on 20 nm diameter colloidal silica nanoparticles.

We previously identified substantial unfolding at low %SC with intrinsic fluorescence spectroscopy analysis. This was attributed to a facilitated adsorption pathway where surface-protein interactions most likely lead to the observed conformational changes. This tendency of enzymes to undergo orientational or conformational changes to maximize surface-protein interactions has been recently reconciled using FRET imaging¹²⁰. The tertiary conformational analysis also revealed that an increase in the initial enzyme concentration resulted in an even higher extent of unfolding at low %SC.

Panel B in Figure 6.4 confirms a similar trend for the secondary structure. In fact, when the initial enzyme concentration is increased, a substantial loss of α -helical content with respect to the native enzyme is clearly observed. This suggests that structural perturbations leading to disruption of the optimized hydrogen bond network associated to the secondary structure is favored in crowded adsorption environments.

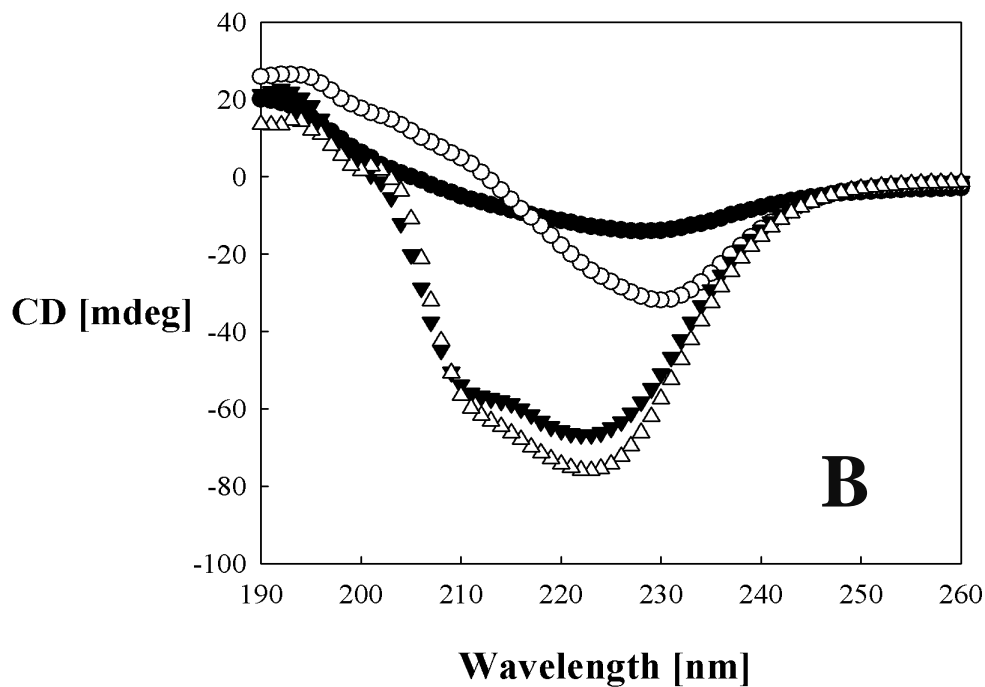
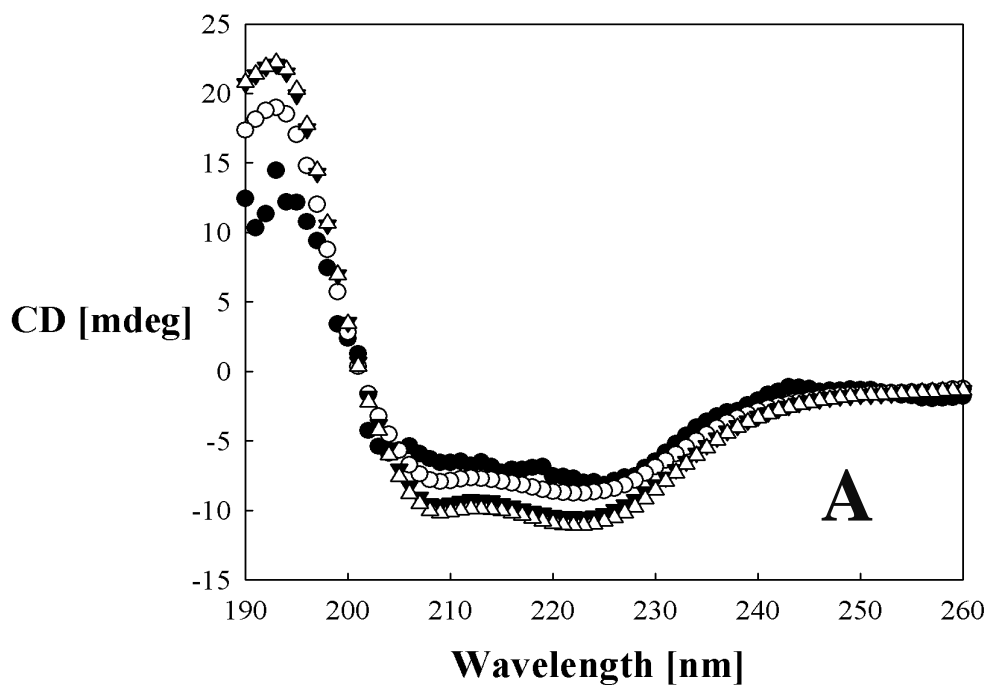


Figure 6.4. CD spectra for CALB adsorbing on fumed silica nanoparticles at different %SC and at initial enzyme concentrations of: (A) 0.7 mg/mL and (B) 3.3 mg/mL. (Δ) Native, (\bullet) 2%SC, (\circ) 100%SC, (\blacktriangledown) 400%SC. The signal loss at 222 nm is higher at low %SC for both low and high enzyme concentrations. This was attributed to reduced α -helical content. These results support the notion that increased surface interactions may lead to substantial conformational changes.

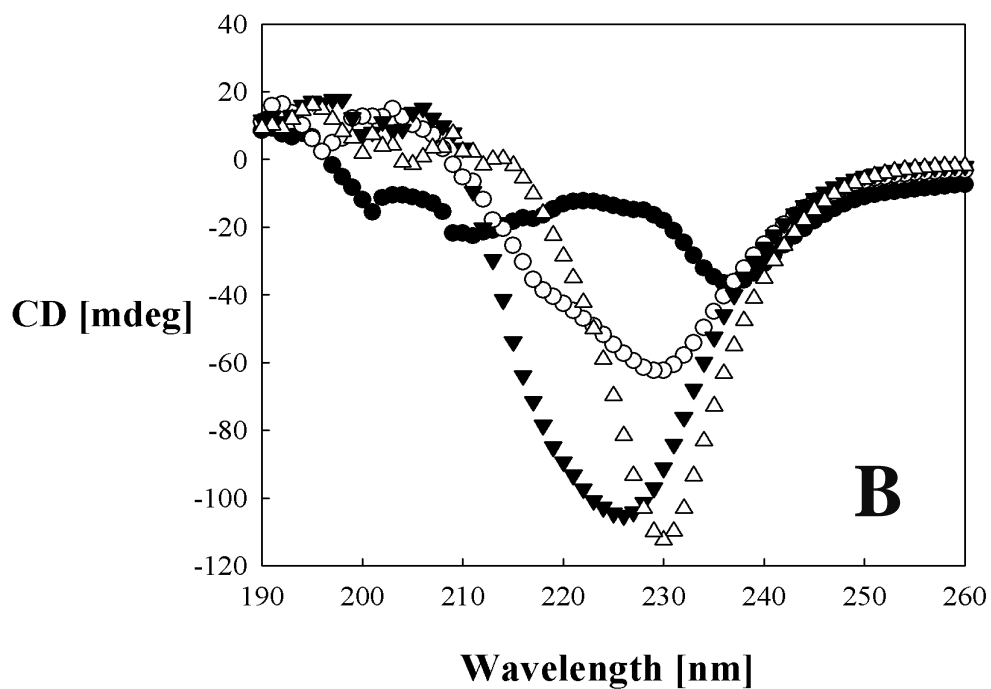
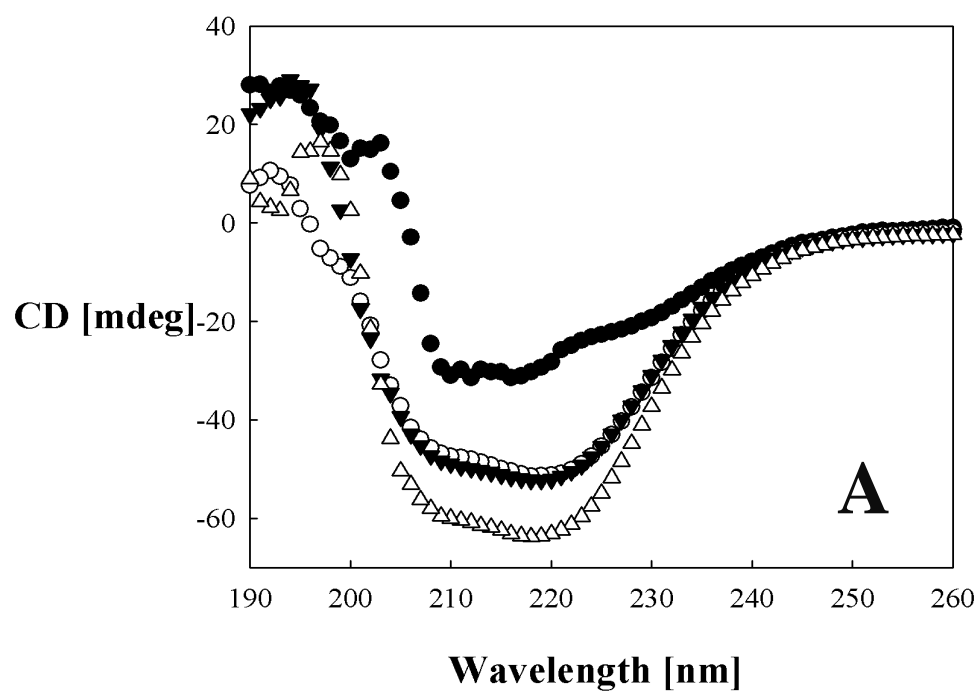


Figure 6.5. CD spectra for *s. Carlsberg* adsorbing on fumed silica nanoparticles at different %SC and at initial enzyme concentrations of: (A) 0.7 mg/mL and (B) 3.3 mg/mL. (Δ) Native, (\bullet) 2%SC, (\circ) 100%SC, (\blacktriangledown) 400%SC. As for CALB, the signal loss at 222 nm is higher at low %SC for the two concentrations under consideration. This was attributed to a reduction in the α -helical content due to conformational changes upon contact with the surface.

Figure 6.5 compares the CD spectrum in aqueous buffer solution for native *s. Carlsberg* with those in the presence of fumed silica nanoparticles at different %SC. As for CALB, a loss of α -helical content was detected. It appears, however, that an even higher structural perturbation occurs for *s. Carlsberg* at 2%SC. This could be attributed to a different native α -helical content, given that there are 5 α helices for *s. Carlsberg* as opposed to 10 α helices for CALB. Panel B in Figure 6.5 shows two different aspects in the CD spectra when moving to higher initial enzyme concentrations. First, the presence of a minimum in the spectrum at around 235 nm, and second a significantly higher loss in the α -helical content compared to low enzyme concentrations. The minimum at 235 nm has been previously reported and was ascribed to α -helical components¹²¹. Loss in signal at this wavelength can also be attributed to unfolding events. Further analyses involving *s. Carlsberg* at enzyme concentrations of 3.3 mg/mL and higher took this into account.

Figure 6.6 superimposes the CD spectra in aqueous buffer solution for native TLL and in the presence of fumed silica at different %SC. Panel A shows the case of low initial enzyme concentrations. As for CALB and *s. Carlsberg*, the nanoparticles appeared to be responsible for decreasing the α -helical content when abundant surface area is provided for interaction, i.e., at low %SC. When the initial enzyme concentration is increased (Figure 6.6 panel B), a lower extent of unfolding was detected than those observed for both *s. Carlsberg* and CALB. This is most likely due to the high conformational stability exhibited by this enzyme.

In all cases, adsorbates obtained at high %SC exhibited highly stable conformations. This supports the idea that protein-protein interactions preclude structural perturbations.

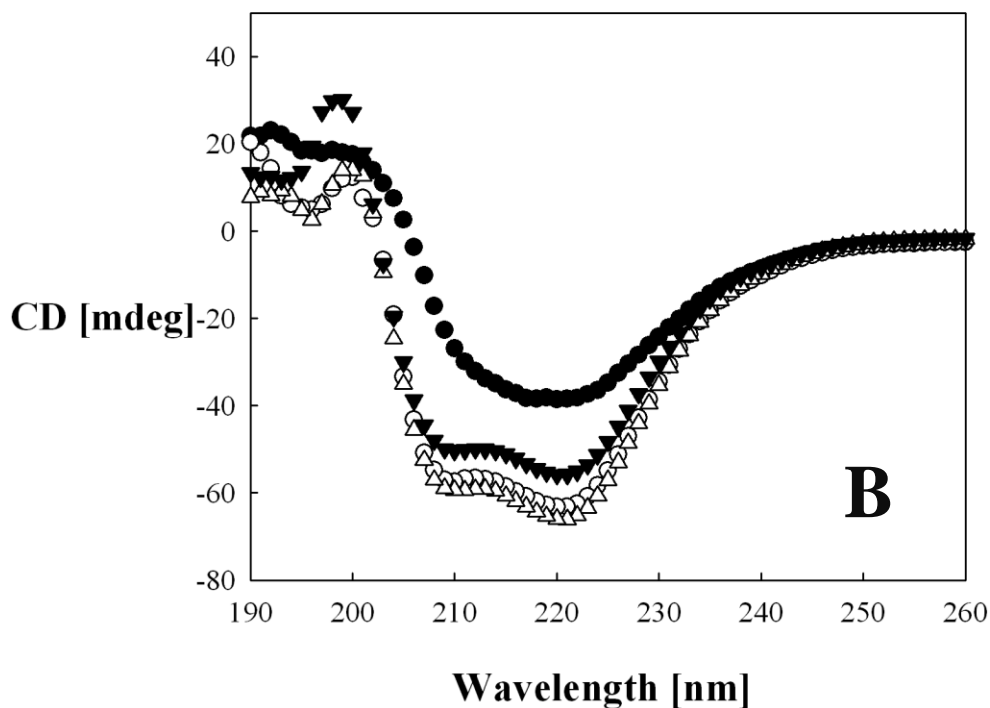
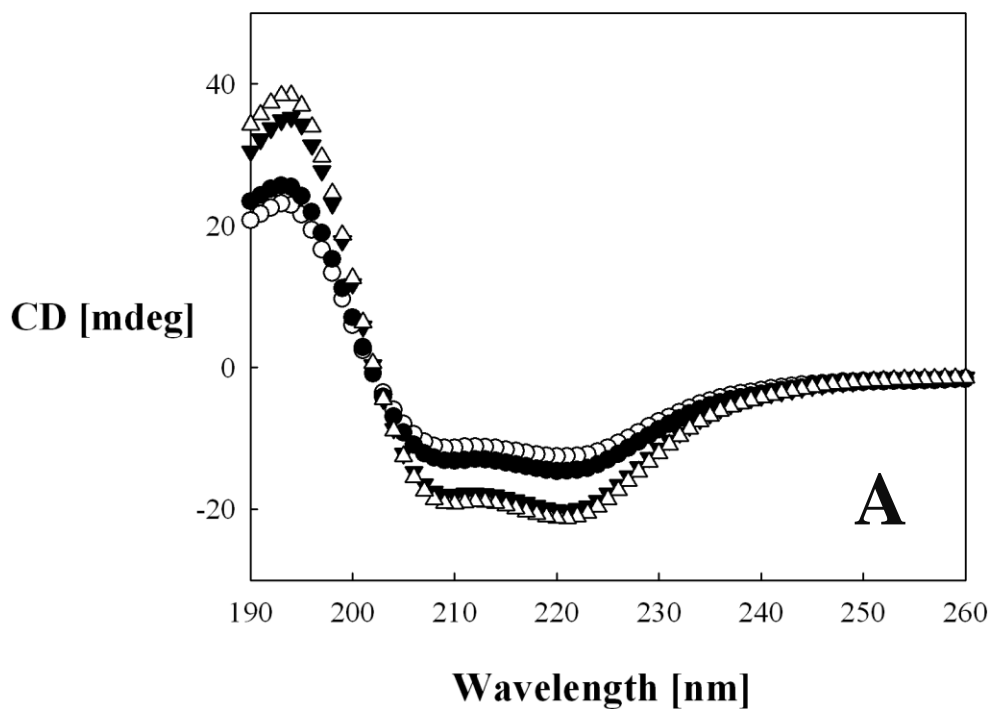


Figure 6.6. CD spectra for TLL adsorbing on fumed silica nanoparticles at different %SC and at initial enzyme concentrations of: (A) 0.7 mg/mL and (B) 3.30 mg/mL. (Δ) Native, (\bullet) 2%SC, (\circ) 100%SC, (\blacktriangledown) 400%SC. At low enzyme concentration, there is an observable loss of signal at 222 nm for 2%SC and 100%SC. When the enzyme concentration is increased, there is no significant loss of signal for 100%SC and 400%SC. This is most likely due to TLL's conformationally stable structure.

6.4.2 Regions of Conformational Stability for Enzyme/Fumed Silica Adsorbates

A general view of secondary conformational stability for *s. Carlsberg* and CALB adsorbing on fumed silica was obtained by conducting multiple unfolding experiments for various %SC and initial enzyme concentrations according to Table 6.1.

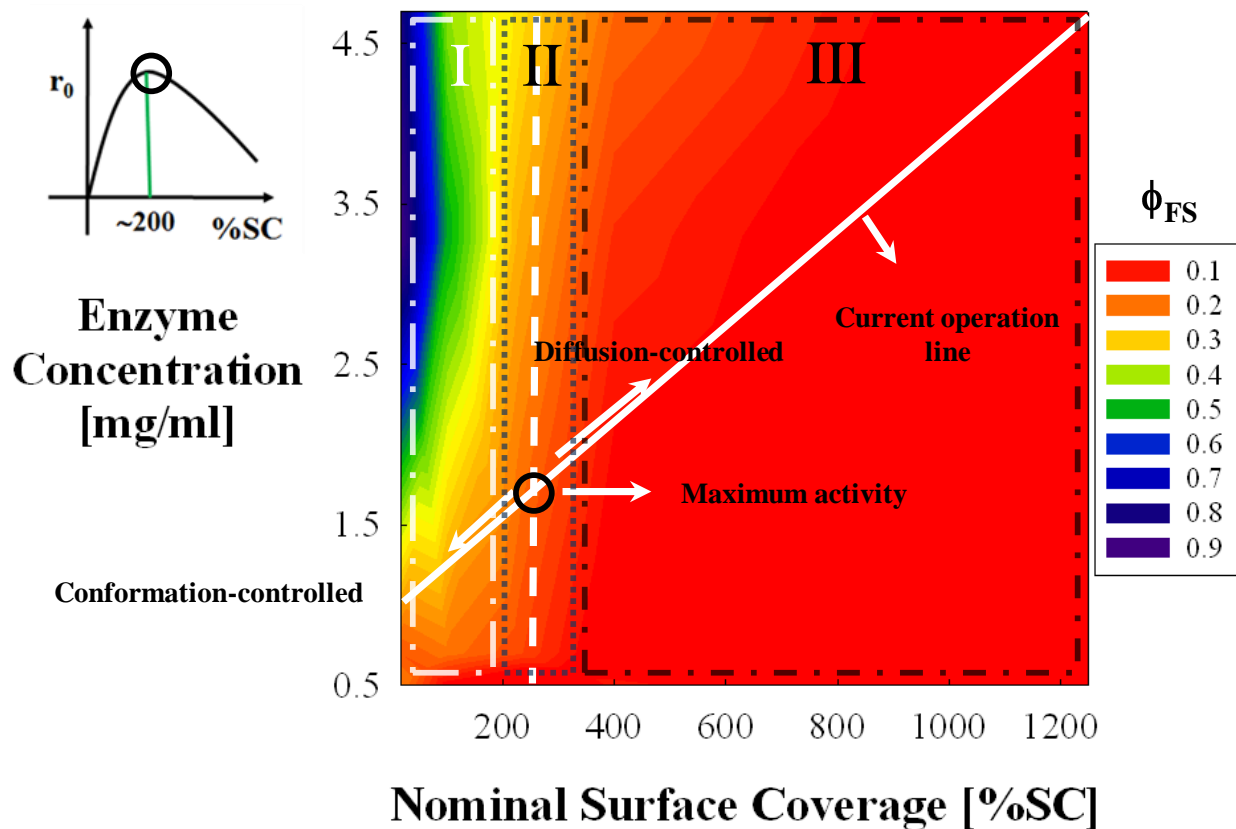


Figure 6.7. Regions of secondary conformational stability for CALB/Fumed Silica adsorbates. The dotted vertical line at ~250%SC separates two different regions of conformational stability: Region I delimited by a long-dash-dot line where adsorbates exhibit low conformational stability, and Region III delimited by a short-dash-dot line where highly stable enzyme ensembles are adsorbed on the surface. The presence of these two regions is likely to be responsible for the observed catalytic activity (r_0) of the lyophilized adsorbates in hexane (inset). The poor catalytic competency observed at low %SC can be linked to Region I while low activities at high %SC are linked to Region III where catalysis is severely reduced by mass transfer limitations. The maximum in activity between those two regions can be attributed to an optimal arrangement on the surface where the structure is relatively well maintained without excessive clustering (Region II, delimited by a dotted line). A very similar conformational diagram was previously found from intrinsic fluorescence spectroscopy experiments.

This approach was successfully applied previously to identify three regions of tertiary conformational stability from intrinsic fluorescence spectroscopy experiments for the same

hydrolases adsorbing on fumed silica in aqueous buffer solutions. These regions correlated well with the catalytic competency of the lyophilized adsorbates measured in hexane. The secondary structure of globular enzymes is assembled with the aid of a strong and well ordered hydrogen bonding network along the enzyme backbone. A major disruption in it requires structural perturbations to be stronger than those required for the tertiary structure. The conformational maps shown below helped to determine whether the structural perturbations introduced upon adsorption on fumed silica can impact the intramolecular hydrogen bonding associated with the stability of the secondary structural topologies.

Figure 6.7 combines the unfolded fractions of CALB adsorbing on fumed silica nanoparticles in a conformational stability diagram. Two different regions of conformational stability are observed at surface coverages above and below approximately 250%SC. Adsorbates obtained at high surface coverages (i.e., above 250%SC) exhibit highly stable conformations (region III). The secondary structure is very well maintained in this region (red shading). Below 250%SC (region I), however, the enzyme molecules unfolded significantly (green and blue areas). Values of unfolding near unity indicate that some adsorbed enzyme ensembles approach to complete denaturation. Region II is a region of transitional conformational stability. The catalytic competency in hexane of lyophilized adsorbates obtained along the diagonal line (Figure 6.7) is schematically shown in the inset (Figure 6.7). A simple inspection of the diagram reveals the proposed positive correlation model between catalytic competency and conformational stability for “soft” CALB previously postulated from tertiary structural analysis. The findings shown here also support our hypothesis that the surface loading regimes are essentially determined during the initial adsorption step of our immobilization protocol.

Figure 6.8 shows the corresponding conformational stability diagram for “hard” *s. Carlsberg*. Three regions of conformational stability were also identified for *s. Carlsberg*. When carefully examined, however, the lower section of region I (i.e., below 0.7 mg/mL) shows conformations that unfolded to a lower extent than those observed for CALB in the same region. This could be seen as support for our hypothesis that “hard” *s. Carlsberg* has a less pronounced tendency to unfold in the presence of abundant surface area than “soft” CALB. The presence of these highly stable and functional conformations in region I is most likely responsible for the high catalytic competency in hexane of the lyophilized adsorbates in this regime (inset in Figure 6.8).

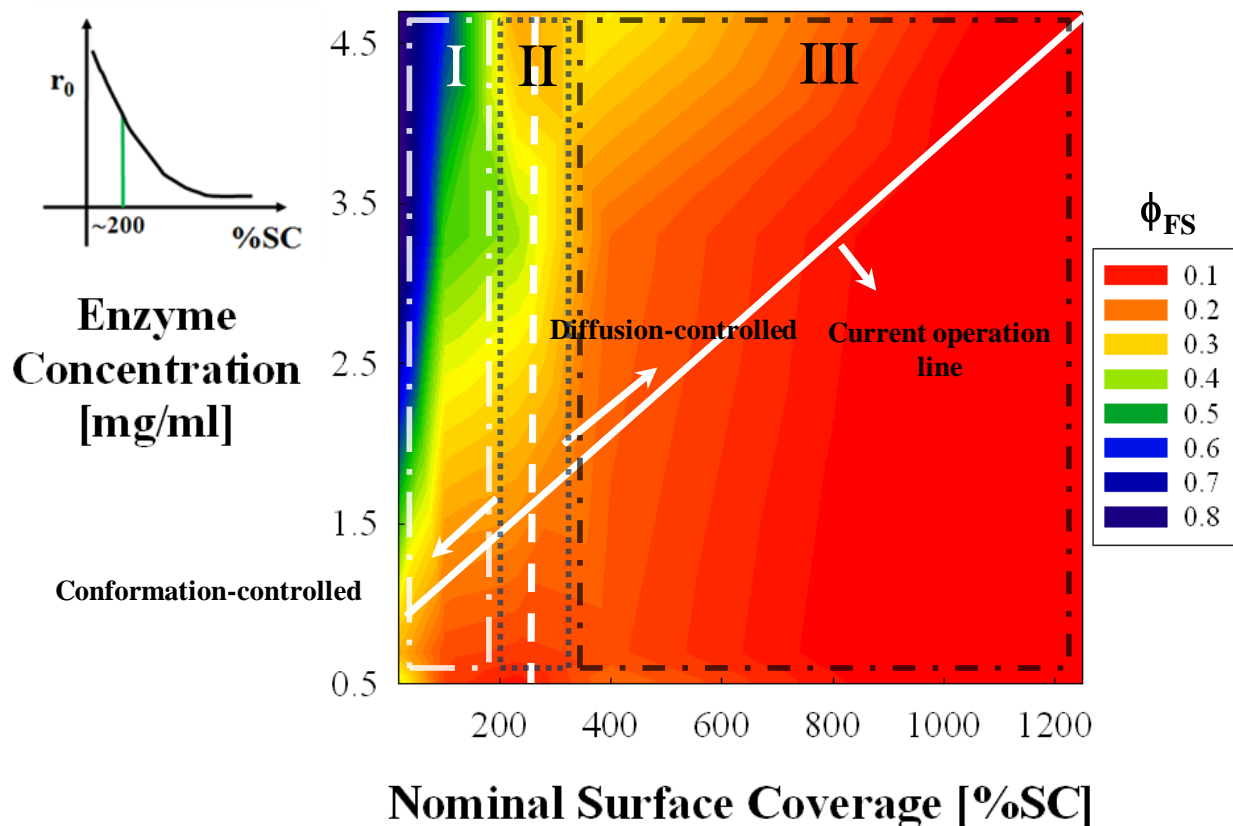


Figure 6.8. Regions of secondary conformational stability for *s. Carlsberg*/Fumed Silica adsorbates. The dotted vertical line at $\sim 250\%$ SC separates two different regions of conformational stability. Region I and III of low and high conformational stability, respectively. In this case, the catalytic activity (r_0) of the lyophilized adsorbates in hexane (inset) is constantly increasing. It appears that the extent of unfolding while operating in the lower part of Region I is less than that observed for CALB in the same region. This resilience to denaturation could be seen as a plausible explanation for the higher activities in this regime of surface loading compared with CALB.

In summary, our findings confirm that the three regions of conformational stability previously identified by probing the structure with Trp fluorescence spectroscopy can be also seen at a shorter structural scale as probed with CD spectroscopy. It appears, therefore, that the structural perturbations upon adsorption at low %SC are strong enough to disrupt the hydrogen bonding network responsible for stabilizing the secondary structure of the analyzed hydrolases. Additionally, the usefulness of conformational diagrams is validated here for designing highly active and stable nanobiomaterials. Our findings also corroborate the importance of the enzyme “hardness” in defining the physical arrangement and ultimately the functionality of enzyme molecules immobilized on solid surfaces.

6.4.3 Impact of Structure Modifiers for Enzymes Interacting with Fumed Silica in Aqueous Buffer Solution

To examine the types of interactions leading to the formation of the identified regions of secondary conformational stability for enzymes interacting with fumed silica, structure modifiers (2,2,2-trifluoroethanol (TFE) and Dithiothreitol (DTT)) were added prior to adsorption. TFE has the ability to disrupt hydrophobic segments and DTT is a potent reducing agent of disulfide bonds. Figure 6.9 panel A shows the impact of TFE and DTT on the secondary structure of CALB adsorbing on fumed silica at different %SC. A decrease in the extent of unfolding is observed for 17%SC and 100%SC in the presence of 30% (v/v) TFE respect to the experiments with untreated enzymes (Figure 6.9 panel A). Similar results were found from Trp fluorescence spectroscopy analyses. We proposed that the flexible unfolded state of CALB molecules has reduced dynamism leading to fewer opportunities for unfolding. This statement agrees with recent studies on proteins adsorbing on solid surfaces that suggest a direct link between spreading and mobility¹²⁰. Low mobility on solid surfaces appears to suppress the tendency of enzyme molecules to spread¹²⁰. As the %SC was increased, the presence of TFE promoted increased secondary unfolding that exceeded the values for the experiments with untreated enzyme molecules. The progressive reduction in unfolding as %SC increases could be attributed to the contribution of an increasing population of chemically-unfolded enzyme molecules forming aggregates. As suggested recently, these aggregates may act as barriers for surface-induced spreading if they adsorb on a dense protein layer, which is likely the case at high %SC¹²⁰. When 0.5 mg/mL DTT is added, the 4 disulfide bonds in CALB's structure are chemically reduced. It is evident from the slightly increased unfolding that the less rigid segments have increased affinity for the surface. This effect seems to be exacerbated at low %SC where the opportunities for surface interaction are favored. We suggest that in this case, the exposed regions in the oxidized native structure are not very mobile.

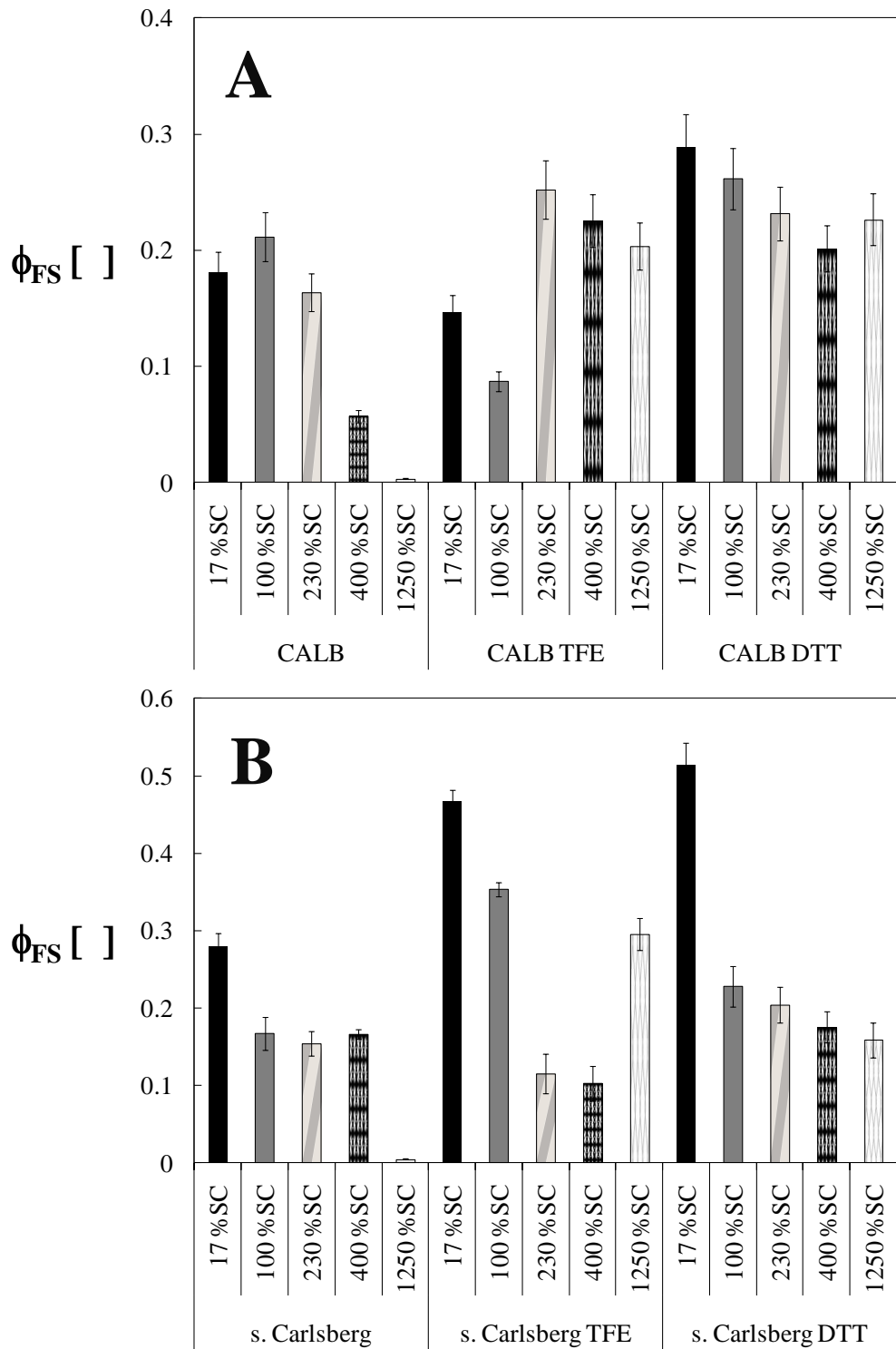


Figure 6.9. Secondary unfolding of (A) CALB and (B) *s. Carlsberg* adsorbing on fumed silica nanoparticles in the presence of 30% (v/v) TFE and 0.5 mg/mL DTT. Unfolding data for the untreated enzymes were added for comparison. The unfolded fraction (ϕ_{FS}) was calculated according to Equation 6.2.

Panel B in Figure 6.9 shows the impact of TFE and DTT on the secondary structure for *s. Carlsberg* adsorbing on fumed silica at different %SC. As opposed to CALB, 30 % (v/v) TFE addition for *s. Carlsberg* at 17%SC and 100%SC resulted in higher unfolding levels than those observed for the untreated enzymes. This could be attributed to the rigid structure of *s. Carlsberg*. It appears that upon TFE-induced unfolding, the exposed regions become more rapidly attached to the abundant nanoparticle surface that prevails at low %SC. As the %SC is increased to 230% and 400%, the unfolding values remained at approximately the same levels observed for the untreated enzymes. This is likely the result of the formation of highly rigid enzyme clusters stabilized upon contact with the nanoparticles. The rigid unfolded state of *s. Carlsberg* could act as a barrier for unfolding. Surprisingly, the unfolding at 1250%SC had a very high value relative to the experiment performed in the absence of TFE. This could be explained by association-induced conformational transitions. When 0.5 mg/mL DTT was added, unexpectedly high values of unfolding were detected at both the lowest and the highest loading values (17%SC and 1250%SC). This could be attributed to additional interactions of DTT that promote intramolecular instabilities and ultimately unfolding. Unfolding values for the intermediate %SC of 100, 230, and 400; however, remained approximately at the levels detected in the absence of DTT. It appears that the interactions among the enzyme molecules and with the surface are such that the induced unfolding is dampened.

6.4.4 Secondary Conformational Changes of Lyophilized Adsorbates

Figure 6.10 shows the FT-infrared spectra of native lyophilized CALB and lyophilized adsorbates of CALB/Fumed silica with different %SC loadings. The absorbance increases with increasing surface coverage towards the absorbance of the native lyophilized CALB with no silica. Because the silica does not absorb in this region of the spectrum, the FTIR signal emerges only from the enzyme and corroborates an increasingly higher packing density with increasing surface coverage. The position and number of the secondary structural components for the preparations obtained at 1250%SC and 2%SC are shown in Figure 6.11 panels A and B, respectively. These components were determined with the second derivative and assigned according to Table 6.3. The 1250%SC lyophilized preparation clearly shows two dominant bands at 1636.4 cm⁻¹ and 1656.8 cm⁻¹. These two peaks can be attributed to the β -sheets and α -helices, respectively. These two bands have been associated with the CALB's native conformation¹¹⁸. A

minor contribution was detected from peaks at 1680.9 cm^{-1} and 1690.3 cm^{-1} . These two bands can be correlated with turns and β -sheets. These findings support the notion that at high %SC, only a small distortion on the enzyme secondary structure is introduced by the presence of the nanoparticles.

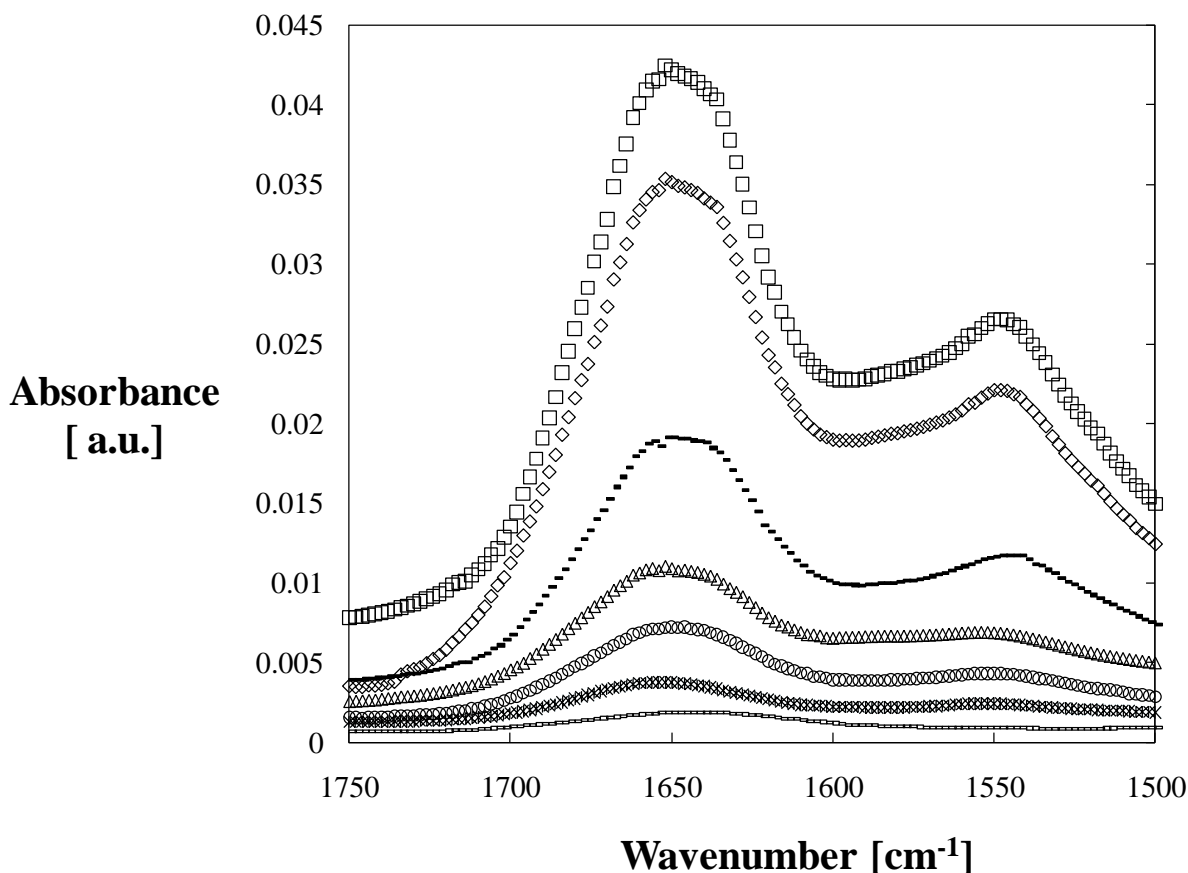


Figure 6.10. FTIR spectra in the amide I and II regions of native lyophilized CALB (\square) and lyophilized CALB/Fumed silica adsorbates: ($\square\square$) 2%SC, ($*$) 100%SC, (\circ) 150%SC, (Δ) 230%SC, ($\blacksquare\blacksquare$) 300%SC, and (\diamond) 1250%SC. A clear progression in the surface loading is evidenced by the higher signal intensities as the surface coverage increases.

The 2%SC preparation, however, has a dominant broad band that peaks at 1645.1 cm^{-1} . This could be attributed to disordered components most likely resulting from rearrangements within the enzyme secondary structure as expected upon spreading on the surface. Bands at 1672.4 cm^{-1} and 1628.1 cm^{-1} can be assigned to turns and β -sheets, respectively, which are also present when significant rearrangements occur in the secondary structure.

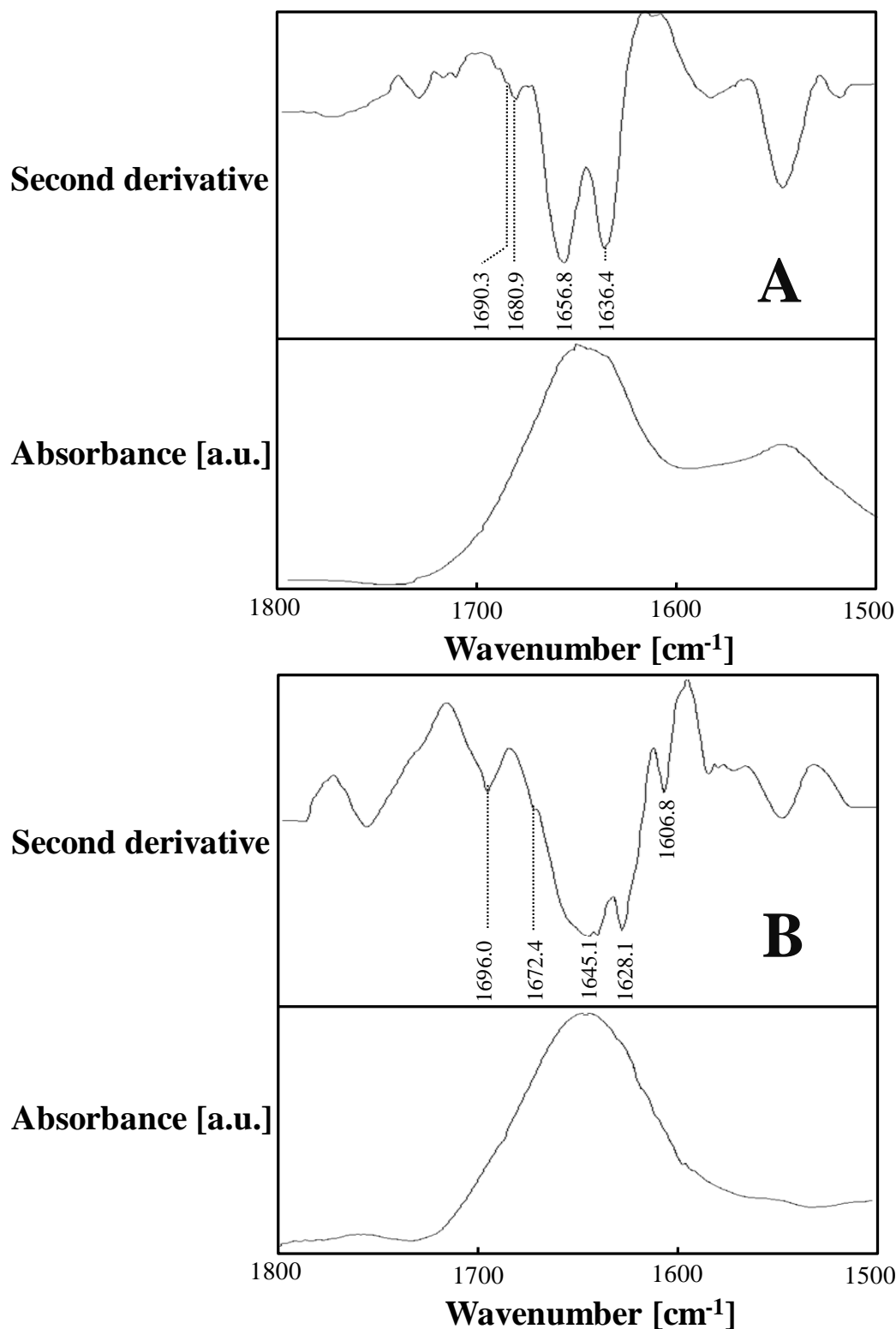


Figure 6.11. Second derivative of the amide I-FTIR spectra of CALB/Fumed silica lyophilized adsorbates. (A) 1250%SC and (B) 2%SC. The secondary structural components associated with the resolution-enhanced peaks obtained with this approach are subsequently identified according to Table 6.3.

The amide I-FTIR analysis confirms the substantial loss of α -helical content relative to the native state that was detected with CD for adsorbates obtained at low %SC. It also supports the idea of very well maintained structures at high %SC.

Prevention of conformational changes to maintain catalytic competency is clearly an important issue. It has been suggested that increasing the enzyme concentration in the aqueous phase during immobilization would be beneficial to reduce detrimental conformational changes¹²². Our results from CD and fluorescence spectroscopy, however, suggest that this approach could lead to substantial conformational changes in both the secondary and tertiary structure at low %SC. The 2%SC lyophilized preparations were prepared, therefore, with increasing initial enzyme concentrations of 0.15, 0.20, and 0.50 mg enzyme/mL solution. The preparation is generally prepared with an enzyme concentration of 0.10 mg/mL. Figure 6.12 panel A shows the FTIR spectra of the 2%SC lyophilized nanobiocatalysts obtained at increased initial enzyme concentrations. As the concentration increased, the enzyme loading was progressively higher as indicated by an increase in the relative signal intensity. Figure 6.12 panel B shows the second derivative of the FTIR spectrum of 2%SC nanobiocatalysts obtained from an initial enzyme concentration of 0.15 mg/mL. The dominant band for this preparation is located at 1641.0 cm^{-1} , which corresponds to disordered components. Bands at 1634.4 cm^{-1} and 1629.4 cm^{-1} assigned to β -sheet and at 1673.0 cm^{-1} assigned to turns did not contribute significantly to the spectrum. Panel C in Figure 6.12 shows the second derivative of the FTIR spectrum for the 2%SC nanobiocatalysts obtained from an initial enzyme concentration of 0.5 mg/mL. It appears that the contribution due to disordered structural components is reduced; however, the β -sheet extended conformations (1635.3 cm^{-1}) and turns (1669.9 cm^{-1}) remained visible in the spectrum. A minor contribution from α -helical components was observed in both cases.

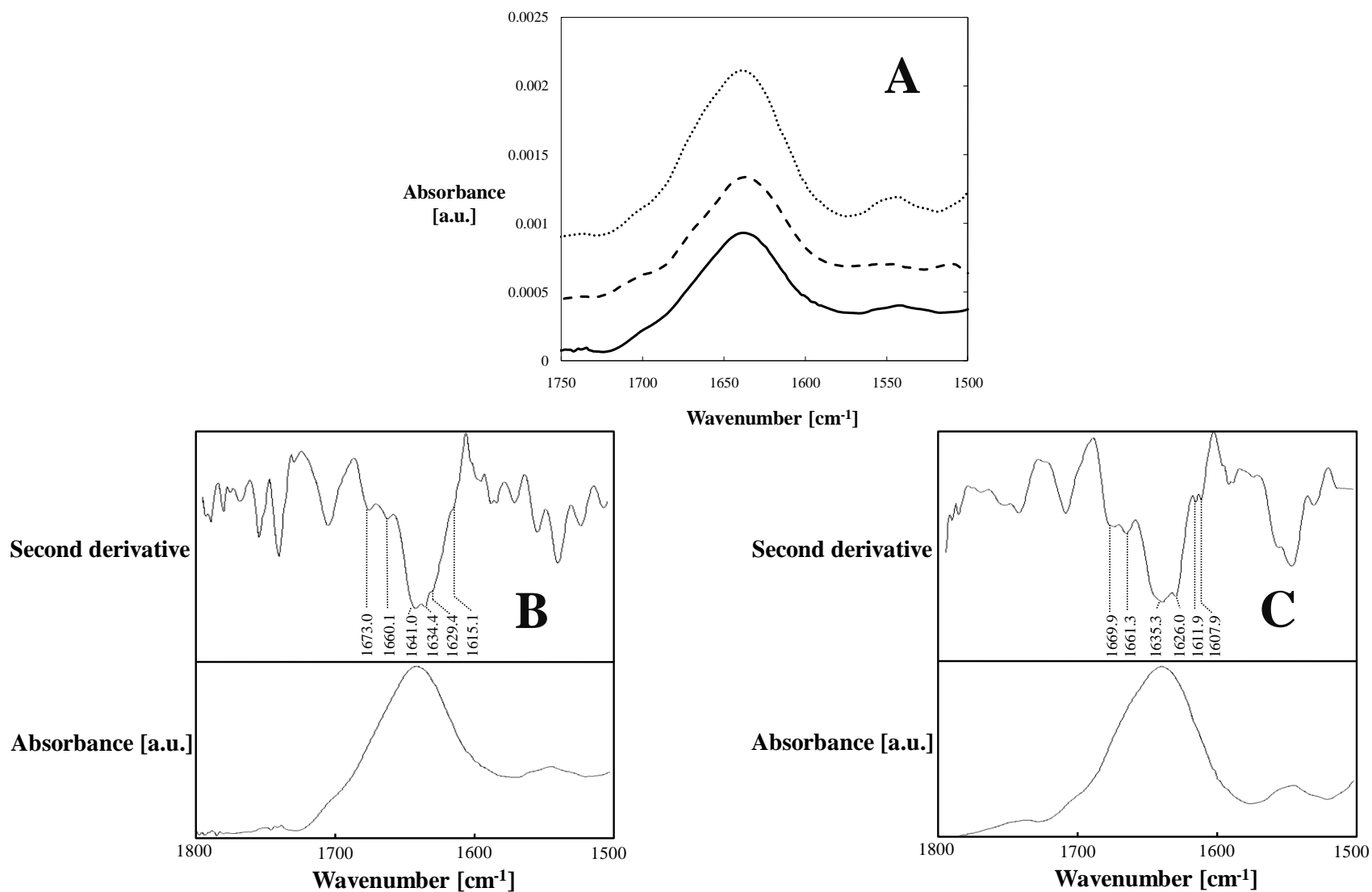


Figure 6.12. (A) FTIR spectra in the amide I and II regions of lyophilized CALB/Fumed silica adsorbates with 2%SC. Lyophilized nanobiocatalysts were prepared from enzyme solutions with different initial concentrations: (—) 0.15 mg/mL, (--) 0.25 mg/mL, (··) 0.5 mg/mL. Second derivative of the amide I-FTIR spectrum of nanobiocatalysts obtained from enzyme solutions with concentrations of (B) 0.15 mg/mL and (C) 0.5 mg/mL. The secondary structural components associated with the resolution-enhanced peaks obtained with this approach are subsequently identified according to Table 6.3.

Similar experiments at increased initial enzyme concentrations were conducted for 17%SC preparations. The initial concentrations explored were 0.3, 0.5, 2.9, and 4.7 mg enzyme/mL solution. Figure 6.13 panel A shows the FTIR spectra for 17%SC lyophilized biocatalysts. Surprisingly, moving from an initial enzyme concentration of 0.3 mg/mL to 0.5 mg/mL resulted in a lower IR signal. Increasing further to a concentration of 2.9 mg/mL resulted in an even lower signal, however, at 4.7 mg/mL no additional signal loss was observed. The presence of CALB/FS aggregates could be responsible for masking the IR signal. The ability of CALB molecules to form aggregates while adsorbing on similar inorganic supports has been recently suggested¹¹⁸. The occurrence of secondary structure conformational changes was examined by taking the second derivative. Figure 6.13 panel B shows the second derivative for 17%SC nanobiocatalysts obtained from an initial enzyme concentration of 0.3 mg/mL. Two dominant bands were identified at 1660.5 cm^{-1} and 1649.0 cm^{-1} , which can be assigned to α -helix and disordered components, respectively (Table 6.3). Less intense signals were detected at 1673.5 cm^{-1} and 1627.7 cm^{-1} , that are normally attributed to turns and β -sheets (Table 6.3). This suggests partially folded structures since the α -helical ordered components are still relatively abundant. Figure 6.13 panel C shows the 4.7 mg/mL case. A substantial loss of signal at 1660.0 cm^{-1} was detected relative to that observed at low concentration. This can be explained by a significant decrease in the α -helical content. The contribution of disordered components (1644.0 cm^{-1}), turns (1673.5 cm^{-1}), β -aggregates (1626.5 cm^{-1}) and β -sheets (1635.5 cm^{-1}) significantly increased.

In summary, obtaining adsorbates under crowding conditions and especially in the region of low %SC should be avoided as it may lead to considerable unfolding. Similar studies for lyophilized preparations have identified a loss of α -helical components concomitantly with an increase in the β -sheet, turns, and disordered components and suggested association-induced conformational transitions occurring either pre- or post- immobilization as a possible trigger mechanism.

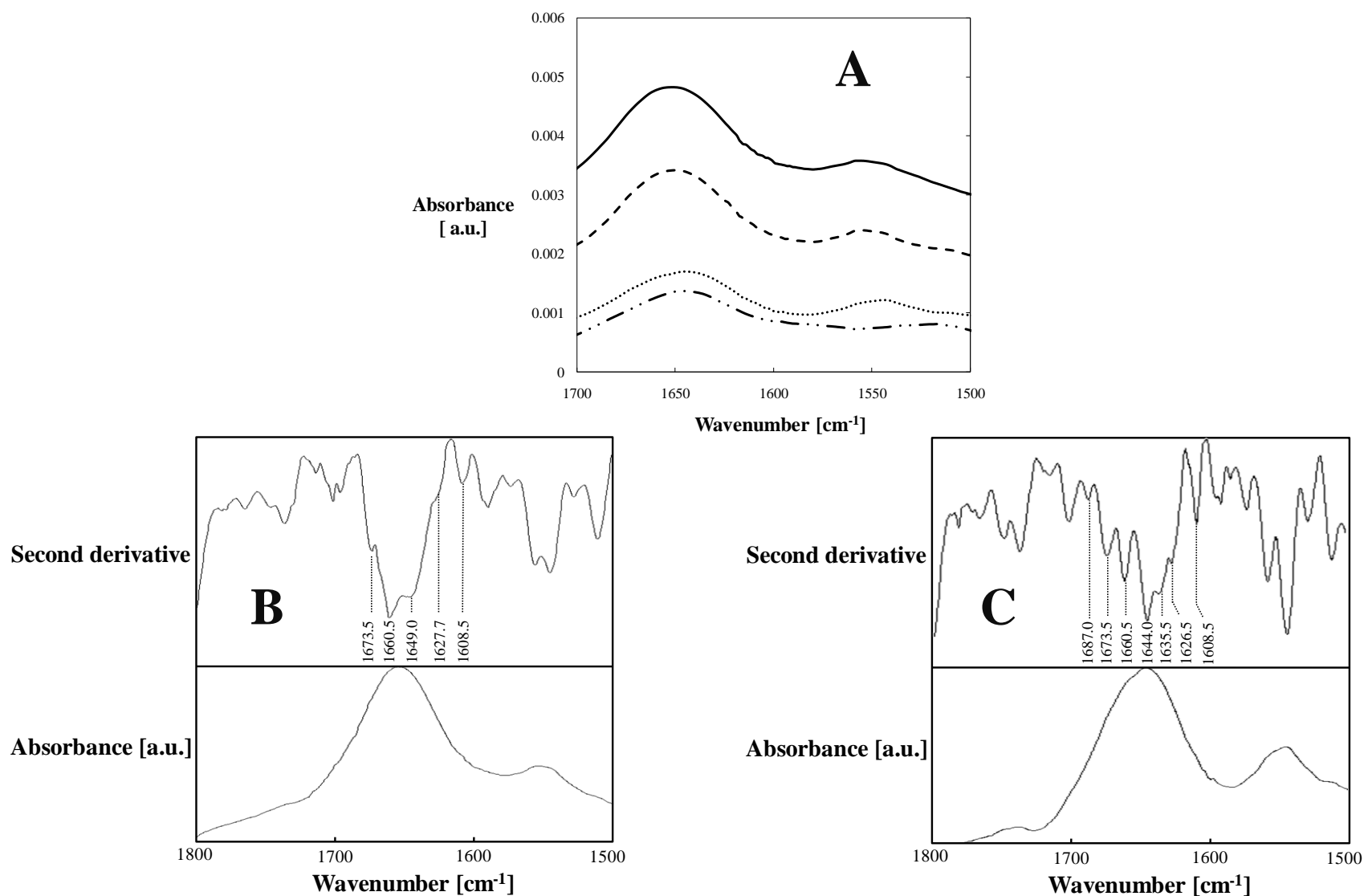


Figure 6.13. (A) FTIR spectra in the amide I and II regions of lyophilized CALB/Fumed silica adsorbates with 17%SC. Lyophilized nanobiocatalysts were prepared from enzyme solutions with different initial concentrations: (—) 0.3 mg/mL, (---) 0.5 mg/mL, (- · - ·) 2.9 mg/mL, (· · ·) 4.7 mg/mL. Second derivative of the amide I-FTIR spectrum of nanobiocatalysts obtained from enzyme solutions with concentrations of (B) 0.3 mg/mL and (C) 4.7 mg/mL. The secondary structural components associated with the resolution-enhanced peaks obtained with this approach are subsequently identified according to Table 6.3.

6.5 Conclusions

We have confirmed that the existence of three regions of conformational stability for hydrolases adsorbing on fumed silica as a function of the nominal surface coverage (%SC) can be seen at the secondary structural level upon disruption of the well organized intramolecular hydrogen bonding network of these enzyme molecules. Unfolding data was inferred from far-UV CD spectra of adsorbing hydrolases on fumed silica. At low %SC, enzyme molecules are seen to undergo major conformational changes. This region of low conformational stability is thought to occur due to increased interactions of the enzyme molecules with excess silica surface area. This phenomenon was exacerbated for CALB, which is an enzyme with a poorly packed or “soft” structure. The loss in catalytic activity in hexane for fumed silica based CALB nanobiocatalysts prepared in this region can be, therefore, correlated with this surface-induced structural distortion as it may ultimately lead to disruption of the active site. The “hard” *s. Carlsberg* enzyme at low %SC showed a relatively higher tolerance to surface-induced unfolding, which appears to correlate well with the high activity in hexane of lyophilized adsorbates at low %SC. At an intermediate %SC of about 250%, a region of transitional stability was identified where enzyme molecules have stable conformations and clustering appears to be absent. This region could be correlated with an optimum in catalytic activity for CALB in hexane. At high %SC, enzyme structure is well maintained which could be attributed to a different energy landscape where strong interactions with the surface are suppressed and protein-protein interactions dominate. This region is characterized by enzyme multilayer packing on the surface, which resulted in a substantial loss of catalytic activity of nanobiocatalysts in hexane mainly by mass transfer limitations.

TFE (30% v/v) addition revealed the importance of hydrophobic segments in maintaining the CALB’s structure at high %SC. At low %SC, however, this approach seemed to support the idea that suppression of protein dynamics could be a useful strategy to avoid spreading on surfaces. The static structure of *s. Carlsberg* is postulated to be responsible for the even higher levels of unfolding in the presence of TFE at low %SC. DTT addition increased the unfolding levels of CALB for all %SC cases, which suggested that the exposed regions had increased affinity for the surface as well as poor mobility.

Amide-I FTIR secondary analysis for CALB lyophilized adsorbates with low %SC showed a marked decrease in the α -helical component signal. This further supported the notion of induced structural perturbation when sufficient surface area is provided for immobilization. Filled contour conformational maps suggested that an increase in the initial enzyme concentration at low %SC gives rise to a pronounced unfolding most likely due to association-induced conformational transitions. The FTIR analysis corroborated that for the lyophilized adsorbates of CALB with low %SC, turns and β -sheets dominated over α -helical components.

6.6 References

1. Gupta, M. N., Enzyme Function in Organic-Solvents. *European Journal of Biochemistry* **1992**, 203, (1-2), 25-32.
2. Kise, H., Ester and Peptide-Synthesis by Proteases in Organic-Solvents. *Journal of Synthetic Organic Chemistry Japan* **1991**, 49, (1), 42-51.
3. Klibanov, A. M., Improving enzymes by using them in organic solvents. *Nature* **2001**, 409, (6817), 241-246.
4. Klibanov, A. M., Asymmetric enzymatic oxidoreductions in organic solvents. *Current Opinion in Biotechnology* **2003**, 14, (4), 427-431.
5. Rich, J. O.; Khmelnitsky, Y. L., Phospholipase D-catalyzed transphosphatidylation in anhydrous organic solvents. *Biotechnology and Bioengineering* **2001**, 72, (3), 374-377.
6. Ru, M. T.; Hirokane, S. Y.; Lo, A. S.; Dordick, J. S.; Reimer, J. A.; Clark, D. S., On the salt-induced activation of lyophilized enzymes in organic solvents: Effect of salt kosmotropicity on enzyme activity. *Journal of the American Chemical Society* **2000**, 122, (8), 1565-1571.
7. Ru, M. T.; Wu, K. C.; Lindsay, J. P.; Dordick, J. S.; Reimer, J. A.; Clark, D. S., Towards more active biocatalysts in organic media: Increasing the activity of salt-activated enzymes. *Biotechnology and Bioengineering* **2001**, 75, (2), 187-196.
8. Zaks, A.; Russell, A. J., Enzymes in Organic-Solvents - Properties and Applications. *Journal of Biotechnology* **1988**, 8, (4), 259-270.
9. Clark, D. S., Characteristics of nearly dry enzymes in organic solvents: implications for biocatalysis in the absence of water. *Philosophical Transactions of the Royal Society of London Series B-Biological Sciences* **2004**, 359, (1448), 1299-1307.

10. Kamat, S.; Barrera, J.; Beckman, E. J.; Russell, A. J., Biocatalytic Synthesis of Acrylates in Organic-Solvents and Supercritical Fluids .1. Optimization of Enzyme Environment. *Biotechnology and Bioengineering* **1992**, 40, (1), 158-166.
11. Gupta, A.; Khare, S. K., Enzymes from solvent-tolerant microbes: Useful biocatalysts for non-aqueous enzymology. *Critical Reviews in Biotechnology* **2009**, 29, (1), 44-54.
12. Ghanem, A., Trends in lipase-catalyzed asymmetric access to enantiomerically pure/enriched compounds. *Tetrahedron* **2007**, 63, (8), 1721-1754.
13. Ghanem, A.; Aboul-Enein, H. Y., Application of lipases in kinetic resolution of racemates. *Chirality* **2005**, 17, (1), 1-15.
14. Carrea, G.; Riva, S., Properties and synthetic applications of enzymes in organic solvents. *Angewandte Chemie-International Edition* **2000**, 39, (13), 2226-2254.
15. Dordick, J. S., Designing Enzymes for Use in Organic-Solvents. *Biotechnology Progress* **1992**, 8, (4), 259-267.
16. Dordick, J. S.; Khmelnitsky, Y. L.; Sergeeva, M. V., The evolution of biotransformation technologies. *Current Opinion in Microbiology* **1998**, 1, (3), 311-318.
17. Akkara, J. A.; Ayyagari, M. S. R.; Bruno, F. F., Enzymatic synthesis and modification of polymers in nonaqueous solvents. *Trends in Biotechnology* **1999**, 17, (2), 67-73.
18. Khmelnitsky, Y. L.; Rich, J. O., Biocatalysis in nonaqueous solvents. *Current Opinion in Chemical Biology* **1999**, 3, (1), 47-53.
19. Halling, P. J., Biocatalysis in low-water media: understanding effects of reaction conditions. *Current Opinion in Chemical Biology* **2000**, 4, (1), 74-80.
20. Ogino, H.; Ishikawa, H., Enzymes which are stable in the presence of organic solvents. *Journal of Bioscience and Bioengineering* **2001**, 91, (2), 109-116.
21. Castro, G. R.; Knubovets, T., Homogeneous biocatalysis in organic solvents and water-organic mixtures. *Critical Reviews in Biotechnology* **2003**, 23, (3), 195-231.
22. Serdakowski, A. L.; Dordick, J. S., Enzyme activation for organic solvents made easy. *Trends in Biotechnology* **2008**, 26, (1), 48-54.
23. Persson, M.; Wehtje, E.; Adlercreutz, P., Factors governing the activity of lyophilised and immobilised lipase preparations in organic solvents. *ChemBiochem* **2002**, 3, (6), 566-571.
24. Cruz, J. C.; Pfromm, P. H.; Rezac, M. E., Immobilization of *Candida antarctica* Lipase B on fumed silica. *Process Biochemistry* **2009**, 44, (1), 62-69.

25. Pfromm, P. H.; Rezac, M. E.; Wurges, K.; Czermak, P., Fumed silica activated subtilisin Carlsberg in hexane in a packed-bed reactor. *AIChE Journal* **2007**, *53*, (1), 237-242.
26. Wurges, K.; Pfromm, P. H.; Rezac, M. E.; Czermak, P., Activation of subtilisin Carlsberg in hexane by lyophilization in the presence of fumed silica. *Journal of Molecular Catalysis B-Enzymatic* **2005**, *34*, (1-6), 18-24.
27. Dabulis, K.; Klibanov, A. M., Dramatic Enhancement of Enzymatic-Activity in Organic-Solvents by Lyoprotectants. *Biotechnology and Bioengineering* **1993**, *41*, (5), 566-571.
28. Triantafyllou, A. O.; Wehtje, E.; Adlercreutz, P.; Mattiasson, B., How do additives affect enzyme activity and stability in nonaqueous media? *Biotechnology and Bioengineering* **1997**, *54*, (1), 67-76.
29. Carvalho, C. M. L.; Cabral, J. M. S., Reverse micelles as reaction media for lipases. *Biochimie* **2000**, *82*, (11), 1063-1085.
30. Biasutti, M. A.; Abuin, E. B.; Silber, J. J.; Correa, N. M.; Lissi, E. A., Kinetics of reactions catalyzed by enzymes in solutions of surfactants. *Advances in Colloid and Interface Science* **2008**, *136*, (1-2), 1-24.
31. Lindsay, J. P.; Clark, D. S.; Dordick, J. S., Penicillin amidase is activated for use in nonaqueous media by lyophilizing in the presence of potassium chloride. *Enzyme and Microbial Technology* **2002**, *31*, (3), 193-197.
32. Yan, A. X.; Li, X. W.; Ye, Y. H., Recent progress on immobilization of enzymes on molecular sieves for reactions in organic solvents. *Applied Biochemistry and Biotechnology* **2002**, *101*, (2), 113-129.
33. Chen, B.; Hu, J.; Miller, E. M.; Xie, W. C.; Cai, M. M.; Gross, R. A., Candida antarctica lipase B chemically immobilized on epoxy-activated micro- and nanobeads: Catalysts for polyester synthesis. *Biomacromolecules* **2008**, *9*, (2), 463-471.
34. Chen, B.; Miller, E. M.; Miller, L.; Maikner, J. J.; Gross, R. A., Effects of macroporous resin size on Candida antarctica lipase B adsorption, fraction of active molecules, and catalytic activity for polyester synthesis. *Langmuir* **2007**, *23*, (3), 1381-1387.
35. Chen, B.; Miller, M. E.; Gross, R. A., Effects of porous polystyrene resin parameters on Candida antarctica Lipase B adsorption, distribution, and polyester synthesis activity. *Langmuir* **2007**, *23*, (11), 6467-6474.

36. Gun'ko, V. M.; Mironyuk, I. F.; Zarko, V. I.; Turov, V. V.; Voronin, E. F.; Pakhlov, E. M.; Goncharuk, E. V.; Leboda, R.; Skubiszewska-Zieba, J.; Janusz, W.; Chibowski, S.; Levchuk, Y. N.; Klyueva, A. V., Fumed silicas possessing different morphology and hydrophilicity. *Journal of Colloid and Interface Science* **2001**, 242, (1), 90-103.
37. Gun'ko, V. M.; Mironyuk, I. F.; Zarko, V. I.; Voronin, E. F.; Turov, V. V.; Pakhlov, E. M.; Goncharuk, E. V.; Nychiporuk, Y. M.; Vlasova, N. N.; Gorbik, P. P.; Mishchuk, O. A.; Mishchuk, O. A.; Chuiko, A. A.; Kulik, T. V.; Palyanytsya, B. B.; Pakhovchishin, S. V.; Skubiszewska-Zieba, J.; Janusz, W.; Turov, A. V.; Leboda, R., Morphology and surface properties of fumed silicas. *Journal of Colloid and Interface Science* **2005**, 289, (2), 427-445.
38. Iler, R. K., *The Chemistry of Silica*. John Wiley & Sons, Inc.: 1979; p 896.
39. Gun'ko, V. M.; Mikhailova, I. V.; Zarko, V. I.; Gerashchenko, II; Guzenko, N. V.; Janusz, W.; Leboda, R.; Chibowski, S., Study of interaction of proteins with fumed silica in aqueous suspensions by adsorption and photon correlation spectroscopy methods. *Journal of Colloid and Interface Science* **2003**, 260, (1), 56-69.
40. Gun'ko, V. M.; Voronin, E. F.; Nosach, L. V.; Pakhlov, E. M.; Guzenko, N. V.; Leboda, R.; Skubiszewska-Zieba, J., Adsorption and migration of poly(vinyl pyrrolidone) at a fumed silica surface. *Adsorption Science & Technology* **2006**, 24, (2), 143-157.
41. Gun'ko, V. M.; Zarko, V. I.; Voronin, E. F.; Goncharuk, E. V.; Andriyko, L. S.; Guzenko, N. V.; Nosach, L. V.; Janusz, W., Successive interaction of pairs of soluble organics with nanosilica in aqueous media. *Journal of Colloid and Interface Science* **2006**, 300, (1), 20-32.
42. Gun'ko, V. M.; Zarko, V. I.; Voronin, E. F.; Turov, V. V.; Mironyuk, I. F.; Gerashchenko, II; Goncharuk, E. V.; Pakhlov, E. M.; Guzenko, N. V.; Leboda, R.; Skubiszewska-Zieba, J.; Janusz, W.; Chibowski, S.; Levchuk, Y. N.; Klyueva, A. V., Impact of some organics on structural and adsorptive characteristics of fumed silica in different media. *Langmuir* **2002**, 18, (3), 581-596.
43. Uppenberg, J.; Hansen, M. T.; Patkar, S.; Jones, T. A., Sequence, Crystal-Structure Determination and Refinement of 2 Crystal Forms of Lipase-B From *Candida antarctica*. *Structure* **1994**, 2, (4), 293-308.
44. Uppenberg, J.; Ohrner, N.; Norin, M.; Hult, K.; Kleywegt, G. J.; Patkar, S.; Waagen, V.; Anthonsen, T.; Jones, T. A., Crystallographic and molecular-modeling studies of lipase B from

Candida antarctica reveal a stereospecificity pocket for secondary alcohols. *Biochemistry* **1995**, 34, (51), 16838-16851.

45. Skjot, M.; De Maria, L.; Chatterjee, R.; Svendsen, A.; Patkar, S. A.; Ostergaard, P. R.; Brask, J., Understanding the Plasticity of the alpha/beta Hydrolase Fold: Lid Swapping on the *Candida antarctica* Lipase B Results in Chimeras with Interesting Biocatalytic Properties. *Chembiochem* **2009**, 10, (3), 520-527.

46. Hult, K.; Berglund, P., Enzyme promiscuity: mechanism and applications. *Trends in Biotechnology* **2007**, 25, (5), 231-238.

47. Svedendahl, M.; Carlqvist, P.; Branneby, C.; Allner, O.; Frise, A.; Hult, K.; Berglund, P.; Brinck, T., Direct Epoxidation in *Candida antarctica* Lipase B Studied by Experiment and Theory. *Chembiochem* **2008**, 9, (15), 2443-2451.

48. Neidhart, D. J.; Petsko, G. A., The Refined Crystal-Structure of Subtilisin Carlsberg at 2.5 Å Resolution. *Protein Engineering* **1988**, 2, (4), 271-276.

49. Asuri, P.; Bale, S. S.; Karajanagi, S. S.; Kane, R. S., The protein-nanomaterial interface. *Current Opinion in Biotechnology* **2006**, 17, (6), 562-568.

50. Kotov, N. A.; Winter, J. O.; Clements, I. P.; Jan, E.; Timko, B. P.; Campidelli, S.; Pathak, S.; Mazzatenta, A.; Lieber, C. M.; Prato, M.; Bellamkonda, R. V.; Silva, G. A.; Kam, N. W. S.; Patolsky, F.; Ballerini, L., Nanomaterials for Neural Interfaces. *Advanced Materials* **2009**, 21, (40), 3970-4004.

51. Wang, X.; Liu, L. H.; Ramstrom, O.; Yan, M. D., Engineering Nanomaterial Surfaces for Biomedical Applications. *Experimental Biology and Medicine* **2009**, 234, (10), 1128-1139.

52. Noy, A.; Artyukhin, A. B.; Misra, N., Bionanoelectronics with 1D materials. *Materials Today* **2009**, 12, (9), 22-31.

53. Katz, E.; Willner, I., Biomolecule-functionalized carbon nanotubes: Applications in nanobioelectronics. *Chemphyschem* **2004**, 5, (8), 1085-1104.

54. Sarma, A. K.; Vatsyayan, P.; Goswami, P.; Minteer, S. D., Recent advances in material science for developing enzyme electrodes. *Biosensors & Bioelectronics* **2009**, 24, (8), 2313-2322.

55. Mi, L. J.; Zhang, X.; Yang, W. C.; Wang, L. H.; Huang, Q.; Fan, C. H.; Hu, J., Artificial Nano-Bio-Complexes: Effects of Nanomaterials on Biomolecular Reactions and Applications in Biosensing and Detection. *Journal of Nanoscience and Nanotechnology* **2009**, 9, (4), 2247-2255.

56. Chen, D.; Wang, G.; Li, J. H., Interfacial bioelectrochemistry: Fabrication, properties and applications of functional nanostructured biointerfaces. *Journal of Physical Chemistry C* **2007**, 111, (6), 2351-2367.
57. Kane, R. S.; Stroock, A. D., Nanobiotechnology: Protein-nanomaterial interactions. *Biotechnology Progress* **2007**, 23, (2), 316-319.
58. Asuri, P.; Karajanagi, S. S.; Vertegel, A. A.; Dordick, J. S.; Kane, R. S., Enhanced stability of enzymes adsorbed onto nanoparticles. *Journal of Nanoscience and Nanotechnology* **2007**, 7, (4-5), 1675-1678.
59. Asuri, P.; Karajanagi, S. S.; Yang, H. C.; Yim, T. J.; Kane, R. S.; Dordick, J. S., Increasing protein stability through control of the nanoscale environment. *Langmuir* **2006**, 22, (13), 5833-5836.
60. Asuri, P.; Bale, S. S.; Pangule, R. C.; Shah, D. A.; Kane, R. S.; Dordick, J. S., Structure, function, and stability of enzymes covalently attached to single-walled carbon nanotubes. *Langmuir* **2007**, 23, (24), 12318-12321.
61. Shamim, N.; Liang, H.; Hidajat, K.; Uddin, M. S., Adsorption, desorption, and conformational changes of lysozyme from thermosensitive nanomagnetic particles. *Journal of Colloid and Interface Science* **2008**, 320, (1), 15-21.
62. Shang, W.; Nuffer, J. H.; Dordick, J. S.; Siegel, R. W., Unfolding of ribonuclease A on silica nanoparticle surfaces. *Nano Letters* **2007**, 7, (7), 1991-1995.
63. Shang, W.; Nuffer, J. H.; Muniz-Papandrea, V. A.; Colon, W.; Siegel, R. W.; Dordick, J. S., Cytochrome c on Silica Nanoparticles: Influence of Nanoparticle Size on Protein Structure, Stability, and Activity. *Small* **2009**, 5, (4), 470-476.
64. Norde, W., Driving forces for protein adsorption at solid surfaces. In *Biopolymers at Interfaces*, 2nd edn ed.; Marcel Dekker, Inc.: New York, 2003.
65. Roach, P.; Farrar, D.; Perry, C. C., Surface tailoring for controlled protein adsorption: Effect of topography at the nanometer scale and chemistry. *Journal of the American Chemical Society* **2006**, 128, (12), 3939-3945.
66. Ganesan, A.; Moore, B. D.; Kelly, S. M.; Price, N. C.; Rolinski, O. J.; Birch, D. J. S.; Dunkin, I. R.; Halling, P. J., Optical Spectroscopic Methods for Probing the Conformational Stability of Immobilised Enzymes. *Chemphyschem* **2009**, 10, (9-10), 1492-1499.

67. Barth, A., Infrared spectroscopy of proteins. *Biochimica et Biophysica Acta-Bioenergetics* **2007**, 1767, (9), 1073-1101.
68. Ganesan, A.; Price, N. C.; Kelly, S. M.; Petry, I.; Moore, B. D.; Halling, P. J., Circular dichroism studies of subtilisin Carlsberg immobilised on micron sized silica particles. *Biochimica et Biophysica Acta-Proteins and Proteomics* **2006**, 1764, (6), 1119-1125.
69. Hidajat, K.; Uddin, M.; Peng, Z., Conformational change of adsorbed and desorbed bovine serum albumin on nano-sized magnetic particles. *Colloids and Surfaces B: Biointerfaces* **2004**, 33, (1), 15-21.
70. Kondo, A.; Oku, S.; Higashitani, K., Structural-Changes in Protein Molecules Adsorbed on Ultrafine Silica Particles. *Journal of Colloid and Interface Science* **1991**, 143, (1), 214-221.
71. Pribic, R.; Vanstokkum, I. H. M.; Chapman, D.; Haris, P. I.; Bloemendal, M., Protein Secondary Structure from Fourier-Transform Infrared and/or Circular-Dichroism Spectra. *Analytical Biochemistry* **1993**, 214, (2), 366-378.
72. Wu, X.; Narsimhan, G., Characterization of secondary and tertiary conformational changes of beta-lactoglobulin adsorbed on silica nanoparticle surfaces. *Langmuir* **2008**, 24, (9), 4989-4998.
73. Wu, X. Y.; Narsimhan, G., Effect of surface concentration on secondary and tertiary conformational changes of lysozyme adsorbed on silica nanoparticles. *Biochimica et Biophysica Acta-Proteins and Proteomics* **2008**, 1784, (11), 1694-1701.
74. Zhu, K.; Jutila, A.; Tuominen, E. K. J.; Patkar, S. A.; Svendsen, A.; Kinnunen, P. K. J., Impact of the tryptophan residues of Humicola lanuginosa lipase on its thermal stability. *Biochimica Et Biophysica Acta-Protein Structure and Molecular Enzymology* **2001**, 1547, (2), 329-338.
75. Kelly, S. M.; Jess, T. J.; Price, N. C., How to study proteins by circular dichroism. *Biochimica et Biophysica Acta-Proteins and Proteomics* **2005**, 1751, (2), 119-139.
76. Ranjbar, B.; Gill, P., Circular Dichroism Techniques: Biomolecular and Nanostructural Analyses- A Review. *Chemical Biology & Drug Design* **2009**, 74, (2), 101-120.
77. Bandekar, J., Amide Modes and Protein Conformation. *Biochimica et Biophysica Acta* **1992**, 1120, (2), 123-143.
78. Krimm, S.; Bandekar, J., Vibrational Spectroscopy and Conformation of Peptides, Polypeptides, and Proteins. *Advances in Protein Chemistry* **1986**, 38, 181-364.

79. Arrondo, J. L. R.; Muga, A.; Castresana, J.; Goni, F. M., Quantitative Studies of the Structure of Proteins in Solution by Fourier-Transform Infrared-Spectroscopy. *Progress in Biophysics & Molecular Biology* **1993**, 59, (1), 23-56.
80. Oberg, K. A.; Ruyschaert, J. M.; Goormaghtigh, E., The optimization of protein secondary structure determination with infrared and circular dichroism spectra. *European Journal of Biochemistry* **2004**, 271, (14), 2937-2948.
81. Fu, F. N.; Deoliveira, D. B.; Trumble, W. R.; Sarkar, H. K.; Singh, B. R., Secondary Structure Estimation of Proteins Using the Amide-III Region of Fourier-Transform Infrared-Spectroscopy - Application to Analyze Calcium Binding-Induced Structural-Changes in Calsequestrin. *Applied Spectroscopy* **1994**, 48, (11), 1432-1441.
82. Cai, S. W.; Singh, B. R., A distinct utility of the amide III infrared band for secondary structure estimation of aqueous protein solutions using partial least squares methods. *Biochemistry* **2004**, 43, (9), 2541-2549.
83. Cai, S. W.; Singh, B. R., Identification of beta-turn and random coil amide III infrared bands for secondary structure estimation of proteins. *Biophysical Chemistry* **1999**, 80, (1), 7-20.
84. Chirgadze, Y. N.; Nevskaya, N. A., Infrared-Spectra and Resonance Interaction of Amide-I Vibration of Anti-Parallel-Chain Pleated Sheet. *Biopolymers* **1976**, 15, (4), 607-625.
85. Chirgadze, Y. N.; Nevskaya, N. A., Infrared-Spectra and Resonance Interaction of Amide-I Vibration of Parallel-Chain Pleated Sheet. *Biopolymers* **1976**, 15, (4), 627-636.
86. Kauffmann, E.; Darnton, N. C.; Austin, R. H.; Batt, C.; Gerwert, K., Lifetimes of intermediates in the beta-sheet to alpha-helix transition of beta-lactoglobulin by using a diffusional IR mixer. *Proceedings of the National Academy of Sciences of the United States of America* **2001**, 98, (12), 6646-6649.
87. Fabian, H.; Mantsch, H. H.; Schultz, C. P., Two-dimensional IR correlation spectroscopy: Sequential events in the unfolding process of the lambda Cro-V55C repressor protein. *Proceedings of the National Academy of Sciences of the United States of America* **1999**, 96, (23), 13153-13158.
88. Reinstadler, D.; Fabian, H.; Naumann, D., New structural insights into the refolding of ribonuclease T1 as seen by time-resolved Fourier-transform infrared spectroscopy. *Proteins-Structure Function and Genetics* **1999**, 34, (3), 303-316.

89. Dyer, R. B.; Gai, F.; Woodruff, W. H., Infrared studies of fast events in protein folding. *Accounts of Chemical Research* **1998**, 31, (11), 709-716.
90. Ramajo, A. P.; Petty, S. A.; Starzyk, A.; Decatur, S. M.; Volk, M., The alpha-helix folds more rapidly at the C-terminus than at the N-terminus. *Journal of the American Chemical Society* **2005**, 127, (40), 13784-13785.
91. Backmann, J.; Fabian, H.; Naumann, D., Temperature-Jump-Induced Refolding of Ribonuclease-A - A Time-Resolved FTIR Spectroscopic Study. *FEBS Letters* **1995**, 364, (2), 175-178.
92. Surewicz, W. K.; Szabo, A. G.; Mantsch, H. H., Conformational Properties of Azurin in Solution as Determined from Resolution-Enhanced Fourier-Transform Infrared-Spectra. *European Journal of Biochemistry* **1987**, 167, (3), 519-523.
93. Reinstadler, D.; Fabian, H.; Backmann, J.; Naumann, D., Refolding of thermally and urea-denatured ribonuclease A monitored by time-resolved FTIR spectroscopy. *Biochemistry* **1996**, 35, (49), 15822-15830.
94. Fabian, H.; Naumann, D., Methods to study protein folding by stopped-flow FT-IR. *Methods* **2004**, 34, (1), 28-40.
95. Gooding, E. A.; Ramajo, A. P.; Wang, J. W.; Palmer, C.; Fouts, E.; Volk, M., The effects of individual amino acids on the fast folding dynamics of alpha-helical peptides. *Chemical Communications* **2005**, (48), 5985-5987.
96. Brewer, S. H.; Song, B. B.; Raleigh, D. P.; Dyer, R. B., Residue specific resolution of protein folding dynamics using isotope-edited infrared temperature jump spectroscopy. *Biochemistry* **2007**, 46, (11), 3279-3285.
97. Kauppinen, J. K.; Moffatt, D. J.; Mantsch, H. H.; Cameron, D. G., Fourier Self-Deconvolution - A Method for Resolving Intrinsically Overlapped Bands. *Applied Spectroscopy* **1981**, 35, (3), 271-276.
98. Mantsch, H. H.; Moffatt, D. J.; Casal, H. L., Fourier-Transform Methods for Spectral Resolution Enhancement. *Journal of Molecular Structure* **1988**, 173, 285-298.
99. Susi, H.; Byler, D. M., Resolution-Enhanced Fourier-Transform Infrared-Spectroscopy of Enzymes. *Methods in Enzymology* **1986**, 130, 290-311.

100. Barth, A., Fine-structure enhancement - assessment of a simple method to resolve overlapping bands in spectra. *Spectrochimica Acta Part a-Molecular and Biomolecular Spectroscopy* **2000**, 56, (6), 1223-1232.
101. Dong, A.; Huang, P.; Caughey, W. S., Redox-Dependent Changes in Beta-Extended Chain and Turn Structures of Cytochrome-C in Water Solution Determined by 2nd Derivative Amide-I Infrared-Spectra. *Biochemistry* **1992**, 31, (1), 182-189.
102. Susi, H.; Byler, D. M., Fourier-Transform Infrared Study of Proteins with Parallel Beta-Chains. *Archives of Biochemistry and Biophysics* **1987**, 258, (2), 465-469.
103. Byler, D. M.; Susi, H., Examination of the Secondary Structure of Proteins by Deconvolved FTIR Spectra. *Biopolymers* **1986**, 25, (3), 469-487.
104. Sarver, R. W.; Krueger, W. C., Protein Secondary Structure from Fourier-Transform Infrared-Spectroscopy - A Data-Base Analysis. *Analytical Biochemistry* **1991**, 194, (1), 89-100.
105. Baumruk, V.; Pancoska, P.; Keiderling, T. A., Predictions of secondary structure using statistical analyses of electronic and vibrational circular dichroism and Fourier transform infrared spectra of proteins in H₂O. *Journal of Molecular Biology* **1996**, 259, (4), 774-791.
106. Jutila, A.; Zhu, K.; Patkar, S. A.; Vind, J.; Svendsen, A.; Kinnunen, P. K. J., Detergent-induced conformational changes of Humicola lanuginosa lipase studied by fluorescence spectroscopy. *Biophysical Journal* **2000**, 78, (3), 1634-1642.
107. Jutila, A.; Zhu, K.; Tuominen, E. K. J.; Kinnunen, P. K. J., Fluorescence spectroscopic characterization of Humicola lanuginosa lipase dissolved in its substrate. *Biochimica et Biophysica Acta-Proteins and Proteomics* **2004**, 1702, (2), 181-189.
108. Zhu, K.; Jutila, A.; Kinnunen, P. K. J., Steady state and time resolved effects of guanidine hydrochloride on the structure of Humicola lanuginosa lipase revealed by fluorescence spectroscopy. *Protein Science* **2000**, 9, (3), 598-609.
109. Schafer, T.; Borchert, T. W.; Nielsen, V. S.; Skagerlind, P.; Gibson, K.; Wenger, K.; Hatzack, F.; Nilsson, L. D.; Salmons, S.; Pedersen, S.; Heldt-Hansen, H. P.; Poulsen, P. B.; Lund, H.; Oxenboll, K. M.; Wu, G. F.; Pedersen, H. H.; Xu, H., Industrial enzymes. In *White Biotechnology*, Springer-Verlag Berlin: Berlin, 2007; Vol. 105, pp 59-131.
110. Guo, F.; Friedman, J. M., Osmolyte-Induced Perturbations of Hydrogen Bonding between Hydration Layer Waters: Correlation with Protein Conformational Changes. *Journal of Physical Chemistry B* **2009**, 113, (52), 16632-16642.

111. Bai, S. F.; Dong, A. C., Effects of immobilization onto aluminum hydroxide particles on the thermally induced conformational behavior of three model proteins. *International Journal of Biological Macromolecules* **2009**, 45, (1), 80-85.
112. Dong, A. C.; Jones, L. S.; Kerwin, B. A.; Krishnan, S.; Carpenter, J. F., Secondary structures of proteins adsorbed onto aluminum hydroxide: Infrared spectroscopic analysis of proteins from low solution concentrations. *Analytical Biochemistry* **2006**, 351, (2), 282-289.
113. Natalello, A.; Ami, D.; Brocca, S.; Lotti, M.; Doglia, S. M., Secondary structure, conformational stability and glycosylation of a recombinant *Candida rugosa* lipase studied by Fourier-transform infrared spectroscopy. *Biochemical Journal* **2005**, 385, 511-517.
114. Barth, A.; Zscherp, C., What vibrations tell us about proteins. *Quarterly Reviews of Biophysics* **2002**, 35, (4), 369-430.
115. Dong, A. C.; Meyer, J. D.; Kendrick, B. S.; Manning, M. C.; Carpenter, J. F., Effect of secondary structure on the activity of enzymes suspended in organic solvents. *Archives of Biochemistry and Biophysics* **1996**, 334, (2), 406-414.
116. Dong, A. C.; Prestrelski, S. J.; Allison, S. D.; Carpenter, J. F., Infrared Spectroscopic Studies of Lyophilization-Induced and Temperature-Induced Protein Aggregation. *Journal of Pharmaceutical Sciences* **1995**, 84, (4), 415-424.
117. van de Weert, M.; Haris, P. I.; Hennink, W. E.; Crommelin, D. J. A., Fourier transform infrared spectrometric analysis of protein conformation: Effect of sampling method and stress factors. *Analytical Biochemistry* **2001**, 297, (2), 160-169.
118. Foresti, M. L.; Valle, G.; Bonetto, R.; Ferreira, M. L.; Briand, L. E., FTIR, SEM and fractal dimension characterization of lipase B from *Candida antarctica* immobilized onto titania at selected conditions. *Applied Surface Science* 256, (6), 1624-1635.
119. Vertegel, A. A.; Siegel, R. W.; Dordick, J. S., Silica nanoparticle size influences the structure and enzymatic activity of adsorbed lysozyme. *Langmuir* **2004**, 20, (16), 6800-6807.
120. Rabe, M.; Verdes, D.; Seeger, S., Surface-induced spreading phenomenon of protein clusters. *Soft matter* **2009**, 5, (5), 1039-1047.
121. Lee, S.; Jang, D. J., Progressive rearrangement of subtilisin Carlsberg into orderly and inflexible conformation with Ca²⁺ binding. *Biophysical Journal* **2001**, 81, (5), 2972-2978.

122. Unsworth, L. D.; van der Oost, J.; Koutsopoulos, S., Hyperthermophilic enzymes - stability, activity and implementation strategies for high temperature applications. *FEBS Journal* **2007**, 274, (16), 4044-4056.

CHAPTER - 7 Conclusions and Recommendations

7.1 Conclusions

The need for affordable enzymatic technologies has been revitalized by the current economic incentives offered by the U.S. Government to promote consumers and businesses to incorporate green technologies and chemistries. When enzymes are incorporated in industrial processes, chances are high that yields can be improved and energy consumption can be reduced. This is a consequence of the ability of enzymes to operate at lower temperatures, perform complicated stereospecific chemistries that otherwise require multi-step processes, and selectively convert substrates for simpler downstream separation schemes and ultimately higher overall efficiencies. All these attributes are particularly attractive for industrial sectors dedicated to manufacturing specialty chemicals and pharmaceuticals. Some of these compounds are conventionally synthesized with complicated multi-step schemes that frequently involve extreme process conditions, by-products, and toxic chemical compounds as catalysts. The major challenges when incorporating enzymes in these processes are their marked tendency to cluster and their continuously decaying operational stability when suspended in the common non-aqueous processing media. This research project provides guidelines to remediate these major hurdles for hydrolases, the most widely used enzymes in industrial biocatalysis. Our strategy mainly relies on the electrostatic assembly of the enzyme molecules on fumed silica. This material is a nanoparticulated fractal aggregate that offers facilitated hydrophilic adsorption pathways for various organic compounds including proteins and polymers.

Selected hydrolases were immobilized on fumed silica to prepare highly active, selective, and stable nanobiocatalysts for applications in organic solvents. The immobilization protocol presented here offers a cost-effective alternative that could potentially expand the applicability of enzyme-based bioprocesses to the production of a wider variety of compounds of commercial interest. This is due to the low cost of fumed silica and the simplicity of the immobilization protocol, which requires only two steps. The buffered enzymes are adsorbed on fumed silica from aqueous solutions and then lyophilized. This strategy has been assessed with two hydrolases of industrial importance, *subtilisin Carlsberg* and *Candida antarctica* Lipase B (CALB).

Lyophilized adsorbates of *s. Carlsberg* showed increasing catalytic activity in hexane as more nominal surface area was provided for immobilization. This was attributed to a substantial release of the aforementioned mass transfer limitations for the native enzyme molecules suspended in the organic phase. The observed activities reached those obtained with nonbuffer salt based preparations. CALB/fumed silica preparations also showed remarkable catalytic activities in hexane for both chiral and non-chiral esterification reactions, roughly doubling those of the widely successful commercial preparation Novozyme 435®. An intriguing result for CALB/fumed silica preparations was the presence of a maximum in catalytic activity when the nominal surface coverage by the enzyme molecules reached an intermediate loading value. The presence of this maximum in activity was rationalized in light of three different surface loading regimes after lyophilization: 1. low surface coverages where multiple surface-protein interactions are most likely responsible for detrimental conformational changes, 2. intermediate surface coverages where both surface-protein and protein-protein interactions are balanced such that a large population of catalytically competent enzyme molecules is maintained on the surface, 3. high surface coverages where a multi-layer packing on the surface lead to a substantial loss in apparent catalytic activity.

Temperature stability studies for CALB/fumed silica preparations corroborated typical Arrhenius activation as reported in the literature. Preparations with low surface coverages showed no substantial deactivation with respect to the fresh preparation, which was attributed to the multi-attachment to the surface. Preparations that exhibited optimal catalytic performance remained active at temperatures as high as 70°C where they even exceeded Novozyme 435®. This further supported the crucial role of neighboring molecules in stabilizing a large population of properly functioning enzyme molecules at intermediate surface coverages. Prolonged exposure of CALB/fumed silica preparations to solvent reduced the activity by about 50% in a simple esterification reaction, and remained at approximately the initial level in an enantioselective transesterification. This suggested that the fine 3D active site arrangement required for chiral conversion is likely to remain unaffected after continuous exposure to solvents. CALB/fumed silica preparations with low surface coverages that were stored at 4°C for approximately 1 year showed no significant reduction in activity relative to the fresh preparations. This was interpreted as evidence for stabilization due to enzyme-support

interactions. Preparations with higher surface coverages, however, exhibited a reduction in activity of approximately 25% with respect to the fresh preparations.

The central hypothesis of this project was that the surface loading regimes of the lyophilized nanobiocatalysts were essentially formed during the adsorption step of our protocol. It was also postulated that the extent of the conformational change observed with the low surface coverage regime is mainly defined by the intrinsic conformational stability or packing density of the enzyme molecules. The conformational state of enzymes adsorbing on fumed silica as a function of the surface coverage was inferred from intrinsic fluorescence and CD spectroscopy data.

The kinetics of tertiary conformational changes for enzymes adsorbing on fumed silica was probed with Trp fluorescence spectroscopy. The kinetic studies confirmed a marked tendency for CALB molecules to undergo dramatic unfolding/refolding events while adsorbing on fumed silica under the conditions of regime 1. This was attributed to both CALB's loosely packed structure or "softness" and conformational molecular dynamism. As the surface coverage increased, the unfolding events proceeded more gradually. In the more packed environment a higher energy barrier of adsorption could ultimately preclude conformational fluctuations. The kinetic studies of unfolding for the "hard" *s. Carlsberg* and Lipase from *Thermomyces lanuginosus* (TLL), however, showed more gradual unfolding pathways. These two enzymes are considered "hard" due to their tightly packed and rigid native state ensembles. The final conformational stability of the nanobioadsorbates was visualized through 3D contour filled conformational diagrams. Each diagram contains the steady-state unfolding data as a function of the initial protein concentration and nominal surface coverage. The diagrams revealed three distinct regions of conformational stability as a function of the surface coverage. A region of low conformational stability at low surface coverages was detected where enzyme ensembles with unfolded regions most likely dominate. At an intermediate surface coverage of approximately 2 monolayers, the conformational stability analysis showed a significant increase in the fraction of folded enzyme ensembles. As the surface coverage was increased even further, a large population of folded ensembles conferred very high conformational stability to the adsorbates. The presence of these three regions of conformational stability correlated well with the postulated surface loading regimes for the lyophilized adsorbates.

CD spectroscopy was used to corroborate the presence of these regions of conformational stability from the secondary structural viewpoint. In this case, the impact of the nanoparticles on the intramolecular stability of the hydrogen bonding network maintaining the secondary structural topologies was addressed. The CD signal at 222 nm was correlated to the α -helical content during adsorption on the nanoparticles. Secondary conformational changes were, therefore, inferred from the decrease signal at this wavelength. The unfolding data were plotted in 3D contour filled conformational diagrams as described above for the tertiary unfolding data. The diagrams of secondary and tertiary conformational stability were remarkably similar confirming, therefore, the presence of the three regions of stability as a function of the surface coverage even at the shorter scales associated with the secondary structure. This also suggested that the structural perturbations introduced by adsorption on abundant fumed silica are strong enough to disrupt or even strip off very well organized water molecules holding together complex secondary topologies such as the α -helix.

In an attempt to gain an insight into the type and role of protein-protein interactions in each of the identified regions of conformational stability, structure modifiers were added to the aqueous buffer prior to adsorption. The impact of promoting structural changes in hydrophobic regions and reducing disulfide bonds was assessed with TFE and DTT, respectively. For the hydrolases considered here, the remarkable conformational stability at high surface coverages was reduced by nearly 50% when TFE was added. This suggested that buried hydrophobic regions were responsible for maintaining a high structural integrity in this region. At low surface coverages, however, the maximum extent of unfolding for both CALB and *s. Carlsberg* was reduced. In the case of CALB, this was attributed to the suppression of the molecular dynamism inherently associated to this enzyme. It appears that upon disruption, the flexible unfolded state promoted a gradual attachment of the exposed groups to the abundant surface available leading thereby to the decrease of conformation space and ultimately the ability to unfold/refold to a larger extent. In the case of *s. Carlsberg*, a rapid initial unfolding is followed by attachment to the surface through a low energy barrier pathway. Due to the rigidity of the unfolded state of this enzyme, further unfolding events were largely repressed. The addition of DTT to CALB's adsorbing mixtures showed no significant changes in the unfolding levels at high surface coverages or low enzyme concentrations. This suggested that the disruption of CALB's disulfide bonds were compensated by the enzyme-enzyme interactions dominating in this region. At low

surface coverages, however, unfolding was again largely reduced. Due to the reduced interactions with neighboring molecules, CALB molecules exposed some segments upon disulfide bond disruption. In line with the aforementioned postulated loss of dynamism, these exposed regions are thought to be responsible for promoting a gradual unfolding through an adsorption pathway with an increasingly higher energy barrier.

The conformational state of the lyophilized CALB/fumed silica adsorbates was probed with FTIR spectroscopy. The amide I-FTIR spectra of preparations with different levels of surface coverage were collected and band-narrowed to determine the position of the contributing secondary structural components. As the surface coverage increased, the FTIR signal was higher and approached that of the native enzyme. At low surface coverages, band-narrowing of the spectra with the second derivative revealed a substantial loss in the α -helical content and a concomitant increase of disordered components relative to the native enzyme. The presence of a region of substantial conformational change when operating at low surface coverages and high initial enzyme was evaluated for the lyophilized adsorbates with amide I-FTIR analysis. These preparations certainly have significant contributions of β -aggregates and turns. This has been explained by the formation of aggregates that apparently initiate the disruption of the very well organized secondary structural components of individual molecules. A complete understanding of the unfolding-aggregation events for enzymes adsorbing in crowded environments is particularly important for pharmaceutical companies. During the manufacture and storage of protein biopharmaceuticals, proteins come in contact with a variety of surfaces and interfaces. The effect of these protein-surface interactions on the protein solutions is not well understood especially at high protein solution concentrations. Pharmaceutical companies are urgently looking for tools to examine the dynamics of protein adsorption and the effect of surfaces/interfaces on the structure, conformation, and physical stability of the protein molecules.

7.2 Recommendations

7.2.1 Strategies to Increase Conformational Stability

One of the major findings of this research project was the tendency of “soft” enzymes for conformational change in the presence of abundant surface area, which in turn leads to decreased catalytic competency. A simple strategy to minimize structural fluctuations and therefore to maximize the catalytic productivity could be to add small rigid molecules prior to adsorption on the fumed silica. Through protein-protein interactions, these molecules could act as barriers for the detrimental surface-protein interactions at low surface coverages. Rigid small molecules that could be used for this purpose include the protein lysozyme and polymers of low molecular weight like polyethylene glycol (PEG). Recent studies have reported that lysozyme has the ability to maintain a relatively stable structure when adsorbed on colloidal silica nanoparticles^{1,2}. PEG coils has been successfully incorporated as supporting cushions in surface supported lipid bilayer platforms for studying lateral association of membrane proteins³.

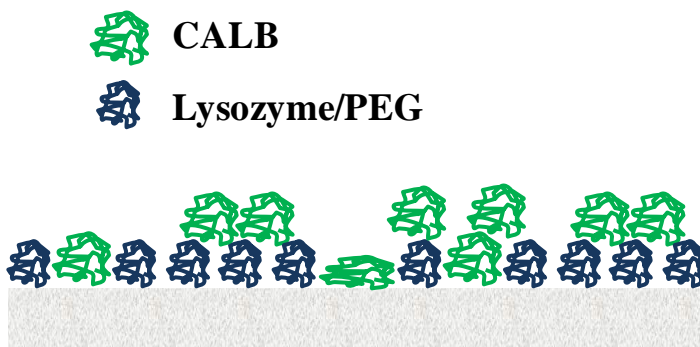


Figure 7.1. Adding small molecules prior to adsorption could help to increase the stabilizing protein-protein interactions for “soft” enzymes at low surface coverages.

Figure 7.1 shows a schematic of the role of small molecules in preventing conformational changes when “soft” enzymes adsorb on solid surfaces. One can also consider a crosslinking agent to increase the packing density and consequently the conformational stability of “soft” enzymes. This strategy should be followed with special care as some functional groups at the enzyme surface could be absent or occluded for further interaction with the fumed silica. Additionally, it is very likely that the energetics of the resulting ensemble could lead to a substantially different arrangement of the enzyme molecules on the surface, and consequently to completely new regions of conformational stability. This suggests that instead of adding modifiers that would likely change the surface chemistry of the enzyme molecules, one should

look for alternative means to locally modify regions of low stability. One potential avenue is to mechanically induce changes in the structure with AFM, optical tweezers, or glass needles. In these techniques single molecules are mechanically stretched and their elastic response is recorded in real time. The use of these techniques is, however, disadvantageous due to the need of an external method to correlate with structural data and its low throughput: only to one molecule at a time. An alternative approach is the production of recombinant enzymes where poorly packed or mobile residues (that generally confer low stability) are replaced, removed or locked (with the aid of disulfide bonds). The major challenge is to identify the regions of interest. This identification needs to be performed with the aid of both computational and experimental tools as discussed below.

7.2.1.1 Computational Tools to Identify Regions of Low Conformational Stability in Proteins

An interesting computational approach to calculate regional stability variations within protein structures was developed by Hilser et al.⁴⁻⁹. They proposed an algorithm that considers the enzyme molecules as dynamic or fluctuating entities with high conformational heterogeneity. The COREX algorithm models the native state as an ensemble of conformational states to determine the response to energetic perturbations. The method starts by creating an exhaustive enumeration of the possible conformational states. The structure is partitioned into sub-units (generally of 10 residues) of local folding or unfolding. All possible combinations form a statistical thermodynamic ensemble of the energy landscape. For each microstate, the statistical weight K_i can be, therefore, defined as:

$$K_i = e^{-\frac{\Delta G_i}{RT}} \quad \text{Equation 7.1}$$

where ΔG_i is the free Gibbs energy of the state, R is the gas constant, and T is the temperature.

It is possible to calculate the Boltzmann-weighted probability P_i of each state as the ratio of the statistical weight of that state over all N states in the ensemble:

$$P_i = \frac{K_i}{\sum_{i=1}^N K_i} = \frac{K_i}{Q} \quad \text{Equation 7.2}$$

where K_i is calculated according to Equation 7.1 and Q is the sum of all statistical weights, also known as the partition function for the system.

This approach allows determining any number of statistical thermodynamic descriptors of the equilibrium. Of particular importance for this project, however, is the residue stability constant $\kappa_{f,j}$:

$$\kappa_{f,j} = \frac{\sum P_{f,j}}{\sum P_{nf,j}} \quad \text{Equation 7.3}$$

where $\sum P_{f,j}$ are the summed probabilities of the states in the ensemble in which a residue is in a folded conformation, and $\sum P_{nf,j}$ are the summed probabilities of the states in the ensemble in which a residue is in an unfolded conformation.

Based on Equation 7.3, residues with high stability constants are likely to be folded in most of the probable states while residues with low stability constants are likely to be unfolded in most of the probable states.

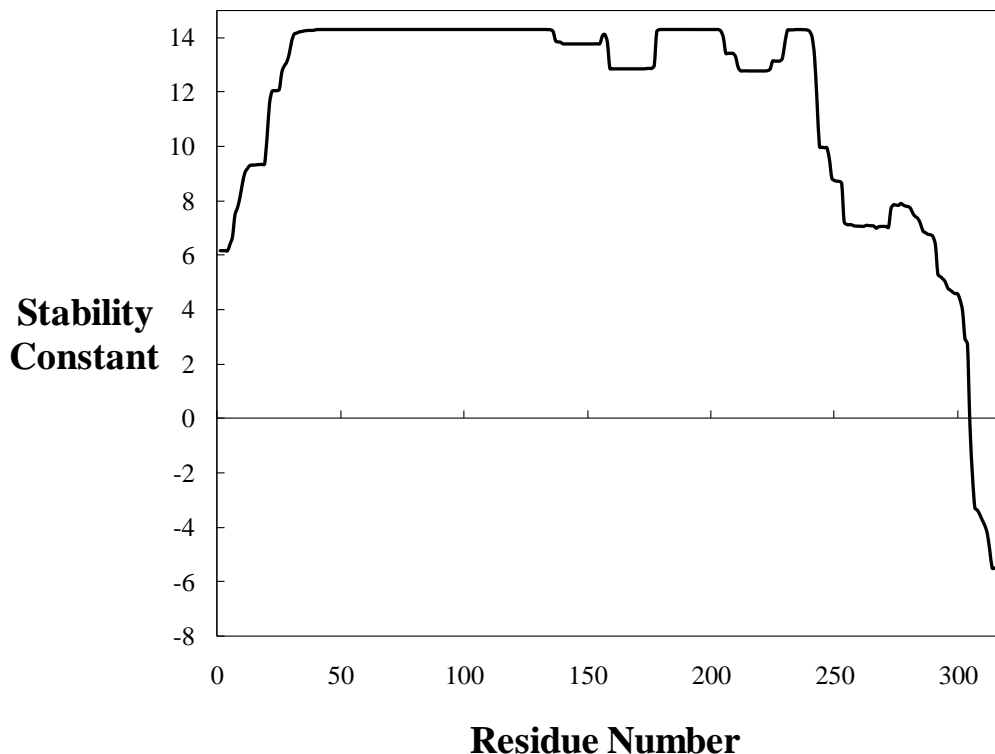


Figure 7.2. Stability constants for CALB residues as calculated from the statistical thermodynamic analysis of conformational ensembles implemented in the COREX algorithm. Residues 295 to 317 exhibit low stability and are good candidates for protein engineering.

This approach has been successfully validated with experimental data. Moreover, it has been proven useful to understanding a number of biological processes including signal transduction^{10, 11}, protein homeostasis¹², and substrate ligand recognition^{7, 11}.

The COREX algorithm can be accessed online (<http://www.best.utmb.edu/BEST/>). Using this tool, the most probable ensembles and residue stability constants for CALB, *s. Carlsberg*, TLL were calculated.

Table 7.2. List of residues with the lowest conformational stability constants for CALB ensembles.

Residue Name	Residue Number
PRO	295
ASP	296
LEU	297
MET	298
PRO	299
TYR	300
ALA	301
ARG	302
PRO	303
PHE	304
ALA	305
VAL	306
GLY	307
LYS	308
ARG	309
THR	310
CYS	311
SER	312
GLY	313
ILE	314
VAL	315
THR	316
PRO	317

After uploading CALB's structure to the COREX server, the most probable conformational states were determined in approximately 6 hours. The sequences of 15 most probable ensembles are shown in Table 7.1. The stability constants for each residue were subsequently calculated as discussed above. The analysis showed that residues 295 to 317 have low stability. The names of these residues are listed in Table 7.2 for reference. A graphical view of the residue stability is provided in Figure 7.3. Our experimental findings for CALB agree well with the COREX analysis and even serve as external confirmation for CALB's molecular dynamism. Similar calculations were performed for *s. Carlsberg* and TLL to check whether the COREX algorithm also supports the experimental data reported here for these two enzymes.

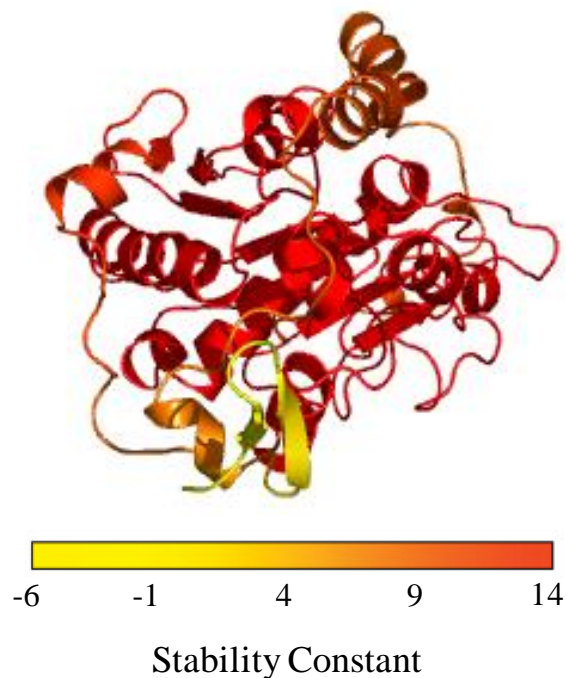


Figure 7.3. Single-molecule schematic of the different regions of stability in CALB's structure. Residues in red exhibit the highest stability while those in yellow the lowest. In agreement with our experimental findings, CALB has regions of low stability that provide mobility and dynamism.

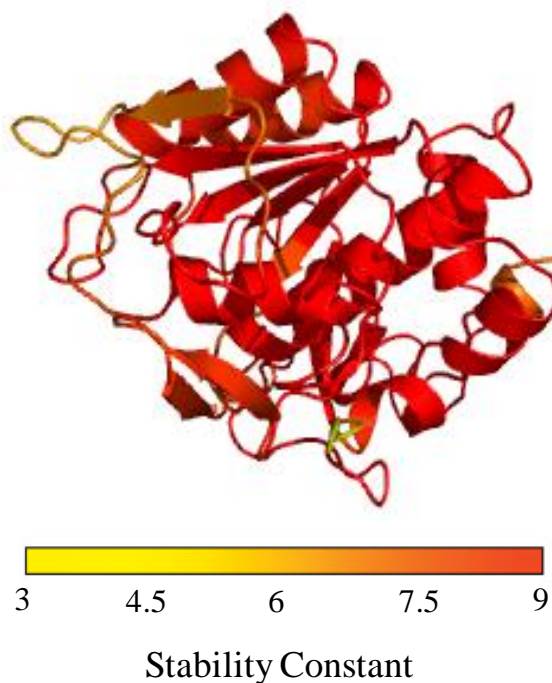


Figure 7.4. Single-molecule schematic of the different regions of stability in *s. Carlsberg*'s structure. Residues in red exhibit the highest stability while those in yellow the lowest. In agreement with our experimental findings, *s. Carlsberg* as opposed to CALB exhibit a relatively stable structure.

Figure 7.4 shows the single molecule representation from COREX residue stability analysis of *s. Carlsberg*. The lowest value for the stability constant was approximately 3.5 while the highest was of about 8. This further supports the notion of a static structure with high resilience to propagate structural perturbations. The numerical values of stability for each residue are shown in Figure 7.5.

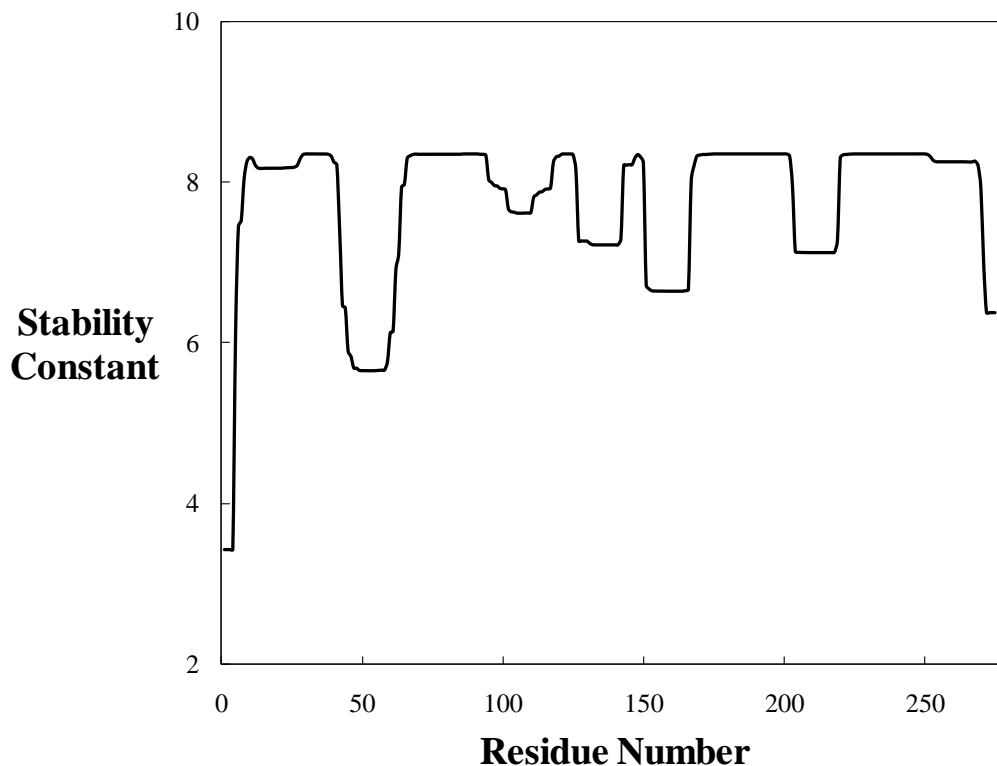


Figure 7.5. Stability constants for *s. Carlsberg* residues as calculated from the statistical thermodynamic analysis of conformational ensembles implemented in the COREX algorithm.

Figure 7.6 shows the single molecule representation from COREX residue stability analysis of TLL. In this case, the lowest value for the stability constant was approximately -0.1 while the highest was of about 10. This demonstrates that TLL can also tolerate structural fluctuations to a larger extent than CALB. The numerical values of stability for each residue are shown in Figure 7.7.

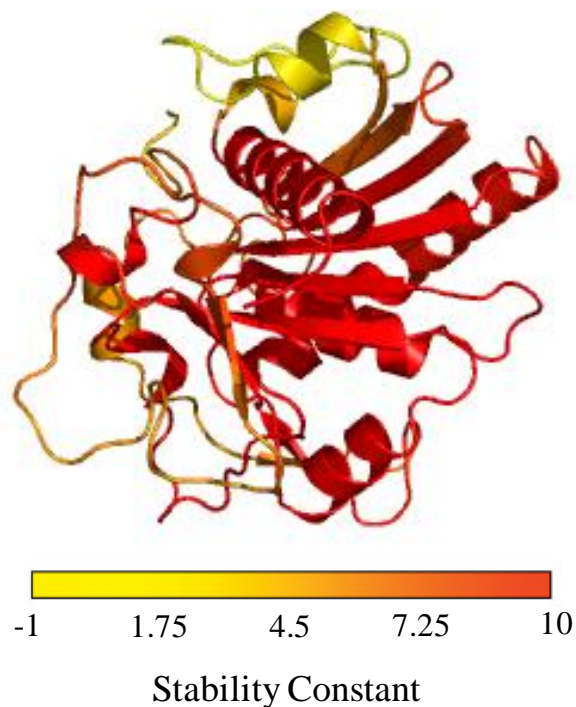


Figure 7.6. Single-molecule schematic of the different regions of stability in TLL's structure. Residues in red exhibit the highest stability while those in yellow the lowest. In agreement with our experimental findings, TLL shows resilience to conformational fluctuations.

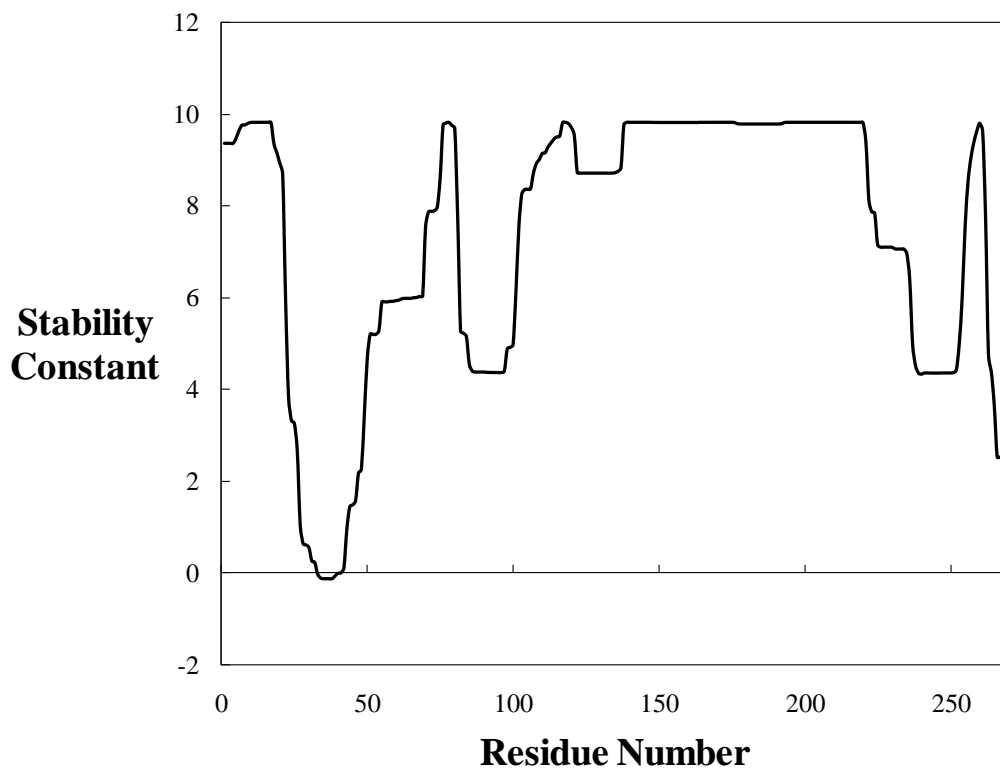


Figure 7.7. Stability constants for TLL residues as calculated from the statistical thermodynamic analysis of conformational ensembles with the COREX algorithm.

Another parameter that appears to be related to the tendency of enzymes to unfold is the packing density. A reasonable estimate of this parameter can be obtained by calculating the fraction of the volume occupied by internal cavities in the protein structure¹³. These cavities are thought to be involved in the unfolding mechanisms of proteins. Cavities were calculated in the Swiss PDB viewer v4.0.1 for CALB, *s. Carlsberg*, and TLL. The results are summarized in Table 7.3, Table 7.4, and Table 7.5; respectively.

Table 7.3. Surface exposed and volume of internal cavities for CALB. The calculation was performed with Swiss PDB viewer.

Region (Color)	Area (Å ²)	Volume (Å ³)
Exposed surface (yellow)	10175	39287
Cavity 1 (Blue)	53	28
Cavity 2 (Red)	41	19
Cavity 3 (Green)	35	14

Table 7.4. Surface exposed and volume of internal cavities for *s. Carlsberg*. The calculation was performed with Swiss PDB viewer.

Region Color	Area (Å ²)	Volume (Å ³)
Exposed surface (yellow)	8208	32001
Cavity 1 (Blue)	39	17
Cavity 2 (Green)	36	17

Table 7.5. Surface exposed and volume of internal cavities for TLL. The calculation was performed with Swiss PDB viewer.

Region Color	Area (Å ²)	Volume (Å ³)
Exposed surface (yellow)	9535	35045
Cavity 1 (Blue)	158	139
Cavity 2 (Red)	154	114
Cavity 3 (Green)	60	28

The location of the cavities in the structure is shown in Figure 7.8, Figure 7.9, and Figure 7.10 for CALB, *s. Carlsberg*, and TLL; respectively.

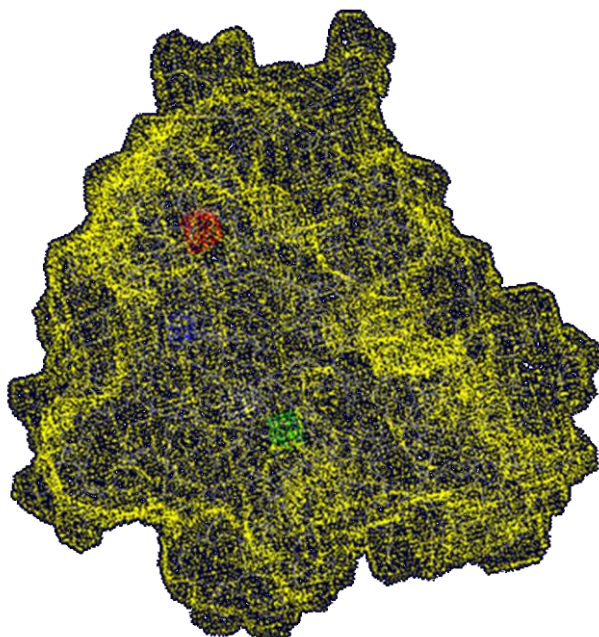


Figure 7.8. Location of CALB's cavities (blue, red, and blue regions) as calculated from Swiss PBD viewer. Internal cavities account for approximately 0.2% of the total volume.

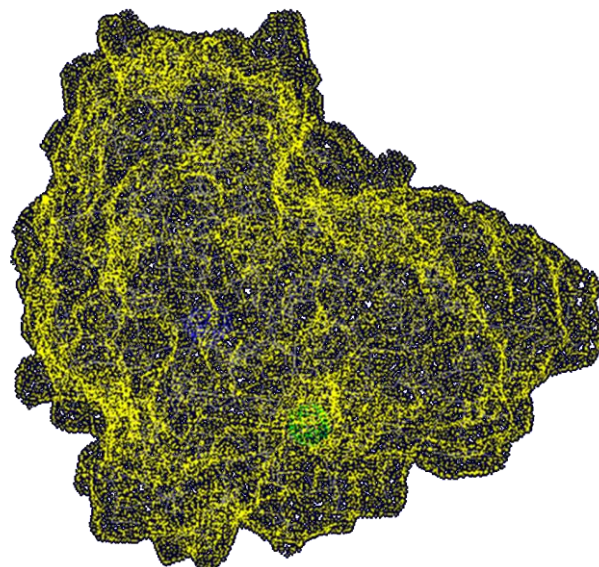


Figure 7.9. Location of *s. Carlsberg*'s cavities (blue and green regions) as calculated from Swiss PBD viewer. Internal cavities account for approximately 0.1% of the total volume.

It appears that there is a connection between the void volumes at the interior of proteins with the tendency to propagate structural perturbations as indicated by the higher volume of

cavities for “soft” CALB when compared with “hard” *s. Carlsberg*. Surprisingly, TLL, a “hard” enzyme, appears to have a higher cavity volume than that of CALB.

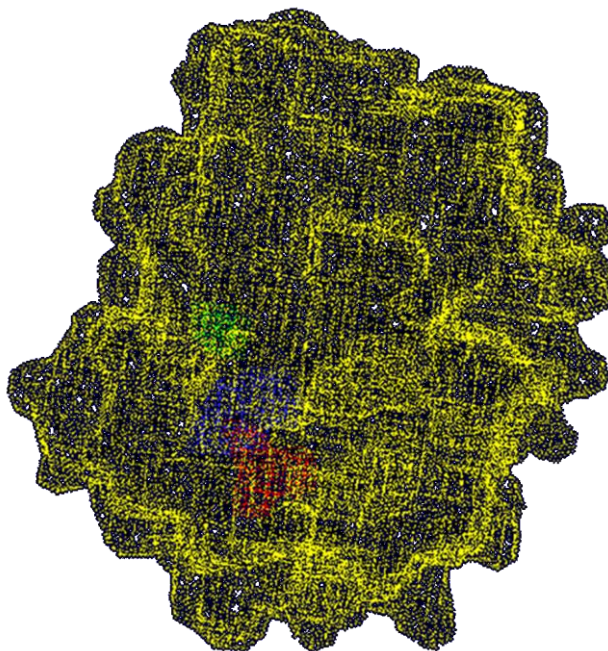


Figure 7.10. Location of TLL’s cavities (blue, green, and red regions) as calculated from Swiss PBD viewer. Internal cavities account for approximately 0.8% of the total volume.

With the locations of the cavities, selected mutations would probably help to estimate if by reducing the void volume, the tendency of “soft” enzymes to propagate structural perturbations can be suppressed. This initiative can be supported with CALB’s packing density per residue provided in Table 7.6. Packing density calculations were performed with Voronoia¹⁴. A further correlation with the stability data provided above would help to determine which residues are suitable for protein engineering. Those residues with both low stability and low packing density will be the best candidates.

Table 7.6. Packing density per residue for native CALB. Data calculated with Voronoia¹⁴.

Residue number	Residue type	Van derWaals volume [Å³]	Solvent excluded volume [Å³]	Total volume [Å³]	Packing density
295	PRO	37.80	21.16	58.96	0.71
296	ASP	19.83	4.68	24.51	0.80
297	LEU	66.86	43.84	110.70	0.64
298	MET	24.47	9.63	34.10	0.73
299	PRO	5.67	1.07	6.74	0.84
300	TYR	41.89	28.98	70.87	0.68
301	ALA	60.02	32.64	92.66	0.70
302	ARG	37.66	14.41	52.07	0.74
303	PRO	12.22	2.84	15.06	0.82
304	PHE	53.85	23.17	77.02	0.73
305	ALA	46.28	24.25	70.53	0.68
306	VAL	19.49	3.76	23.25	0.85
308	LYS	24.38	10.19	34.57	0.71
309	ARG	19.81	5.13	24.94	0.79
310	THR	44.17	23.39	67.56	0.72
311	CYS	9.56	3.41	12.97	0.74
312	SER	9.48	3.63	13.11	0.72
314	ILE	13.01	2.04	15.05	0.86
315	VAL	26.82	7.05	33.87	0.80
316	THR	19.63	5.81	25.44	0.77
317	PRO	19.50	8.49	27.99	0.72

7.2.1.2 Experimental Techniques to Identify Regions of Low Conformational Stability in Proteins

Complementary to the computational methods presented previously, both calorimetric and force spectroscopy techniques could help to confirm if the introduced structural modifications are effectively increasing the overall conformational stability.

7.2.1.2.1 Calorimetric Techniques

An interesting avenue to determine the impact of structural changes in protein stability through fundamental thermodynamic parameters was developed by Makhatadze et al.^{13, 15}. In this approach, changes in specific volume upon protein unfolding can be directly calculated from thermodynamic data. The method relies on pressure perturbation calorimetry (PPC) and differential scanning calorimetry (DSC) to estimate the linear thermal expansion coefficient and the partial molar heat capacity, respectively. The data is fitted simultaneously to a set of equations that allow accessing the change of volume upon protein unfolding. If the introduced structural changes promote a higher packing density, the change of volume upon unfolding is likely to decrease. This change can be monitored very accurately with this approach.

7.2.1.2.2 Force Spectroscopy

Once the enzyme is genetically engineered, the stability of the modified regions can be also assessed by promoting unfolding with force. This can be accomplished by pulling the enzyme with a single-molecule force-clamp spectroscopy system. Fernandez et al.^{15, 16} have applied this technique to investigate the chemical kinetics of disulfide bond cleavage. In force-clamp spectroscopy, an AFM system is connected to a feedback system that maintains a constant force while the extension of the molecule being stretched is recorded as a function of time. The major advantages of these systems are their high resolution and low signal to noise ratios. A simple comparison of the unfolding fingerprints of the native and engineered proteins would allow for an unambiguous quantitative analysis of subtle changes in the overall conformational stability.

7.2.2 Strategies to Control Interfacial Dynamics of Enzymes Adsorbing on Hydrophilic Surfaces

The view of enzymes as dynamic entities with a significant conformational heterogeneity was superficially explored in this dissertation. This aspect, however, is thought to be of considerable importance when assembling proteins on surfaces. Both inter- and intra- molecular mechanisms of adsorption, surface translational diffusion, and molecular orientational states of the enzyme molecules are most likely controlled by this heterogeneity. Hitherto, our knowledge of these phenomena and their correlation with the functionality of the obtained nanobiomaterials remains poorly explored.

The major challenge is to assess the structural dynamics and function simultaneously. Most biophysical tools allow for static structural details of proteins but they often do not explain what the molecule does and how it does it. Additional challenges are posed by the fact that sometimes the assembly process proceeds under crowding conditions which gives rise to important technical difficulties. Several experimental tools to address this issue are discussed below.

7.2.2.1 Adsorption Studies and Surface Chemistry Modification

The first step to understand the dynamics of interaction of enzymes with the surface is to calculate adsorption isotherms. The type of interactions, the level of orientational and conformational change, and the binding strength can be inferred from the isotherms. The experimental data could be fitted to one of the main models available in the literature to describe such processes. Two type of models have been associated to protein adsorption on surfaces¹⁷: (i) those based on statistical and geometrical aspects, e.g., the random sequential adsorption model (RSA), and (ii) those based on diffusional considerations, e.g., the ballistic deposition model (BD). A recent experimental study of the adsorption of CALB on TiO₂ suggested that this protein follows the RSA model¹⁷. CALB molecules first occupy the empty space on the surface and then continue to aggregate, everything in a random manner. This was evidenced by the shape of the isotherms, a very steep increase of rapid deposition followed by a relaxation stage where aggregation occurs. The validity of this model for other hydrophilic surfaces is yet to be proved.

Additionally, the impact of changing the surface coverage on the dynamics of adsorption is not clear.

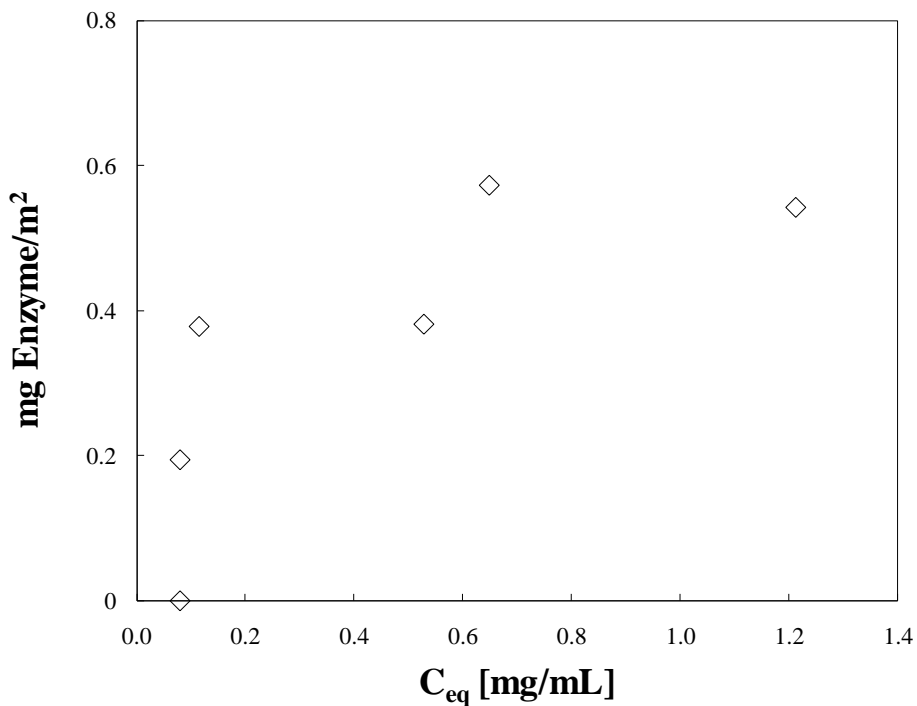


Figure 7.11. Adsorption isotherm for CALB on fumed silica at a surface coverage of 17%. C_{eq} is the equilibrium concentration of enzyme.

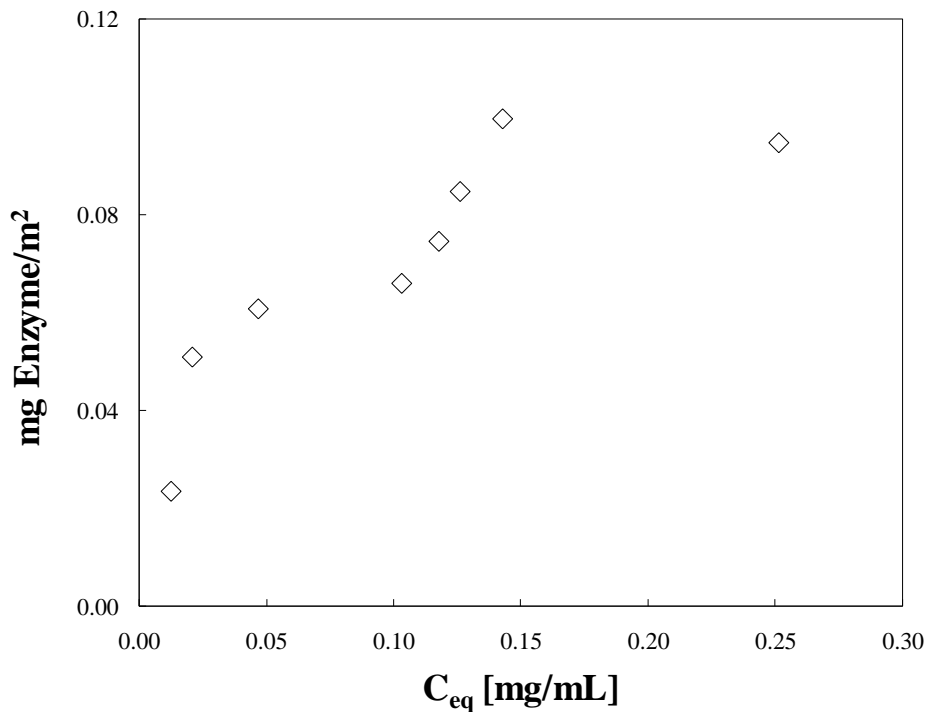


Figure 7.12. Adsorption isotherm for TLL on fumed silica at a surface coverage of 2%. C_{eq} is the equilibrium concentration of enzyme.

Preliminary isotherms for CALB and TLL adsorbed on fumed silica were calculated in our laboratory and are shown here for reference in Figure 7.11 and Figure 7.12, respectively. It appears that these two enzymes followed the RSA model as evidenced by the presence of two regimes of adsorption: an initial saturation step of high affinity followed a stage of lower affinity where bigger aggregates continue to adsorb. CALB seems to have a higher affinity towards the surface in the early stages of adsorption. The adsorbed amounts could be corroborated with TGA.

The presence of an intermediate step in the adsorption isotherm where a second regime is likely to be present brings out the possibility of orientational changes. We have suggested that these events are most likely a direct consequence of an energy minimization when the ensemble of enzymes needs to accommodate on the surface. Recent studies have spent considerable effort in defining strategies to promote the assembly of proteins with a desired orientation/organization on the surface¹⁸⁻²⁵. This has resulted in a new set of surface activation/functionalization techniques that allow for surfaces with highly controlled protein patterns and nanoscale resolution¹⁸. Some of the most successful avenues for chemically tailoring surfaces to preferentially adsorb one or several protein orientations include silanization, dendrimer-functionalization, and SAMs¹⁸. This is conventionally followed by coupling of a surface spacer between the protein and the reactive group on the surface. A myriad of spacers are commercially available with different chemical functionalities, lengths, rigidities, and hydrophobicities (Table 7.7).

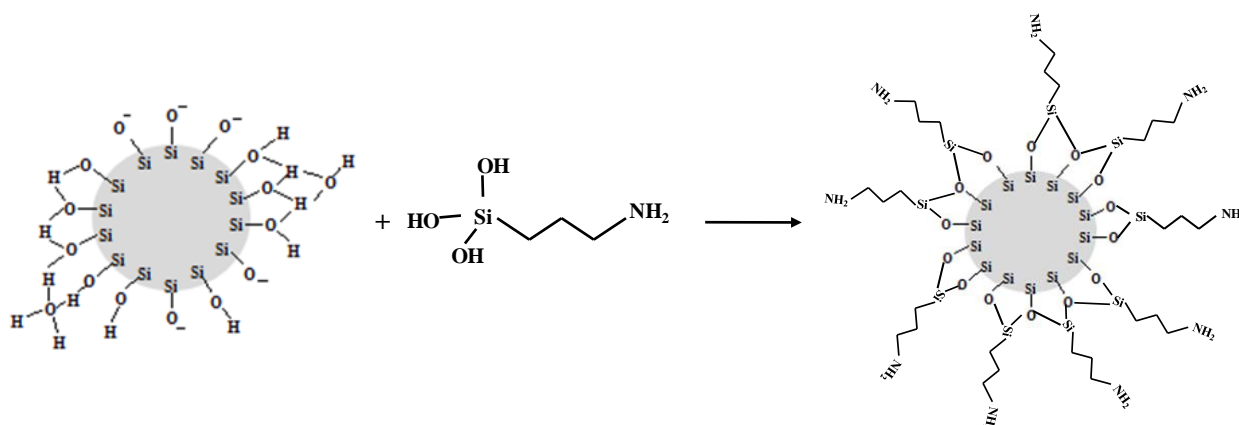


Figure 7.13. Silanization of fumed silica with aminopropyltriethoxysilane (APTES)¹⁸. The functionalized fumed silica can be subsequently coupled with one of the spacers in Table 7.7. This could help to control the number of reactive groups on the surface and ultimately the surface coverage, orientation, and conformation of the adsorbed enzymes.

The silanol chemistry of fumed silica offers a number of opportunities for chemical modification. Two strategies that can be tested are silanization with aminopropyltriethoxysilane (Figure 7.13) and dendrimer formation with poly-(propylene imine) (Figure 7.14).

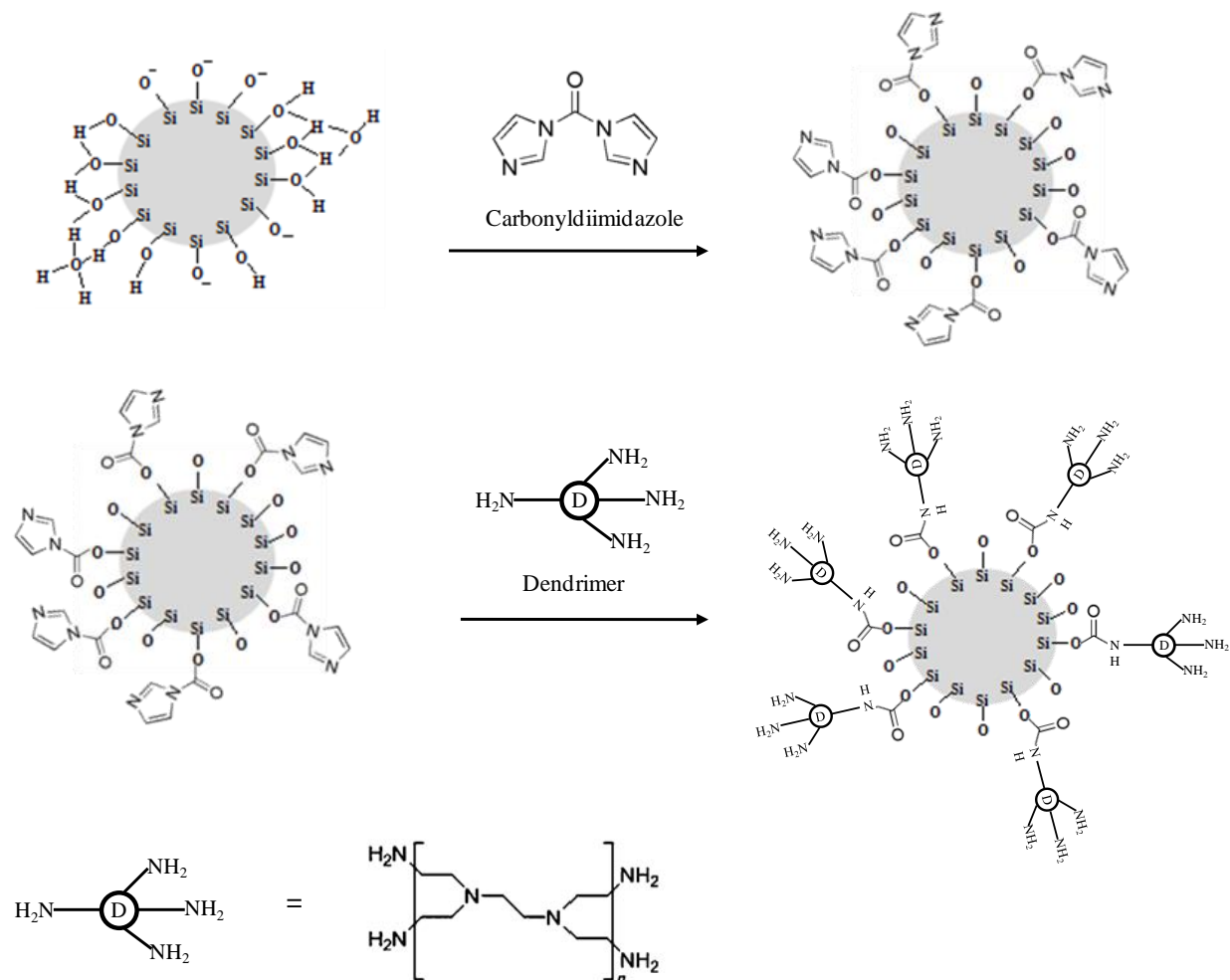
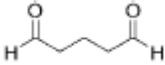
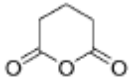

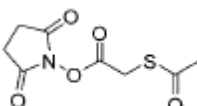

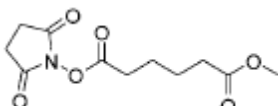
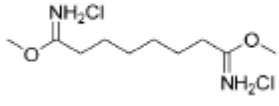
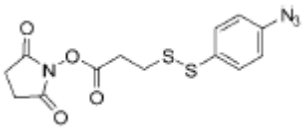
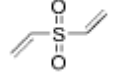
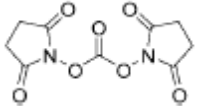
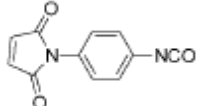
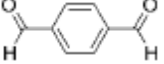
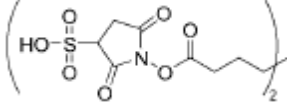
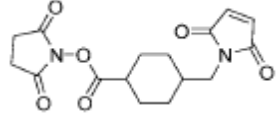
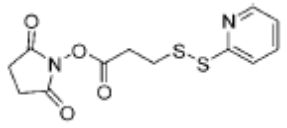
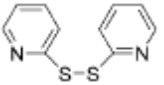
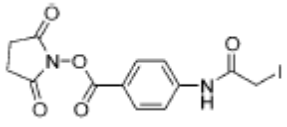
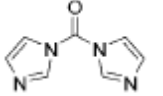


Figure 7.14. Dendrimer-functionalization of fumed silica with poly-(propylene imine) dendrimers¹⁸. This approach is aimed at promoting an oriented assembly of enzymes on fumed silica. Orientational changes are thought to be present during the random adsorption events that normally occur on virgin fumed silica.

One of the major challenges is to prevent self-condensation of the nanoparticles and consequently their clustering. The selection of the proper surface chemistry would require a trial and error process due to the large number of possible combinations.

Table 7.7. Commercially available spacer molecules¹⁸. Potentially any desired functional group can be incorporated for further interaction with the enzyme molecules.

Spacers			
Homobifunctional Amine-reactive		Heterobifunctional Amine-reactive	
Glutaraldehyde		Glutaric anhydride	
1,4-butanediol diglycidyl ether		SATA (protected thiol)	
1,4-phenylene diisothiocyanate		MSA (protected acid)	
Dimethylsuberimidate		SADP (photoreactive)	
Divinylsulfone		Amine- and hydroxy-reactive	
Disuccinimidyl carbonate		PMPI	
Terephthalaldehyde		Amine- and thiol-reactive	
Bis(sulfosuccinimidyl) suberate		SMCC	
Thiol Reactive		SDPD	
2,2'-dipyridyl disulfide		SIAB	
<i>N,N'</i> -carbonyldiimidazole			

7.2.2.2 Real-time Monitoring of Translational and Rotational Dynamics

A flat hydrophilic surface appears to be a good approximation of fumed silica's surface chemistry.

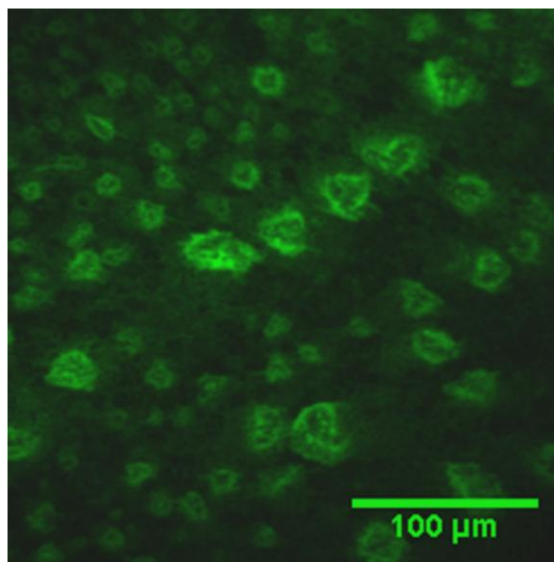


Figure 7.15. Confocal image of CALB adsorbed on a silica wafer with a SiO₂ layer of 100 nm. The nominal surface coverage was 150%.

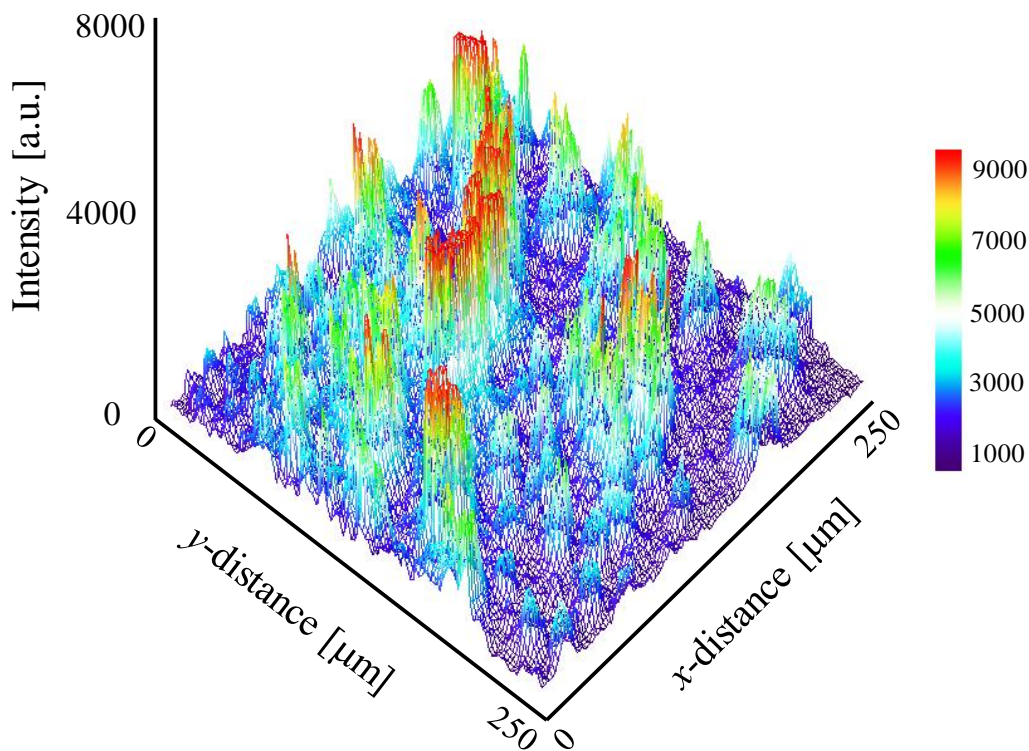


Figure 7.16. 3D intensity profile of image shown in Figure 7.15. Substantial enzyme aggregation was observed. This could support the idea that the structure is well maintained in this surface coverage regime due to the multi-layer packing.

To determine the impact of surface coverage on enzyme distribution upon adsorption, silica wafers were used as model surfaces. The enzyme molecules were first labeled with the fluorochrome Alexa Fluor 488 and then adsorbed on the silica wafers at different surface coverages. A confocal image of labeled CALB adsorbed on a silica wafer with an oxide layer of 100 nm is shown in Figure 7.15. In this case, the expected surface coverage was 100%. The corresponding 3D intensity profile is shown in Figure 7.16.

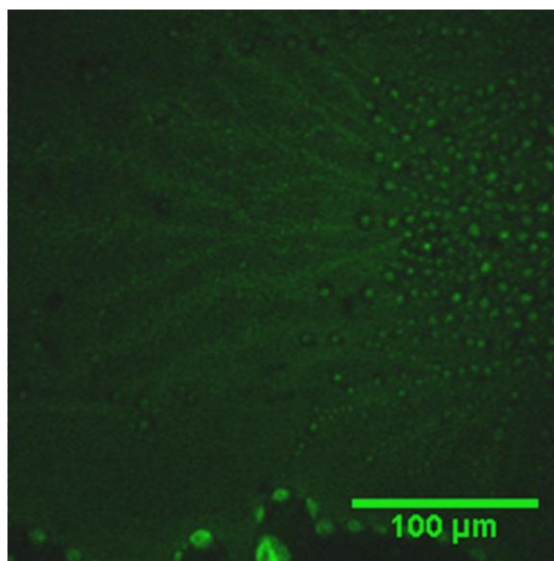


Figure 7.17. Confocal image of CALB adsorbed on a silica wafer with a SiO₂ layer of 100 nm. The nominal surface coverage was 50%.

As the expected surface coverage was decreased to 50%, the enzyme molecules distributed more evenly on the wafer (Figure 7.17). This is a direct consequence of the increased surface availability in this surface loading regime. The 3D intensity profile for this situation is shown in Figure 7.18.

The enzyme distribution as a function of the surface coverage on model silica surfaces appears, therefore, to be in good agreement with that identified on fumed silica and shown in Chapter 3. This is encouraging to continue to incorporate them in prospective experiments as those described below.

Due to the similarity to the fumed silica chemistry, the model silica surfaces could be also modified according to the chemical schemes described in Figure 7.13 and Figure 7.14. The use of spacers (Table 7.7) can be further considered for fine tuning of the surface chemical properties. One of the challenges of using flat surfaces to model nanoparticles is to mimic the

curvature. A similar 3D architecture on the surface can be attempted through nanolithography techniques.

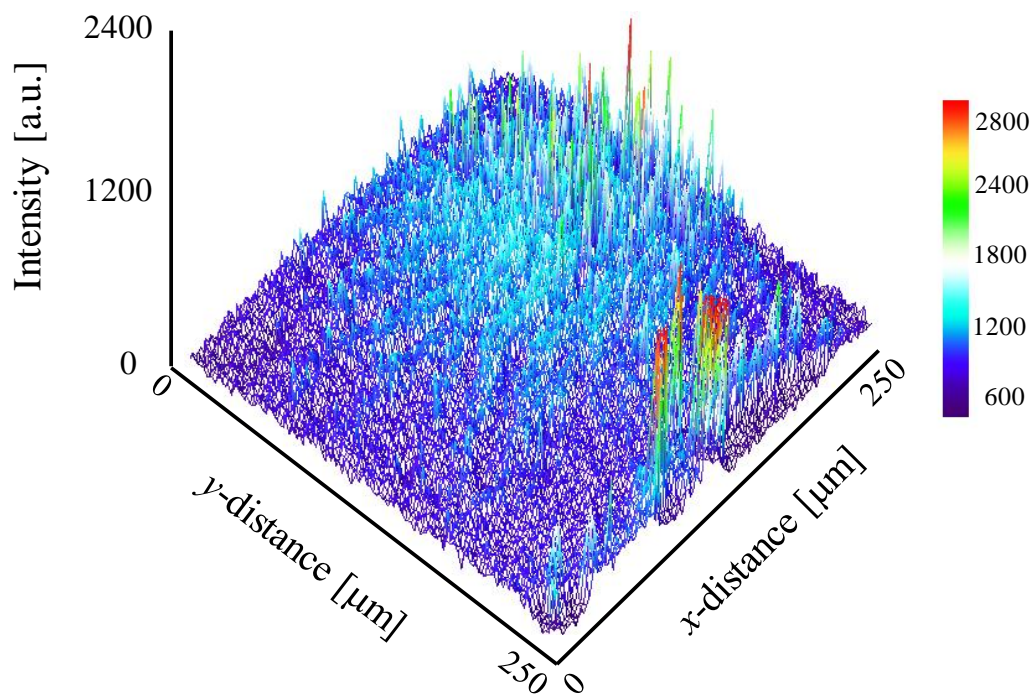


Figure 7.18. 3D intensity profile of image shown in Figure 7.17. The enzyme molecules distributed more homogenously on the wafer. This could support the notion of increased surface-protein interactions that most likely lead to conformational changes.

Recent advances in nanolithography allow for manipulation and organization of the surface chemistry with nanoscale precision^{26, 27}.

Adsorption kinetics could be a good starting point to characterize the interaction of enzyme molecules with the modified silica surfaces. This analysis can be potentially done with the aid of a Surface Plasmon Resonance read-out or a Quartz Crystal Microbalance system. Preliminary experiments were conducted with labeled enzymes in a confocal microscope (data not shown). The next step could be to implement high-resolution imaging techniques such as Total Internal Reflection Fluorescence (TIRF)^{28, 29}, dual objective multifocal plane microscopy³⁰ or noninvasive Supercritical Angle Fluorescence microscopy (SAF)³¹. Commercially available flow cells can be mounted in the imaging stage for adding the buffered enzymes under carefully controlled flow conditions. These techniques allow for a real-time measurement of the enzyme distribution. A schematic description of these experiments is shown in Figure 7.19. Conformational changes of the adsorbed enzymes can be assessed with AFM^{29, 32} and surface

spectroscopic techniques such as linear dichroism^{33, 34} and reflectance absorption infrared spectroscopy³⁵. The kinetic data can be further analyzed at the single molecule level to recover information about the translational and rotational dynamics of the enzyme molecules. The preferred method to analyze the distribution of the heterogeneous states that form the ensemble of molecular behaviors is fluorescence correlation spectroscopy^{36, 37}. This approach has been successfully applied to determine individual diffusion coefficients for various molecules interacting with surfaces^{36, 38, 39}.

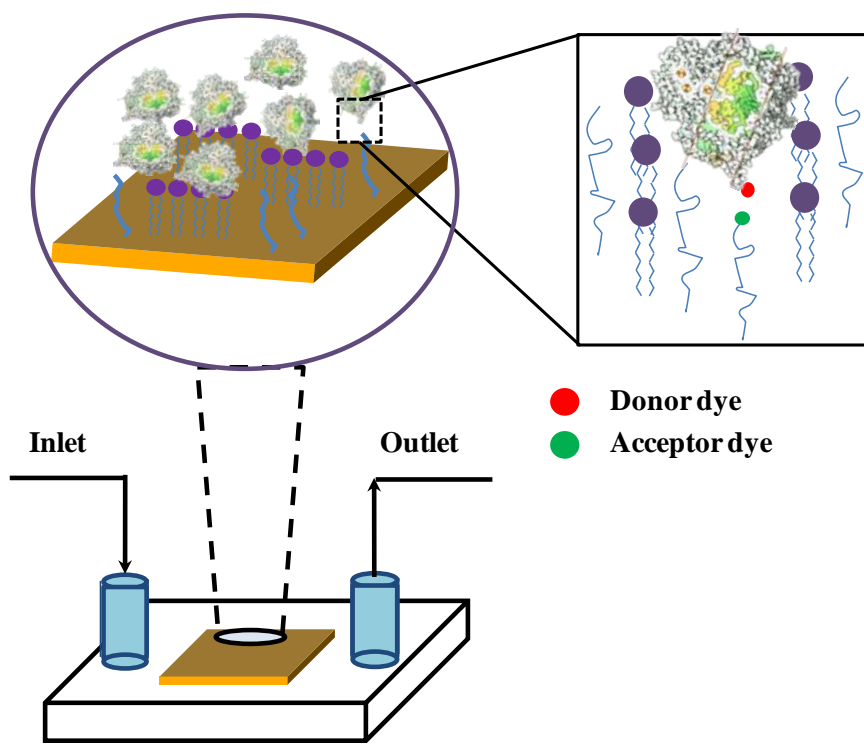


Figure 7.19. The dynamics of surface-protein interaction can be studied at the single-molecule level with the aid of state-of-the-art fluorescence imaging techniques. The complexity of this interaction is mainly due to the multidimensional landscape generated by the heterogeneity of the enzyme molecules. The ultimately goal of these studies is to engineer strategies to control the motion of the enzyme molecules as they assemble on the surface. A FRET strategy that involves energy transfer between donor and acceptor can be attempted to map small changes in the intermolecular distances between neighboring enzyme molecules and respect to the surface functional groups.

A direct correlation of the conformational stability and the mobility of enzymes can be accomplished by performing co-adsorption experiments with enzyme molecules of different conformational stabilities. This approach could also help to validate the proposed strategy of incorporating small molecules prior to adsorption to minimize protein-surface interactions. A

FRET strategy can be also attempted where fluorochrome molecules are incorporated in both the surface and the protein^{31, 40}. Excited enzyme molecules could act as donors to transfer energy to acceptor fluorochrome molecules on the surface. The energy transfer strongly depends on the distances between donor and acceptor. This can be further exploited to map subtle changes in the intermolecular distances between the adsorbed enzymes and the functional groups on the surface. Similarly, information about the distances between neighboring enzyme molecules can be collected. In the end, one should be able to propose a complete mechanistic description of conformational changes and their correlation with the mobility on surfaces.

Most of the proposed experiments to this point involve the measurement of translational mobilities. Nevertheless, orientational mobilities can be also tracked in a very similar manner. In this case, however, local orientation is determined by measuring either the fluorescence polarization anisotropy⁴¹⁻⁴³ or polarization-dependent absorption⁴⁴ of a probe molecule coupled to the system of interest. The major difficulty is to find a probe with a high degree of polarization anisotropy. Fluorescent probes have proven particularly well suited for these applications. Some examples include organic dye molecules^{42, 44}, fluorescent polymers⁴⁵, and inorganic semiconductor nanoparticles⁴⁶.

7.2.2.3 Conformational Dynamics and Unfolding Events at Short-time Scales

In addition to the direct observation of the interaction of enzymes with model surfaces that would allow for determining enzyme conformational dynamics, it would be pertinent to study how the inherent dynamics of the enzyme molecules changes upon immobilization on fumed silica. Preliminary analyses involving dynamics were discussed in Chapters 5 and 6; nevertheless, it would be interesting to explore additional aspects such as the evolution of local conformational fluctuations at shorter time scales, the presence and distribution of intermediate conformational states, and the relative mobility, flexibility, and accessibility of enzyme segments prior to and during catalysis.

Conformational fluctuations at the femto- or pico- second scale during the adsorption on fumed silica can be accessed with ultrafast laser spectroscopy^{47, 48}, time-resolved UV Raman spectroscopy⁴⁹, and time-resolved FTIR spectroscopy^{50, 51}. Details of the typical experimental setups can be found elsewhere^{49, 52}. To calibrate the method, transient conformational species need to be generated and characterized⁵². The transient species are conventionally generated with laser pulses, temperature jumps, electron transfer, bond breaking or isomerization⁵². Once these

species are formed, the system moves to a nonequilibrium state⁵². The system then relaxes back to the original state. Conformational events occurring during this relaxation stage are recorded as a function of time, thereby, leading to transient decay profiles that allow for kinetic parameter calculation. This requires a site-specific structural probe that could be either an intrinsic⁴⁷ or an extrinsic⁴⁸ fluorochrome. As discussed in Chapter 5, Trp residues are generally the preferred choice for these studies. The extension to unfolding in the presence of fumed silica would allow for an estimate of the surface-induced local structural perturbations. From these experiments is also possible to characterize the unfolding landscape in the presence of fumed silica, in other words, the relative abundance of partially folded intermediate states while adsorbing on the nanoparticles. Figure 7.20 schematically describes the presence of multiple stages during the unfolding of proteins in solution. A similar landscape could be expected for surface-induced unfolding as in the case of hydrolases adsorbing on fumed silica. This opens an interesting opportunity for a direct correlation of the folding landscape with the conformational maps presented in Chapters 5 and 6.

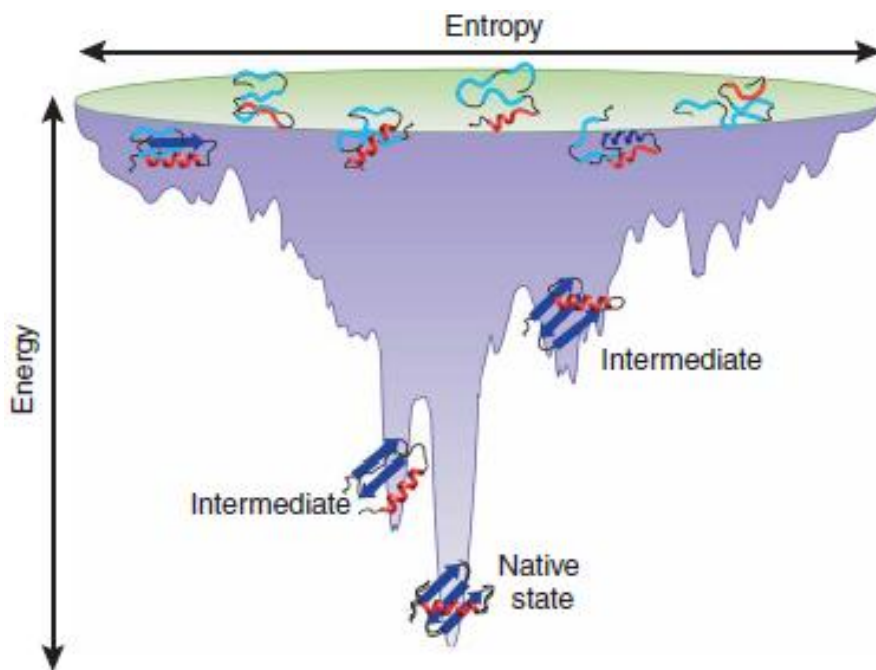


Figure 7.20. Schematic representation of a theoretically predicted folding funnel for proteins in solution⁵³. This has been mainly predicted with the aid of computational tools. A similar landscape where enzyme ensembles contain a number of non-native intermediate species are likely to be generated upon interaction with solid surfaces. The inherent structural heterogeneity of these ensembles poses significant challenges for a complete experimental biophysical characterization⁵³. The arrival of ultra-high resolution methods will help to refine the structural ensembles produced.

Compelling questions could be answered from this analysis such as how many routes can be taken by an unfolding enzyme to arrive to the fully denatured state?, can those routes be potentially manipulated to obtain a particular intermediate folding state?, and how is the route map connected to the “hardness” of the enzyme and the surface coverage?.

The lyophilized adsorbed state can be also analyzed with some of the previously described biophysical techniques in conjunction with hydrogen/deuterium (H/D) exchange methods. In this approach, D₂O is added to the lyophilized powders to exchange the mobile protons in the enzyme structure. This can be also done in the presence of organic solvents. The rate of exchange is directly related to the solvent accessibility and the strength of their hydrogen bond, consequently it is a measurement of the enzyme conformational flexibility. The preferred biophysical techniques to monitor the H/D exchange are FTIR and NMR, depending on the desired level of resolution. FTIR is well suited for providing an average of the entire system while NMR enables site-specific information. The exchange can be followed with FTIR by monitoring both amide I and amide II bands either in transmission or ATR experiments. The time course of the exchange is typically plotted as decay and subsequently fitted by three to four exponentials for amide groups with fast, medium, and slow exchange^{54, 55}. To track the exchange process with NMR, one can consider either ¹H NMR or ²H NMR⁵⁶. The former has been successfully applied to buried hydrogen atoms while the latter has been used to exchange all the hydrogens⁵⁶. The time evolution of the exchange can be subsequently fitted to a tri-exponential equation that accounts for protons with different exchanging rates⁵⁶.

NMR relaxation dispersion spectroscopy is also an interesting avenue to determine dynamical information of specific regions for both free and adsorbed enzyme molecules⁵⁷. The idea is to obtain a spectral density function at different frequencies which can be fitted to a model to recover the relaxation rates. The model is defined according to the observed relaxation mechanisms for proteins that very often include dipolar interactions for protons, C, and N, and chemical shift anisotropy for carbonyl carbons and amide nitrogen. Selectively labeled regions in the enzyme molecules can be studied with this approach by estimating various parameters including the rotational and translational motion of solvent molecules around the region(s) of interest, the relative motion of these regions respect to the rest of the molecule, and the impact of the support on the overall molecular flexibility as a function of the surface coverage.

Figure 7.21 shows an overview of the applicability of some biophysical techniques in addressing dynamical processes that occur in proteins at different time scales and structural levels. This arsenal of techniques offers numerous opportunities for direct observation of enzymes at work. As our molecular-level knowledge of these dynamical processes advances, robust predictive models can be postulated to design highly efficient protein-based applications.

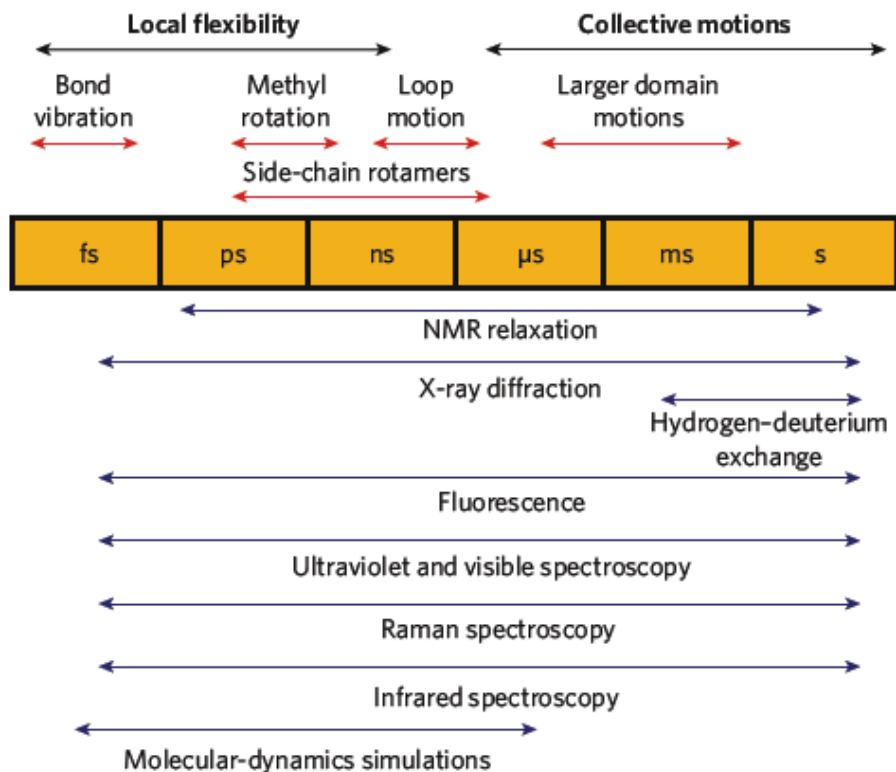


Figure 7.21. Overview of the major dynamical processes in proteins and their timescales. Some of the experimental and computational techniques that can be potentially used to access this information are added for reference⁵⁸.

7.2.3 Method Development

Additional aspects of the immobilization method itself could be further investigated to improve its robustness. A size exclusion chromatography step for the enzyme molecules prior to adsorption could help to obtain a more uniform size distribution especially for enzymes like CALB that have a marked tendency to aggregate. The impact of adding this step to the protocol can be evaluated by monitoring the time evolution of the enzyme distribution on fumed silica. This can be accomplished with SEM or confocal microscopy. The enzymes need to be labeled with heavy metals for the SEM analyses and with a suitable fluorochrome for the confocal ones.

The enzyme/fumed silica adsorbates are subsequently formed as usual. Samples of the adsorbing mixtures need to be withdrawn in a timely manner and quickly centrifuged for imaging.

Recent reports have suggested that the presence of co-solvents and co-solutes during the immobilization process might have a significant impact on both protein-protein and protein-surface interactions⁵⁹. Tested co-solvents include ethanol, 1-propanol, 2-propanol, and glycerol⁵⁹. A buffer containing 10% (v/v) ethanol could be prepared for the adsorption of CALB on fumed silica. The adsorbate can be subsequently lyophilized and tested for activity in hexane as usual. It would be also interesting to try to stabilize CALB's "soft" structure through the formation of cross-linked enzyme aggregates (CLEAs) prior to adsorption⁶⁰. Strategies to form the aggregates as well as to control their size are described elsewhere⁶⁰. The impact of the presence of co-solvents or the formation of CLEAs on the surface packing density and morphology upon adsorption could be assessed with hydrophilic surfaces and AFM.

7.2.4 Additional Aspects of Enzyme Conformational Stability

A rational design of highly active and stable nanobioconjugates would require quantitative studies of the energetics for the enzyme/fumed silica adsorbates with different surface coverages. The enzyme ensembles can be perturbed either with chemical or thermal denaturants to form partially folded intermediates that can be subsequently adsorbed on the nanoparticles. If chemical denaturation is applied, subtle changes in the structure can be monitored with either fluorescence or CD spectroscopy. These changes generally lead to a sigmoidal-shape curve for the unfolded fraction as a function of the denaturant concentration that can be then fitted to a two-state model. This approach allows for determining the Gibbs free energy of unfolding (ΔG_u), which is a measure of the thermodynamic stability of the enzyme molecules in the different enzyme loading regimes. The thermodynamic stability can be also inferred from thermally unfolded enzyme ensembles. In such a case, structural changes are monitored as the temperature is increased, leading again to a similar sigmoidal plot for the unfolded fraction. In the two-state model enthalpy (ΔH) and entropy (ΔS) are defined as⁶¹:

$$\Delta H(T) = \Delta H(T_m) + (T - T_m) \cdot \Delta C_p \quad \text{Equation 7.4}$$

and

$$\Delta S(T) = \Delta S(T_m) + \ln(T/T_m) \cdot \Delta C_p \quad \text{Equation 7.5}$$

where ΔC_p is the heat capacity and T_m is the melting temperature.

The Gibbs free energy can be approximated according to⁶¹:

$$\Delta G(T) = [(1 - T/T_m) \cdot \Delta H(T_m)] + (T - T_m) \cdot \Delta C_p - \ln(T/T_m) \cdot T \cdot \Delta C_p$$

Equation 7.6

where $\Delta H(T_m)$ is the enthalpy for melting.

Very accurate estimates of T_m , ΔC_p , and $\Delta H(T_m)$ in the absence of the nanoparticles can be obtained from DSC analysis in aqueous buffer solution. The data for the thermal unfolding in the presence of the nanoparticles collected previously can be then fitted to Equation 7.4, Equation 7.5, and Equation 7.6. In the end, reliable estimates for the thermodynamic parameters can be expected as a function of the surface coverage.

The question of how the kinetic and thermodynamic stability of the lyophilized preparations may change in the presence of an organic solvent remains open for discussion. A possible avenue to address this question is to calculate the Gibbs free energy of unfolding from the H/D experiments as described by Griebenow et al⁶². Another alternative could be to suspend them out in the solvent and directly measure the conformational state with fluorescence and CD spectroscopy.

Finally, it would be interesting to try to correlate the conformational stability data with the operational stability of the preparations. For instance, the preparations obtained at low surface coverages appeared to be very resistant to prolonged solvent exposure. One can try to determine whether the enzyme remains attached to the nanoparticles or desorbs by monitoring protein concentration on the organic solvent during time course of reactions. This would allow for correlation adsorption strength with stability.

7.2.5 Additional Applications

Due to the high activity and stability of enzyme/fumed silica preparations, a number of possible applications can be envisioned in various fields including non-aqueous detergency, synthesis of pharmaceutical compounds, development of biosensors, design of multifunctional nanoparticles for biomedical applications, and bioremediation.

7.3 References

1. Wu, X. Y.; Narsimhan, G., Effect of surface concentration on secondary and tertiary conformational changes of lysozyme adsorbed on silica nanoparticles. *Biochimica et Biophysica Acta-Proteins and Proteomics* **2008**, 1784, (11), 1694-1701.
2. Wu, X. Y.; Narsimhan, G., Coarse grain molecular dynamics simulation for the prediction of tertiary conformation of lysozyme adsorbed on silica surface. *Molecular Simulation* **2009**, 35, (10-11), 974-985.
3. Merzlyakov, M.; Li, E.; Gitsov, I.; Hristova, K., Surface-supported bilayers with transmembrane proteins: Role of the polymer cushion revisited. *Langmuir* **2006**, 22, (24), 10145-10151.
4. Vertrees, J.; Barritt, P.; Whitten, S.; Hilser, V. J., COREX/BEST server: a web browser-based program that calculates regional stability variations within protein structures. *Bioinformatics* **2005**, 21, (15), 3318-3319.
5. Hilser, V. J.; Garcia-Moreno, B.; Oas, T. G.; Kapp, G.; Whitten, S. T., A statistical thermodynamic model of the protein ensemble. *Chemical Reviews* **2006**, 106, (5), 1545-1558.
6. Manson, A.; Whitten, S. T.; Ferreon, J. C.; Fox, R. O.; Hilser, V. J., Characterizing the Role of Ensemble Modulation in Mutation-Induced Changes in Binding Affinity. *Journal of the American Chemical Society* **2009**, 131, (19), 6785-6793.
7. Schrank, T. P.; Bolen, D. W.; Hilser, V. J., Rational modulation of conformational fluctuations in adenylate kinase reveals a local unfolding mechanism for allostery and functional adaptation in proteins. *Proceedings of the National Academy of Sciences of the United States of America* **2009**, 106, (40), 16984-16989.
8. Vertrees, J.; Wrabl, J. O.; Hilser, V. J., Energetic Profiling of Protein Folds. In *Methods in Enzymology: Biothermodynamics, Vol 455, Part A*, Elsevier Academic Press Inc: San Diego, 2009; Vol. 455, pp 299-327.
9. Whitten, S. T.; Kurtz, A. J.; Pometun, M. S.; Wand, A. J.; Hilser, V. J., Revealing the nature of the native state ensemble through cold denaturation. *Biochemistry* **2006**, 45, (34), 10163-10174.
10. Hilser, V. J., An Ensemble View of Allostery. *Science* **2010**, 327, (5966), 653-654.

11. Hilser, V. J.; Thompson, E. B., Intrinsic disorder as a mechanism to optimize allosteric coupling in proteins. *Proceedings of the National Academy of Sciences of the United States of America* **2007**, 104, (20), 8311-8315.
12. Gu, J.; Hilser, V. J., Sequence-Based Analysis of Protein Energy Landscapes Reveals Nonuniform Thermal Adaptation within the Proteome. *Molecular Biology and Evolution* **2009**, 26, (10), 2217-2227.
13. Schweiker, K. L.; Fitz, V. W.; Makhatadze, G. I., Universal Convergence of the Specific Volume Changes of Globular Proteins upon Unfolding. *Biochemistry* **2009**, 48, (46), 10846-10851.
14. Rother, K.; Hildebrand, P. W.; Goede, A.; Gruening, B.; Preissner, R., Voronoia: analyzing packing in protein structures. *Nucleic Acids Research* **2009**, 37, D393-D395.
15. Garcia-Manyes, S.; Liang, J.; Szoszkiewicz, R.; Kuo, T. L.; Fernandez, J. M., Force-activated reactivity switch in a bimolecular chemical reaction. *Nature Chemistry* **2009**, 1, (3), 236-242.
16. Liang, J.; Fernandez, J. M., Mechanochemistry: One Bond at a Time. *ACS Nano* **2009**, 3, (7), 1628-1645.
17. Foresti, M. L.; Valle, G.; Bonetto, R.; Ferreira, M. L.; Briand, L. E., FTIR, SEM and fractal dimension characterization of lipase B from *Candida antarctica* immobilized onto titania at selected conditions. *Applied Surface Science* **2010**, 256, (6), 1624-1635.
18. Jonkheijm, P.; Weinrich, D.; Schroder, H.; Niemeyer, C. M.; Waldmann, H., Chemical Strategies for Generating Protein Biochips. *Angewandte Chemie-International Edition* **2008**, 47, (50), 9618-9647.
19. Weinrich, D.; Jonkheijm, P.; Niemeyer, C. M.; Waldmann, H., Applications of Protein Biochips in Biomedical and Biotechnological Research. *Angewandte Chemie-International Edition* **2009**, 48, (42), 7744-7751.
20. Young, J. F.; Nguyen, H. D.; Yang, L. T.; Huskens, J.; Jonkheijm, P.; Brunsveld, L., Strong and Reversible Monovalent Supramolecular Protein Immobilization. *ChemBiochem* **11**, (2), 180-183.
21. Zheng, Z. J.; Daniel, W. L.; Giam, L. R.; Huo, F. W.; Senesi, A. J.; Zheng, G. F.; Mirkin, C. A., Multiplexed Protein Arrays Enabled by Polymer Pen Lithography: Addressing the Inking Challenge. *Angewandte Chemie-International Edition* **2009**, 48, (41), 7626-7629.

22. Bano, F.; Fruk, L.; Sanavio, B.; Glettenberg, M.; Casalls, L.; Niemeyer, C. M.; Scoles, G., Toward Multiprotein Nanoarrays Using Nanografting and DNA Directed Immobilization of Proteins. *Nano Letters* **2009**, 9, (7), 2614-2618.
23. Kohn, M., Immobilization strategies for small molecule, peptide and protein microarrays. *Journal of Peptide Science* **2009**, 15, (6), 393-397.
24. Lempens, E. H. M.; Helms, B. A.; Merkx, M.; Meijer, E. W., Efficient and Chemoselective Surface Immobilization of Proteins by Using Aniline-Catalyzed Oxime Chemistry. *ChemBiochem* **2009**, 10, (4), 658-662.
25. Wan, J. D.; Thomas, M. S.; Guthrie, S.; Vullev, V. I., Surface-Bound Proteins with Preserved Functionality. *Annals of Biomedical Engineering* **2009**, 37, (6), 1190-1205.
26. Subramani, C.; Ofir, Y.; Patra, D.; Jordan, B. J.; Moran, I. W.; Park, M. H.; Carter, K. R.; Rotello, V. M., Nanoimprinted Polyethyleneimine: A Multimodal Template for Nanoparticle Assembly and Immobilization. *Advanced Functional Materials* **2009**, 19, (18), 2937-2942.
27. Escalante, M.; Zhao, Y. P.; Ludden, M. J. W.; Vermeij, R.; Olsen, J. D.; Berenschot, E.; Hunter, C. N.; Huskens, J.; Subramaniam, V.; Otto, C., Nanometer arrays of functional light harvesting antenna complexes by nanoimprint lithography and host-guest interactions. *Journal of the American Chemical Society* **2008**, 130, (28), 8892-+.
28. Axelrod, D., Total Internal Reflection Fluorescence Microscopy. In *Biophysical Tools for Biologists, Vol 2: In Vivo Techniques*, 2008; Vol. 89, pp 169-221.
29. Toscano, A.; Santore, M. M., Fibrinogen adsorption on three silica-based surfaces: Conformation and kinetics. *Langmuir* **2006**, 22, (6), 2588-2597.
30. Ram, S.; Prabhat, P.; Ward, E. S.; Ober, R. J., Improved single particle localization accuracy with dual objective multifocal plane microscopy. *Optics Express* **2009**, 17, (8), 6881-6898.
31. Rabe, M.; Verdes, D.; Seeger, S., Surface-induced spreading phenomenon of protein clusters. *Soft Matter* **2009**, 5, (5), 1039-1047.
32. Yu, L.; Lu, Z. S.; Gan, Y.; Liu, Y. S.; Li, C. M., AFM study of adsorption of protein A on a poly(dimethylsiloxane) surface. *Nanotechnology* **2009**, 20, (28).
33. Bulheller, B. M.; Rodger, A.; Hicks, M. R.; Dafforn, T. R.; Serpell, L. C.; Marshall, K. E.; Bromley, E. H. C.; King, P. J. S.; Channon, K. J.; Woolfson, D. N.; Hirst, J. D., Flow Linear

Dichroism of Some Prototypical Proteins. *Journal of the American Chemical Society* **2009**, 131, (37), 13305-13314.

34. Ennaceur, S. M.; Hicks, M. R.; Pridmore, C. J.; Dafforn, T. R.; Rodger, A.; Sanderson, J. M., Peptide Adsorption to Lipid Bilayers: Slow Processes Revealed by Linear Dichroism Spectroscopy. *Biophysical Journal* **2009**, 96, (4), 1399-1407.

35. Thakur, G.; Leblanc, R. M., Conformation of Lysozyme Langmuir Monolayer Studied by Infrared Reflection Absorption Spectroscopy. *Langmuir* **2009**, 25, (5), 2842-2849.

36. Khatua, S.; Guerrero, J. M.; Claytor, K.; Vives, G.; Kolomeisky, A. B.; Tour, J. M.; Link, S., Micrometer-Scale Translation and Monitoring of Individual Nanocars on Glass. *ACS Nano* **2009**, 3, (2), 351-356.

37. Tcherniak, A.; Reznik, C.; Link, S.; Landes, C. F., Fluorescence Correlation Spectroscopy: Criteria for Analysis in Complex Systems. *Analytical Chemistry* **2009**, 81, (2), 746-754.

38. Reznik, C.; Darugar, Q.; Wheat, A.; Fulghum, T.; Advincula, R. C.; Landes, C. F., Single ion diffusive transport within a poly(styrene sulfonate) polymer brush matrix probed by fluorescence correlation spectroscopy. *Journal of Physical Chemistry B* **2008**, 112, (35), 10890-10897.

39. Reznik, C.; Estillore, N.; Advincula, R. C.; Landes, C. F., Single Molecule Spectroscopy Reveals Heterogeneous Transport Mechanisms for Molecular Ions in a Polyelectrolyte Polymer Brush. *Journal of Physical Chemistry B* **2009**, 113, (44), 14611-14618.

40. Taylor, J. N.; Makarov, D. E.; Landes, C. F., Denoising Single-Molecule FRET Trajectories with Wavelets and Bayesian Inference. *Biophysical Journal* **2010**, 98, (1), 164-173.

41. Gould, T. J.; Gunewardene, M. S.; Gudheti, M. V.; Verkhusha, V. V.; Yin, S. R.; Gosse, J. A.; Hess, S. T., Nanoscale imaging of molecular positions and anisotropies. *Nature Methods* **2008**, 5, (12), 1027-1030.

42. Forkey, J. N.; Quinlan, M. E.; Shaw, M. A.; Corrie, J. E. T.; Goldman, Y. E., Three-dimensional structural dynamics of myosin V by single-molecule fluorescence polarization. *Nature* **2003**, 422, (6930), 399-404.

43. Rosenberg, S. A.; Quinlan, M. E.; Forkey, J. N.; Goldman, Y. E., Rotational motions of macromolecules by single-molecule fluorescence microscopy. *Accounts of Chemical Research* **2005**, 38, (7), 583-593.

44. Nishizaka, T.; Oiwa, K.; Noji, H.; Kimura, S.; Muneyuki, E.; Yoshida, M.; Kinosita, K., Chemomechanical coupling in F-1-ATPase revealed by simultaneous observation of nucleotide kinetics and rotation. *Nature Structural & Molecular Biology* **2004**, 11, (2), 142-148.
45. Link, S.; Chang, W. S.; Yethiraj, A.; Barbara, P. F., Orthogonal orientations for solvation of polymer molecules in smectic solvents. *Physical Review Letters* **2006**, 96, (1).
46. Toprak, E.; Enderlein, J.; Syed, S.; McKinney, S. A.; Petschek, R. G.; Ha, T.; Goldman, Y. E.; Selvin, P. R., Defocused orientation and position imaging (DOPI) of myosin V. *Proceedings of the National Academy of Sciences of the United States of America* **2006**, 103, (17), 6495-6499.
47. Kamal, J. K. A.; Xia, T. B.; Pal, S. K.; Zhao, L.; Zewail, A. H., Enzyme functionality and solvation of Subtilisin Carlsberg: from hours to femtoseconds. *Chemical Physics Letters* **2004**, 387, (4-6), 209-215.
48. Pal, S. K.; Peon, J.; Zewail, A. H., Ultrafast surface hydration dynamics and expression of protein functionality: alpha-Chymotrypsin. *Proceedings of the National Academy of Sciences of the United States of America* **2002**, 99, (24), 15297-15302.
49. Balakrishnan, G.; Weeks, C. L.; Ibrahim, M.; Soldatova, A. V.; Spiro, T. G., Protein dynamics from time resolved UV Raman spectroscopy. *Current Opinion in Structural Biology* **2008**, 18, (5), 623-629.
50. Gerwert, K., Molecular reaction mechanisms of proteins monitored by time-resolved FTIR-spectroscopy. *Biological Chemistry* **1999**, 380, (7-8), 931-935.
51. Kotting, C.; Gerwert, K., Proteins in action monitored by time-resolved FTIR spectroscopy. *Chemphyschem* **2005**, 6, (5), 881-888.
52. Stevens, J. A.; Link, J. J.; Kao, Y. T.; Zang, C.; Wang, L. J.; Zhong, D. P., Ultrafast Dynamics of Resonance Energy Transfer in Myoglobin: Probing Local Conformation Fluctuations. *Journal of Physical Chemistry B* **2010**, 114, (3), 1498-1505.
53. Bartlett, A. I.; Radford, S. E., An expanding arsenal of experimental methods yields an explosion of insights into protein folding mechanisms. *Nature Structural & Molecular Biology* **2009**, 16, (6), 582-588.
54. Barth, A., Infrared spectroscopy of proteins. *Biochimica et Biophysica Acta-Bioenergetics* **2007**, 1767, (9), 1073-1101.

55. Barth, A.; Zscherp, C., What vibrations tell us about proteins. *Quarterly Reviews of Biophysics* **2002**, 35, (4), 369-430.
56. Fasoli, E.; Ferrer, A.; Barletta, G. L., Hydrogen/Deuterium Exchange Study of Subtilisin Carlsberg During Prolonged Exposure to Organic Solvents. *Biotechnology and Bioengineering* **2009**, 102, (4), 1025-1032.
57. Lundstrom, P.; Vallurupalli, P.; Hansen, D. F.; Kay, L. E., Isotope labeling methods for studies of excited protein states by relaxation dispersion NMR spectroscopy. *Nature Protocols* **2009**, 4, (11), 1641-1648.
58. Henzler-Wildman, K.; Kern, D., Dynamic personalities of proteins. *Nature* **2007**, 450, (7172), 964-972.
59. Laszlo, J. A.; Evans, K. O., Influence of cosolvents on the hydrophobic surface immobilization topography of *Candida antarctica* lipase B. *Journal of Molecular Catalysis B-Enzymatic* **2009**, 58, (1-4), 169-174.
60. Lopez-Serrano, P.; Cao, L.; van Rantwijk, F.; Sheldon, R. A., Cross-linked enzyme aggregates with enhanced activity: application to lipases. *Biotechnology Letters* **2002**, 24, (16), 1379-1383.
61. Streicher, W. W.; Makhatadze, G. I., Unfolding thermodynamics of Trp-cage, a 20 residue miniprotein, studied by differential scanning calorimetry and circular dichroism spectroscopy. *Biochemistry* **2007**, 46, (10), 2876-2880.
62. Pagan, M.; Sola, R. J.; Griebenow, K., On the Role of Protein Structural Dynamics in the Catalytic Activity and Thermostability of Serine Protease Subtilisin Carlsberg. *Biotechnology and Bioengineering* **2009**, 103, (1), 77-84.